

**COMPUTATIONAL MODELING OF THERMAL
MANAGEMENT IN ELECTRONIC PACKAGING DESIGN
AND OPERATIONS**

Wen Wei

B.S., Xi'an Jiaotong University, 1984

M.S., Shanghai Institute of Mechanical Engineering, 1987

A dissertation presented to the faculty of the
Oregon Graduate Institute of Science and Technology
in partial fulfillment of the requirements for the degree of
Doctor of Philosophy
in Materials Science and Engineering

June 1998

The dissertation "Computational Modeling of Thermal Management in Electronic Packaging Design and Operations," by Wen Wei has been examined and approved by the following Examination committee:

Dr. Lemmy Meekisho, Dissertation Advisor
Associate Professor

Dr. Martin Becker
Professor

Dr. David G. Atteridge
Professor

Dr. Jack Devletian
Professor

Dr. Milton Scholl
Associate Professor

ACKNOWLEDGMENTS

I would like to acknowledge the support and guidance of my advisor and friend Dr. Lemmy Meekisho, without which this work could neither have been initiated nor completed. I greatly appreciate his many insightful suggestions, as well as his wise counsel during my study at OGI.

I also greatly appreciate the time and effort that my thesis committee members, Dr. Lemmy Meekisho, Dr. David Atteridge, Dr. Martin Becker, Dr. Jack Devletian, and Dr. Milton Scholl, invested in reviewing this document and examining its contents as well as my oral presentation and defense. A special thanks to Dr. Ronald Linton, Dr. Therese Chopin, Dr. Ann Anderson, Dr. Terry X. Yan, Dave Baker, etc. from industry, and other universities for their help and encouragement which led to the completion of this thesis.

I am also appreciative of the time from my fellow students such as Dr. A. Bansal, Dr. Victor M. Li, Kevin Searles, Dr. Lu Fang invested in me during my years in OGI. To those dear classmates who I will always remember (David Christilaw, Leo Chen, Mia Park, and Jim Van Winkle), many thanks!

I would like to express my sincere thanks to the Oregon Graduate Institute of Science and Technology for funding me during my study and research on my dissertation for four years in the Department of Materials Science and Engineering. Also, to our department secretary Roxanne Metzker, director of Personnel, Janet Chandler, and librarians Julianne Williams, Nancy Henderson many thanks for putting up with me for all the academic and legal documentation details and indeed for assistance in putting this document into compliance with required specifications.

I gratefully acknowledge the encouragement and continued sacrifice of my wife, Wen Zhu, who has supported me through both failures and successes, in my frustration and fulfillment. Without patience, understanding, and love on her part, this work would never have been realized. To my lovely daughter, Ching-Ching (Yuqing), you are both my joy and motivation.

DEDICATION

Dedicated to my parents,
Ranggao Wei and Yuying Wang,
my wife and daughter,
Wen Zhu and Yuqing Wei

TABLE OF CONTENTS

Acknowledgment	iii
Dedication	iv
Table of Contents	v
Abstract	vii
1. Literature Review and Recommendation	1
1.1. Objectives, Significance and Scope	1
1.2. Background	3
1.3. Approach and Strategies	7
2. Theoretical and Numerical Solutions for Electronic Packaging	24
2.1. Conduction Heat Transfer	25
2.2. Contact Heat Transfer	29
2.2.1. Thermal Contact Resistance	32
2.3. Finite Element Analysis	42
2.4. Convective Heat Transfer	59
2.4.1. Laminar and Turbulence	61
2.4.2. External Forced Convective Heat Transfer Solutions	64
2.4.3. Internal Forced convective Heat Transfer Solutions	70
2.4.4. Natural Convection Flow Solution	75
2.4.5. Computational Fluid Dynamics, Finite Volume Approach	77
2.5. Radiation Heat Transfer Solutions	82
3. Case Studies	113
3.1. Component Level Simulation	113
3.1.1. Modeling of Multi-chip Modules(MCM) with Thermal Vias	113
3.2. System Level Simulation	119
3.2.1. Heat Transfer Prediction for In-line Arrays of Modules in Air Channel	119
4. Special Topics and Discussions	154
4.1. Component Level Simulation	154

4.1.1.	Sensitivity Analysis of thermal Via Configuration	156
4.1.2.	Sensitivity Analysis for Pins	158
4.1.3.	Sensitivity Analysis of Interlayer Thickness	161
4.2.	System Level Simulation	165
4.2.1.	Fan Design	165
4.2.2.	Heat Sink Design	167
4.2.3.	Results of Heat Transfer Analysis for In-line Arrays of Modules in Air Channel Flows	169
	References	201
	Vita	208

ABSTRACT

COMPUTATIONAL MODELING OF THERMAL MANAGEMENT IN ELECTRONIC PACKAGING DESIGN AND OPERATIONS

Wen Wei

Oregon Graduate Institute of Science and Technology

Supervising Professor: Dr. Lemmy L. Meekisho

Thermal phenomena associated with electronic packaging were introduced and explored in detail. Packaging refers to the silicon integrated circuits (IC), cards and boards. The mechanisms of multi-mode heat transfer in electronic packaging are summarized and approaches to the design and operation by means of conjugate thermal-flow simulations and testing are explored. Simulations were accomplished by numerical modeling with the aid of finite element method (FEM) and finite volume method (FVM) techniques.

The component level designs included the structural design and material management. Structural designs focused on the substrate, die, lid, board, thermal vias, heat sink, adhesive layer design. These configurations are associated with thermal conductivity, convective heat transfer coefficient, emissivity, view factor and other parameters which involve conduction, convection and radiation heat transfer over the IC components, ASICs and other packaging components. Material selections were based on the thermal conductivity performance for IC substrate, die, thermal vias, printed circuit board (PCB), and interfacial materials between heat sinks and lid, die and substrate. A three dimensional (3D) simulation case study of a multi-chip module (MCM) in surface mounted technology (SMT) ball-grid-array (BGA) hybrid packaging on multi-layer printed circuit boards illustrated the component level design.

Device system level designs are mainly associated with forced convection over all components and board level systems. 3D computational fluid dynamics (CFD) FVM

models were used to compute system level solutions numerically. These numerical solutions were compared with experimental results. The models involved arrays of electronics modules in a channel.

The simulations involved conduction heat transfer, conjugate conduction/flow, convection and radiation heat transfer. The flows were assumed to be viscous and incompressible laminar or turbulent fluid flow conjugated with heat conduction or radiation. In computational fluid dynamics of system models for turbulence flow, the k- ϵ and LEVEL algebraic turbulence models were used. Application of different thermal and flow boundaries including interfacial thermal resistance were explored and a discussion is initiated. The relative error of simulation results were found to lie in the range 0.64% - 7.67% in comparison with standard benchmark tests. Future trends of thermal management issues as they apply to electronic packaging are discussed.

CHAPTER 1

LITERATURE REVIEW AND RECOMMENDATION

1.1 Objectives, Significance and Scope

The target of this dissertation was to address the needs of the thermal management design for the different levels associated with electronic packaging. Specific emphasis was placed on heat transfer analysis and the thermal design processes in electrical circuit boards, semiconductor components, associated materials and sizes, and their interactions with the cooling fluid.

In the 1960's bipolar transistors predominantly comprised the integrated circuit (IC) market. Since 1975, however, digital complementary metal-oxide semiconductors (CMOS) ICs have prevailed. With the development of very-large-scale integration (VLSI) technique, the number of components per IC chip has grown exponentially (Fig.1-1)⁽⁷⁷⁾. The circuit designers have been placing components, chips, modules, cards, motherboards, and I/Os as compactly as possible to increase computer speed⁽³⁾ and decrease computer size and weight. Design of electronics system and component packaging is subject to continuous miniaturization. This trend has been associated with a reduction in the minimum feature size⁽⁴²⁾ (Fig.1-2) from approximately 1 to 0.1 μm ⁽⁷²⁾ and it is predicted that the number of components per chip will increase from more than 10^6 ⁽⁶⁷⁾ to 100 million in the year 2000⁽⁷²⁾.

With exponentially increasing power trends (Fig.1-3) by the year 2005 individual IC power dissipation levels can become as high as 200 Watts. Correspondingly, heat fluxes have ranged from 100 Watts/cm² for a small package size and 50 Watts/cm² for the larger packages^(52, 6) “The heat flux of the microelectronics chip is only two orders of magnitude less than that on the surface of the sun, but the sun's surface temperature is

6000°C compared with 125-150°C operating temperature of a typical semiconductor device”⁽⁸⁵⁾. The junction temperature of an IC would tend to increase accordingly, and it has been documented⁽³⁰⁾, that higher operating temperatures directly to accelerate various failure modes mechanisms such as creep, local deflections, and severe thermal stresses⁽³⁰⁾ as shown in Fig.1-4a, Fig.1-4b and Fig.1-4c. Other failure mechanism are triggered by corrosion and electromigration phenomena as shown in Fig.1-5. In addition to high operating temperatures, frequent temperature cycling between power-off and power-on conditions can also be detrimental to component reliability due to failures in solder points⁽⁶⁷⁾.

Electronic components are very reliable at room temperature and can theoretically be expected to operate continuously for more than 10,000 years. The acceptable maximum operating temperature of a CMOS device is about 85°C⁽⁸⁸⁾. It is documented that a 10°C-20°C increase in the device temperature can increase its failure rate by 100%. On the other hand, 1°C decrease in its temperature may lower its failure rate by as much as 4%⁽⁵²⁾ and the relationship between the temperature and its functional reliability is associated with fatigue as⁽⁷⁶⁾ Fig.1-6. This indicates that the reliability of standard CMOS assemblies drops dramatically with increasing temperature. Thermal management for electronic packaging reliability (Fig.1-7) has thus become one imperative and critical aspect to limit the IC packaging dimension and density level⁽⁷⁷⁾ of components.

In the 1990's, significant thermal loads have typically been from advanced computing and military applications such as multi-chip modules (MCMs) or ultra thin small outline packages (UTSOP), surface mounted technology (SMT), packages, and ball grid arrays (BGA) or chip scale packages (CSPs)⁽⁶¹⁾. For densely packaged electronics, the required cooling often exceeds the capability of traditional passive cooling such as conduction and natural convection. Advanced cooling schemes such as heat sinks, direct impingement cooling, encapsulated highly conductive slabs, thermal vias *et al* have to be introduced to match the increased power densities.

The current cooling methods include air-cooling, hybrid-cooling, indirect liquid cooling, and direct liquid cooling⁽³⁾. Generally, air-cooling system is for low power

dissipation packages or devices by means of natural or forced convection to directly cool the electronic modules. For the packages with higher power dissipation levels of less than 100 Watts such as ASIC and Pentium microprocessors, air-cooling methods can be sufficiently efficient if aided by applying heat sinks and additional local internal fans on the surfaces of chips to improve convective heat transfer. Hybrid cooling is for considerably higher-level power dissipation packages usually in two steps, namely liquid cooled heat exchangers to cool the air, then air cools the modules. Indirect liquid cooling is used for even higher power dissipation systems by mounting the electronic modules on liquid cooled or two-phase fluid cooled cold plates. For such high power dissipation systems, direct liquid cooling techniques become necessary.

1.2 Background

The traditional method for industry to seek solutions for thermal problems is that: first to make the thermal design based on simple correlations taken from experimental data on related geometry, then measure the system performance with full scale tests. If the design does not meet specifications, this necessitates adjusting some parameters, for instance, for air cooling system, adjust the air flow rate using larger cubic feet per minute (CFM) fans or changing air flow path by air dams, vents and so on, until an acceptable temperature distribution is achieved. This development process is neither efficient in time nor economical in cost⁽³⁾. Sometimes after the product is developed, unexpected severe problems are reported by the end-users due to the differences between the operating conditions of end-users. Product development schemes from the manufactures such as different environment or room temperatures, different flow path of the clean rooms and any conditions which are different compared to the so called full scale tests based on the experimental data for the design model geometry configuration and dimensions. In the 1980s, Przekwas, Jiang, and Wang et al⁽⁶¹⁾ conceptually developed a Virtual Prototyping Environment (VPE) for thermal packaging and testing of MCMs. In 1977, a group led by Moffat at Stanford University started an air-cooling research program to develop the superposition technique to electronic component cooling with the aim of improving the accuracy of predictions and to extend the application of air-cooling

under realistic operating condition for the electronics industry. The success of this group has resulted in the significant progress of cooling technologies in general and to electronic cooling in particular. Arvizu and Moffat⁽⁴⁾ applied the superposition method to calculate the temperature distribution on an array of arbitrarily heated components in forced convection. By combining the model for thermal wake function and heat transfer coefficient as a function of Reynolds number, they predicted the temperatures in an arbitrarily heated array of modules. Ortega and Moffat⁽⁵⁷⁾ demonstrated that superposition could also be applied to free convection flow if the local Grashof number was small compared to the induced flow Reynolds number. Investigators at Stanford like Biber and Sammakia⁽¹²⁾ also improved this technique theoretically and experimentally.

There are other researchers in the electronics cooling field who did not use superposition techniques however, they provided heat transfer coefficient results for a variety of combinations of different geometries and inlet/outlet flow conditions. Notably these include Sparrow et al⁽⁷¹⁾ who explored heat transfer analysis of arrays of rectangular modules encountered in electronic equipment. Davalath⁽¹⁹⁾, Asako et al⁽⁵⁾ also analyzed, three dimensional heat transfer of arrays of heated rectangular and square blocks, Faghri et al⁽²¹⁾ did a preliminary experimental study of forced air-cooling of rectangular blocks typically encountered in electronic equipment, and Incropera⁽³⁷⁾ addressed the application of convection heat transfer in electronic equipment cooling.

The aim of all the studies referred above was to obtain the local heat transfer coefficient on a particular element or module with heat source in an array of elements. The results cannot be compared directly due to the difference among the geometries studied⁽³⁾. Anderson⁽²⁾ tried the superposition approach to calculate the operating temperature of components in an arbitrarily heated array of modules by numerical techniques using superposition kernel function. This method could evaluate component temperatures in non-uniform heat dissipation situations from electronic modules in arrays instead of individual units arranged arbitrarily. The superposition model is one dimensional, and the adiabatic heat transfer coefficient is generally not applied to heat convection and conduction problems. Schmidt⁽⁶⁵⁾ did a numerical study of laminar forced convection across heated rectangular blocks in two-dimensional ducts. But for arbitrarily

distributed components, for example, radial distributed components, cards and boards with components on them, and irregular duct or channel, it is even more difficult to predict the component temperatures. This is especially true with the consideration of the card or board conduction, with fans next to vents using traditional methods. Oosthuizen⁽⁵⁶⁾ tried numerical methods to analyze the effect of a deflector wedge on forced convection from heated rectangular blocks on a channel wall. With the development of simulation tools, increasing number of researchers like Lee⁽⁴⁴⁾, Biber⁽¹³⁾, Lee^(45, 46), Linton⁽⁴⁷⁾ et al. predicted the semiconductor junction temperatures, system temperature distributions, design fans, heat sinks, *et al* using advanced numerical software for the increasingly more complicated electronics packaging and electronics systems.

A general numerical model is represented in Fig.1-8, which shows the ways to interpret the actual constraints or the prescribed conditions to the boundary conditions on the numerical model. For the thermal problem options include isothermal, adiabatic, heat flux, heat generation, heat convection, radiation as thermal load; and displacements, and stress, strains as structural load. The analysis domain is defined by the physical interactions in the form of fundamental equations, and the domain is discretized into a finite number of elements for the FEA approach and finite number of control volumes for FVM approach. The equations are applied to these units. With the different computational codes or programs all the variables from the equations can finally be iterated into or converged to a target accuracy range so as to provide local temperature, convection coefficient, flow velocity under the specified geometric and operation conditions. Structural boundary conditions typically involve contact interfaces. The corresponding displacement, strain and stress fields can have a significant effect on the thermal performance through a phenomenon known as interfacial thermal resistance⁽⁸²⁾.

The electronics packaging design process involves analysis tools from different scenarios including electronics, mechanics, thermal, thermal/structural, electromagnetic, and manufacturing. Cost, complexity, ergonomics and reliability are all implicit in the design of the package. Interoperability between these software tools is essential to facilitate interactive trade-off between conflicting requirements from different disciplines.

Unfortunately, contemporary packaging software tools are uni-disciplinary and seldom involve advanced 3D-capability⁽⁷⁾. Thermal and thermal/structural analyses are usually used to validate the electrical scheme and thermally “over-design with larger safety factors after the IC design has been accomplished. Integrated multi-disciplinary simulation tools for electronic packaging are non-existent.

The two efforts to model thermal performance are implemented by using component level codes and system level codes. The component level codes model the portion of problem emphasizing the interaction of heat conduction among the solid objects such as substrates, dies, interlayer, lid, heat sink, vias and so on. Normally this portion is effectively done by FEA for the arbitrary geometry of domains and objects in conduction heat transfer. If the domains of objects are shaped like a rectangle, FVM is as good as FEA to conduct the component level simulation. Rectangular shape cause tremendous trouble in addressing the complete problem as they result in the flow separation, which is notorious for causing divergent solutions⁽³⁾. The system level codes basically deal with flow or thermal/flow problem ignoring the details in component level, but most are confined to low Reynolds number flows and are only as good as the turbulence models incorporated in them⁽³⁾. Although many FVM codes are developed to overcome those problems and replace the FEA for solving the flow problems, it still facing difficulty handling the non-rectangular dominant systems, multiphase flow, impingement flow, *et al.* Recently, more and more FVM codes are specially designed for the electronic packaging industry like FLOTHERM from Flomerics®, ICEPAK from Fluent®, HOTBOX from Phoenix®, *et al.* Table 1-1 summarizes some key features of these codes.

Unfortunately, because only a small portion of the problem and the model simplification are not easy to generalize and not based on the relevant physics of the problem. This often results in a multitude of heat transfer correlations⁽³⁾. It is impossible to rely on one software to perform *a priori*, thermal analysis for most electronics companies⁽³⁾. The need to establish a general approach to the problem and a better prediction method becomes crucial. The objectives of this study, as outlined in sections 1.3, represent the vision ideas of the efforts to understand the coupled thermal-flow

phenomena associated with electronic packaging with the aim of identifying ways to contribute to this fascinating technology area.

1.3 Approaches and Strategies

The task of the packaging engineer is to integrate all considerations and requirements from the electrical design, mechanical design and the operating characteristics into an optimal design of a cooling system⁽³⁾. The thermal performance of individual electronic components and cards in a system for electronic packaging is a complex issue due to its multi-mode heat transfer. It becomes reasonable to predict thermal behavior by breaking the assemblies down into a set of lumped capacitances or a set of units classified into different packaging levels, and divide the design procedure into five steps. A detailed prediction of performance and susceptibility to failure can be achieved by analyzing their thermal interaction with each other.

The thermal performance prediction of the semiconductor devices or components, and the systems under different specific applications, the maturity process for a successful thermal design is the key issue for the semiconductor industry.

To successfully predict heat transfer and fluid flow, experimental investigation and theoretical calculations are the two general approaches. Experimental investigation provides the most convincing conclusion for a thermal design or cooling system if the measurement is reliable, the test model is fully identical or emulates the actual equipment under the same operating conditions. But, unfortunately, it is near impossible to implement most tests at full scale for the tests are expensive, time consuming, and sometimes, impossible to set up. Small scale or partial size models are very useful but can tend to become less reliable. The limitation of the measuring techniques is another constraint which limits our ability to conduct the thermal and flow measurement for the increasingly smaller and denser electronics equipment.

Compared to experimental investigation, the significant benefit we can get by theoretical calculations are lower cost, high speed, and complete information for any points in the model corresponding to any specific time. It can also simulate the worst and ideal cases which may be impossible from an experimental test approach. But theoretical

calculations have some profound disadvantages as well, for example, limitation of our understanding of some physical phenomena like complex turbulent flows, non-Newtonian flows *et al*, which deems it difficult to get the correct or complete mathematical descriptions, thus reducing the accuracy and reliability of theoretical prediction. However, most electronics cooling problems do not belong in this blind area and with the development of advanced numerical codes, computed solutions have become more feasible and acceptable for design and operating requirements.

Due to the advantages of experimental test and theoretical calculations, a combination of experimental investigation and numerical simulation processes present a potentially optimal method to predict and design a cooling system. The procedure for developing a thermal design is summarized in Fig 1-9, and it can also be represented by a relation between the simulation and test, typically in five stages (Fig.1-10) which was introduced above. The first stage (zone I) is a preliminary design process; the design is based upon the assumptions for the material properties, geometric configurations, existing geometry (if mechanical design is complete), operating conditions like temperature, pressure ranges, flow type. This scheme is a conceptual design and rudimentary estimation. This estimation has to be achieved in one of three ways such as empirical estimation, closed-form calculation and numerical simulation. The goal of the simulation at this stage is to provide a series of thermal solutions. The solutions determine the methods of cooling, the choice of material and structural configuration for the package on the system, or component or both levels. Mock-ups are made from the optimal solutions among all the preliminary designs.

Stage II is a data acquisition test period on the mock-up. The purpose of the test is not only to validate the choice of the cooling system, but it also is expected to extract data for the critical parameters to the whole system. The data will be used to modify the assumptions for the material properties, which are unknown but can significantly influence the thermal performance. For example, the thermal conductivity for the multi-layer printed circuit board varies with the number of layers, density of the printed wires, electrical vias, thermal vias, the normal and in-plane directions inside circuit boards, and board material *et al*. The differences in the thermal conductivity boards result in different

cases, namely, the lid, substrate, heat sink temperatures and ultimately junction temperature at the die. To keep the CMOS circuit performance in stable working conditions, many semiconductor devices or systems have thermal compensation systems to lock the thermal load so as to keep the IC chips working at a relatively stable temperature range. This makes the allowable temperature fluctuation range relatively low, and typically a couple of degree centigrade. The small percentage of estimation error resulting from thermal conductivity of circuit board and even the thin adhesive layer may cause larger errors in temperature prediction and system calibration.

If the IC temperature cannot meet with the specified junction temperature requirement, stage III which modifies the original design is needed after a relatively reliable data set is obtained. The goal of this stage is to provide a series of improved thermal solutions by the thermal simulation on the component, or system, or both level. The modifications deals with

- methods of cooling,
- the choices of material and structural,
- design and selection of fans,
- flow path including opening,
- vents and ducts for system,

under different combination of operating conditions such as specific power dissipation, ambient temperature, flow impedance, *et al.* The cooling scheme, component, board and system structures are presented by 2D or 3D numerical model, the functioning conditions confine the boundary condition or load for numerical models. An efficient and feasible design is selected after comparing all the plots, and correspondingly, preparing the mechanical prototype for the validation test.

Validation of the thermal performance of selected system is the objective of stage IV. It submits the performance data to stage V to do the modification, development and correlation of the design. Iteration between stages IV and V may be repeated until specified target performance criteria are met. Another most important aspect of stage V is temperature prediction for the modified conditions and the final mechanical design.

In this dissertation, two examples were used to address thermal management in three different levels and intent to present a series of thermal design method by means of numerical solutions and test. The first case is a component level packaging design using ANSYS ⁽⁴¹⁾ FEA method for an MCM package. The second example is forced convection cooling system level analysis using 3D FVM model. Results are summarized and the future directions are discussed.

Table 1-1 Brief Summary Of Numerical Codes For Electronic Packaging (By 1998)

	FLOTHERM	ICEPAK	HOTBOX	ANSYS
Geometry	Rectangular	Partial arbitrary	Rectangular	Arbitrary
Arbitrary geometry		UNS Version	General Version	Flotran
Multiphase		UNS Version	General Version	yes
Structural	no	UNS Version	yes*	yes
Fan Curve	yes	yes	yes	no
Heat sink	yes	yes	no	no
CPU Time	fast	fast	fast	
Method	FVM	FVM/FEA	FVM	FEA
Interface	Good	Best	Good	Best
Version	1.4	2.1.2	2.2.2	5.3

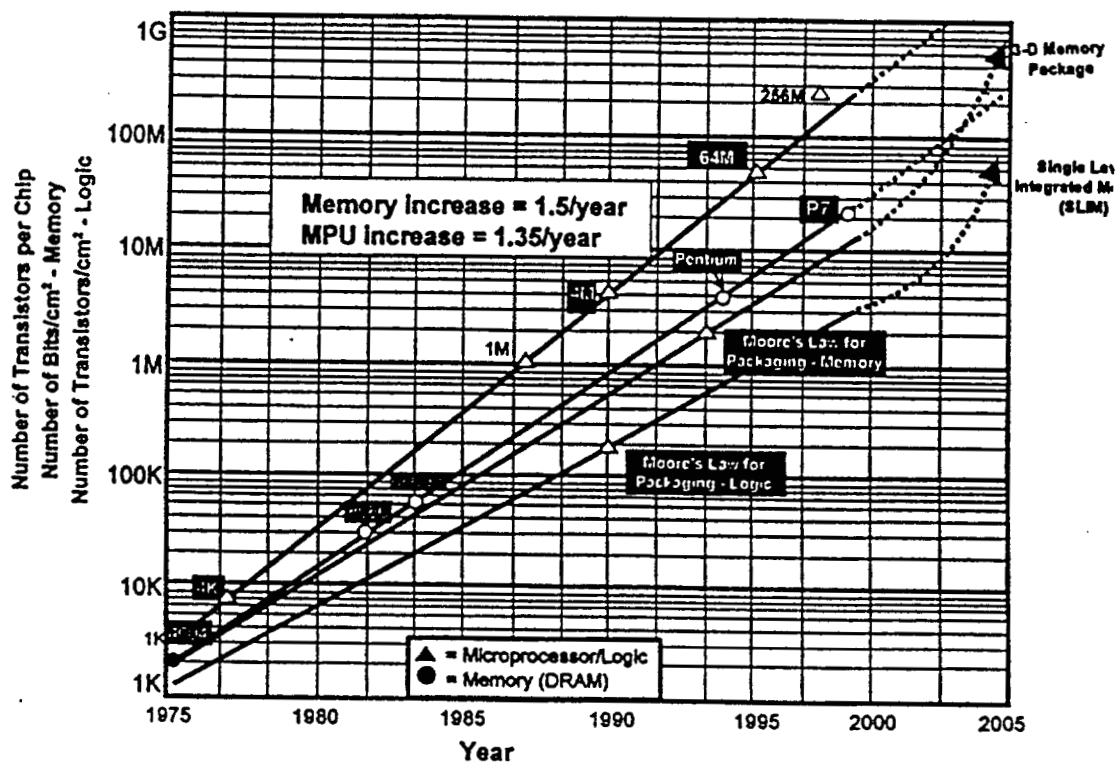


Fig.1-1 Microelectronics Density Trends (Adapted From Ref. 77)

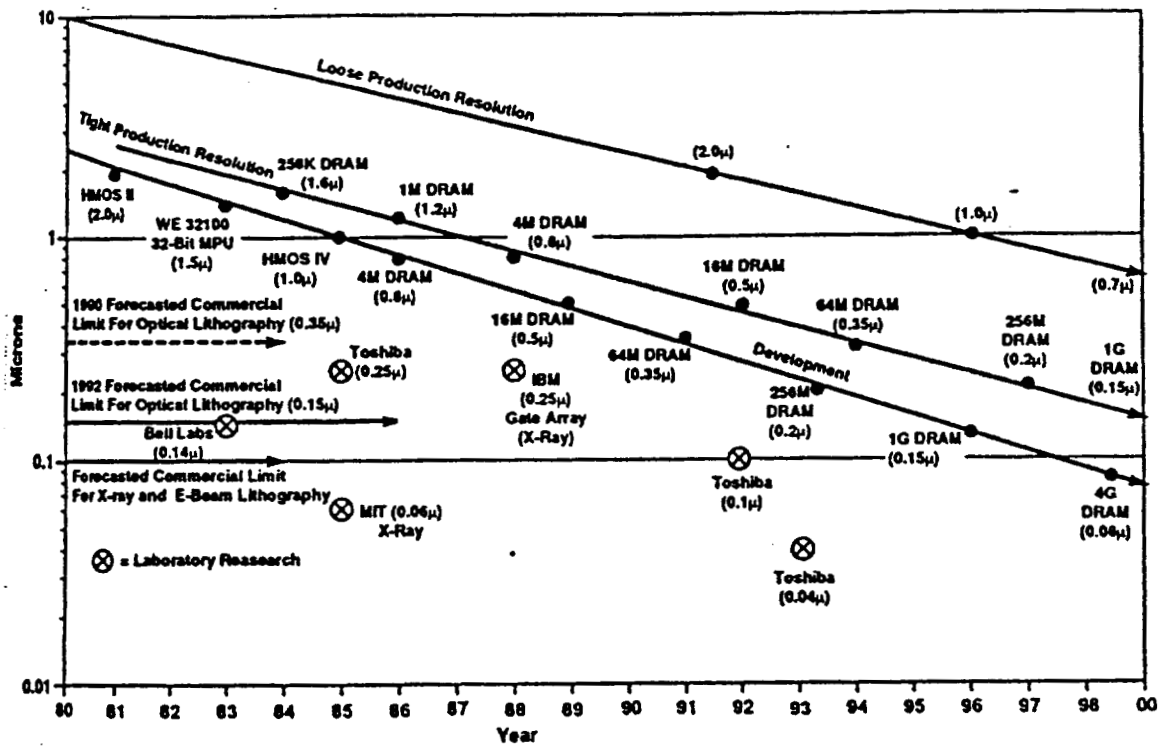


Fig.1-2 IC Feature Size Trends (Adapted From Ref. 42)

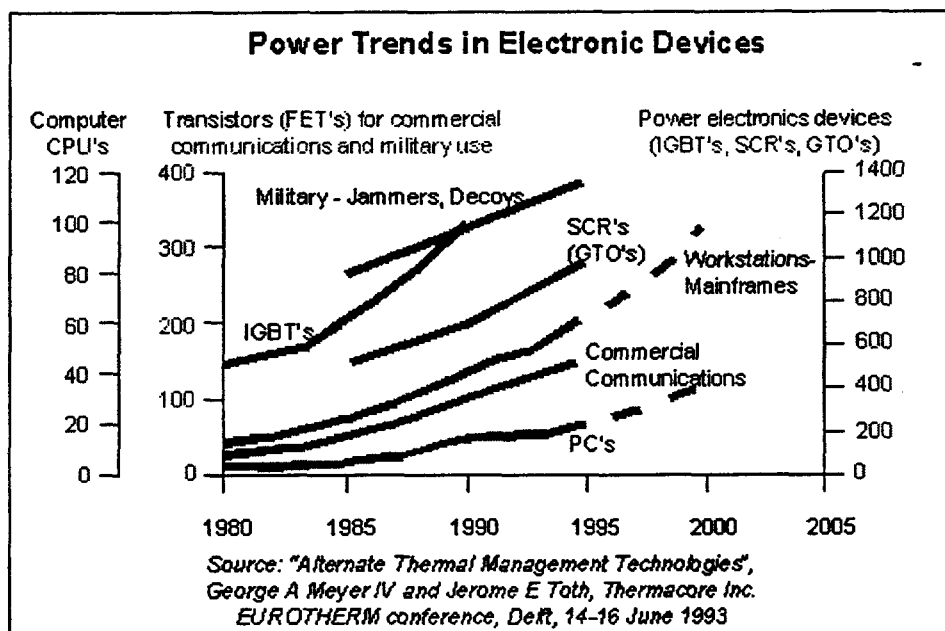


Fig.1-3 Power Trends In Electronic Devices (Adapted From Ref. 51)

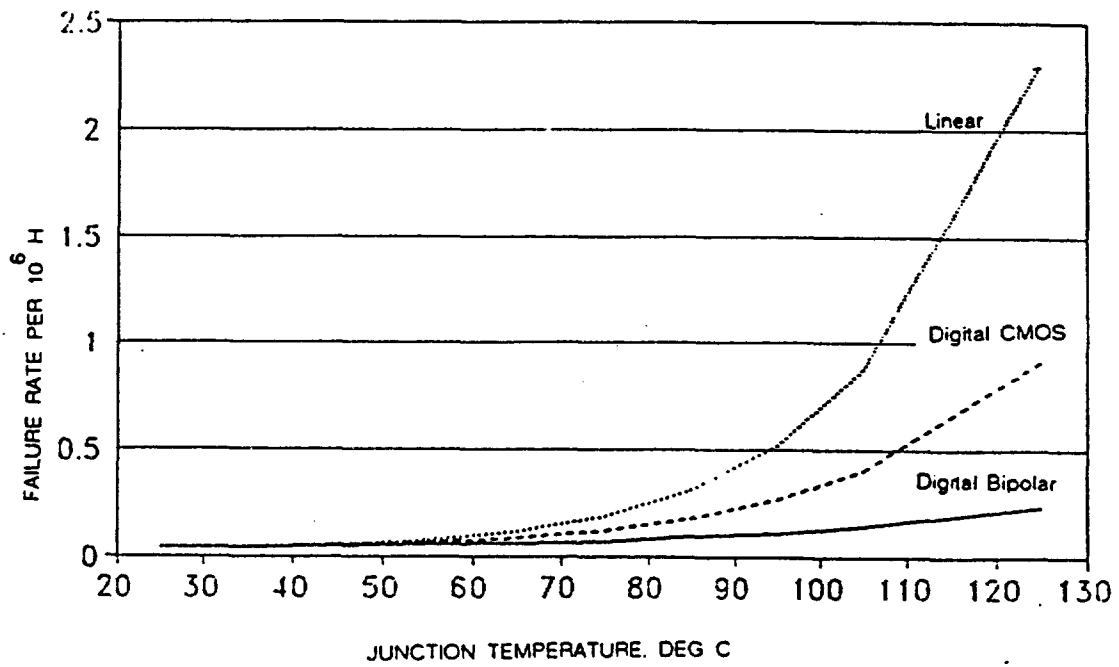


Fig.1-4a Digital And Analog Component Failure Rates Over Temperature
(From MIL-HDBK-217) (Adapted From Ref. 30)

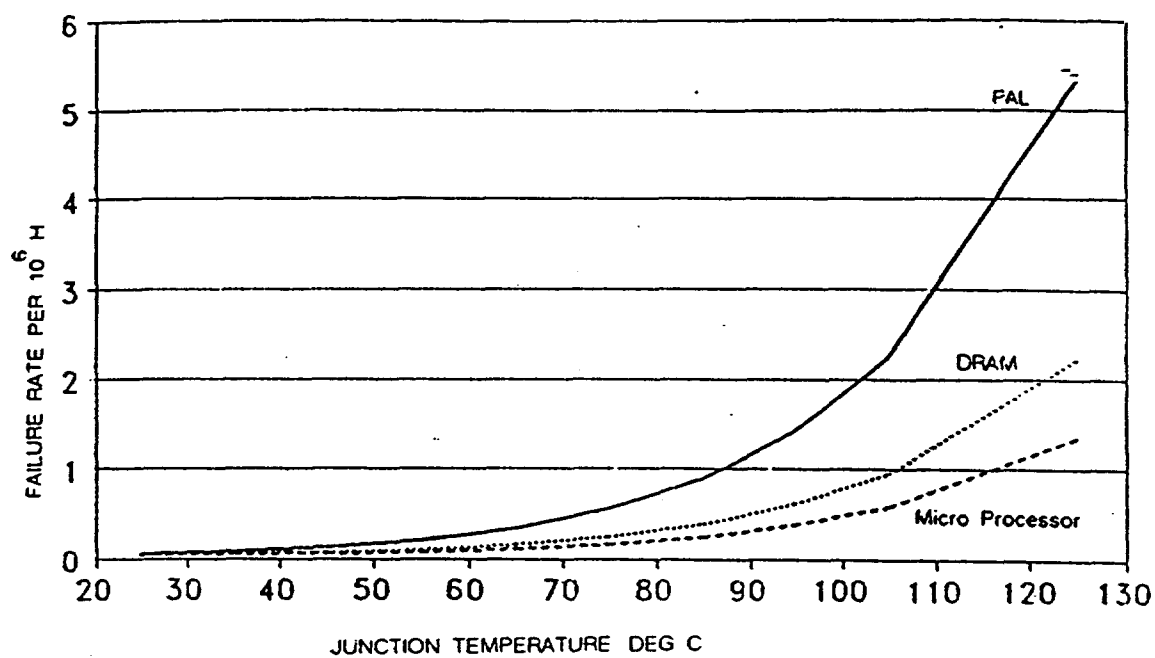


Fig.1-4b Digital Component Failure Rates Over Temperature (From Mil-hdbk-217) (Adapted From Ref. 30)

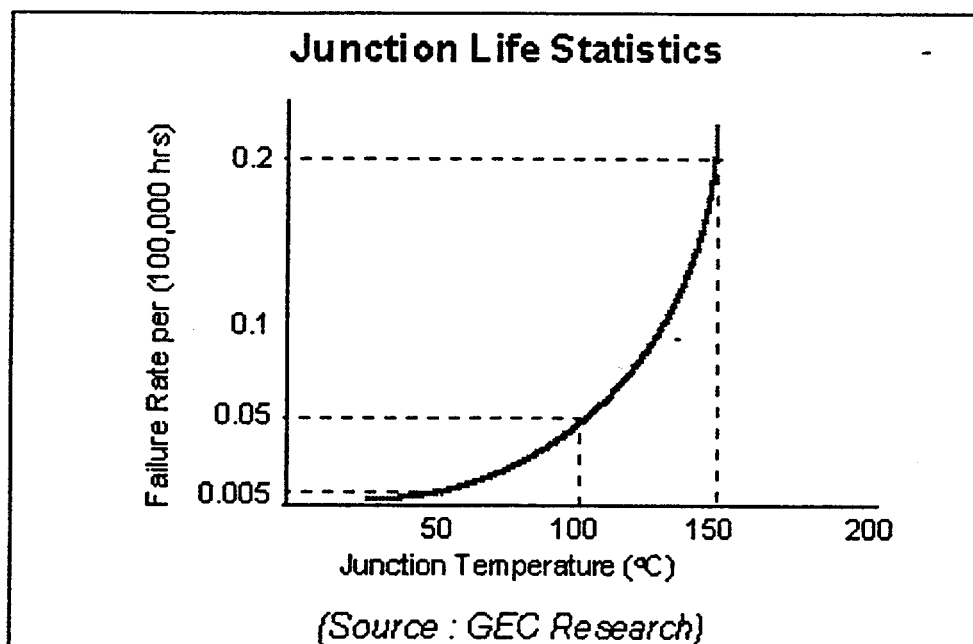


Fig.1-4c Junction Life Statistics(Source: GEC Research) (Adapted From Ref. 22)

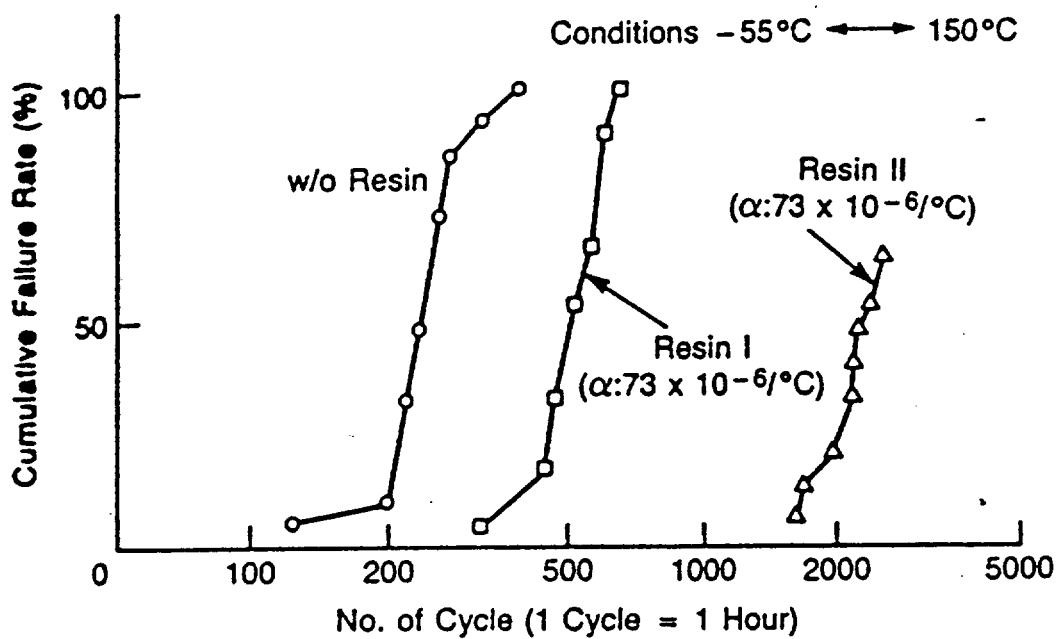


Fig.1-5 C4 Life Extension By The Use Of Thermal Expansion Matched (To Solder) Resins (Adapted From Ref. 30)

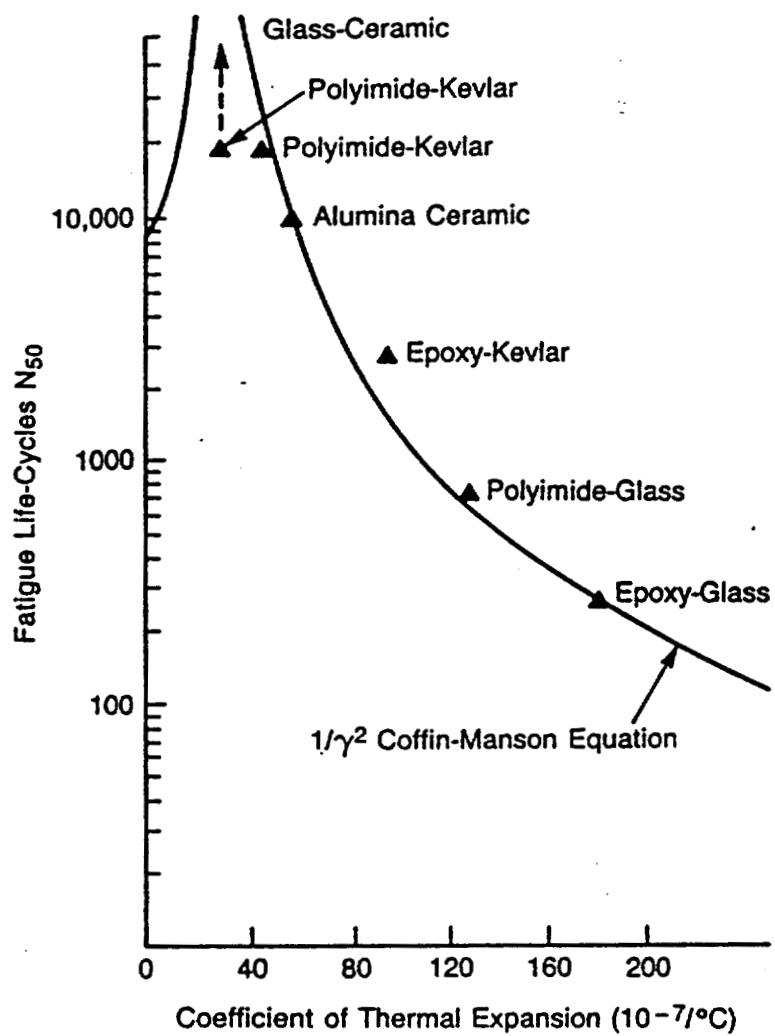


Fig.1-6 Effect of Thermal Expansion Coefficient On Fatigue Life(Adapted From Ref. 30)

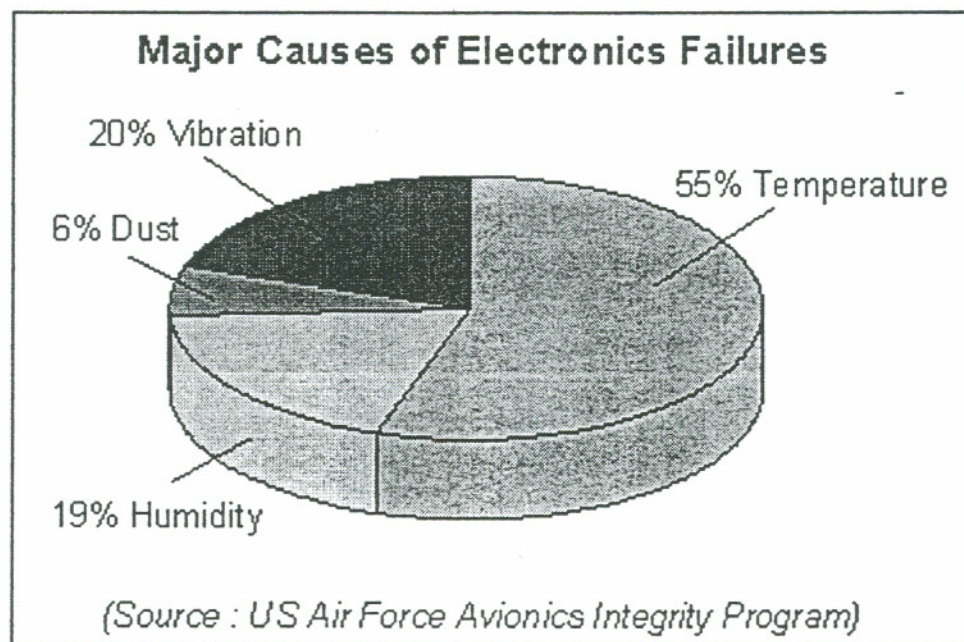


Fig.1-7 Major Causes Of Electronics Failures (Source: US Air Force Avionics Integrity Program (Adapted From Ref. 23))

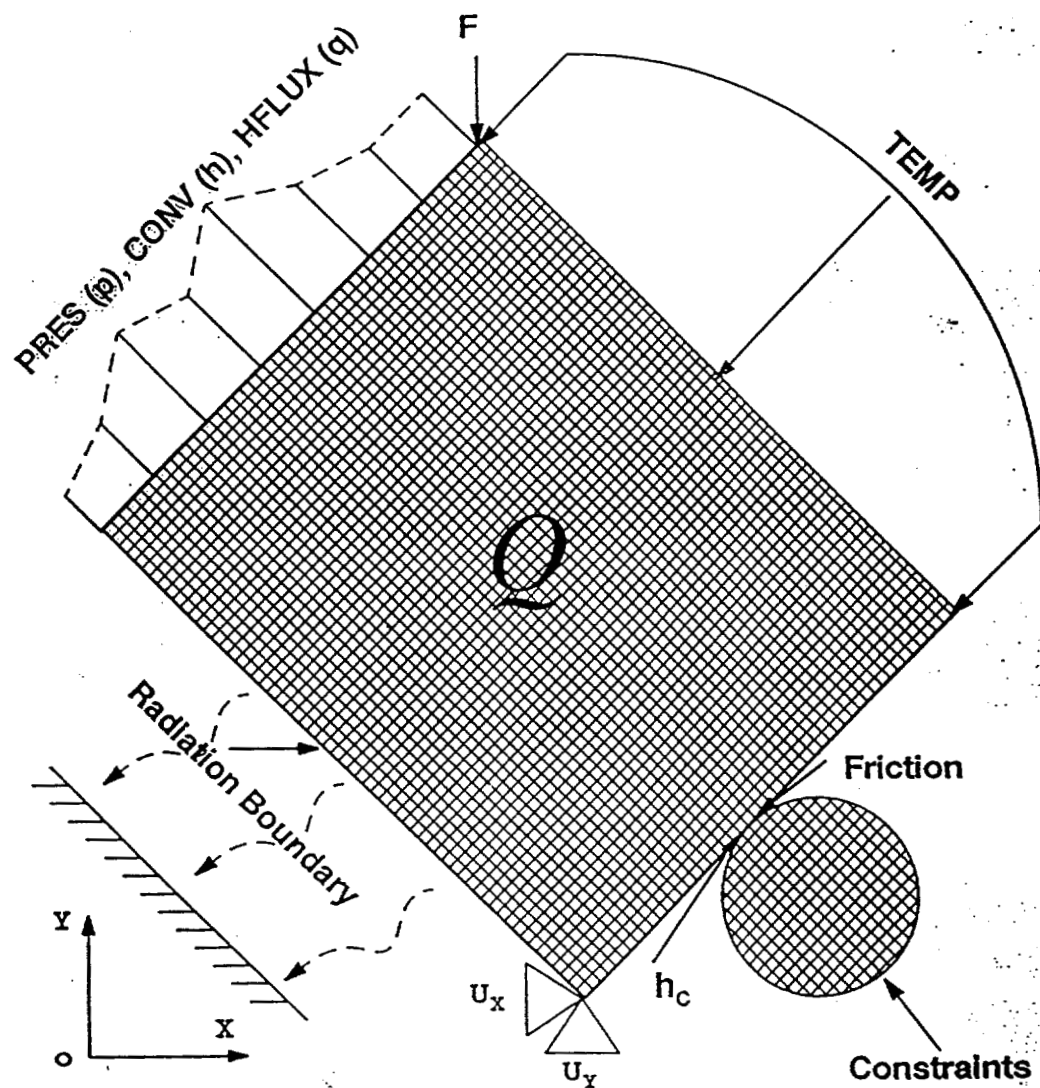


Fig.1-8 Numerical Model With Domain And Specified Boundaries

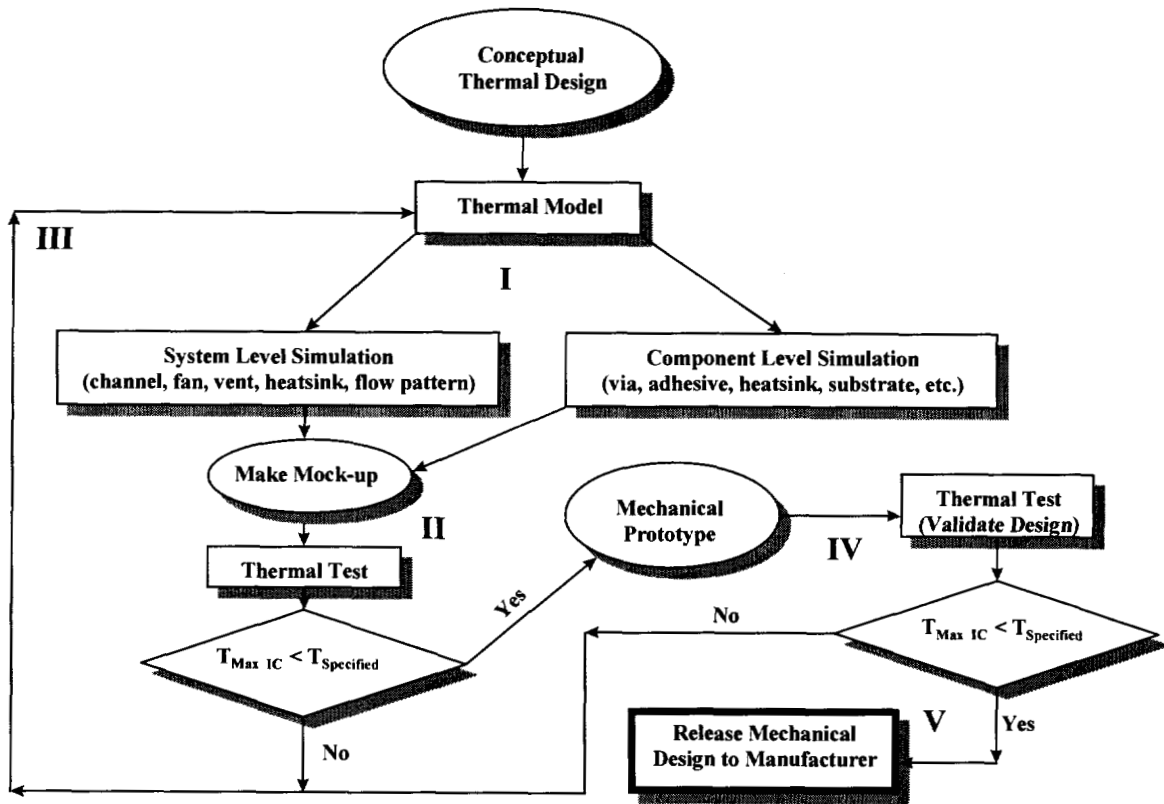


Fig.1-9 Thermal Design And Development Procedures

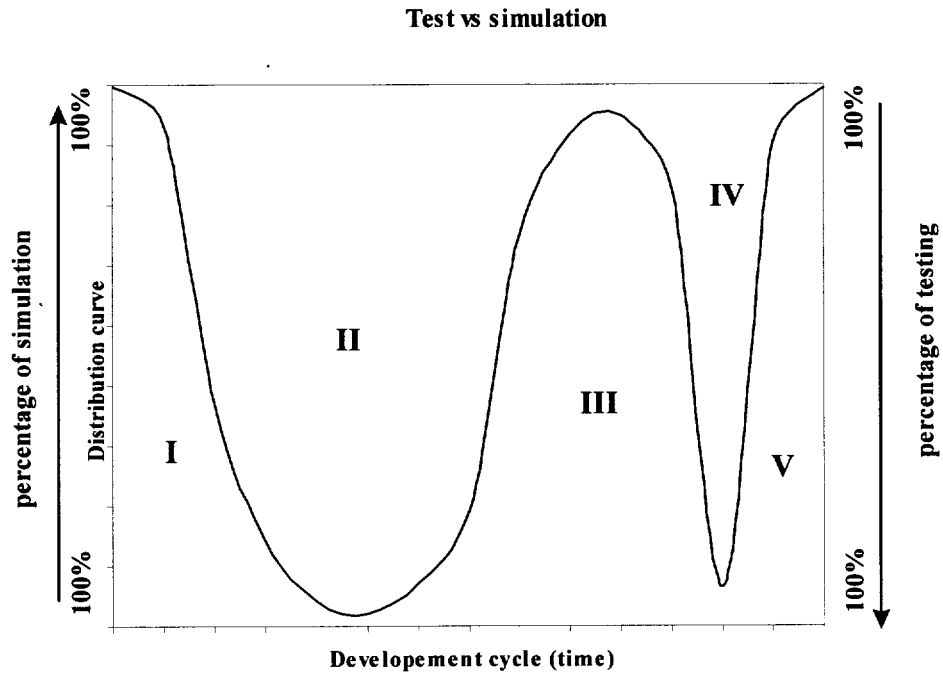


Fig.1-10 Simulation And Test Cycles For The Thermal Management

CHAPTER 2

THEORETICAL AND NUMERICAL SOLUTIONS FOR ELECTRONIC PACKAGING

Modern VLSI thermal design and operation, involves individual and a variety of different combinations of components including substrate, circuit board, adhesive layers, lid, heat sink, thermal vias of different size and materials. The most critical parameters for thermal design are associated with the number of thermal vias present in the substrate, thickness of the heat sink base, substrate, lid, the adhesive or solder material like epoxy layer between the substrate and dies. Other parameters include the cap and heat sink, the chip or module active area, the number of pins or fins and height of the heat sink, and their materials with different thermal conductivity.

It is difficult to achieve an optimal choice from numerous combinations of all parameters cited above through experiments. The example of thermal management for an MCM mounted on a ceramic board with and without Tungsten thermal vias is relevant here. Actually, the variables for this case are thermal vias, thickness of the board, material for the epoxy layer, and the chip temperature usually confined within a very small range. Any little change in these parameters may change the chip temperature. If we have two options for the number of vias, and two options for the vias material, two options for the thickness of board, and two options for the adhesive layer thickness and material, the total number of choice becomes 2^6 which amounts to 64 options. With the traditional method, we have to prepare for 64 mock-ups to validate for a package with only six variables. If we have to conduct tests for two different power dissipation rates under two different environments, the number of tests would be 256. It is not only time and money consuming, but also makes the actual problem solving process practically impossible. Numerical solutions provide an efficient way to derive the optimal design. A component

level model example detailing the steps to achieve an optimal design will be given in Chapter 3.

2.1 Conduction Heat Transfer

Conduction is the transfer of energy from the more energetic to the less energetic particles of a substance due to interaction between the particles via atomic and molecular vibration, translational or rotational motions without bulk motion⁽³⁸⁾. The thermal energy level is associated with temperature. The heat diffusion equation also known as heat equation for heat conduction in a three dimensional space is described by the second order partial differential in Cartesian coordinates as:

$$\rho c \frac{\partial T}{\partial t} = \frac{\partial}{\partial x} \left(k \frac{\partial T}{\partial x} \right) + \frac{\partial}{\partial y} \left(k \frac{\partial T}{\partial y} \right) + \frac{\partial}{\partial z} \left(k \frac{\partial T}{\partial z} \right) + \dot{Q} \quad (2-1)$$

where T is the temperature as a function of space and time, k is the thermal conductivity, ρ is the density, c is the specific heat capacity, and \dot{Q} is the rate of heat generated per unit volume of the medium.

If the thermal conductivity is a constant and isotropic, the heat diffusion equation can be simplified as:

$$\frac{1}{\alpha} \frac{\partial T}{\partial t} = \frac{\partial^2 T}{\partial x^2} + \frac{\partial^2 T}{\partial y^2} + \frac{\partial^2 T}{\partial z^2} + \frac{\dot{Q}}{k} \quad (2-2)$$

where α is the thermal diffusivity.

If the heat conduction occurs under steady-state conditions, there can be no change in the amount of energy storage, hence equation (2-1) can be reduced to:

$$\frac{\partial}{\partial x} \left(k \frac{\partial T}{\partial x} \right) + \frac{\partial}{\partial y} \left(k \frac{\partial T}{\partial y} \right) + \frac{\partial}{\partial z} \left(k \frac{\partial T}{\partial z} \right) + \dot{Q} = 0 \quad (2-3)$$

The heat equation in cylindrical coordinates is expressed as:

$$\rho c \frac{\partial T}{\partial t} = \frac{1}{r} \frac{\partial}{\partial r} \left(kr \frac{\partial T}{\partial r} \right) + \frac{1}{r^2} \frac{\partial}{\partial \Phi} \left(k \frac{\partial T}{\partial \Phi} \right) + \frac{\partial}{\partial z} \left(k \frac{\partial T}{\partial z} \right) + \dot{Q} \quad (2-4)$$

The heat equation in spherical coordinates:

$$\rho c \frac{\partial T}{\partial t} = \frac{1}{r^2} \frac{\partial}{\partial r} \left(kr^2 \frac{\partial T}{\partial r} \right) + \frac{1}{r^2 \sin^2 \theta} \frac{\partial}{\partial \Phi} \left(k \frac{\partial T}{\partial \Phi} \right) + \frac{1}{r^2 \sin \theta} \frac{\partial}{\partial \theta} \left(k \sin \theta \frac{\partial T}{\partial \theta} \right) + \dot{Q} \quad (2-5)$$

To predict temperatures of electronic packages and boards numerically, the conduction heat transfer equation has to be solved. Equation (2-1) is a typical and general quasi-harmonic equation for transient heat transfer within a domain of interest. The complete mathematical description for a particular heat conduction problem is composed of the general equation and the actual heat transfer conditions happening at the boundaries as boundary conditions, the boundary conditions being classified into two types as follows:

- 1) Dirichlet boundary condition, which requires that a temperature field, be specified.

This is also termed an “essential” or prescribed temperature boundary condition.

$$T = T_0 \quad (2-6)$$

- 2) Von Neumann Boundary condition which involves a thermal load resulting a temperature gradient being specified at the boundary. This is also termed the “natural” boundary condition, which is further broken down as:

- a) A perfectly insulated or isothermal boundary, for which

$$\frac{\partial T}{\partial n} = 0 \quad (2-7)$$

where n is the vector along normal direction of the interface.

- b) A flux boundary which involves a finite thermal gradient being prescribed due to the presence of a thermal flux q_0 on that boundary.

$$-k \frac{\partial T}{\partial n} = q_0 \quad (2-8)$$

- c) A convection boundary in which a thermal gradient is prescribed or results from the presence of heat transfer via convection.

$$-k \frac{\partial T}{\partial n} = h(T - T_\infty) \quad (2-9)$$

- d) A radiation boundary in which a thermal gradient is prescribed or results from the presence of heat transfer via film radiation.

$$-k \frac{\partial T}{\partial n} = \epsilon \sigma (T^4 - T_\infty^4) \quad (2-10)$$

where ϵ is emissivity, σ is Boltzmann constant.

The solution to equation (2-1) will be sought in accordance with boundary conditions for equations (2-2) to (2-10) as well as the initial thermal equilibrium condition given by:

$$T|_{t=0} = T_0 \quad (2-11)$$

In heat transfer analysis for transient problems, thermal diffusivity is a major thermal property of material expressed as:

$$\alpha = \frac{k}{\rho c} \quad (2-12)$$

Which is the ratio of the thermal conductivity to the heat energy storage capacity of a material. Generally, materials with large α respond quickly and take shorter times to reach the equilibrium state corresponding to their thermal environment under the thermal load. For steady-state problems, since all the variables are time independent, α is not taken into consideration.

The thermal conductivity is defined from Fourier's law as:

$$k = -\frac{q}{\frac{\partial T}{\partial n}} \quad (2-13)$$

where q is the heat flux across the surface of the conduction medium $\frac{\partial T}{\partial n}$ is the temperature gradient in a direction normal to the surface.

Thermal conductivity depends on the temperature and material characteristics. In general, the thermal conductivity of a solid is larger than that of a liquid and the thermal conductivity of a liquid is larger than that of a gas. The thermal conductivity level of a solid can be as much as four orders of magnitude as that of a gas⁽³⁸⁾. For solids, thermal conductivity has contributions due to effects of free electrons and atoms bound in lattice. The transport of thermal energy is therefore affected by the migration of free electrons and lattice vibrational waves so that the thermal conductivity k can be considered the sum of the electronic effect k_e and the lattice effect k_l ⁽³⁸⁾:

$$k = k_e + k_l \quad (2-14)$$

where k_e is inversely proportional to the electrical resistivity, ρ_e .

Metals typically have low ρ_e because they have a rather large number of free electrons that move about in the lattice structure and correspondingly have large k_e . For pure metals like silver, copper, tungsten, electrical resistivity is negligible, thus their k_e becomes dominant to k_l , and the overall thermal conductivity k is relatively large. For alloys, due to their larger ρ_e , the contribution of k_l can not be neglected and their thermal conductivity is lower than that of pure metals. For nonmetallic solids, since their electrical resistivity ρ_e is substantially larger, the k_e approaches zero. Thus, the k_l primarily determines the thermal conductivity k , which depends on the frequency of interactions between the atoms and the lattice. Crystalline materials which have better lattice regularity such as quartz, diamond and beryllium oxide, k_l can even exceed the values of k associated with good conductors like aluminum. But most nonmetallic materials like glass and ceramics are amorphous, and typically have relatively low k_l and k as well. Thermal conductivity k usually increases with temperature for gases, and stays nominally constant for most liquids, and decreases for good solid conductors.

For electronic packaging applications, the multi-layer circuit board, card, module, and chips all use dielectric materials⁽⁵³⁾ such as ceramic, fiber glass, plastics like epoxy⁽⁶³⁾, urethane or cyanate, metal oxide, and so on. The main disadvantage of these materials with low ρ_e , and low thermal conductivity is their less efficient heat conduction. This results in high temperature of individual modules, cards, and boards, which finally limits the reliability of electronic devices and products due to the higher power dissipation rate from the electronic components and lower heat transfer rate.

Among all the material properties for the electronics packaging, thermal conductivity for the circuit board varies from in-plane conduction and through plane conduction. The conduction at in-plane direction is determined by FR4 matrix material, the fraction of copper for signal layer, power and ground planes⁽¹⁾ (Fig 2-1). It is also a function of the circuit thickness. The in-plane conductivity k_p is much larger than through plane conductivity k_n , making it easier for heat to be transmitted along the board than through the thickness dimension of the board. Heat generated from hot integrated circuit components would tend to build up in the board making the board emulate a heat sink.

However, the enhanced in-plane conductivity from the copper and FR4 layers effectively acting as resistors in parallel conduct the heat away⁽¹⁾ (Fig.2-2):

$$k_p = \frac{1}{T} \sum_N t \cdot k_{av} \quad (2-15)$$

Where t is the thickness of each layer, T is total thickness of the board, N is the number of layers, and k_{av} is the area weighted average conductivity for each layer:

$$k_{av} = \alpha \cdot k_{Cu} + (1 - \alpha)k_{FR4} \quad (2-16)$$

Where, α is the percentage of copper in the layer, and if power or ground planes are embedded, α will become 100%. k_{Cu} and k_{FR4} are the thermal conductivity for copper and matrix respectively.

The equivalent through-plane conductivity may be considered as resistors in series (Fig.2-3):

$$k_n = \frac{T}{\sum_N t \cdot k_{av}} \quad (2-17)$$

Table 2-1 shows data for a typical 2S-2P-layer board⁽¹⁾, and the average board details as Table 2-2. Thermal conductivity for through-plane direction is only 3.5% of that in-plane direction.

2.2 Contact Heat Transfer

Heat transfer through contact interfaces can not be described adequately by equation (2-1) for the temperature distribution as a function of geometry due to the discontinuity of the geometry and the thermal conductivity. The heat flow and temperature are dependent upon thermal behavior at the interface and the material and geometric characteristics of the interface formed by the contacting solid bodies. Generally, when two solids are in perfect contact, the temperatures for the two bodies at the interface is identical, making this an ideal contact⁽⁸²⁾. Such a contact region usually results from smooth surfaces in intimate contact⁽³⁰⁾ (Fig.2-4), and there is no thermal resistance across the interface.

In engineering applications, real surfaces are not perfectly smooth, rather they appear as peaks and valleys with waviness and roughness. Therefore a measurable

temperature drop or difference at the contact plane or surface between the two materials exists⁽⁸²⁾ (Fig.2-5) (Fig.2-6) resulting from profile of the surfaces which are determined by surface preparation techniques. In this case, actual intimate contact occurs at just a few discrete locations. Typically intimate contact accounts for less than 5%⁽⁶⁸⁾ of the nominal contact area (Fig.2-7). For electronic ball-grid-array(BGA), the solder bump array existing between module and the wiring substrate is another type of contact interface⁽⁴²⁾(Fig.2-8).

For two big solid plates in contact (Fig 2-9) with heat flux happens only in the normal direction. The heat fluxes across the plates can be calculated using equation (2-18):

$$Q = k_A A_c \frac{T_1 - T_A}{t_A} = k_B A_c \frac{T_B - T_2}{t_B} \quad (2-18)$$

where k_A and k_B are the thermal conductivity for the two materials respectively, A_c is the area of the contact surface, T_1 and T_2 are the temperatures at the ends of the two bars. T_A and T_B are the temperatures at the contact ends of the two bars and t_A and t_B are the thickness of the two plates respectively.

The heat flux across the contact interface can be expressed by equation (2-19):

$$q = \frac{T_A - T_B}{R_c} \quad (2-19)$$

where R_c is called the thermal contact resistance.

R_c is defined as:

$$R_c = \frac{1}{h_c A} \quad (2-20)$$

where h_c is named the contact coefficient, then q can also be computed as equation (2):

$$q = \frac{T_1 - T_2}{\frac{t_A}{k_A A_c} + \frac{1}{h_c A_c} + \frac{t_B}{k_B A_c}} \quad (2-21)$$

Thus, the temperature difference $\Delta T_c = T_A - T_B$ at the interface is obtained by extrapolating the steady-state unidirectional temperature distribution from the regions away from the interface. The imperfect contact condition, which creates the thermal

resistance to heat flow in the contact region specifically, is characterized by several important aspects⁽⁶⁸⁾ as follows:

1. Intimate contact occurs only at discrete parts of the nominal interface.
2. The ratio of the real contact area to the nominal contact area is usually less than 5%.
3. The real contact pressure, which is associated with the yield strength of the contacting peaks, is much larger than the apparent pressure.
4. The gap between the non-intimate contact is usually occupied by a third substance.
5. The third substance in the gap can be air, other gases, liquid, grease, metals or a vacuum.
6. The interface is idealized as a line with the actual depth of the interfaces from 60×10^{-6} inches which is relatively smooth to about 1000×10^{-6} inches which is relatively rough.

Heat transfer across the interface involves the heat conduction through the intimate contact interfaces and the substance in the gap, and radiation across the gap in a vacuum. Two or three modes of heat transfer could occur simultaneously. Radiation heat transfer may be normally ignored when the $\Delta T_c < 1000^\circ \text{F}$ compared with the heat conduction through the contact interfaces and the substance in the gap.

Therefore, there are two major heat exchange processes across a real surface, and sometimes in combination as follows:

1. A solid to solid conduction at the contact spots or areas.
2. Conduction through the substance filled in the voids in the interface region (Fig.2-10).

The amount of heat transfer could therefore be expressed as:

$$q = q_s + q_g = \frac{T_A - T_B}{\frac{\delta_c}{k_A A_c} + \frac{\delta_c}{k_B A_c}} + k_g A_g \frac{T_A - T_B}{2\delta_c} = \frac{T_A - T_B}{\frac{1}{h_c A}} \quad (2-22)$$

Where q_s and q_g are heat conduction through the contact areas and entrapped substance respectively; k_g is the thermal conductivity of the entrapped substance. A_c and A_g are solid

contact area and the effective area of the voids; δ_c is the average depth of the roughness for the two contact surfaces:

$$\delta_c = \frac{\delta_A + \delta_B}{2} \quad (2-23)$$

δ_A and δ_B are average depth of the roughness for their surfaces. A is the total cross sectional area of the contact zone. The effective contact coefficient h_c is then computed as:

$$h_c = \frac{1}{2\delta_c} \left(\frac{A_c}{A} \frac{2k_A k_B}{k_A + k_B} + \frac{A_g}{A} k_g \right) \quad (2-24)$$

and the interfacial thermal resistance is:

$$R_c = \frac{1}{h_c A} = \frac{2\delta_c (k_A + k_B)}{2A_c k_A k_B + A_g k_g (k_A + k_B)} \quad (2-25)$$

The thermal resistance or the contact resistance R_c is the principal parameter that determined the characteristics of heat transfer across the interfaces within the contact region.

2.2.1 Thermal Contact Resistance

This section will emphasize on analysis for the influence factors to the Thermal contact resistance and contact coefficient, and the general procedure to calculate the contact coefficient numerically.

From equation (2-25) we may tentatively conclude that R_c is determined by the surface characteristics of the contact region such as A_c , A_g , A , δ_c which define the depth of roughness and the gap, the solid to solid contact area, effective gap surfaces, and by the thermal conductivity such as k_A , k_B , k_g , of the solids and the entrapped substances. These ultimately control heat flow across contact interfaces.

Generally, the thermal contact resistance decreases with the increase of the ambient gas pressure for it results in an increase in the density of the entrapped fluid especially gas which increases the effective thermal conductivity of the fluid in the gap. The thermal contact resistance may also be decreased with by increasing of the joint

pressure for this causes larger deformation of the discrete contact spots thus enlarging the contact area between the contacting solids.

Factors that influence the thermal conductivity and surface geometry of the materials which ultimately influence the thermal contact resistance are analyzed into three categories⁽⁶⁸⁾ namely; geometry related factors, thermal conductivity factors, and other factors. The relationships are also illustrated in Fig.2-11a to Fig.2-11l.

Geometry Related Factors

Generally, the apparent contact pressure P applied on the two solids is the chief parameter affecting R_c dominantly by changing the deformation at the contacting surface. For smooth surfaces (depth of the interface $<60 \times 10^{-6}$ inches) with spherical waviness,

$$R_c \propto \frac{1}{P^{-3}}$$

This implying that the physical interaction between the solids is primarily elastic.

When the contacting surface has larger roughness with relatively smaller waviness,

$$R_c \propto \frac{1}{P^{-1}}$$

This suggests that plastic deformation of the asperities is important. When the contacting surfaces are very smooth and a fluid such as air fills the gap:

$$R_c \propto P$$

R_c is also affected by the surface roughness; when roughness increases by a factor of 2, it may result in a four to five times increase in R_c . It is especially significant when P is small and the surface is relatively smooth, and it will contribute the least when P is larger. Most surfaces have essentially a Gaussian distribution⁽⁶⁸⁾ of asperity heights about some mean plane lying in the surface. The surface was prepared from milling, grinding, and lapping, which results in a large difference in asperity distribution over the mean plane.

Surface waviness plays an important role to R_c ; when the waviness is large, the R_c ; will increase. It has also been shown that when P is relatively small, a small amount

of surface roughness has a pronounced effect upon the waviness. Generally the presence of some roughness reduces the waviness influence.

The effect of material hardness is always positive to R_c . The correlation between the hardness and R_c is linear with large surface roughness and smaller waviness under larger P .

The effect of modulus of elasticity is also positive to R_c . It is apparent that for certain surface and load conditions for objects in contact, Young's modulus is mainly taken into account based on the classical elasticity theory to predict the important geometric parameters such as the Hertz parameters defining the contact regions, which in turn determine the value of R_c .

The effect of mean contact temperature has a negative effect on R_c ; when the temperature level increases, the thermal resistance decreases because of the decrease of the material properties such as the hardness and the elastic modulus which tend to decrease when temperature increases. In addition, when mean contact temperature exceeds 1000°F, radiation heat transfer across the gap becomes significant so that primarily the radiation resistance governs R_c . Therefore the thermal resistance will be decreased with the increase of the temperature level.

Thermal Conductivity Related Factors

In general, thermal conductivity contributes negatively to the thermal contact resistance; large thermal conductivity induces smaller thermal contact resistance. Any factors that tend to increase thermal conductivity will decrease the R_c . When the interstitial fluid pressure $P > 100 \text{ mm Hg}$ the effects of pressure become significant because the resulting gas interstitial fluid decreases R_c . The increased pressure arises results in an improvement in the thermal conductivity of the entrapped fluid, and this is effectively what decreases R_c .

Thermal conductivity of the interstitial fluid increases R_c linearly because the mean free path of the molecules is at the same level as the characteristic dimension of the void space. There is no convection in the fluid trapped in the gap between the two solid bodies, therefore the heat transfer is entirely by heat conduction through the fluid layer.

It has been shown that the solid material thermal conductivity also increases R_c although it may not be exactly linear because usually the mechanical properties of the solid bodies do not remain constant when thermal conductivity is changed. But altering any of the other parameters cannot change the thermal conductivity effect.

When the filler material is a solid materials placed between contacting solid bodies, the effects of filler material may either reduce or increase the thermal resistance. The variables depend on the filler thickness, filler thermal conductivity, and filler hardness or elasticity. It has been observed that increasing the filler material thickness within one thousandth of an inch range generally decreases R_c . As the thickness increases further, R_c goes through a minimum value and then begins to increase. Any further increase in filler material results in yet a higher R_c . The criteria which make the thickness of the filler material attain a minimum R_c depend on the surface geometry, the filler material properties, and pressure P as a load.

Other Related Factors

There are some parameters other than geometry and thermal conductivity could change the thermal contact resistance. For example, the relaxation time negatively contributes to the resistance R_c and usually takes place over a period of hours, days or even weeks. With increasing time, R_c decreases continuously and finally attains to a constant value.

Directional effect is another phenomenon that results in the change of thermal contact resistance. When two dissimilar solids A and B are in contact R_c may be different when the heat flows from A to B compared to flowing from B to A . It has been observed that there is a significant directional effect on R_c , between when heat flows from aluminum to stainless steel compared to heat flow from stainless steel to aluminum for aluminum-stainless steel contact. The magnitude of this difference depends upon the surface shape factors such as roughness, waviness, the material properties, P as a load, and the level of heat flux. The reason for this phenomenon is due to local thermal strains caused by the local temperature gradients which actually finally changed the surface

characteristics. The number and size of contacts will be influenced differently as the heat flows from A to B or from B to A .

In summary, loading conditions are the most dominant factors affecting thermal contact resistance. The interstitial fluid, filler material, the radiation effect, and the directional effects apply their influence to the thermal contact resistance through the gap, the surface geometry and the interaction of the solid bodies. The major factors, which determine the intimate contact areas between contiguous solids, are surface geometry such as roughness, waviness and surface irregularities, and surface interaction like plasticity, elasticity and hardness.

For the practical contact process, the contact interaction between the two solids is generally in the behavior of elasto-plastic deformation. It is impossible to perform purely elastic or purely plastic deformation of the microscopic asperities. The initial contact occurs only between the highest asperities in few percentage in number which bear the total applied load. After the first contacting asperities have been crushed, redistribution of the pressure to the other asperities occurs subsequently. The entire surface layer of the bodies finally supports the total applied load. It is possible that the microscopic surface deviations (waviness) can change during the loading. Also, there may be a permanent change in the characteristics of the roughness during the compression. Therefore important physical or mechanical properties like the modulus of elasticity and the hardness or yield pressure of the asperities in the determination of the real contact pressure. Other parameters that determine the actual area of contact spots include displacement or the relative approach of the surfaces as a result of the deformation of the surfaces under compression.

There are a variety of ways to find R_c experimentally and theoretically, but the classical Hertzian approach is an efficient way to it. R_c is determined by finding the contact stress and normal pressure at the contact interface and which is then applied by the semi-empirical formulas to calculate the h_c for the counterformal contact problem⁽⁶⁰⁾.

The contact problems are classified into two categories; counterformal and conformal. If the dimensions of the area of contact are small compared to the radii of curvature of the contacting surfaces near the contact region, the problems are classified as

involving counterformal contact. If the dimensions of the area of contact are relatively large with reference to the radii of curvature of the contacting surfaces near the contact region, the problems are conformal in nature. If the contacting surfaces can be approximated by quadratic functions in the contact region, the counterformal problem is defined as Hertzian. Numerous engineering problems involve Hertzian-type contact such as the plane to plane contact, cylinder to cylinder, cylinder to plane, sphere to plane or sphere *et al.* By solving the Hertz equations, contact stress distribution and the displacement can be computed hence characterizing the problem in reference.

Hertz was the first one to solve the arbitrary sphere to sphere point contact problem with the dimensions of the contact area and pressure distribution over the contact region in 1881. The calculation provided the basis to Belajev⁽¹⁰⁾ and Thomas and Hoersch⁽⁷⁴⁾ to calculate the displacement and stress field near the contact region and inside the contacting bodies.

In reference to two solid bodies with curved surfaces⁽⁸²⁾ shown in Fig.2-12, when a force F is applied to the bodies to press them together, the elastic compression changes the contact region from one point to a finite flat area. The area is tangent to the undeformed surfaces of the contact bodies and is perpendicular to the line of action of the force F . The curvature of a surface is presented at any location by the largest and smallest values of the radii of curvature ρ and ρ' . The two planes containing the ρ and ρ' are orthogonal. If the radius of curvature at the point of the surface is positive then the corresponding center of curvature lies on the same side of the solid body from the surface, otherwise, it is negative. The two solids are supposed to be elastic, isotropic, and homogeneous, and the contacting surfaces are smooth and free of frictional or adhesive forces. The four principal radii of the two surface curvature at the contact point are large compared to the dimension of the contact area, and plastic deformation is negligible. For the resultant elliptical contact area, the semi-major axis a and semi-minor axis b can be expressed as:⁽⁸²⁾

$$a = m \left(\frac{3}{4} \pi F \Delta \right)^{\frac{1}{3}} \quad (2-26)$$

$$b = n \left(\frac{3}{4} \pi F \Delta \right)^{\frac{1}{3}} \quad (2-27)$$

where

$$\Delta = \frac{1}{(A+B)} \left(\frac{1-v_1^2}{\pi E_1} + \frac{1-v_2^2}{\pi E_2} \right) \quad (2-28)$$

$$\alpha = \cos^{-1} \left(\frac{B-A}{A+B} \right) \quad (2-29)$$

$$A+B = \frac{1}{2} \left(\frac{1}{\rho_1} + \frac{1}{\rho_1'} + \frac{1}{\rho_2} + \frac{1}{\rho_2'} \right) \quad (2-30)$$

$$B-A = \frac{1}{2} \left[\left(\frac{1}{\rho_1} - \frac{1}{\rho_1'} \right)^2 + \left(\frac{1}{\rho_2} - \frac{1}{\rho_2'} \right)^2 + 2 \left(\frac{1}{\rho_1} - \frac{1}{\rho_1'} \right) \left(\frac{1}{\rho_2} - \frac{1}{\rho_2'} \right) \cos 2\phi \right]^{\frac{1}{2}} \quad (2-31)$$

where ϕ is the angle between the planes of maximum (or minimum) curvature of the two contacting bodies; F is the total normal load acting on the contact area; E_i are the Young's moduli; ν_i are Poisson's ratios; ρ_i are the local radii of curvature of the contacting solids; ϕ is defined as the angle between the principal planes which pass through the contacting solids; m and n are called the Hertz elastic parameters; A and B are geometric parameters; Δ is physical parameter; i refers to the two contact solids; and m, n can be determined from the Table 2-3. Thus, the pressure distribution over the contact area is semi-elliptical

$$p(x, y) = p_0 \sqrt{1 - \left(\frac{x^2}{a^2} \right) - \left(\frac{y^2}{b^2} \right)} \quad (2-32)$$

where

$$p_0 = \frac{3F}{2\pi ab} \quad (2-33)$$

is the maximum pressure at the center of the elliptic contact region.

This relationship is used to compute pressure distribution and displacement fields for contacts for a variety of contacts e.g. ball and arbitrary curved surface, ball and inner race, ball and out race, ball and plane, two balls, two circular cylinders. The representative radii of curvature need to be identified and substituted accordingly.

For contact between nominally flat and rough solids, between rough and wavy surfaces, methods for calculating a and b developed by Williamson and Greenwood^(28, 29) may be

applied. In these methods, a “plasticity index” $\left(\frac{E'}{H}\right)\left(\frac{\sigma}{\rho}\right)^{\frac{1}{2}}$ is introduced

where

$$\frac{1}{E'} = \frac{1 - \nu_1^2}{E_1} + \frac{1 - \nu_2^2}{E_2} \quad (2-34)$$

H is hardness of the softer solid; σ is the *RMS* roughness; ρ is radius of curvature of a typical asperity.

These relationships may also be applied to rectangular contact areas produced when two ideal circular cylinders are initially in line contact, or an ideal cylinder and a flat surface are in contact which produce special cases of elliptical contact areas^(82, 83, 84). Unfortunately, for contact problems with irregular geometry, contact configurations, sliding at the contact interface, or any other complicated contact problems, application of the Hertz method ceases to be valid. Castleberry⁽¹⁶⁾ and Seely⁽¹⁴⁾ realized this limitation, and they point out that using Hertz's formulas alone for the calculations involving machine components for which service stresses exceed design contact stresses and have been attributed to a number of failures. Consequently with this circumstance, many modifications and new methods based upon the Hertz method toward each concrete contact problem had been developed. For example, Castleberry⁽¹⁶⁾ suggested using Smith-Liu equations⁽⁵⁰⁾ to solve line contact problems.

During the 1960's and 1970's, a so-called a second generation of contact researchers emphasized on solving the contact problems theoretically by introducing new concepts and assumptions. Researchers such as Kalker⁽³⁹⁾ and Paul⁽⁵⁹⁾ are noteworthy. Kalker developed a computer package for the analysis of fatigue and wear mechanisms by solving rolling contact problems in wheel-rail interactions which were subsequently adopted for railroad applications internationally. Paul⁽⁵⁹⁾ developed a local ellipsoidal contact patch assumption and provided detailed and complex geometric-trigonometric analysis of patches and shapes to solve contact problems in a considerably more flexible way.

The efforts to model contact problems by the first two generations were only focused on contacting objects with simple or typical geometries which can be described with simple mathematical equations. In real contact problems with arbitrary geometry, the contact area is usually cumbersome to predict. As the objects are forced together the contact area changes continuously resulting in nonlinear boundary conditions. This phenomenon makes the contact problem difficult to solve and requires special solution methods.

The first successful effort to solve a two-dimensional model with a linear variation of slip between interacting surfaces was first proposed by Goodman *et al*⁽²⁷⁾ in 1968. around that time, a third generation of analysts emerged. Examples include Ghaboussi *et al*⁽²⁶⁾, Buragohain and Shah⁽¹⁵⁾, Zienkiewicz⁽⁸⁷⁾, Francavilla⁽²⁵⁾, Wilcox⁽⁷⁹⁾ and Oden⁽⁵⁵⁾ began to introduce the new numerical analysis methods, notably the finite element method to deal with contact problems. Buragohain and Shah⁽¹⁵⁾ developed a more advanced interface element with a wider range of property values. Zienkiewicz⁽⁸⁶⁾ studied curved isoparametric line and axisymmetric elements for the analysis of physical problems with straight or curved contacting surfaces using 2-D models. Oden⁽⁵⁵⁾ computed flexibility matrices for the nodes of two contacting elastic bodies using a form of substructuring and reduced the severity of the nonlinearity of the problems and the computation time as well. He also gave a detailed description of the finite element approach to a class of contact problems generally referred to as Signorini's problem, and addressed the common problem in contact analysis. Significant improvement of the numerical conditioning of contact problems was made by Wilson and Parsons⁽⁸⁰⁾, using differential displacements across the contact interfaces rather than the use of absolute nodal displacements proposed earlier by Burragohain and Shah, Ghaboussi *et al*. Bathe⁽⁹⁾, Noor *et al*⁽⁵⁴⁾. For the dynamic analysis like impact problems finite element analysis, Benson and Hallquist^(11a) proposed a method of combining structural dynamics with rigid body dynamics. For some problems, the trade-off between the accuracy and the saving in the computation costs by using this method on a portion of the problem and deformable body dynamics in another portion is quite satisfactory. Hughes⁽³⁵⁾ also studied contact-impact problems by including inertia and damping terms to the equation of equilibrium

along with a number of integration parameters associated with the central difference method.

In the present study, definition of thermal contact resistance R_c is based on the Boussinesq point load model and the Hertz distributed load mode. R_c is then used to solve for Hertz parameters for circular, elliptic, rectangular, band, contact areas with the assumption of the smooth contact surfaces, perfectly elastic contact bodies, and much smaller the contact area dimensions compared to the dimensions of the bodies. The applied load is static and normal to the plane of the contact area in elliptical shape having semi-major axes a, b shown⁽⁶⁰⁾ on Fig.2-13 respectively. Circular contact area occurs in two special cases involving two spheres or a sphere and a flat are in contact. Several regular shapes such as circular, elliptic, rectangular, band are reliable to analytical solutions and these shapes can be used to model real problems with the specific correlation for solving for R_c . The correlations are usually semi-empirical formulas, which are based on the work of Yovanovich⁽⁸²⁾. The thermal resistance model is based on the assumption that both contacting bodies can be modeled as half spaces.

The correlation of Clausing and Chao⁽¹⁸⁾ is based on the model with the conditions of smooth, wavy surfaces in vacuum. Tien⁽⁷⁵⁾ developed a contact conductance correlation for modeling nominally flat, rough surfaces in vacuum. Barkan and Tuohy⁽⁸⁾ obtained a correlation for rough, wavy surfaces in vacuum. Yovanovich⁽⁸²⁾ proposed a correlation for turned surfaces in vacuum. Shlykov⁽⁶⁹⁾ developed a semi-empirical correlation expression for effect of interstitial fluids.

The present study with the finite element analytical methods for solving thermal contact resistance is based on the work of Meekisho⁽⁵⁰⁾ who developed a contact stress algorithm based on the penalty method. The method is able to sufficiently handle arbitrary shaped contacting bodies. He applied an implicit dynamic algorithm and interfaced with the contact algorithm to analyze dynamic- contact problems such as those found in production processes like rolling⁽⁵⁰⁾ (Fig.2-14). The transient contact thermal analysis is modeled as heat transfer process and limited to conduction for the heat transfer across contacts and small gaps. A fully coupled contact thermal-stress analysis was done and used to model the peening of welds⁽⁵⁰⁾.

Based on the theory of Yovanovich⁽⁸²⁾ and its subsequent implementation in a finite element study of contact problems⁽⁵⁰⁾ Meekisho computed the normal stress distribution for a long cylinder on a semi-infinite flat plate using finite element method with the closed form solution from Hertz's equations, and he applied the pressure distribution to the contact coefficient correlation which he provided to compute the contact coefficient:

$$h_c = 1.25 \left(\frac{P}{H} \right)^{0.95} \quad (2-35)$$

where P is normal interface pressure and H is the microhardness of the softer material at the interface. This result was validated experimentally by the work of Hegazy⁽³²⁾.

2.3 Finite Element Analysis

The finite element method (FEM) is a numerical analysis technique for obtaining approximate solutions to a large range of engineering problems. Usually we encounter the need to obtain the approximate solutions for the modern engineering problems such as computing the load capacity of a train wheel with several stiffeners and odd-shaped holes. Other examples include, computing the concentration of chemical vapor deposited on the surfaces of the semiconductor device at different wall temperatures and the heat transfer coefficients at the surface. The electronic component modules caused by forced cooling air through a channel with arbitrary shape at the interior surface represents another practical application. In all cases we have to write down the mathematical descriptions including governing or fundamental equations and boundary conditions associated with the corresponding physical significance for these problems. It is found it is relatively easy to write down the mathematical descriptions, but it is difficult or sometime impossible to obtain the analytical solutions from the multi-dimensional partial different equations for the multi-variables and irregular boundaries.

To solve these engineering dilemmas, there are several options. One choice is to make simplifying assumptions to reduce the number of dimensions, the number of the variables, the order of the derivative equations, and even the physical configurations to avoid the difficulties so that to handle the problems. This procedure does not always

work; it leads to serious bias and even wrong solutions. With the advent of powerful computers, a more challenging and effective alternative, numerical analysis, has become widely available without losing important relevant values, which are always sacrificed by the simplified assumptions.

There have been several approximate numerical analysis methods developed or still under development. They are finite element method (FEM), finite difference method (FDM), finite volume method (FVM) and boundary element method (BEM). All of these methods are based on the same concept, i.e., to discretize the partial differential equations into a linear algorithm matrix which are solvable and iterated efficiently by modern computers. But the different methods have their own schemes for approaching the governing equations approximately and have corresponding weaknesses and strengths. For example, the finite difference method gives a pointwise approximation to the fundamental equations by transforming the equations into a group equations referred to an arrays of grid points. Generally the more the grid points the better the computed solution. This method is most effective for regular rectangular domains and rather weak with irregular or arbitrary domains.

Compared with finite difference method, finite element method has emerged from many numerical analysis methods due to its unique feature for handling arbitrary domains with its higher order approximation functions. The FEM discretizes the domain of interest into an assemblage of sub-regions or elements interconnected at the nodes and seeks a piecewise approximation to the governing equations. The domain can be discretized into elements of different shape and size. The FEM thus has superior capabilities to model effectively problems with complex geometries. The FEM was first introduced to solve plane elasticity problems by Clough⁽³⁴⁾ in 1960, and evolved into applications for solving complex aerospace structure problems for the stiffness coefficients of shell-type structures reinforced by ribs and spars⁽³⁴⁾. The method is nowadays widely applied to solve continuum problems for both solids and fluids of any dimension in both steady state equilibrium problems and time dependent problems. It is now routinely used to compute the displacements and stresses at any point of the solid body under mechanical and thermal loading in structural problems, and pressure, velocity profiles and temperature,

density, heat transfer coefficient distributions for thermal-fluid in the space and time domains.

An example⁽³⁸⁾ (Fig.2-15) to use finite element analysis formulation to solve one dimensional conduction heat transfer problem with the conduction equation (2-1) in accordance with the initial and boundary conditions given in equations (2-6)~(2-11). Assuming there is no internal heat source or heat generation, so that \dot{Q} is zero, both side of the wall are fixed to uniform temperature T_1 and T_2 respectively, and each layer of material, the left side temperature T_1 is greater than the right side temperature T_2 and each layer is a homogeneous solid of thermal conductivity in the direction of heat flow, while the heat flux, temperature, thermal conductivity, and the layer thickness are the pertinent parameters. In this approach, the domain is a section of layered material with different thickness along x direction, and infinitely long along y direction. The heat will flow through the material along the x -direction only because of its infinite length along the y -direction. This also presents an effective way to simplify or lower the dimension of the domain so as to lower the order of the governing equations, hence ultimately ease the solution method and associated cost.

If we discretize this wall (Fig.2-15) into a number of elements, and each layer of material presents one finite element with the nodes at the crossing points between the boundary and the heat flux line at both sides of each layer, then heat transfer in each element is governed by the heat equation given in equation (2-1).

At each node, we can apply Fourier's law to relate the heat crossing a unit area per unit time in the x direction is then given as

$$Q_i = -k_i A \frac{dT}{dx} \quad (2-36)$$

For constant thermal conductivity, it can also be written as

$$Q_i = k_i A \frac{\Delta T}{L_i} \quad (2-37)$$

where ΔT is the temperature drop across the layer, and L_i is one layer thickness.

Thus for element i , the heat flux into the wall on the left hand side Q_i is written in terms of the element nodal temperature as:

$$Q_i = \frac{k_i A}{L_i} (T_i - T_{i+1}) \quad (2-38)$$

which is balanced to the heat flux out of the layer Q_{out} as

$$Q_i = -Q_{i+1} \quad (2-39)$$

or

$$Q_{i+1} = -\frac{k_i A}{L_i} (T_i - T_{i+1}) \quad (2-40)$$

In matrix notation the equation is expressed as

$$\frac{k_i A}{L_i} \begin{bmatrix} 1 & -1 \\ -1 & 1 \end{bmatrix} \begin{Bmatrix} T_i \\ T_{i+1} \end{Bmatrix} = \begin{Bmatrix} Q_i \\ Q_{i+1} \end{Bmatrix} \quad (2-41)$$

or

$$[K]^e \{T\}^e = \{Q\}^e \quad (2-42)$$

where

$$[K]^e = \frac{k_i A}{L_i} \begin{bmatrix} 1 & -1 \\ -1 & 1 \end{bmatrix} \quad (2-43)$$

is the matrix of thermal conductance coefficients for the i th element, also called “stiffness” matrix obeying the Maxwell-Betti reciprocal theorem, which states that all stiffness matrices for linear structures referred to orthogonal coordinate systems must be symmetric(54). Equation (2-42) represents the so called element equations, where

$\{T\}^e = \begin{Bmatrix} T_i \\ T_{i+1} \end{Bmatrix}$ is the column vector of the nodal temperatures, and $\{Q\}^e = \begin{Bmatrix} Q_i \\ Q_{i+1} \end{Bmatrix}$ is the

column vector of nodal heat flux. The components of $[K]^e$ are composed of the element k_{ij} at their positions in the i th row and j th column in the stiffness matrix. In this example, the values in the matrix are determined exactly by the Fourier’s law, but for the more complicated situations the stiffness matrix coefficients can only be determined by approximate temperature functions. The interpretation of the k_{ij} in a typical stiffness matrix is that the load required, which is heat flux for this simple example, at node i is to produce a variable change, which is the temperature for this case, at node j . Note that the

stiffness matrix equation(2-43) is defined in the local coordinate system, (x_L, y_L) . If we want to solve the problem for the whole wall, we have to assemble the element characteristics in the local coordinate into the global system. The steps are as follows:

At node 1:

$$Q_1 = \frac{k_1 A}{L_1} (T_1 - T_2) \quad (2-44)$$

$$Q_2 = -\frac{k_1 A}{L_1} (T_1 - T_2) \quad (2-45)$$

At node 2:

$$Q_2 = \frac{k_2 A}{L_2} (T_2 - T_3) \quad (2-46)$$

$$Q_3 = -\frac{k_2 A}{L_2} (T_2 - T_3) \quad (2-47)$$

At node 3:

$$Q_3 = \frac{k_3 A}{L_3} (T_3 - T_4) \quad (2-48)$$

$$Q_4 = -\frac{k_3 A}{L_3} (T_3 - T_4) \quad (2-49)$$

At node 4:

$$Q_4 = \frac{k_4 A}{L_4} (T_4 - T_5) \quad (2-50)$$

$$Q_5 = -\frac{k_4 A}{L_4} (T_4 - T_5) \quad (2-51)$$

At node 5:

$$Q_5 = \frac{k_5 A}{L_5} (T_5 - T_6) \quad (2-52)$$

$$Q_6 = -\frac{k_5 A}{L_5} (T_5 - T_6) \quad (2-53)$$

It is then can be expressed as:

$$\left\{ \begin{array}{l} \frac{k_1 A}{L_1} T_1 - \frac{k_1 A}{L_1} T_2 \\ \frac{k_1 A}{L_1} T_1 - \left(\frac{k_1 A}{L_1} - \frac{k_2 A}{L_2} \right) T_2 - \frac{k_2 A}{L_2} T_3 \\ \frac{k_2 A}{L_2} T_2 - \left(\frac{k_2 A}{L_2} - \frac{k_3 A}{L_3} \right) T_3 - \frac{k_3 A}{L_3} T_4 \\ \frac{k_3 A}{L_3} T_3 - \left(\frac{k_3 A}{L_3} - \frac{k_4 A}{L_4} \right) T_4 - \frac{k_4 A}{L_4} T_5 \\ \frac{k_4 A}{L_4} T_4 - \frac{k_4 A}{L_4} T_5 \end{array} \right. = \begin{array}{l} Q_1 \\ 0 \\ 0 \\ 0 \\ -Q_5 \end{array} \quad (2-54)$$

Using matrix notation, the system equations can be written as

$$\begin{bmatrix} \frac{k_1 A}{L_1} & -\frac{k_1 A}{L_1} & 0 & 0 & 0 \\ \frac{k_1 A}{L_1} & -\left(\frac{k_1 A}{L_1} - \frac{k_2 A}{L_2} \right) & -\frac{k_2 A}{L_2} & 0 & 0 \\ 0 & \frac{k_2 A}{L_2} & -\left(\frac{k_2 A}{L_2} - \frac{k_3 A}{L_3} \right) & -\frac{k_3 A}{L_3} & 0 \\ 0 & 0 & \frac{k_3 A}{L_3} & -\left(\frac{k_3 A}{L_3} - \frac{k_4 A}{L_4} \right) & -\frac{k_4 A}{L_4} \\ 0 & 0 & 0 & \frac{k_4 A}{L_4} & -\frac{k_4 A}{L_4} \end{bmatrix} \begin{Bmatrix} T_1 \\ T_2 \\ T_3 \\ T_4 \\ T_5 \end{Bmatrix} = \begin{Bmatrix} Q_1 \\ 0 \\ 0 \\ 0 \\ -Q_5 \end{Bmatrix} \quad (2-55)$$

or

$$[K]\{T\} = \{Q\} \quad (2-56)$$

If we expand the dimension of $[K]^e$ for one element from 2×2 to the whole square matrix of dimensions 5×5 , the matrix has become $[\bar{K}]^e$:

for element 1:

$$[\bar{K}]^{(1)} = \begin{bmatrix} k_{11}^{(1)} & k_{12}^{(1)} & 0 & 0 & 0 \\ k_{21}^{(1)} & k_{22}^{(1)} & 0 & 0 & 0 \\ 0 & 0 & 0 & 0 & 0 \\ 0 & 0 & 0 & 0 & 0 \\ 0 & 0 & 0 & 0 & 0 \end{bmatrix} \quad (2-57)$$

for element 2:

$$[\bar{K}]^{(2)} = \begin{bmatrix} 0 & 0 & 0 & 0 & 0 \\ 0 & k_{22}^{(2)} & k_{23}^{(2)} & 0 & 0 \\ 0 & k_{32}^{(2)} & k_{33}^{(2)} & 0 & 0 \\ 0 & 0 & 0 & 0 & 0 \\ 0 & 0 & 0 & 0 & 0 \end{bmatrix} \quad (2-58)$$

for element 3:

$$[\bar{K}]^{(3)} = \begin{bmatrix} 0 & 0 & 0 & 0 & 0 \\ 0 & 0 & 0 & 0 & 0 \\ 0 & 0 & k_{33}^{(3)} & k_{34}^{(3)} & 0 \\ 0 & 0 & k_{43}^{(3)} & k_{44}^{(3)} & 0 \\ 0 & 0 & 0 & 0 & 0 \end{bmatrix} \quad (2-59)$$

for element 4:

$$[\bar{K}]^{(4)} = \begin{bmatrix} 0 & 0 & 0 & 0 & 0 \\ 0 & 0 & 0 & 0 & 0 \\ 0 & 0 & 0 & 0 & 0 \\ 0 & 0 & 0 & k_{44}^{(4)} & k_{45}^{(4)} \\ 0 & 0 & 0 & k_{54}^{(4)} & k_{55}^{(4)} \end{bmatrix} \quad (2-60)$$

where

$$k_{ii}^i = \frac{k_i A}{L_i} \quad (2-61)$$

$$k_{ii+1}^i = k_{i+1i}^i = -\frac{k_i A}{L_i} \quad (2-62)$$

So this results in the global stiffness matrix $[K]$ as

$$[K] = \sum_{e=1}^4 [\bar{K}]^{(e)} \quad (2-67)$$

and the same expansion and summation principle can also apply to determine the column vectors of the external nodal constraints or driven force like heat flux across the boundary as:

$$\{Q\} = \sum_{e=1}^4 \{\bar{Q}\}^{(e)} \quad (2-68)$$

and the variable column vectors $\{T\}$ can finally solved through the matrix equation (2-56).

Although this example is for one dimensional conduction heat transfer, the procedures and the principles are the same all problems, and the complete system equations can be written as:

$$[K] \{X\} = \{R\} \quad (2-69)$$

where n is the number of system nodal variables or the degree of freedom of the system.

The stiffness matrix is

$$[K] = \sum_{e=1}^m [K]^{(e)} \quad (2-70)$$

where m is the number of elements.

In the whole domain, when

$$\begin{cases} \frac{\partial [K]}{\partial \{X\}} = 0 \\ \frac{\partial [K]}{\partial \{R\}} = 0 \end{cases} \quad (2-71)$$

we say that the problem is linear, otherwise, it is nonlinear due to the variable being dependent on material properties and variable boundary conditions.

No matter how many elements are involved with many variables, if we can find the column vectors of resultant external nodal actions from the elements, and we can write the stiffness matrix, we can finally obtain the values for the variable vectors in the unknown vector column with the aid of computers.

In general, not all of the element equations may be developed from the physical principles like the principle of minimum potential energy for structure mechanics, heat energy conservation law for conduction problems. In reality for most problems the element equations can not be written directly if they are nonlinear, have two or more dimensions or transient in nature, the only way to interpret the element equations is through a mathematical approximation approach. Among mathematical approximations, the variational approach is the basic concept for most finite element methods to derive the finite element equations. The classical variational method is the method of weighted-residual (MWR) which can handle a global approximate solutions to linear and nonlinear partial differential equations. If we replace the variables with the approximate functions as the solutions into the differential equations to satisfy the boundary conditions, an error

between the exact solutions and the approximate results, and this error is referred to as a residual. The MWR techniques aims to minimize this residual close to zero in an average sense over the entire solution domain.

Assuming we want to obtain the approximate solution for a variable c governed by a partial differential equation:

$$F(c) - f = 0 \quad (2-72)$$

in the domain of Ω bounded by the surface Γ ; f is a known function of the independent variables. The first step of MWR is build an approximated function \hat{c} to replace the exact solution c in the equation in the form of

$$c \approx \hat{c} = \sum_{i=1}^n \varphi_i c_i \quad (2-73)$$

where c_i is the value of one of the variables; φ_i is the assumed function or shape functions; n is number variables of c_i .

When substitute \hat{c} into equation (2-72), the equation becomes

$$F(\hat{c}) - f = R \neq 0 \quad (2-74)$$

where R is the residual or error that results from approximating \hat{c} by c .

To minimize the R over the entire domain, we can select n linearly independent weighting functions w_i and let

$$\int_{\Omega} [F(\hat{c}) - f] w_i d\Omega = \int_{\Omega} R w_i d\Omega = 0 \quad i= 1, 2, \dots, n \quad (2-75)$$

so that $R \approx 0$ in an average sense.

The methods for determining the weighted functions have resulted in a variety of weighted techniques based on the error distribution principles. If we choose the weighted functions to be the same as the assumed or shape function for the approximate function as $w_i = \varphi_i$, it is called *Galerkin* method, if the $w_i = \partial R / \partial c_i$, it is referred to as the *least-squares* method, and *collocation* methods if $w_i = \delta(x - x_i)$, where the symbol $\delta(\)$ is the Dirac delta function, *et al.* Equation (2-75) is for the entire domain of continuum. Since it holds for any point of the domain, it also holds for all the arbitrary sub-domain or element of the whole domain, and the element equations can be written in the form:

$$c^e \approx \hat{c}^e = \sum_{i=1}^m \varphi_i^e c_i^e \quad (2-76)$$

$$\iint_{\Omega} [F(\hat{c}^e) - f^e] w_i^e d\Omega = 0 \quad i=1, 2, \dots, m \quad (2-77)$$

where c_i^e is the value of one of the variables at node i of a elements; φ_i^e is the assumed function or shape functions for an element; m is the number of nodes on one element; f^e is the driving force function defined over the element. The shape functions φ_i^e usually are the polynomial functions, and the order of the polynomials depends on the configuration of the elements. The polynomial shape functions for the element without midside nodes are usually linear, otherwise they are in second or third order. The element can be divided into two categories as linear elements without midside nodes in the shapes of triangular, tetrahedral, rectangular and hexahedral shapes, and higher order elements as such quadratic elements. The most cost-effective elements ⁽⁶²⁾ for FEA computation, the most frequently used elements are as follows:

- 1) linear triangular elements with 3 nodes in terms of the area coordinates,
- 2) linear tetrahedral elements with 4 nodes,
- 3) linear rectangular elements with 4 nodes and the shape functions are the Lagrange interpolation functions from the tensor product of corresponding one dimensional Lagrange interpolation functions in terms of the normalized coordinates(ξ, η),
- 4) linear hexahedral(brick) elements with 8 nodes in terms of the normalized coordinates.

For quadratic elements, the shape functions are as follows:

- 1) quadratic triangular elements with 6 nodes in terms of the area coordinates,
- 2) quadratic tetrahedral elements with 10 nodes,
- 3) quadratic rectangular Lagrange elements with one interior node, the shape functions are the Lagrange interpolation functions from the tensor product of corresponding one dimensional Lagrange interpolation functions in terms of the normalized coordinates,
- 4) quadratic rectangular serendipity elements without interior nodes,

- 5) quadratic hexahedral (brick) serendipity elements with 20 nodes without interior nodes in terms of the normalized coordinates.

The geometric mapping transformations between the local (ξ, η, ζ) and global coordinates (x, y, z) are based on above shape functions as⁽⁶²⁾(Fig 2-16):

$$x = \sum_{i=1}^n x_i^e \varphi_i^e(\xi, \eta, \zeta) \quad (2-78)$$

$$y = \sum_{i=1}^n y_i^e \varphi_i^e(\xi, \eta, \zeta) \quad (2-79)$$

$$z = \sum_{i=1}^n z_i^e \varphi_i^e(\xi, \eta, \zeta) \quad (2-80)$$

where $n = 3, z = 0 = \zeta$ for 2-D linear triangular elements with 3 nodes,
 $n = 4, z \neq 0 \neq \zeta$ for 3-D linear tetrahedral elements with 4 nodes,
 $n = 4, z = 0 = \zeta$ for 2-D linear rectangular elements with 4 nodes,
 $n = 6, z = 0 = \zeta$ for 2-D quadratic triangular elements with 6 nodes,
 $n = 8, z \neq 0 \neq \zeta$ for 3-D linear hexahedral(brick) serendipity elements with 8 nodes,
 $n = 8, z = 0 = \zeta$ for 2-D quadratic rectangular serendipity elements with 8 nodes,
 $n = 9, z = 0 = \zeta$ for 2-D quadratic rectangular Lagrange elements with 9 nodes,
 $n = 10, z \neq 0 \neq \zeta$ for 3-D quadratic tetrahedral elements with 10 nodes,
 $n = 20, z \neq 0 \neq \zeta$ for 3-D quadratic serendipity elements with 20 nodes.

All the approximation functions in terms of the values of the field variables at the element nodes lying on the element boundaries, where adjacent elements are connected with the constraints on the domain boundaries. With these piecewise local approximation functions, which are to the governing equations for each individual element, the solution can be modeled analytically or approximated⁽³⁴⁾ by assembling discrete elements.

In summary, the general process for solving the practical problems by the finite element method are:

Domain Selection

The first step is to select the numerical model with appropriate geometry and boundaries, and to make right assumptions and pertinent simplifications. Practical

problems sometimes provide overlap of relevant conditions like both temperature and heat flux which are over and above the requirement for the FEM model, sometimes there is lack of sufficient conditions for the FEM model, for instance, the interflow without constraints for the flow at the outlet.

For these circumstances, appropriate boundary conditions must be specified for the over constrained problems into exclusively condition like either temperature or heat flux at the one boundary, and assumed a reasonable constraint like zero relative pressure at the outlet for interflow. For the problems with either symmetric boundary or geometry, the domain may be simplified into corresponding half or a quarter symmetries of the original domain, and even to simplify a 3-D domain into 2-D domain if the variables being investigated have negligible variance along one direction. In 3D, if a variable is principally unchanged in one direction we may introduce cylindrical or spherical 2-D geometry with symmetric boundary specifications. These measures not only make numerical solutions to the problems feasible, but also lowers the cost of calculation and shortens the computation time.

Assumptions

Making reasonable assumptions to transform the practical phenomena into the typical numerical models governed by the fundamental equations and assumptions is very important in modeling. Most practical problems are not trivial. To obtain a solution that meets minimum requirements of the problems, reasonable simplifying assumptions are necessary. It can otherwise be impossible to build the ideal model with corresponding governing equations and boundary conditions to the problems.

For example, numerical models involving isotropic material properties which are independent of geometry, or constant material properties which are time, temperature or pressure invariant, are applied to approximate practical problems that in reality do not satisfy these conditions. Justification for applying simplifying assumption is that if in some operating ranges the factors like temperature and pressure only change the material properties in levels that are within acceptable error norms, the problems can be assumed to be steady. In CFD modeling, single phase and Newtonian fluid assumption is used for a multi-phase problem if one phase is dominant and the temperature and pressure changes

do not alter the original state of the phases, and there are no significantly steep gradient regions using the material properties of the dominant phase or manipulate weighted averaged material properties between the two material with different phases. For non-Newtonian fluid problems, if the Reynolds number is not high so that the relationship between the velocity gradients and the shear stress is linear in a certain range, the fluid may be assumed to be Newtonian in that range, the problems are then solvable with normal CFD modeling.

To simplify the problems without significantly impacting the solution, it is acceptable to confine the conditions of the problems in a narrow range using average material properties on geometry, temperature, time, and other dependent defining parameters, or by dividing the domain into multiple continuum domains where the material properties have less difference in each individual domain so as to satisfy the constant material property requirement.

Mesh Generation

This step involves subdividing the numerical region or domain into a finite number of elements with certain shapes. The meshed domain should adequately represent the geometry of the physical problem domain and boundary accurately, that is, all the elements from the mesh should fill the physical geometry and match its boundary. The mesh should be sufficiently refined to be able to capture large gradients in the solution (temperature and pressure), however, mesh grading should be such that large aspect ratio variation in elements is avoided. Within the domain the elements could be in triangular and rectangular shapes for two dimensional problems, and tetrahedral and brick shapes for three dimensional problems. The order of the elements could be linear, quadratic or higher as needed. The choice of the element type and mesh is problem dependent. Generally, the higher order of the elements, the more nodes per element, the higher order of the shape functions, the more approximated modeling results, and the more computational intensive as well. The more elements, the finer mesh, the more location or the points have been captured even with the linear elements, the more precise solutions and higher CPU cost. But this does not necessarily imply that the higher order elements and more elements are recommended to get the successful solutions.

In fact, the mesh could be coarse with few elements at the small variable gradient regions and refined with more lower order elements at the steep variable gradient areas, and the mesh could also use the combination of different order elements. Mesh generation using the single element type or same element is easy, because the degrees of the elements are the same and compatible with each other; but it becomes difficult and often not feasible when using a combination of elements with different types or orders, for example like linear and quadratic elements which have different number of nodes on common sides of the element is most difficult. Usually there are two ways to accomplish the refinement of the combined mesh. One way is to use transition elements with different numbers of nodes on different sides of the elements to match the numbers of nodes at the same sides of the neighbor elements. The other way is to force the constraints to the extra nodes of the higher order as the same value as that at the node of the neighbor elements⁽⁶²⁾.

There are some other special mesh requirement for computational fluid dynamics modeling when the turbulence flows occur to generate the mesh by the so called “structured mesh”. Especially when the $k-\varepsilon$ model is applied to simulated the turbulent flows. The purpose of structured meshes for the CFD modeling is to provide more consistent representation at the wall to capture the sublayer and the large velocities and pressure gradient region near the walls.

The $k-\varepsilon$ model is not valid immediately adjacent to the walls. A wall turbulence model is used for the wall element by means of a wall function method. A function method is known as the “Log-Law of the wall” to provide a link between the velocity gradient to the wall and the velocity component parallel to the wall at the first nodal point normal to the wall at a certain distance from the wall, and to obtain an approximate iterative solution for the wall shear stress. This method attempts to account for the steep gradients and sharp variations in the velocity and turbulence quantities in the near wall region. The assumption for the formulations is a zero pressure gradient, flat plate boundary layer shape of the near wall flow. It is important to recognize that for general turbulent flows this condition is usually not met. The method is implemented using both

single functions and multiple layer functions in order to model the near wall behavior correctly⁽⁴³⁾. The Log-Law of the wall formula⁽⁷⁰⁾ is given by:

$$\frac{u_{\tan}}{u_{\tau}} = \frac{1}{\kappa} \ln(y^+ E) \quad (2-81)$$

where u_{\tan} is the velocity parallel to the wall, κ is von Karman's constant(=0.41), E is a wall roughness parameter(=9.0 for a smooth wall), u_{τ} is the friction velocity defined as:

$$u_{\tau} = \sqrt{\frac{\tau_w}{\rho}} \quad (2-82)$$

y^+ is the dimensionless normal distance from the wall defined as:

$$y^+ = \frac{\delta u_{\tau}}{\nu} \quad (2-83)$$

The wall viscosity can be calculated as:

$$\mu_w = \frac{\delta \tau}{u_{\tan}} \quad (2-84)$$

Near wall values of the turbulent kinetic energy are obtained from the k- ϵ model. The wall value of the dissipation rate is dominated by the length scale and is given by⁽⁷⁰⁾:

$$\epsilon_{nw} = \frac{C_{\mu}^{0.75} k_{nw}^{1.5}}{\kappa} \delta \quad (2-85)$$

where ϵ_{nw} is near wall dissipation rate, k_{nw} is near wall kinetic energy.

The structured meshing requirement near the wall involves the Log Law of the Wall at a computational element node located within the inner region of the turbulent boundary layer, $11.63 < y^+ < 500$. Outside of the viscous sublayer, the optimum values of y^+ for FLOTRAN CFD code used in this study is between approximately 30 and 1000. If the pressure is decreasing in the direction of flow, values up to 5000 are acceptable. Within this region, the turbulent production and dissipation rate are in approximate balance. In summary, an analyst should be able to make informed decisions, that reflect lower cost or higher efficient approach for the mesh pattern design using different combinations of different order elements and different density of elements and different order of elements at the different region based upon the above principles and also pay attention to the problems which require structured meshes.

Selection of Interpolation Functions⁽³⁴⁾

This step involves assigning nodes to every element and then selecting the interpolation functions to represent the variations of the field or local variables over the elements. The local variables can be scalars, vectors, or higher order tensors. Polynomials are usually chosen as interpolation functions for the local variables because they are easy to integrate and differentiate. The degrees of the shape function in the form of polynomials are determined by the type of elements selected. Actually most numerical codes use their own interpolation procedures such as Galerkin, and such procedures are generally enabled in the element type selected for analysis.

For the heat transfer by conduction of viscous incompressible flow, involves continuous functions to approximate the local variables, all the Lagrange and serendipity family of shape functions are sufficient. For variable pressure in the mixed finite element model in incompressible flow, because the approximation function for the solution of the pressure in the continuity equation is the weighting function and this brings about over-constraining of the system of discrete equations⁽⁶²⁾. In order to prevent this from happening, the interpolation functions selected for pressure should be at least one order lower than that for the fluid velocity and the unequal order interpolation criteria could be relaxed. To solve these types of problems effectively, the most commonly used elements is 9-node quadrilateral (with an interior node) quadratic rectangular element for 2-D flows of viscous incompressible fluids and all the variables including velocity and other auxiliary variables by using quadratic Lagrange functions⁽⁶²⁾. If the velocity approximation is using quadratic Lagrange functions, the interpolation functions for pressure can be chosen either continuous linear rectangular approximation⁽⁶²⁾ in which the pressure is defined at the corner nodes of the element and is made continuous across element boundaries⁽⁶²⁾ (Fig.2-17), or discontinuous linear variation on the element as:

$$\{\varphi_i^e\} = \begin{Bmatrix} 1 \\ x \\ y \end{Bmatrix} \quad (2-86)$$

For 3-D viscous flows of viscous incompressible fluids, the effective element is the 8 node linear hexahedral(brick) element. The velocity variables are using the linear

Lagrange functions⁽⁶²⁾. The pressure approximation is therefore one order lower than the interpolation for velocity as a constant and it is discontinuous between elements.

Element Properties

This step involves applying the material properties such as heat conductivity, density, specific heat capacity and viscosity to the matrix equations for the individual elements. The properties can be constant or they could be on parameters dependent like temperature and geometry. Basically, three methods may be applicable; they are the direct approach, the variational approach and the weighted residual approach. The element properties are then assembled to get the system equations by the nodal equations of individual elements where the elements are interconnected and share the same value at the nodes.

Boundary Conditions

This step involves imposing the known values of the main variable at specific boundary locations. As well boundary loading variables are applied at this stage:

- specified condition is to set degrees of freedom (DOF) constraints at nodes by applying the values such as pressure, force, displacement, temperature, heat flux, heat convection coefficient, flow velocity and so on,
- symmetry condition is used to define the symmetric boundary by applying the zero value of the characteristic degree of freedom in the normal direction to the symmetric boundary such as zero velocity normal to the symmetry boundary, adiabatic condition for the symmetric boundary, etc,
- periodic condition is unknown but identical at multiple boundary locations.

Choice of Matrix Solver and Set the Iteration Parameters

This step involves choosing the algorithm solvers or methods for solving the set of simultaneous equations. The selection of the solvers depends on the whether the problems are transient or steady, linear or nonlinear *et al.* At this stage, other solution time parameters such as convergence criteria, number of steps and substeps are specified.

2.4 Convective Heat Transfer

The convection heat transfer occurs between a moving fluid and a solid surface (Fig.2-18) with different temperatures due to random molecular motion (diffusion) and bulk motion (advection) (Fig.2-19)⁽³⁸⁾ of fluid. In the fluid-surface interaction region, there are two boundary layers; hydrodynamic (velocity) boundary layer through which the velocity changes from zero at stationary surface to a finite value of u_∞ , and thermal boundary layer through which the temperature varies from surface temperature T_w to T_∞ in the outflow. If $T_w > T_\infty$, the convection heat transfer for solid is a cooling process, otherwise, it is a heating process. Convection heat transfer is basically classified into forced convection and free or natural convection by the driving force of flow. The forced convective heat transfer is caused by external flow due to a fan, a pump, or ambient winds *et al.* The free convective heat transfer is caused by buoyancy forces which results from density differences primarily induced by temperature differences in the fluid or between the fluid and the boundary. If the velocity associated with the forced convection flow is small and buoyancy forced free flow is relatively large, a secondary flow that is comparable to the superimposed forced flow may exist. The buoyancy induced flow will be normal to the forced flow and enhance the effect of convection heat transfer⁽³⁸⁾. The mathematical description of convection heat transfer is given by Newton's law of cooling:

$$q'' = h(T_w - T_\infty) \quad (2-87)$$

where q'' is the convective heat flux from solid surface to the fluid. T_w is the local surface temperature or the wall temperature of the solid; T_w is a function of geometry on the wall;

$$T_w = T_{w(x,y,z)} \quad (2-88)$$

where T_∞ is the mainstream fluid temperature; h is the local convection heat transfer coefficient or the film coefficient on the surface $h = h_{(x,y,z)}$. The total convection heat transfer rate is:

$$q = \bar{h}A(\bar{T}_w - T_\infty) \quad (2-89)$$

where q is the convection heat transfer rate along the surface or the wall; A is the surface area of the arbitrary shape wall; \bar{h} is the average convection coefficient over the surface area A ; \bar{T}_w is the average temperature of the surface. The total convection heat transfer coefficient can also be computed from the integration of the local heat flux over the entire surface:

$$q = \int_A q''_{(x,y,z)} dA \quad (2-90)$$

or

$$q = \int_A h_{(x,y,z)} (T_{w(x,y,z)} - T_\infty) dA \quad (2-91)$$

If the wall temperature is uniform, then:

$$q = \int_A h_{(x,y,z)} (T_{w(x,y,z)} - T_\infty) dA \quad (2-92)$$

So that the relationship between local and average convection coefficient is:

$$\bar{h} = \frac{1}{A} \int_A h_{(x,y,z)} dA \quad (2-93)$$

If h varies only with the distance L along one direction on x , equation (2-93) can be reduced to:

$$\bar{h} = \frac{1}{L} \int_0^L h_{(x)} dx \quad (2-94)$$

By equating Fourier's law of conduction heat transfer in the solid or inside the boundary layer of fluid to the Newton's law of cooling to the convection heat transfer,

$$q'' = -k_f \left. \frac{\partial T}{\partial y} \right|_{y=0^+} = -k \left. \frac{\partial T}{\partial y} \right|_{y=0^-} = h(T_w - T_\infty) \quad (2-95)$$

where k_f is thermal conductivity of the fluid at the surface; k is the thermal conductivity of solid; $\left. \frac{\partial T}{\partial y} \right|_{y=0^+}$ is the temperature gradient at the surface inside flow boundary layer along y direction which is normal to the surface; $\left. \frac{\partial T}{\partial y} \right|_{y=0^-}$ is the temperature gradient at the surface inside solid normal to the surface.

Local h could also be expressed as:

$$h = \frac{-k_f \left. \frac{\partial T}{\partial y} \right|_{y=0^+}}{T_w - T_\infty} \quad (2-96)$$

or

$$h = \frac{-k \left. \frac{\partial T}{\partial y} \right|_{y=0^-}}{T_w - T_\infty} \quad (2-97)$$

Generally, convection heat transfer depends on the condition of boundary layer, which is affected by surface geometry, fluid material thermodynamic and transport properties such as fluid viscosity, thermal conductivity, specific heat capacity, density, the nature of fluid motion like velocity, pressure profiles, nature of thermal loads like temperature constraints, heat generation rates and energy transfer rate in the region near the wall.

Some analytical, semi-empirical and empirical solutions are very effective to do the thermal and flow computation for some special electronic packaging with regular boundary configurations. For example, Nusselt number and the dimensionless equations for external flow over a large plate are used to calculate the convective heat coefficient over a small chip on a thin circuit board. Nusselt number and dimensionless equation for the fully developed internal flow under constant temperature and heat flux wall boundary conditions are also effectively applied for different flow. All discussions in this thesis refer to fluid flow of single phase in the laminar and turbulent states.

2.4.1 Laminar and Turbulence

Fluids are generally divided into viscous and ideal, incompressible and compressible, Newtonian and Non-Newtonian fluid. The types of flow can be classified into turbulent and laminar flow⁽³⁸⁾ (Fig.2-20).

When the fluid viscosity is zero or approximately zero, the fluid is considered to be ideal. Otherwise it is viscous. Most real fluid are viscous. When the fluid density does not change with pressure it is considered to be incompressible. Otherwise it is a compressible fluid. In normal applications, if the Mach number, the ratio of an object's

velocity to the speed of sound, is less than 0.3, the fluid can be considered to be incompressible.

A viscous fluid develops a boundary layer when it flows over a solid surface⁽⁶⁴⁾. The fluid particles staying at the contact wall with the zero velocity retard the motion of the particles in the next layer at a distance from the wall to δ which is the normal distance or thickness from the wall. If distance increases from zero at the wall to δ , and the velocity parallel to the wall varies from zero to $0.99u_\infty$ which is 99 percent of the free stream or mainstream value, then δ is considered as the thickness of boundary layer. When the distance is larger than δ or in another words outside the boundary layer, the velocity change or velocity gradient is negligible. The frictional effect which retards the motion acts as a shear stress for flow over flat plate and is expressed as:

$$\tau = \mu \left. \frac{\partial u}{\partial y} \right|_{y < \delta} \quad (2-98)$$

where μ is a fluid property know as dynamic viscosity; $\left. \frac{\partial u}{\partial y} \right|_{y < \delta}$ is the normal velocity gradient. If $\tau \propto \mu \left. \frac{\partial u}{\partial y} \right|_{y < \delta}$ or μ is constant, the fluid is Newtonian, otherwise, it is Non-Newtonian fluid. The friction coefficient C_f for a fluid is defined as:

$$C_f = \frac{\tau|_{y=0}}{\rho u_\infty^2 / 2} \quad (2-99)$$

Essentially, the surface friction and the convection transfer rates are determined by the characteristics of the boundary layer, which is in either a laminar or turbulent state. In laminar boundary layer, the fluid motion is highly ordered and the flow along the streamline can be characterized by velocity components in the three dimensions. The velocity component in the direction normal to the wall dominantly contribute to the transfer of momentum, energy due to microscopic transport on the basis of individual molecules through the boundary layer.

In a turbulent boundary layer, the fluid motion is highly irregular and the flow along the streamline can only be characterized by velocity fluctuations instead of velocity components⁽³⁸⁾. The velocity fluctuations enhance the contribution to the transfer of

momentum, energy due to the transport of larger mass of the macroscopic elements of fluid which increase the surface friction as well as convection heat transfer rates through the boundary layer. This generally results in large boundary layers in turbulent flows in turbulent flows than laminar flows.

The types of the boundary layer determines the characteristics of the fluid flows. In calculating boundary layer behavior, a dimensionless criteria, Reynolds number, is defined as:

$$\text{Re} = \frac{\rho u_{\infty} l}{\mu} \quad (2-100)$$

where l is the characteristic dimension or hydraulic diameter of the fluid. The significance of Reynolds number is that it represents the ratio of inertial force and viscous force for the fluid. The values of critical Reynolds number for laminar and turbulent flow are different.

For turbulent flow, all kinds of physical properties of fluid like velocity, pressure, temperature are changing randomly with time and position. Turbulence is composed of different eddy with different dimension, and the size and the rotation directions for the eddy are randomly distributed. Larger dimensional eddy which is the source of low frequency fluctuation is caused by flowing boundary conditions and the dimension is similar with the flow field. Smaller dimensional eddy which is the source of high frequency fluctuation results from the viscosity stress and the dimension is only one thousandth of flow field. When bigger eddy is destroyed, it is divided into smaller and smaller eddy so that in the fully developed turbulence region the sizes of the eddy vary continuously in a rather wide dimension range. During the flow process, bigger eddy obtain energy from the main flow and then transfer to the smaller eddy by means of the interaction between all sizes of eddy, finally due to the effect of fluid viscosity, smaller eddy disappear and the mechanical energy is transferred or dissipated into thermal energy for the fluid. In the meantime, the boundary disturbs and velocity gradient and generates new eddy, and resulting in turbulence⁽¹¹⁾.

For external flow over a flat plate where the characteristic dimension l is the distance from the leading edge to the end. If the boundary layer is laminar⁽³³⁾, then

$$\text{Re}_l = \frac{u_\infty l}{\nu} < 5 \times 10^5 \quad (2-101)$$

When $\text{Re} > 5 \times 10^5$, the transition from laminar to turbulent flow occurs. The transition ends at $\text{Re} = 2 \times 10^6$ ⁽³³⁾ or 3×10^6 ⁽³⁸⁾ depending on the surface roughness and the turbulence level of the free stream. After the transition section, the flow becomes turbulent.

For internal flow, after the flow is fully developed, when the critical Reynolds number

$$\text{Re}_d = \frac{Ud}{\nu} > 2300 \quad (2-102)$$

turbulent flow can be observed although much larger Reynolds numbers ($\text{Re}_D \approx 10000$) are needed to establish stable turbulence.

The definition for the characteristic dimension d is as follows:

$$d = \frac{4A_c}{P} \quad (2-103)$$

where P is the wetted perimeter; A_c is the flow cross sectional area. The range of critical Reynolds number for the transition section depends on the pipe roughness and smoothness of the flow and the general accepted values are⁽³³⁾:

$$2000 < \text{Re}_d < 4000$$

At the entrance section the viscous effects are important and the boundary layer develops with increasing length. After the flow is fully developed, the velocity profile will no longer change with increasing length. The flow then becomes fully developed and the distance from the entrance to the position at which the fully developed flow is established is called the hydrodynamic entry length. The fully developed velocity profile is parabolic for laminar flow in a circular tube and when the flow is turbulent, a blunter profile is observed.

2.4.2 External Forced Convective Heat Transfer Solutions

For external flow, there are no constraints imposed on the adjacent surfaces and the flow boundary layers are developed freely so that the region of flow outside the boundary layer where the velocity and temperature gradients can be neglected. For some

specific flows like flow over a flat plate, curved surfaces, the local and average convection coefficients may be correlated by dimensionless equations in the form as follows⁽³⁸⁾:

$$Nu_x = f(x, Re_x, Pr) \quad (2-104)$$

$$\overline{Nu}_x = f(Re_x, Pr) \quad (2-105)$$

where x is the particular location on the surface from $x = 0$, the location where boundary layer begins.

Nu_x is the Nusselt number corresponding to the location of x . \overline{Nu}_x is the average Nusselt number corresponding to the characteristic dimension x ; Re_x is the Reynolds number corresponding to the characteristic dimension x ; Prandtl number, Pr , is the relation between velocity field and temperature field with the definition as

$$Pr = \frac{\nu}{\alpha} \quad (2-106)$$

The relation between Nu_x and \overline{Nu}_x is linked by:

$$\overline{h}_x = \frac{1}{x} \int_0^x h_x dx \quad (2-107)$$

$$(h_x = \frac{Nu_x k}{x}) \quad (2-108)$$

These equations are obtained by two approaches; theoretical and empirical. The correlation for empirical or experimental approach is obtained correcting the data in terms of proper dimensionless parameters with the heat transfer measurements based on controlled laboratory conditions. The theoretical approach can only be achieved by solving the boundary layer equations for particular geometry.

For the cooling of electronic packages to remove the heat dissipated from the electronic components or devices with small vertical dimensions mounted on flat printed circuit boards by forcing air across over the board surfaces either on the chip side or on the heat sink side as Fig.2-21⁽³⁸⁾, the heat transfer configuration is associated with the flat plate in the parallel flow. The problems are therefore solved by the dimensionless equation as follows:

for laminar flow ($Re < 5 \times 10^5$), the local h_x is calculated from the equation⁽³⁸⁾:

$$\text{Nu}_x = \frac{h_x x}{k} = 0.332 \text{Re}_x^{\frac{1}{2}} \text{Pr}^{\frac{1}{3}} \quad 0.6 \leq \text{Pr} \leq 50 \quad (2-109)$$

the average h_x is calculated from the following equation⁽³⁸⁾:

$$\overline{\text{Nu}}_x = \frac{\bar{h}_x x}{k} = 0.664 \text{Re}_x^{\frac{1}{2}} \text{Pr}^{\frac{1}{3}} \quad 0.6 \leq \text{Pr} \leq 50 \quad (2-110)$$

for turbulent flow, $\text{Re} > 2 \times 10^6$ ⁽³³⁾ or 3×10^6 ⁽³⁸⁾, the local h_x is calculated from the equation⁽³⁸⁾:

$$\text{Nu}_x = \frac{h_x x}{k} = 0.0296 \text{Re}_x^{\frac{4}{5}} \text{Pr}^{\frac{1}{3}} \quad 0.6 \leq \text{Pr} \leq 60 \quad (2-111)$$

the average \bar{h}_x is calculated by:

$$\bar{h}_x = \frac{1}{x} \int_0^x h_x dx \quad (2-112)$$

For laminar and turbulent mixed boundary (transition) flow ($5 \times 10^5 < \text{Re} < 2 \times 10^6$), if the transition occurs near the end of the plate ($0.95 \leq (x_c / L) \leq 1$), the laminar equations may be used to compute the average convective coefficients to a acceptable approximation. However, when transition happens near the upstream end of the plate ($(x_c / L) \leq 0.95$), the average convective coefficients must take both of turbulent and laminar boundary layers, which is the mixed boundary layer, into account by integrating over the laminar region ($0 \leq x \leq x_c$) and then over the turbulent region ($x_c \leq x \leq L$) by⁽³⁸⁾:

$$\bar{h}_L = \frac{1}{L} \left(\int_0^{x_c} h_{x_L} dx + \int_{x_c}^L h_{x_T} dx \right) \quad (2-113)$$

where x_c is the location where transition suddenly occurs; h_{x_L} is the local convective coefficient for laminar region. h_{x_T} is the local convective coefficient for turbulent region, the average convective coefficient for mixed boundary is then referred as⁽³⁸⁾:

$$\bar{h}_L = \left(\frac{k}{L} \right) \left[0.332 \left(\frac{u_\infty}{\nu} \right)^{\frac{1}{2}} \int_0^{x_c} \frac{dx}{x^{\frac{1}{2}}} + 0.0296 \left(\frac{u_\infty}{\nu} \right)^{\frac{4}{5}} \int_{x_c}^L \frac{dx}{x^{\frac{1}{5}}} \right] \text{Pr}^{\frac{1}{3}} \quad (2-114)$$

or the average Nusselt number is:

$$\overline{\text{Nu}}_L = \left[0.664 \text{Re}_{x_c}^{\frac{1}{2}} + 0.037 \left(\text{Re}_L^{\frac{4}{5}} - \text{Re}_{x_c}^{\frac{4}{5}} \right) \right] \text{Pr}^{\frac{1}{3}} \quad (2-115)$$

All the above equations are applicable under assumption that the surface has uniform temperature. For the situation with an unheated starting length of ξ at which the surface temperature equals to upstream temperature and from $x = \xi$ (Fig.2-22)⁽³⁸⁾ and heat transfer begins only when $x > \xi$. For these special cases, the solutions are⁽³⁸⁾:

for laminar flow:

$$\text{Nu}_x = \frac{\text{Nu}|_{\xi=0}}{\left[1 - \left(\frac{\xi}{x}\right)^{\frac{3}{4}}\right]^{\frac{1}{3}}} \quad (2-116)$$

where $\text{Nu}_x|_{\xi=0}$ is given by equation (2-109) assuming there is no unheated starting length.

for turbulent flow:

$$\text{Nu}_x = \frac{\text{Nu}|_{\xi=0}}{\left[1 - \left(\frac{\xi}{x}\right)^{\frac{9}{10}}\right]^{\frac{1}{9}}} \quad (2-117)$$

where $\text{Nu}_x|_{\xi=0}$ is given by equation (2-111) assuming there is no unheated starting length.

If the surface has a imposed condition as uniform heat flux instead of uniform temperature, for laminar flow:

$$\text{Nu}_x = 0.453 \text{R}_x^{\frac{1}{2}} \text{Pr}^{\frac{1}{3}} \quad (2-118)$$

for turbulent flow:

$$\text{Nu}_x = 0.0308 \text{R}_x^{\frac{4}{5}} \text{Pr}^{\frac{1}{3}} \quad (2-119)$$

Thus, the Nusselt number is 36% and 4% larger than those from the uniform temperature for laminar and turbulent respectively.

For higher dissipation rate chips like the Pentium microprocessor, the heat extraction process involves air jets impinging a dense array of pins on a pin fin heat sink. Normally the jets impinge the top of the pins to achieve enhanced convective heat transfer coefficients (Fig.2-23)⁽⁶¹⁾. For such applications, Nusselt number can be computed by integrating local results over the pin top areas as the representative flat

surface. The corresponding relationships for determining the heat transfer coefficient are as⁽³⁸⁾:

$$\overline{Nu} = f(\text{Re}, \text{Pr}, r/D_H, H/D_H) \quad (2-120)$$

where

$$\overline{Nu} = \frac{\overline{h}D_h}{k} \quad (2-121)$$

$$\text{Re} = \frac{V_e D_h}{\nu} \quad (2-122)$$

and $D_h = D$ (Round nozzle); $D_h = 2W$ (Slot nozzle); V_e is uniform velocity at the nozzle exit; W is the width of slot nozzle. The correlated solutions are recommended from Martin⁽⁴⁹⁾.

For a single round nozzle:

$$\frac{\overline{Nu}}{\text{Pr}^{0.42}} = G\left(\frac{r}{D}, \frac{H}{D}\right)F(\text{Re}) \quad (2-123)$$

where $F(\text{Re}) = 2 \text{Re}^{\frac{1}{2}}(1 + 0.005\text{Re}^{0.55})^{\frac{1}{2}}$ and

$$G = \frac{D}{r} \frac{1 - 1.1 \frac{D}{r}}{1 + 0.1 \left(\frac{H}{D} - 6\right) \frac{D}{r}} \quad (2-124)$$

The ranges of validity are

$$\left[\begin{array}{l} 2000 \leq \text{Re} \leq 400,000 \\ 2 \leq \frac{H}{D} \leq 12 \\ 2.5 \leq \frac{r}{D} \leq 7.5 \end{array} \right] \quad (2-125)$$

where H is the distance between the exit of nozzle and the target surface; D is the diameter of the nozzle; r is the distance from the stagnation or impingement zone along the transverse direction.

For a single slot nozzle:

$$\frac{\overline{\text{Nu}}}{\text{Pr}^{0.42}} = \frac{3.06 \text{Re}^m}{\frac{x}{W} + \frac{H}{W} + 2.78} \quad (2-126)$$

where

$$m = 0.695 - \left[\left(\frac{x}{2W} \right) + \left(\frac{H}{2W} \right)^{1.33} + 3.06 \right]^{-1} \quad (2-127)$$

The ranges of validity are:

$$\left[\begin{array}{l} 3000 \leq \text{Re} \leq 90,000 \\ 2 \leq \frac{H}{W} \leq 10 \\ 4 \leq \frac{r}{W} \leq 20 \end{array} \right] \quad (2-128)$$

For an array of round nozzles:

$$\frac{\overline{\text{Nu}}}{\text{Pr}^{0.42}} = K \left(A_r, \frac{H}{D} \right) G \left(A_r, \frac{H}{D} \right) E(\text{Re}) \quad (2-129)$$

where

$$E(\text{Re}) = 0.5 \text{Re}^{\frac{2}{3}} \quad (2-130)$$

and

$$K = \left[1 + \left(\frac{\frac{H}{D}}{\frac{0.6}{A_r^{\frac{1}{2}}}} \right)^6 \right]^{-0.05} \quad (2-131)$$

and G is the same as equation (2-124) which is the single nozzle function.

The ranges of validity are:

$$\left[\begin{array}{l} 2000 \leq \text{Re} \leq 100,000 \\ 2 \leq \frac{H}{D} \leq 12 \\ 0.004 \leq A_r \leq 0.04 \end{array} \right] \quad (2-132)$$

where A_r is the relative nozzle area which is the ratio of the cross sectional area of the nozzle exit to the cell surface area.

For an array of slot nozzles:

$$\frac{\overline{\text{Nu}}}{\text{Pr}^{0.42}} = \frac{2}{3} A_{r,o}^{\frac{3}{4}} \left(\frac{2 \text{Re}}{\frac{A_r}{A_{r,o}} + \frac{A_{r,o}}{A_r}} \right)^{\frac{2}{3}} \quad (2-133)$$

where

$$A_{r,o} = \left[60 + 4 \left(\frac{H}{2W} - 2 \right)^2 \right]^{-\frac{1}{2}} \quad (2-134)$$

The ranges of validity are

$$\left[\begin{array}{l} 1500 \leq \text{Re} \leq 40,000 \\ 2 \leq \frac{H}{D} \leq 80 \\ 0.008 \leq A_r \leq 2.5A_{r,o} \end{array} \right] \quad (2-135)$$

There are solutions for flows over cylinder, sphere, banks of tubes, packed beds, but since these type of flows have little applications to the electronic packaging, they will not be discussed.

2.4.3 Internal Forced Convective Heat Transfer Solutions

Internal flow such as flow in a pipe is one for which the fluid is confined by a surface. The internal flow configuration may be applied for electronic packaging cooling in the thermal management of microelectronics components which is associated with channel flows between circuit boards or cards. This is because chips are mounted either directly on cards, or on individual modules mounted on the cards. The cards are then arranged parallel to each other and attached on the sides to form a typical package⁽⁷⁷⁾ as shown in Fig.2-24. Such an arrangement forms a number of parallel channels, each containing discretely heated components. The components are cooled either by a buoyancy-induced convective flow (natural convection) or by a forced convective flow produced by forcing air through the channels.

Heat transfer in a channel flow containing heated components is a function of several variables. The flow, as mentioned earlier, could be buoyancy induced or forced. It could also, in turn, be laminar or turbulent, it could undergo transition from laminar to

turbulent at some point in the channel. Depending on the approach to the channel, the flow could be fully developed, and the same is true of the exit section. Other variables that determine the flow regime are the channel dimensions, module dimensions, and module heating rate.

For low power dissipation rates, most of the studies have been concerned with two-dimensional channels with simplified boundary conditions. Channels formed by symmetrically heated isothermal surfaces, symmetrically heated uniform flux surfaces are pertinent examples. Three-dimensional effects due to module sizes and spacing, and to lateral effects have not been studied in detail. Typically electronic packages are made of conductive materials, and the problem should really be approached from both a conductive and convective standpoint. Most designers of microelectronics packages have relied on empirical data specific to their particular technology needs.

For fully developed turbulent channel flow, the thermal and viscous boundary layers are very narrow, and the shape of the duct can be accounted for by using an equivalent hydraulic diameter or characteristic dimension in circular channel correlation. The criteria for the turbulent flow in a circular tube is:

$$\text{Re}_D = \frac{\rho u_m D}{\mu} \approx 2300 \quad (2-136)$$

where D is characteristic dimension; u_m is the means velocity of the fluid.

For incompressible flow in a circular conduit,

$$u_m = \frac{\int_{A_c} \rho u(r, x) dA_c}{\rho A_c} = \frac{2}{r_o^2} \int_0^{r_o} u(r, x) r dr \quad (2-137)$$

where A_c is the area of cross section of the tube; $u(r, x)$ is the velocity profile; r_o is the radius of the tube; r represents the location in the radial direction; and x represents the location in the axis direction.

The entry length for fully developed flow is obtained in the form of:

$$L_{fd} \approx 0.05D \text{ Re}_D \quad (\text{for laminar}) \quad (2-138)$$

$$10D \leq L_{fd} \leq 60D \quad (\text{for turbulent}) \quad (2-139)$$

The condition for the thermal fully development is⁽⁸¹⁾:

$$\frac{\partial \Pi(r, x)}{\partial x} = 0 \quad (2-140)$$

where

$$\Pi(r, x) = \frac{T(r, x) - T_s(x)}{T_m(r, x) - T_s(r, x)} \quad (2-141)$$

$$u_m = \frac{\int_{A_c} \rho u(r, x) dA_c}{\rho A_c} = \frac{2}{r_o^2} \int_0^{r_o} u(r, x) r dr \quad (2-142)$$

and T_s is the conduit surface temperature at location x along axis direction; T is the local fluid temperature at x along axis; r at radial direction; T_m is the mean or bulk temperature of the fluid over the cross section of the duct; c_∞ is the inlet velocity for the incompressible flow; \dot{m} is mass flow rate; A is the cross section area of the pipe.

The surface conditions arise in many electronic packaging cooling applications, such as a constant heat flux which is from the constant power dissipation through the outer surface of modules, or the constant module temperature which may exist if a phase change of condensation or boiling of the fluid inside an enclosed chamber as heat sink of the modules for some high power dissipation electronic modules. These operation conditions result in the variation of T_s with x when the surface heat flux q_s'' is constant, the variation of q_s'' with x when the T_s is constant.

For the constant surface heat flux q_s'' ⁽⁸¹⁾:

$$q_{\text{conv}} = q_s'' \cdot P \cdot x \Big|_{x=L} \quad (2-143)$$

where q_{conv} is the total heat transfer rate on the pipe surface; P is the surface perimeter; L is the length of the pipe. The temperature gradients along axis direction is independent the of the radial location:

$$\frac{\partial T}{\partial x} \Big|_{fd,t} = \frac{dT_s}{dx} \Big|_{fd,t} = \frac{dT_m}{dx} \Big|_{fd,t} = \frac{Pq_s''}{mc_p} = \text{constant} \quad (2-144)$$

Therefore, T_s , and T_m change linearly along axis (x) direction ⁽³⁸⁾ (Fig.2-25a):

$$T_m(x) = T_m \Big|_{x=0} + \frac{Pq_s''}{mc_p} x \quad (2-145)$$

$$T_s(x) = T_s|_{x=0} + \frac{Pq_s''}{mc_p} x \quad (2-146)$$

For the constant conduit surface temperature, $T_s = \text{constant}$, the condition becomes:

$$\frac{\partial T}{\partial x} \Big|_{fd,t} = \frac{(T_s - T)}{(T_s - T_m)} \frac{dT_m}{dx} \Big|_{fd,t} \quad (2-147)$$

Therefore, the bulk temperature varies exponentially with the distance along the axis direction⁽³⁸⁾ (Fig.2-25b)

$$T_m(x) = T_s - (T_s - T_m|_{x=0}) \exp\left(-\frac{Px}{mc_p} \bar{h}\right) \quad (2-148)$$

In the thermally fully developed region, by applying equation (2-140):

$$\frac{\partial}{\partial r} \left(\frac{T_s - T}{T_s - T_m} \right) \Big|_{r=r_0} = \frac{-\frac{\partial T}{\partial r} \Big|_{r=r_0}}{T_s - T_m} \neq F(x) \quad (2-149)$$

Combine the Fourier's law and Newton's cooling law

$$q_s'' = -k \frac{\partial T}{\partial r} \Big|_{r=r_0} = h(T_s - T_m) \quad (2-150)$$

then

$$\frac{h}{k} \neq f(x)$$

Thus, at the beginning of entrance section, h is largest due to the zero boundary layer thickness, and it decreases rapidly as the thermal boundary layer develops. After the thermally fully developed condition has been achieved, in the developed region of a fluid with constant properties, the local convective coefficient becomes constant along the axis direction x ⁽³⁸⁾ (Fig.2-26).

Solution for laminar flow in the thermally fully developed region, the Nusselt number is:

for constant heat flux condition⁽⁸¹⁾:

$$Nu_D = \frac{hD}{k} = 4.36 \quad (2-151)$$

for constant surface temperature condition⁽⁸¹⁾:

$$\text{Nu}_D = \frac{hD}{k} = 3.66 \quad (2-152)$$

For both the entry region and thermally developed region, solutions are the empirical correlations for the average Nusselt number on constant surface temperature conditions.

For thermal entry length problems which assumes the flow has hydraulically developed prior to the thermally developed for the situations like large Prandtl number fluid or the existence of an unheated starting length⁽³³⁾ Nusselt number is computed according to Kays⁽⁴⁰⁾:

$$\overline{\text{Nu}}_D = 3.66 + \frac{0.0668 \left(\frac{D}{L}\right) \text{Re}_D \text{Pr}}{1 + 0.04 \left[\left(\frac{D}{L}\right) \text{Re}_D \text{Pr}\right]^{\frac{2}{3}}} \quad (2-153)$$

For combined entry length problems which assumes the flow has hydraulically and thermally developed simultaneously for the situations like the approximate unit Prandtl number fluid or the smaller ($Pr < 1$) with an appropriate unheated starting length which achieves the hydraulically and thermally fully developed at the same location⁽³³⁾, the Nusselt number is attributed by Sieder and Tate⁽³⁸⁾:

$$\overline{\text{Nu}}_D = 1.86 (\text{Re}_D \text{Pr})^{\frac{1}{3}} \left(\frac{D}{L}\right)^{\frac{1}{3}} \left(\frac{\mu}{\mu_s}\right)^{0.14} \quad (2-154)$$

under the conditions:

$$\left[\begin{array}{l} 0.48 < \text{Pr} < 16700 \\ 0.0044 < \left(\frac{\mu}{\mu_s}\right) < 9.75 \\ \mu_s \text{ is evaluated at } T_s \end{array} \right] \quad (2-155)$$

For turbulent flow in fully developed region inside a smooth pipe, the Colburn empirical equation is modified by Dittus-Boelter⁽³⁸⁾ as:

$$\text{Nu} = 0.023 \text{Re}^{\frac{4}{5}} \text{Pr}^n \quad (2-156)$$

where $n = 0.4$ when heating ($T_s > T_m$), $n = 0.3$ when cooling ($T_s < T_m$)

The ranges of the experimental conditions for the equation are:
$$\left[\begin{array}{l} 0.7 \leq Pr \leq 160 \\ Re_D \geq 10,000 \\ \frac{L}{D} \geq 10 \end{array} \right]$$

2.4.4 Natural Convection Flow Solution

Unlike forced convection, the convection current or flow is induced by the buoyancy which arises from a combination of the density gradient mostly due to the temperature gradient in the heat process and the gravity. The governing equations (2D) are:

$$\frac{\partial u}{\partial x} + \frac{\partial v}{\partial y} = 0 \quad (2-157)$$

$$u \frac{\partial u}{\partial x} + v \frac{\partial u}{\partial y} = g\beta(T - T_\infty) + \nu \frac{\partial^2 u}{\partial y^2} \quad (2-158)$$

$$u \frac{\partial T}{\partial x} + v \frac{\partial T}{\partial y} = \alpha \frac{\partial^2 T}{\partial y^2} \quad (2-159)$$

where g is the gravitational constant along the y direction; β is the volumetric thermal expansion coefficient:

$$\beta = -\frac{1}{\rho} \left(\frac{\partial \rho}{\partial T} \right)_p \quad (2-160)$$

For an ideal gas:

$$\beta = -\frac{1}{\rho} \left(\frac{\partial \rho}{\partial T} \right)_p = \frac{1}{\rho} \frac{p}{RT^2} = \frac{1}{T} \quad (2-161)$$

Generally, by similar consideration, the correlation for natural convection is the dimensionless equation in the form of:

$$Nu_L = f(Re_L, Gr_L, Pr) \quad (2-167)$$

where

$$Gr_L = \frac{g\beta(T_s - T_\infty)L^3}{\nu^2} \quad (2-168)$$

The physical significance of the dimensionless number Grashof number (Gr) is the ratio of the buoyancy force to the viscous force to the fluid.

The empirical correlations for external free convection flows are generally of the form⁽⁸¹⁾:

$$\overline{Nu}_L = C Ra_L^n \quad (2-169)$$

where the Rayleigh number Ra_L refers as:

$$Ra_L = Gr_L Pr \quad (2-170)$$

where C and n are constant based upon several typical regular geometry and free current configurations, and laminar or turbulent states⁽⁸¹⁾ in the different ranges of Ra . For most electronic packaging engineering calculations, the geometry is complicated which may not be typical, Churchill and Chu⁽⁸¹⁾ have recommended a correlation in the range of $10^{-6} \leq Ra_L \leq 10^{13}$ as⁽³⁸⁾:

$$\overline{Nu}_L = \left\{ 0.825 + \frac{0.38 Ra_L^{\frac{1}{4}}}{\left[1 + \left(\frac{0.492}{Pr} \right)^{\frac{9}{16}} \right]^{\frac{8}{27}}} \right\}^2 \quad (2-171)$$

If laminar flow occurs ($0 < Ra_L < 10^9$), a more accurate correlation is suggested to be⁽³⁸⁾:

$$\overline{Nu}_L = 0.68 + \frac{0.670 Ra_L^{\frac{1}{4}}}{\left[1 + \left(\frac{0.492}{Pr} \right)^{\frac{9}{16}} \right]^{\frac{4}{9}}} \quad (2-172)$$

For free convection in an enclosed space such as a vertical or horizontal cavity, the heat transfer rate is in the form of⁽⁸¹⁾:

$$q = \frac{k_{\text{eff}}}{\delta} (T_{s_1} - T_{s_2}) \quad (2-173)$$

where k_{eff} is effective thermal conductivity; δ is the interval between the cavity; T_{s_i} is the surface temperature of the walls.

For air which is mostly used in electronic packaging calculation, the correlations are:

$$\frac{k_{\text{eff}}}{k} = CGr_L^m \left(\frac{\delta}{H} \right)^n \quad (2-174)$$

where H is the height of vertical cavity; m and n are determined by the Gr_L or the flow states. For the flow with the condition of $Gr_L < 2000$, the natural convection current will not be initiated. Therefore, the $k_{\text{eff}} = k$, that indicates that air inside the cavity is solely responsible for conduction heat transfer.

2.4.5. Computational Fluid Dynamics, Finite Volume Method Approach

Most cooling processes for electronic packaging involve forced air flow across arrays of modules mounted on ceramic boards in a channel. The flow type may be internal for the channel and external for the modules with different dimensions. Boundary conditions may not be constant uniform temperature or constant heat flux which are required to obtain the solution using the equations (2-151) or (2-152), instead, the modules usually have different power dissipation rates according to their functions in the circuit. For these sorts of problems, it is impossible to provide a series of widely acceptable equations whether semi-empirically or empirically.

With the advent of powerful digital computers, more and more computational solutions have been developed although there are still various topical areas where the current physical understanding or the theory about the turbulent flow is limited. A number of complex phenomena can be investigated effectively by the numerical solutions which are based on the laws of conservation of mass, momentum, and energy of fluid flow expressed in terms of second order partial differential equations. Mathematical description in three dimensions (3D steady state turbulent fluid flow) is defined by:

Continuity equations:

$$\frac{\partial \rho}{\partial \tau} + \frac{\partial(\rho u)}{\partial x} + \frac{\partial(\rho v)}{\partial y} + \frac{\partial(\rho w)}{\partial z} = 0 \quad (2-175)$$

where u , v , w are the flow velocities along x , y , and z directions.

Momentum equations:

In a Newtonian fluid, the relationship between the stress and rate of deformation of the fluid is written in a Cartesian tensor form as:

$$\tau_{ij} = -\rho \delta_{ij} + \mu \left(\frac{\partial u_i}{\partial x_j} + \frac{\partial u_j}{\partial x_i} \right) + \delta_{ij} \lambda_{ij} \frac{\partial u_i}{\partial x_i} \quad (2-176)$$

where τ_{ij} is the stress tensor at ij plane ($i, j = 1, 2, 3$); 1 is x axis, 2 is y axis, and 3 is z axis; u_i are the orthogonal velocities at i direction; u_1 is defined as u , u_2 is defined as v , u_3 is defined as w ; λ_{ij} is the second coefficient of viscosity. The final term, the product of the second coefficient of viscosity and the divergence of the velocity is zero for an incompressible fluid and is considered small enough to be neglected in a compressible fluid.

Equation (2-2) transforms the momentum equations (Navier-Stokes equations) as follows:

$$\frac{\partial(\rho uu)}{\partial x} + \frac{\partial(\rho vu)}{\partial y} + \frac{\partial(\rho wu)}{\partial z} = -\frac{\partial p}{\partial x} + \frac{\partial}{\partial x}(\mu_e \frac{\partial u}{\partial x}) + \frac{\partial}{\partial y}(\mu_e \frac{\partial u}{\partial y}) + \frac{\partial}{\partial z}(\mu_e \frac{\partial u}{\partial z}) + T_x \quad (2-177)$$

$$\frac{\partial(\rho uv)}{\partial x} + \frac{\partial(\rho vv)}{\partial y} + \frac{\partial(\rho vw)}{\partial z} = -\frac{\partial p}{\partial y} + \frac{\partial}{\partial x}(\mu_e \frac{\partial v}{\partial x}) + \frac{\partial}{\partial y}(\mu_e \frac{\partial v}{\partial y}) + \frac{\partial}{\partial z}(\mu_e \frac{\partial v}{\partial z}) + T_y \quad (2-178)$$

$$\frac{\partial(\rho uw)}{\partial x} + \frac{\partial(\rho vw)}{\partial y} + \frac{\partial(\rho ww)}{\partial z} = -\frac{\partial p}{\partial z} + \frac{\partial}{\partial x}(\mu_e \frac{\partial w}{\partial x}) + \frac{\partial}{\partial y}(\mu_e \frac{\partial w}{\partial y}) + \frac{\partial}{\partial z}(\mu_e \frac{\partial w}{\partial z}) + T_z \quad (2-179)$$

where μ_e is the effective viscosity; for turbulent flows $\mu_e = \mu + \mu_t$, and for laminar flow $\mu_e = \mu$, μ is dynamic viscosity of the fluid, μ_t is turbulent viscosity of the fluid; and T_x, T_y, T_z are viscous loss terms. The order of the differentiation is reversed in each term, reducing the term to a derivative of the continuity, which is zero:

$$T_x = \frac{\partial}{\partial x}(\mu \frac{\partial u}{\partial x}) + \frac{\partial}{\partial y}(\mu \frac{\partial v}{\partial x}) + \frac{\partial}{\partial z}(\mu \frac{\partial w}{\partial x}) \quad (2-180)$$

$$T_y = \frac{\partial}{\partial x}(\mu \frac{\partial u}{\partial y}) + \frac{\partial}{\partial y}(\mu \frac{\partial v}{\partial y}) + \frac{\partial}{\partial z}(\mu \frac{\partial w}{\partial y}) \quad (2-181)$$

$$T_z = \frac{\partial}{\partial x}(\mu \frac{\partial u}{\partial z}) + \frac{\partial}{\partial y}(\mu \frac{\partial v}{\partial z}) + \frac{\partial}{\partial z}(\mu \frac{\partial w}{\partial z}) \quad (2-182)$$

Turbulent flow is the time-mean behavior of these flows that is usually of practical interest. Therefore, the equations for unsteady laminar flow are converted into the time-averaged equations for turbulent flow by an averaging operation in which it is assumed

that there are rapid and random fluctuations about the mean value. The additional terms arising from this operation are the so-called Reynolds stresses, turbulent heat flux, turbulent diffusion flux, *et al.* To express these fluxes in terms of the mean properties of the flow is the task of a turbulence model. The instantaneous turbulent velocity is expressed in terms of:

$$u_i = \bar{u}_i + \bar{u}'_i \quad (2-183)$$

where u_i is mean component of velocity in i -direction; \bar{u}'_i is the fluctuating component of velocity in the i -direction. By introducing this expression in the Navier-Stokes equations and noting that the time average of the fluctuating component is zero, and the time average of the instantaneous value is the average value, the time averaging leads to additional terms. The velocities in the momentum equations are the averaged ones, the absence of a bar implies the mean value, so that the extra terms are:

$$\sigma^R_x = -\frac{\partial}{\partial x}(\rho \bar{u}'u') - \frac{\partial}{\partial y}(\rho \bar{u}'v') - \frac{\partial}{\partial z}(\rho \bar{u}'w') \quad (2-184)$$

$$\sigma^R_y = -\frac{\partial}{\partial x}(\rho \bar{u}'v') - \frac{\partial}{\partial y}(\rho \bar{v}'v') - \frac{\partial}{\partial z}(\rho \bar{v}'w') \quad (2-185)$$

$$\sigma^R_z = -\frac{\partial}{\partial x}(\rho \bar{u}'w') - \frac{\partial}{\partial y}(\rho \bar{v}'w') - \frac{\partial}{\partial z}(\rho \bar{w}'w') \quad (2-186)$$

where σ^R is Reynolds stress terms. The Reynolds stress terms are replaced by using the Boussinesq eddy-viscosity definition ⁽⁷⁰⁾

$$-\rho \bar{u}'u' = 2\mu_t \frac{\partial u}{\partial x} - \rho \frac{2}{3} k \quad (2-187)$$

$$-\rho \bar{v}'v' = 2\mu_t \frac{\partial v}{\partial y} - \rho \frac{2}{3} k \quad (2-188)$$

$$-\rho \bar{w}'w' = 2\mu_t \frac{\partial w}{\partial z} - \rho \frac{2}{3} k \quad (2-189)$$

$$-\rho \bar{u}'v' = -\rho \bar{v}'u' = \mu_t \left(\frac{\partial u}{\partial y} + \frac{\partial v}{\partial x} \right) \quad (2-190)$$

$$-\rho \bar{u}'w' = -\rho \bar{w}'u' = \mu_t \left(\frac{\partial u}{\partial z} + \frac{\partial w}{\partial x} \right) \quad (2-191)$$

$$-\rho \bar{v}'w' = -\rho \bar{w}'v' = \mu_t \left(\frac{\partial v}{\partial z} + \frac{\partial w}{\partial y} \right) \quad (2-192)$$

For incompressible flow, T_x , T_y , T_z are eliminated, and the Boussinesq eddy-viscosity definition leads the final form of the momentum equations as follows:

$$\begin{aligned} \rho u \frac{\partial u}{\partial x} + \rho v \frac{\partial u}{\partial y} + \rho w \frac{\partial u}{\partial z} = -\frac{\partial p}{\partial x} - \frac{2}{3} \rho \frac{\partial k}{\partial x} + \\ 2 \frac{\partial}{\partial x} \left[(\mu + \mu_t) \frac{\partial u}{\partial x} \right] + \frac{\partial}{\partial y} \left[(\mu + \mu_t) \left(\frac{\partial u}{\partial y} + \frac{\partial v}{\partial x} \right) \right] + \frac{\partial}{\partial z} \left[(\mu + \mu_t) \left(\frac{\partial u}{\partial z} + \frac{\partial w}{\partial x} \right) \right] \end{aligned} \quad (2-193)$$

$$\begin{aligned} \rho u \frac{\partial v}{\partial x} + \rho v \frac{\partial v}{\partial y} + \rho w \frac{\partial v}{\partial z} = -\frac{\partial p}{\partial y} - \frac{2}{3} \rho \frac{\partial k}{\partial y} + \\ \frac{\partial}{\partial x} \left[(\mu + \mu_t) \left(\frac{\partial u}{\partial y} + \frac{\partial v}{\partial x} \right) \right] + 2 \frac{\partial}{\partial y} \left[(\mu + \mu_t) \frac{\partial v}{\partial y} \right] + \frac{\partial}{\partial z} \left[(\mu + \mu_t) \left(\frac{\partial v}{\partial z} + \frac{\partial w}{\partial y} \right) \right] \end{aligned} \quad (2-194)$$

$$\begin{aligned} \rho u \frac{\partial w}{\partial x} + \rho v \frac{\partial w}{\partial y} + \rho w \frac{\partial w}{\partial z} = -\frac{\partial p}{\partial z} - \frac{2}{3} \rho \frac{\partial k}{\partial z} + \\ \frac{\partial}{\partial x} \left[(\mu + \mu_t) \left(\frac{\partial u}{\partial z} + \frac{\partial w}{\partial x} \right) \right] + \frac{\partial}{\partial y} \left[(\mu + \mu_t) \left(\frac{\partial v}{\partial z} + \frac{\partial w}{\partial y} \right) \right] + 2 \frac{\partial}{\partial z} \left[(\mu + \mu_t) \frac{\partial w}{\partial z} \right] \end{aligned} \quad (2-195)$$

Energy equations

For a flow without volumetric heat source and viscous work terms, the energy equation in terms of the total temperature for incompressible flow is:

$$\begin{aligned} \frac{\partial}{\partial x} (\rho u C_p T) + \frac{\partial}{\partial y} (\rho v C_p T) + \frac{\partial}{\partial z} (\rho w C_p T) = \\ k \left(\frac{\partial^2 T}{\partial x^2} + \frac{\partial^2 T}{\partial y^2} + \frac{\partial^2 T}{\partial z^2} \right) + \rho c_p (\overline{u'T'} + \overline{v'T'} + \overline{w'T'}) + \Phi + E^k \end{aligned} \quad (2-196)$$

Note that the viscosity dissipation term Φ has been ignored. The kinetic energy term E^k for this flow is small and therefore neglected.

The turbulent heat flux terms are replaced by the Boussinesq eddy viscosity definition and the relationship between the turbulent diffusivity of heat and turbulent viscosity as follows:

$$-\rho c_p \overline{u'T'} = \frac{c_p \mu_t}{\sigma_t} \frac{\partial T}{\partial x} \quad (2-197)$$

$$-\rho c_p \overline{v'T'} = \frac{c_p \mu_t}{\sigma_t} \frac{\partial T}{\partial y} \quad (2-198)$$

$$-\rho c_p \overline{w'T'} = \frac{c_p \mu_t}{\sigma_t} \frac{\partial T}{\partial z} \quad (2-199)$$

This leads to the final form for the incompressible, steady-state energy equation

$$\rho c_p \left(u \frac{\partial T}{\partial x} + v \frac{\partial T}{\partial y} + w \frac{\partial T}{\partial z} \right) = \frac{\partial}{\partial x} \left[\left(k + \frac{c_p \mu_t}{\sigma_t} \right) \frac{\partial T}{\partial x} \right] + \frac{\partial}{\partial y} \left[\left(k + \frac{c_p \mu_t}{\sigma_t} \right) \frac{\partial T}{\partial y} \right] + \frac{\partial}{\partial z} \left[\left(k + \frac{c_p \mu_t}{\sigma_t} \right) \frac{\partial T}{\partial z} \right] \quad (2-200)$$

For turbulent flow, μ varies. Many turbulence models employ the concept of a turbulent viscosity or a turbulent diffusivity to express the turbulent stresses and fluxes. The result is that the time-averaged equations for turbulent flow are of the same form as the equations for laminar flow, but the laminar exchange coefficients such as viscosity, diffusivity, and conductivity are replaced by effective (i.e., laminar plus turbulent) exchange coefficients. From a computational viewpoint, a turbulent flow within this framework is equivalent to a laminar flow with a rather complicated prescription of viscosity.

For high Reynolds k - ε model the turbulence transport equations are the high turbulence Reynolds number k - ε turbulence model as follows:

ε (turbulent kinetic energy dissipation rate) equation:

$$\rho \left(u \frac{\partial \varepsilon}{\partial x} + v \frac{\partial \varepsilon}{\partial y} + w \frac{\partial \varepsilon}{\partial z} \right) = \frac{\partial}{\partial x} \left[\left(\mu + \frac{\mu_t}{\sigma_\varepsilon} \right) \frac{\partial \varepsilon}{\partial x} \right] + \frac{\partial}{\partial y} \left[\left(\mu + \frac{\mu_t}{\sigma_\varepsilon} \right) \frac{\partial \varepsilon}{\partial y} \right] + \frac{\partial}{\partial z} \left[\left(\mu + \frac{\mu_t}{\sigma_\varepsilon} \right) \frac{\partial \varepsilon}{\partial z} \right] + \frac{c_1 \varepsilon}{K} \mu_t \left[2 \left(\frac{\partial u}{\partial x} \right)^2 + 2 \left(\frac{\partial v}{\partial y} \right)^2 + 2 \left(\frac{\partial w}{\partial z} \right)^2 + \left(\frac{\partial u}{\partial x} + \frac{\partial v}{\partial y} + \frac{\partial w}{\partial z} \right)^2 \right] - \frac{c_2 \rho \varepsilon^2}{K} \quad (2-201)$$

k (turbulent kinetic energy) equation:

$$\rho \left(u \frac{\partial K}{\partial x} + v \frac{\partial K}{\partial y} + w \frac{\partial K}{\partial z} \right) = \frac{\partial}{\partial x} \left[\left(\mu + \frac{\mu_t}{\sigma_k} \right) \frac{\partial K}{\partial x} \right] + \frac{\partial}{\partial y} \left[\left(\mu + \frac{\mu_t}{\sigma_k} \right) \frac{\partial K}{\partial y} \right] + \frac{\partial}{\partial z} \left[\left(\mu + \frac{\mu_t}{\sigma_k} \right) \frac{\partial K}{\partial z} \right] + \mu_t \left[2 \left(\frac{\partial u}{\partial x} \right)^2 + 2 \left(\frac{\partial v}{\partial y} \right)^2 + 2 \left(\frac{\partial w}{\partial z} \right)^2 + \left(\frac{\partial u}{\partial x} + \frac{\partial v}{\partial y} + \frac{\partial w}{\partial z} \right)^2 \right] - \rho \varepsilon \quad (2-200)$$

where the turbulent viscosity μ_t is expressed as:

$$\mu_t = \frac{c_\mu \rho K^2}{\varepsilon} \quad (2-203)$$

The five empirical coefficients incorporated in equations (2-201) to (2-203) are tabulated in Table 2-4⁽⁷⁰⁾.

By numerical computational techniques we may discretize high order derivative equations into a linear combination of variables which are solvable by iterative techniques using different algorithms. Current codes for numerical simulations of fluid flows are finite element analysis, finite differential method, and finite volume method. This research will focus on the finite element analysis technique.

2.5 Radiation Heat Transfer Solutions

Radiation is a form of energy transported by electromagnetic waves at the speed of light without incorporating physical medium. Thermal radiation happens in the form of heat energy transferred by electromagnetic waves emitted from a surface caused by its temperature. Thermal radiation waves represent only a small band in the electromagnetic spectrum.

The radiation equation of the rate of heat transfer between two surfaces i and j is mathematically described by the Stefan-Boltzmann law as follows:

$$q_i = A_i F_{ij} \epsilon_i \sigma (T_i^4 - T_j^4) \quad (2-204)$$

where q_i is heat transfer rate from surface i ; A_i is area of the radiating surface; F_{ij} is view factor from surface i to surface j ; ϵ_i is effective emissivity; σ Stefan-Boltzmann constant ($5.67 \times 10^{-8} \text{ W/m}^2 \cdot \text{K}^4$ or $0.119 \times 10^{-10} \text{ Btu/hr-in}^2 \cdot \text{R}^4$); and T_i , T_j are the absolute temperature of the two surfaces.

If there are multiple surfaces (N in number) emitting and receiving thermal radiation, the thermal radiation equation becomes ⁽⁶⁶⁾:

$$\sum_{i=1}^N (\delta_{ji} - F_{ji}) \sigma T^4 = \sum_{i=1}^N \left\{ \frac{\delta_{ij}}{\epsilon_i} - F_{ji} \frac{1 - \epsilon_i}{\epsilon_i} \right\} \frac{1}{A_i} q_i \quad (2-205)$$

where i, j are the surface indices; δ_{ij} is the Kronecker delta; when $j = i$, $\delta_{ij} = 1$, $j \neq i$, $\delta_{ij} = 0$.

Radiation heat is determined by the emitting and receiving surface areas, surface temperatures, and effective emissivity, view factors. The effective emissivity is determined by the materials of surfaces, surface temperature, surface characteristics such as roughness, color *et al*, and the wave length of incoming radiation wave. The view factors between two surfaces i and j are defined as the percentage of the total radiant

energy that is emitted from one surface and reaches the other surface. The view factor from surface i to j is described as ⁽⁷³⁾:

$$F_{ij} = \frac{\text{radiant energy received by surface } j \text{ from } i}{\text{total radiant energy emitted by surface } i} \quad (2-206)$$

$$F_{ji} = \frac{\text{radiant energy received by surface } i \text{ from } j}{\text{total radiant energy emitted by surface } j} \quad (2-207)$$

The relation between any two of the surfaces is:

$$A_i F_{ij} = A_j F_{ji} \quad (2-208)$$

The relation among all the enclosed surfaces is:

$$\sum_{i=1}^N F_{ij} = 1 \quad (2-209)$$

The value of dimensionless view factor is a function of several phenomena as follows:

- the surface geometry involved,
- the distance between the surfaces,
- and the normal direction of the surfaces with respect to each other.

The mathematical description for the view factors can be derived by infinitesimal areas dA_i and dA_j on two surfaces i and j (Fig.2-27) ⁽⁷³⁾ with the equation ⁽⁷³⁾ as:

$$F_{ij} = \frac{1}{A_i} \int_{A_i} \int_{A_j} \frac{\cos\theta_i \cos\theta_j}{\pi r^2} dA_i dA_j \quad (2-210)$$

$$F_{ij} = \frac{1}{A_j} \int_{A_j} \int_{A_i} \frac{\cos\theta_i \cos\theta_j}{\pi r^2} dA_i dA_j \quad (2-211)$$

Table 2-1 Thermal Conductivity Data For A Typical 2S-2P-Layer Board

Layer #	t(μm)	α (%)	K_{av} (W/m K)	Notes
1	34	20	77.5	signal layer
2	595	0	0.6	
3	34	100	385.0	power plane
4	595	0	0.6	
5	34	100	385.0	ground plane
6	595	0	0.6	
7	34	35	135.1	signal layer

Table 2-2 The Average Board Thermal Conductivity Details

T (mm)	K_{FR4} (W/m K)	K_{Cu} (W/m K)	K_p (W/m K)	K_n (W/m K)
1.92	0.59	385	17.9	0.63

Table 2-3 Contact Parameters

α ($^\circ$)	30	40	50	60	70	80	90
m	2.731	2.136	1.754	1.486	1.284	1.128	1.000
n	0.493	0.567	0.641	0.717	0.802	1.893	1.000

Table 2-4 The Empirical Coefficients For κ - ϵ Model

C_μ	C_1	C_2	σ_k	σ_ϵ
0.09	1.44	1.92	1.0	1.3

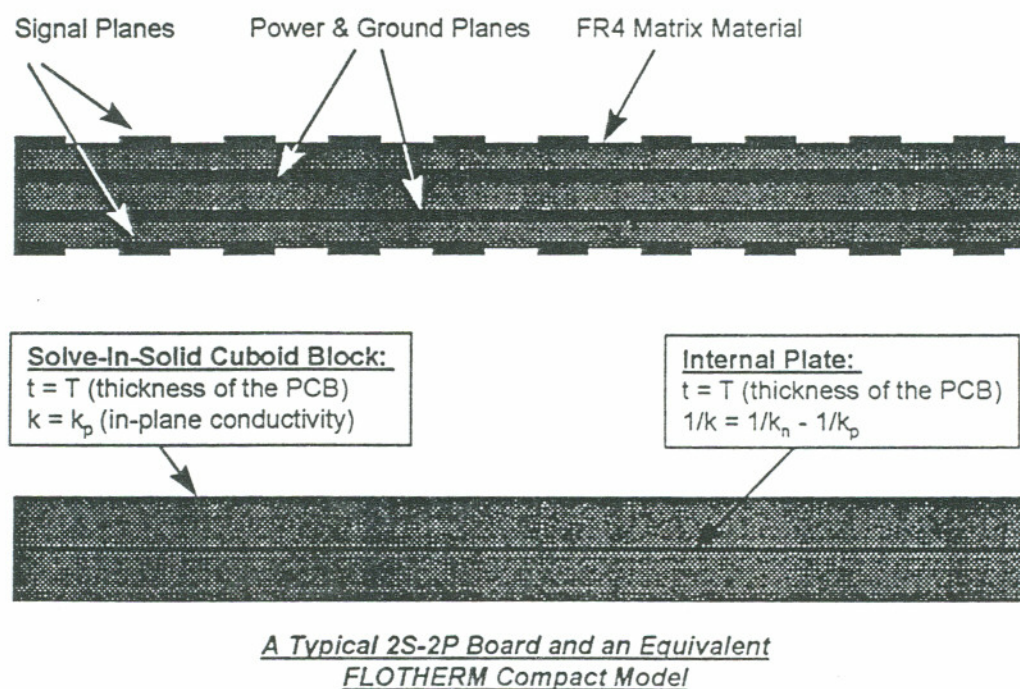


Fig.2-1 A Typical Multiple Layer Circuit Board (Adapted From Ref. 1)

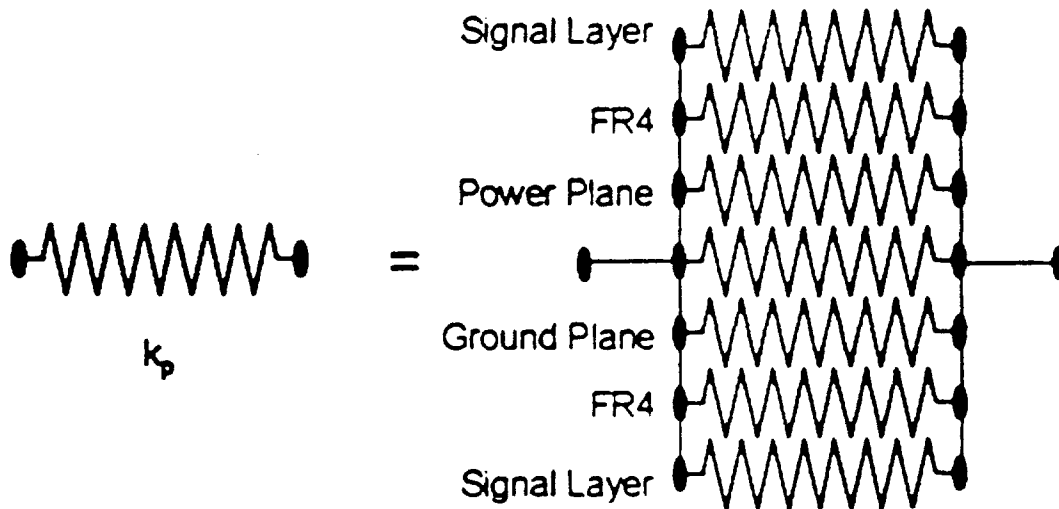


Fig.2-2 **Equivalent In-Plane Conductivity (Adapted From Ref. 1)**

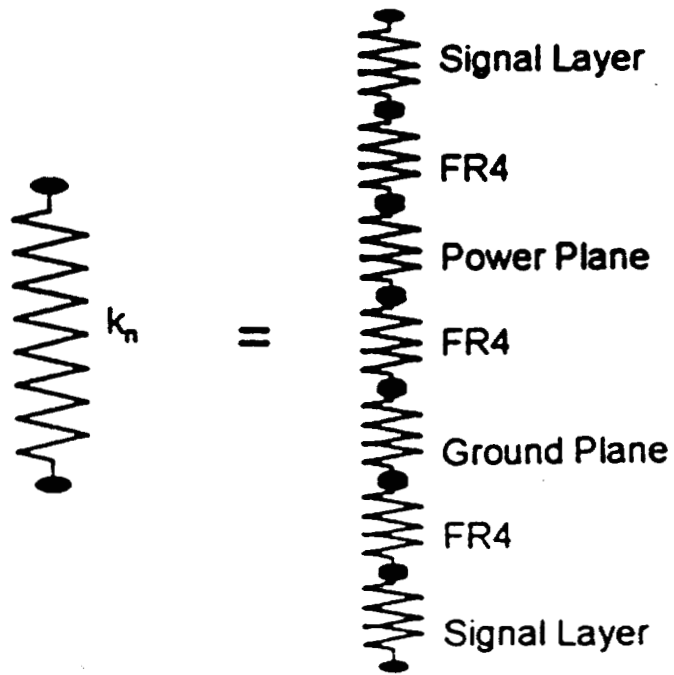


Fig.2-3 **Equivalent Through-Plane Conductivity (Adapted From Ref. 1)**

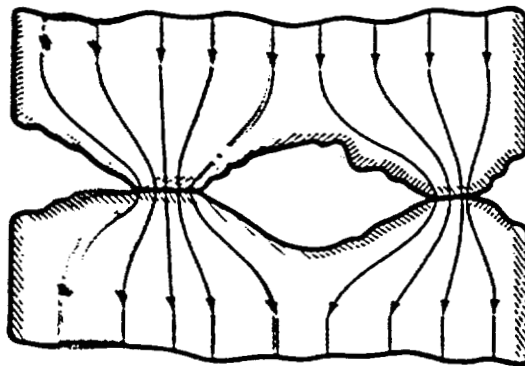


Fig.2-4

Heat Flow Across the Real Contact Surfaces (Adapted From Ref. 30)

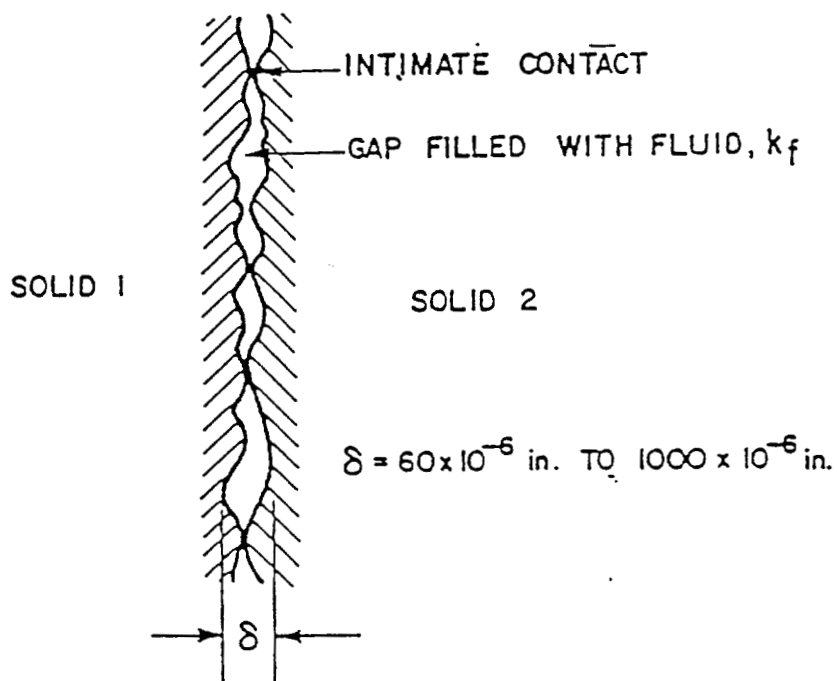


Fig.2-5 Real Contact Interface (Adapted From Ref. 82)

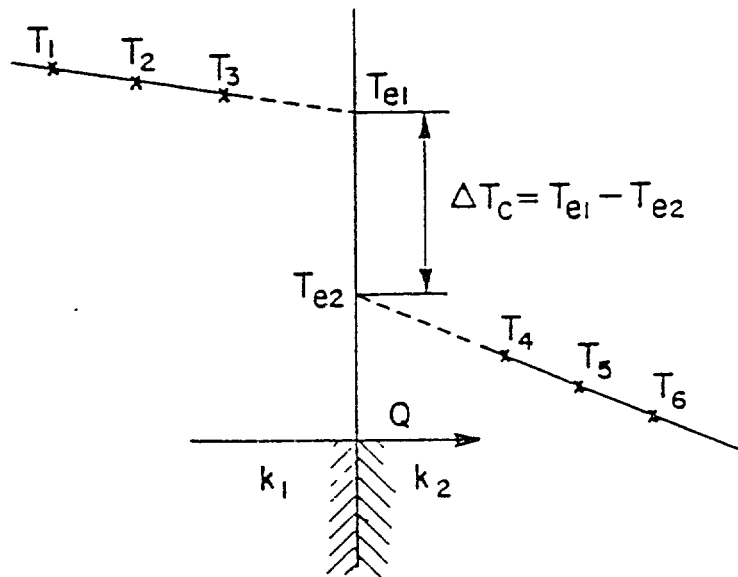


Fig.2-6 Linear Heat Flow Across a Real Contact Interface (Adapted From Ref. 82)

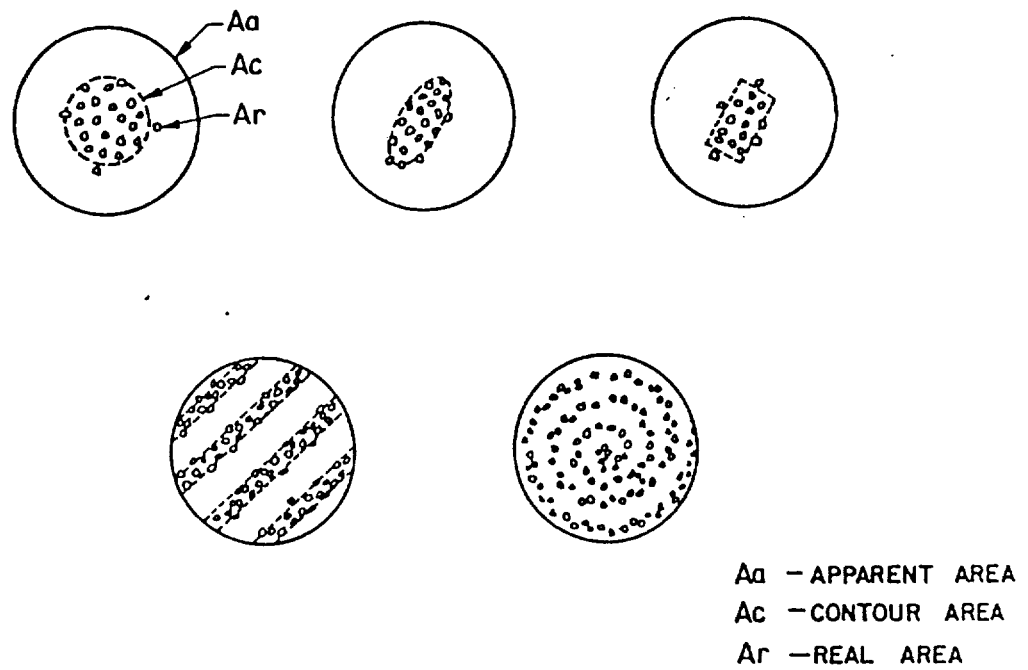


Fig.2-7

Microscopic View of Real Contact Areas (Adapted From Ref. 68)

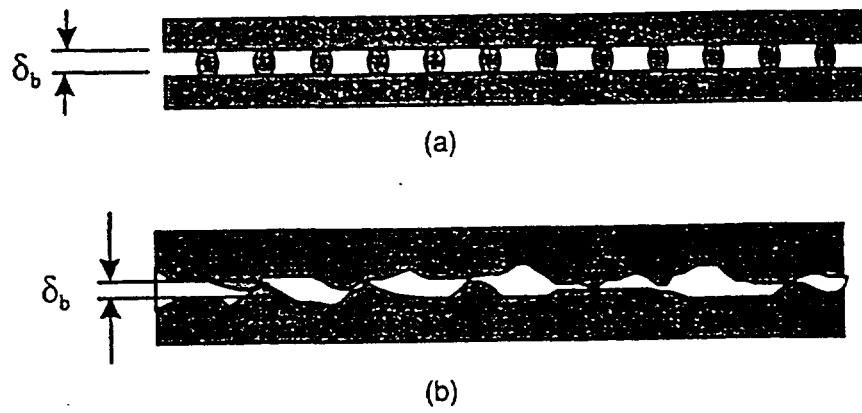


Fig.2-8 Thermal Interfaces; (a) Solder Bump Array; (b) Contact Interfaces (Adapted From Ref. 42)

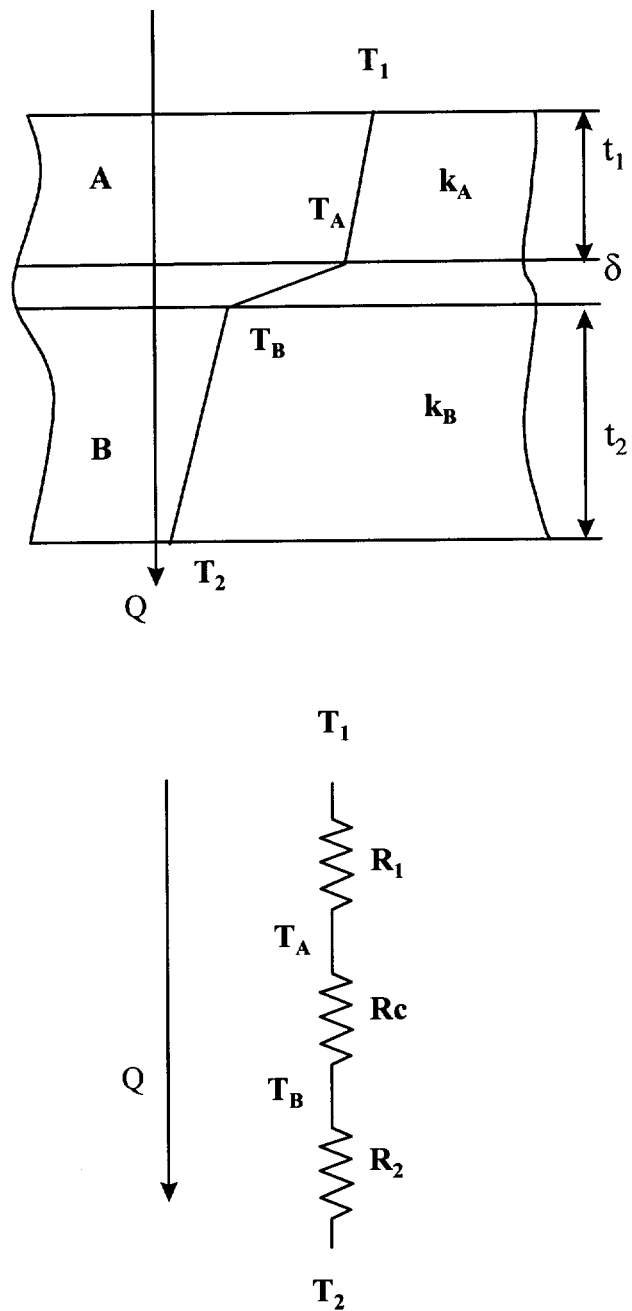


Fig.2-9

Two Solid Plates in Contact with an Interfacial Filler Substance

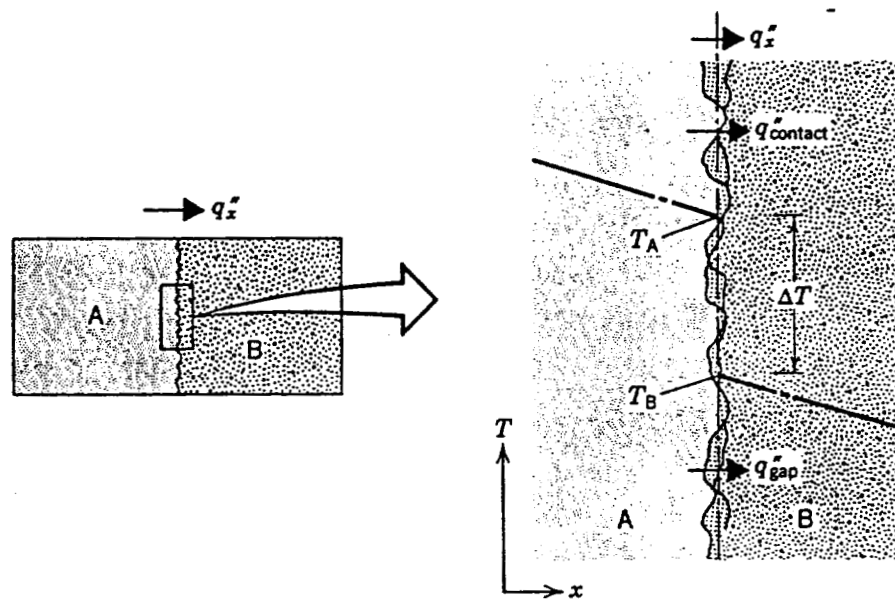


Fig.2-10 Heat Flow Paths and Temperature Drop due to Thermal Resistance
(Adapted From Ref. 38)

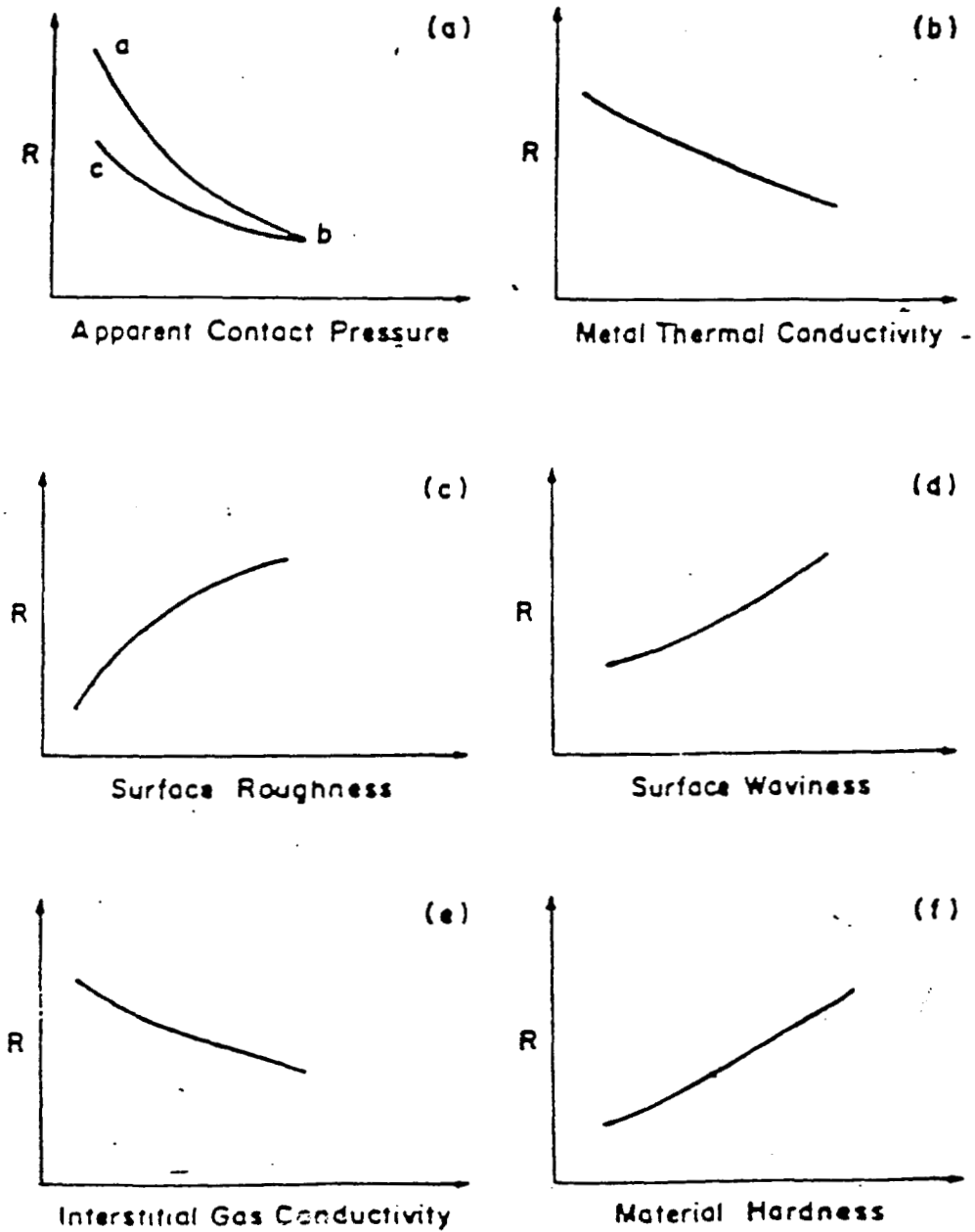


Fig.2-11(a)-(f) The Contact Thermal Resistance Factors (Adapted From Ref. 68)

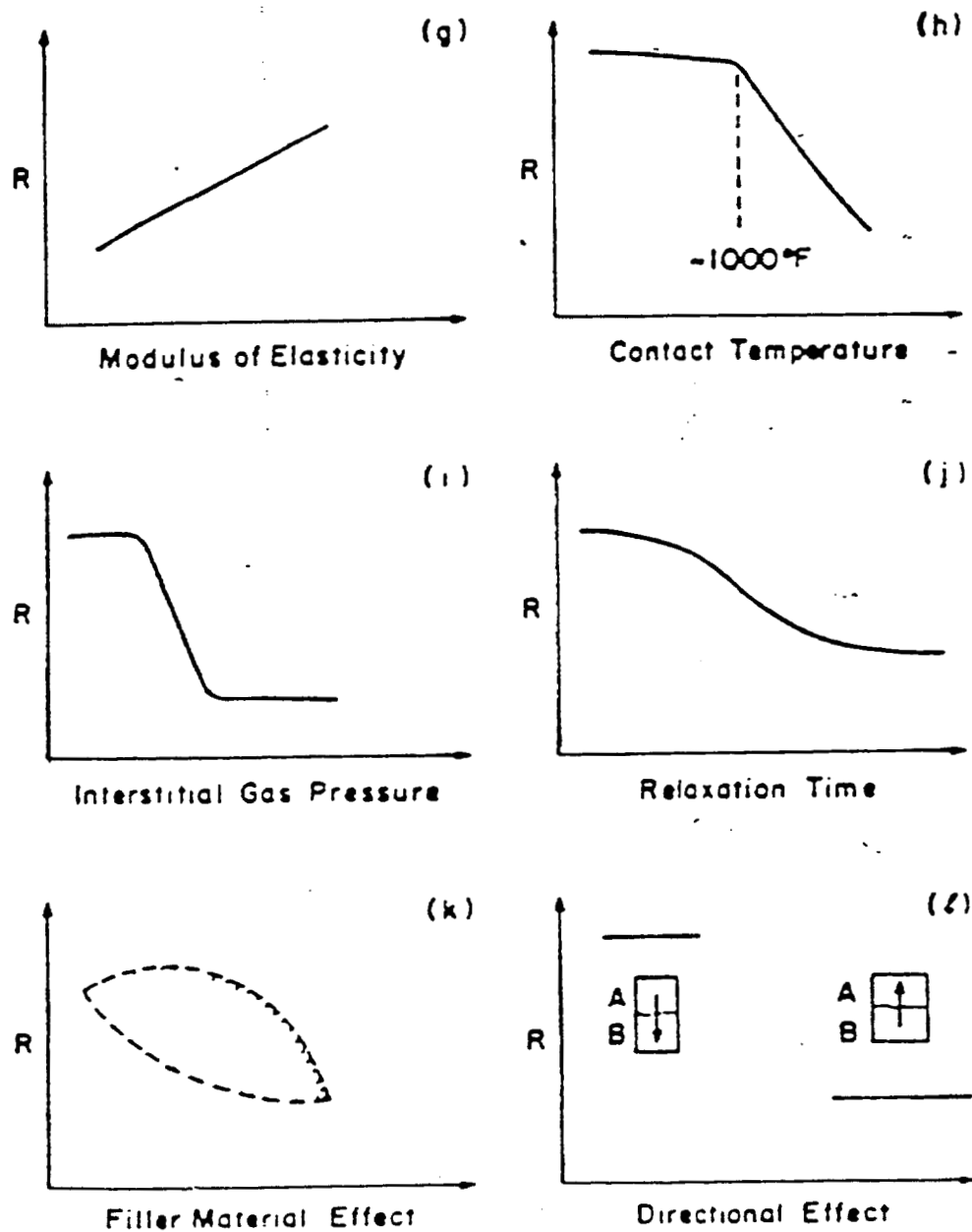


Fig.2-11(g)-(l)

The Thermal Contact Resistance Factors (Adapted From Ref. 68)

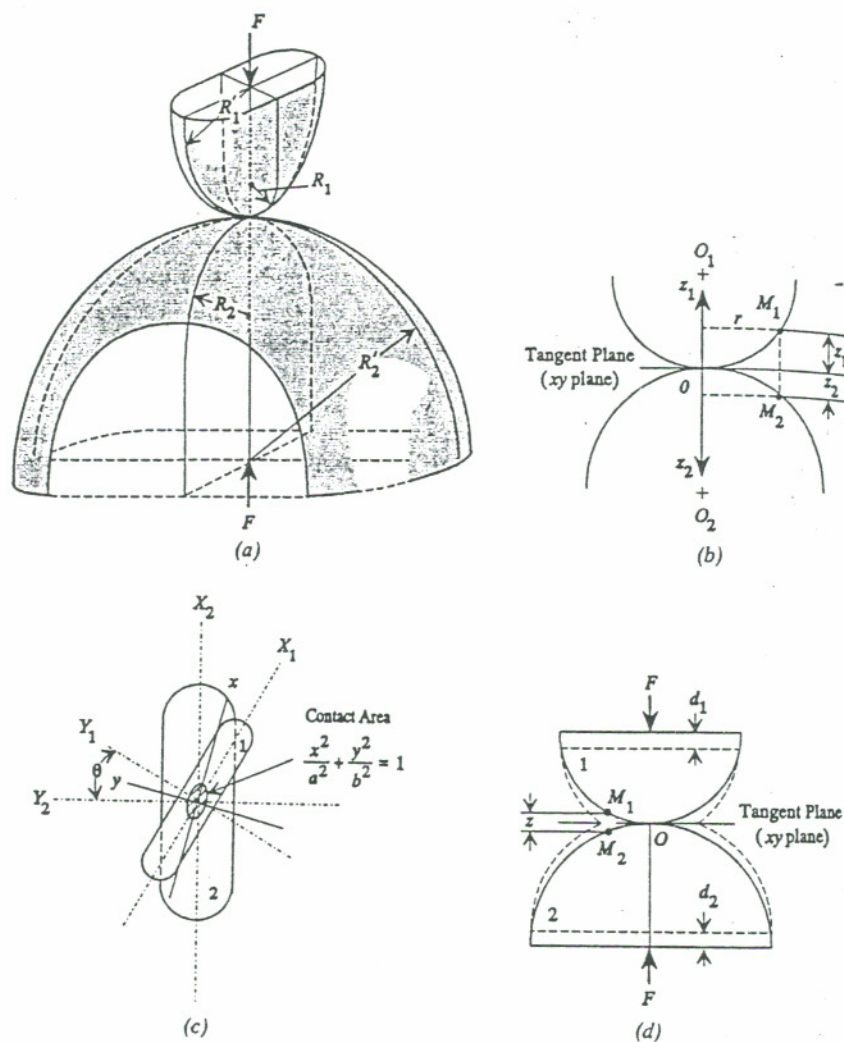
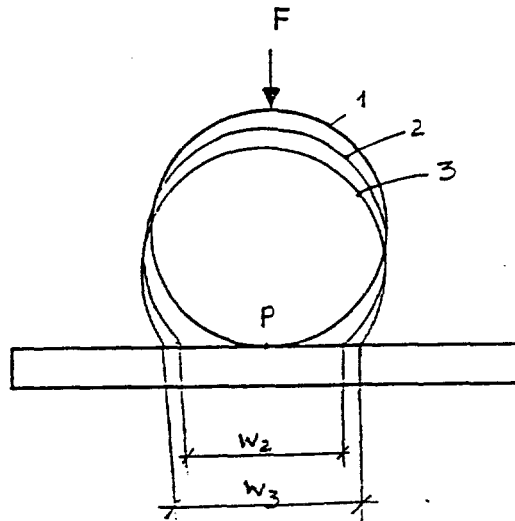
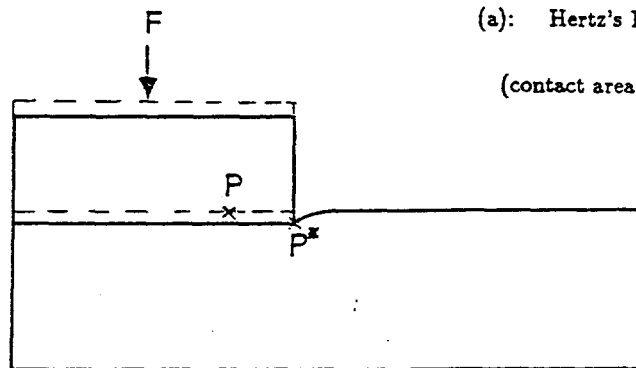


Fig.2-13 Two Elastic Solids in Contact: (a) Contact Configuration; (b) Before Loading; (c) After Loading; (d) Displacement of Contacting Points M_1 and M_2 and Rigid Distance of Approach $d=d_1+d_2$ (Adapted From Ref. 60)



(a): Hertz's Problem.

(contact area exaggerated)



(b): Punch Problem.

Fig.2-14 Nonlinear Boundary Conditions in Contact Problems (Adapted From Ref. 50)

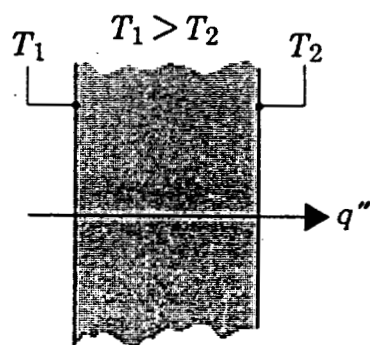


Fig.2-15 **Conduction Through An Solid (Adapted From Ref. 38)**

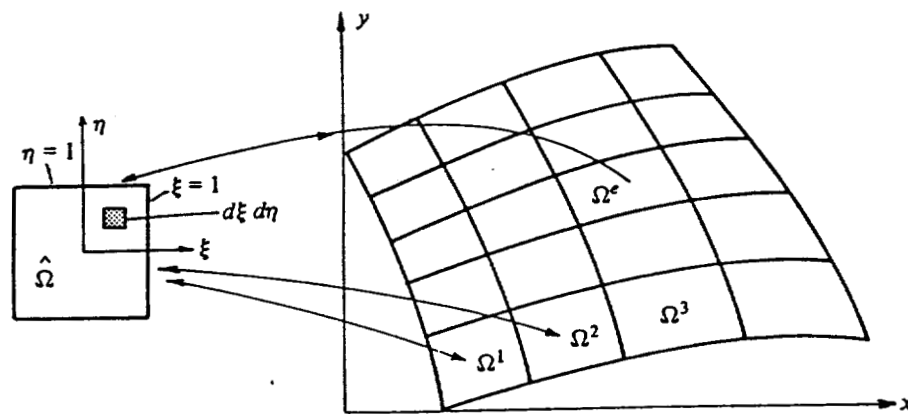


Fig.2-16 Transformation of Arbitrarily Shaped Quadrilateral Elements to the Master Rectangular Element for Numerical Evaluation of Integral Expressions (Adapted from Ref. 62)

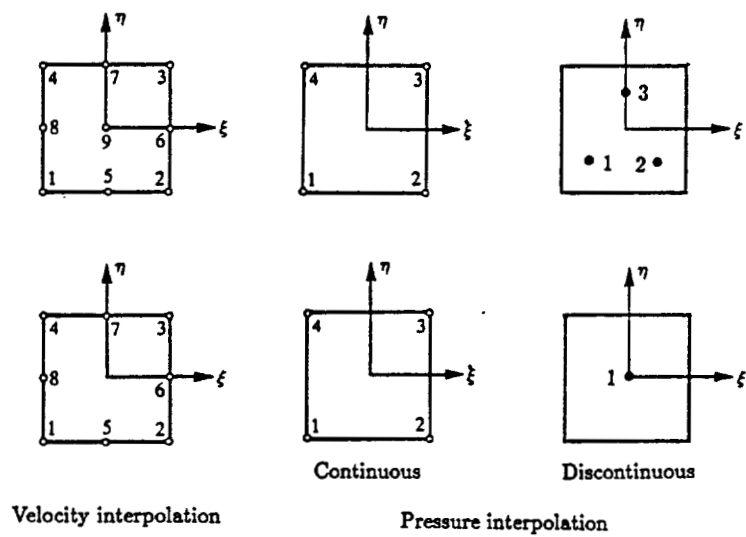


Fig 2-17

The Quadrilateral Elements used for the Mixed Model (Adapted From Ref. 62)

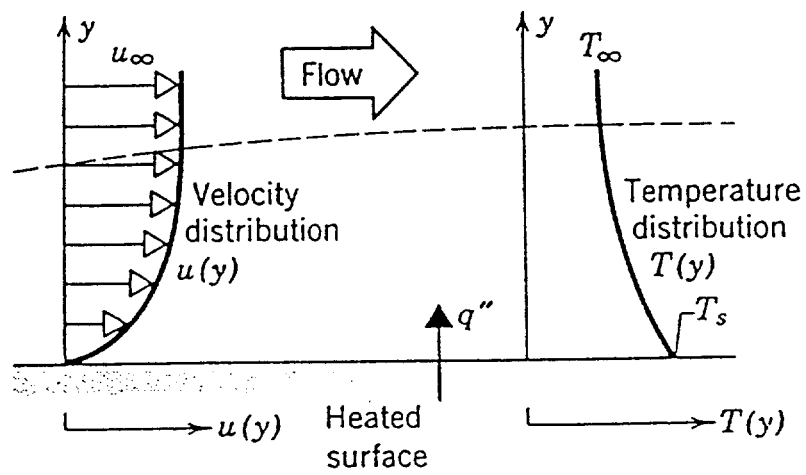


Fig 2-18 Boundary Layer of Fluid Flow at Solid Surface (Adapted From Ref. 38)

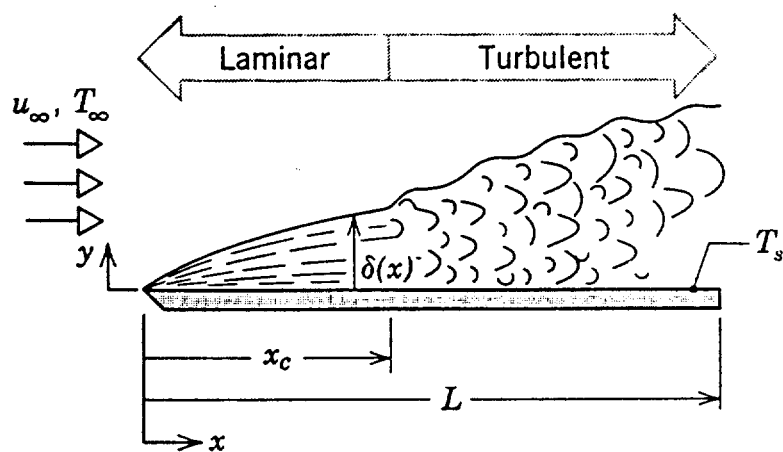


Fig 2-19 Parallel Flow Over a Flat Plate (Adapted From Ref. 38)

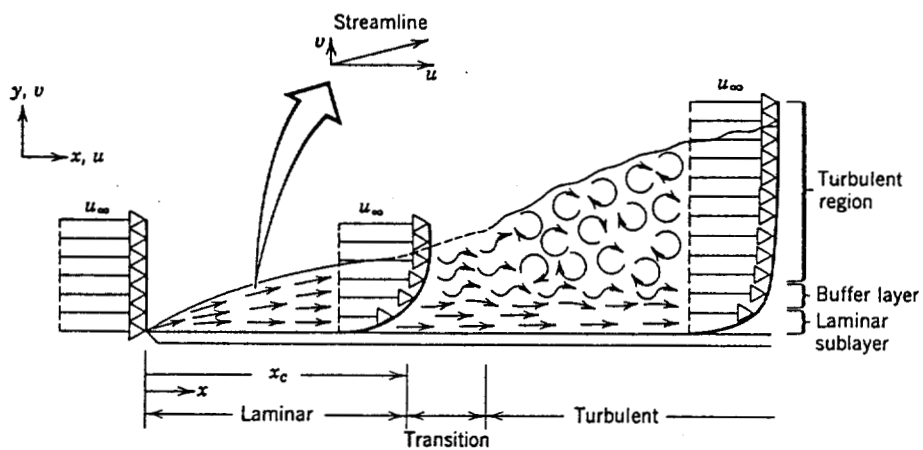


Fig 2-20 Velocity Boundary Layer Development on A Flat Plate (Adapted From Ref. 38)

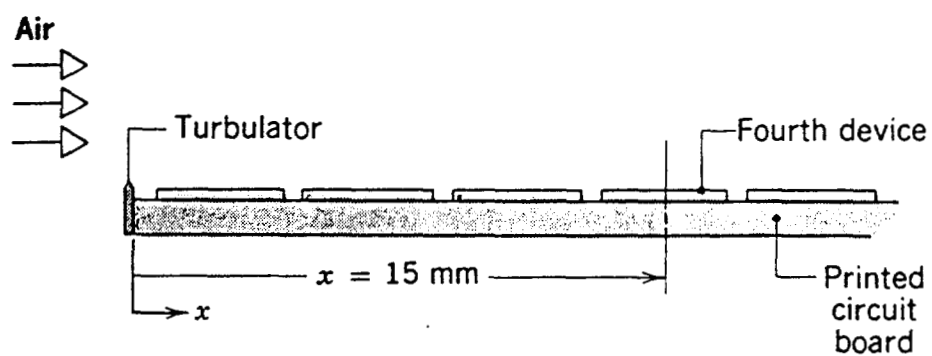


Fig 2-21 Using Parallel Flow Over a Flat Plate to Estimate Surface Temperature of Chips (Adapted From Ref. 38)

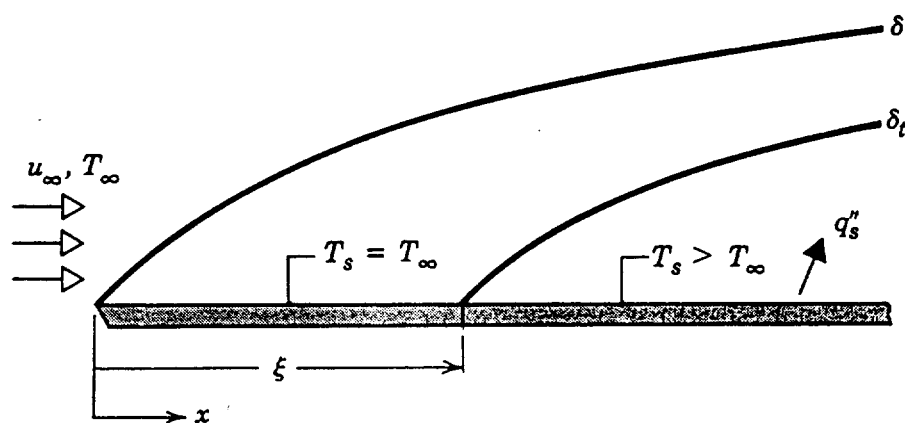


Fig 2-22 Flat Plate in Parallel Flow With Unheated Starting Length (Adapted From Ref. 38)

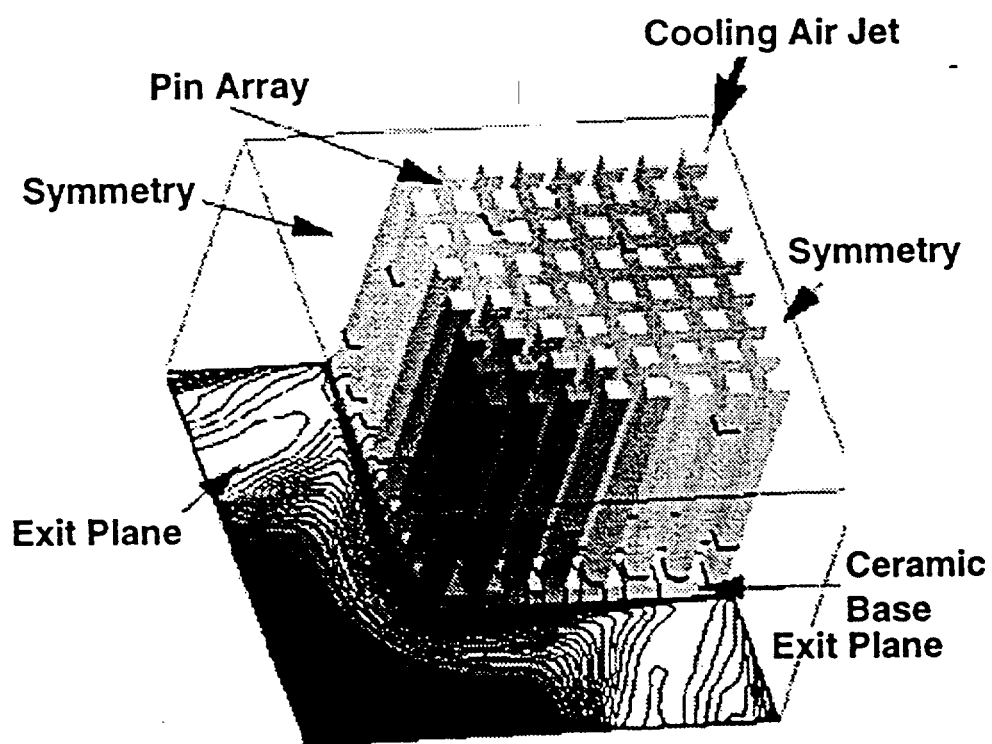


Fig 2-23 Configuration For the Heat Sink Impingement (Adapted From Ref. 61)

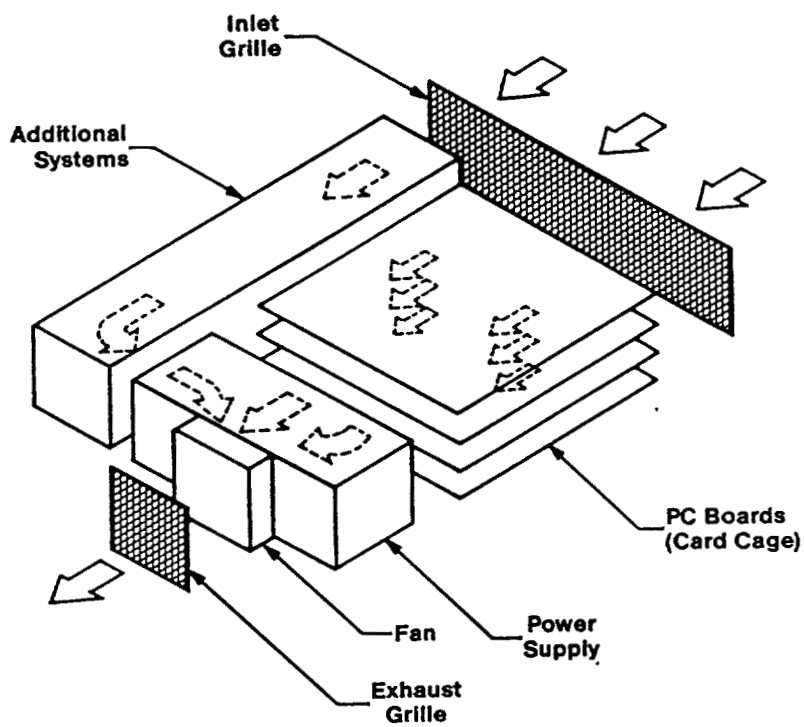


Fig 2-24 Typical Small Machine Air Flow Paths (Adapted From Ref. 64)

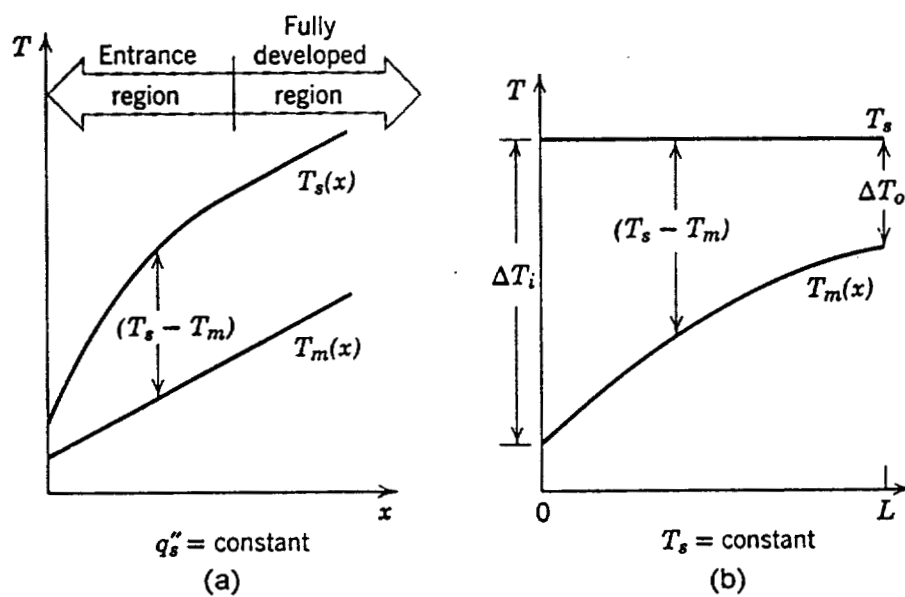


Fig 2-25 Axial Temperature Variations For A Pipe. (a) With Constant Wall Heat Flux; (b) With Constant Wall Temperature (Adapted From Ref. 38)

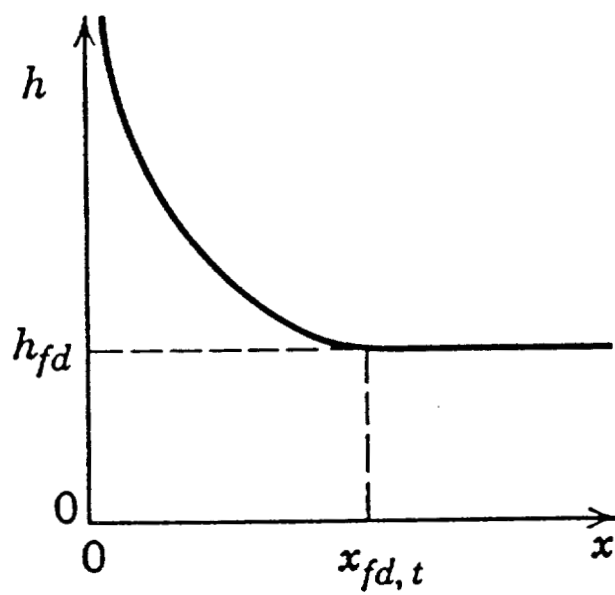


Fig 2-26 Convective Heat Transfer Coefficient For Flow In A Pipe (Adapted From Ref. 38)

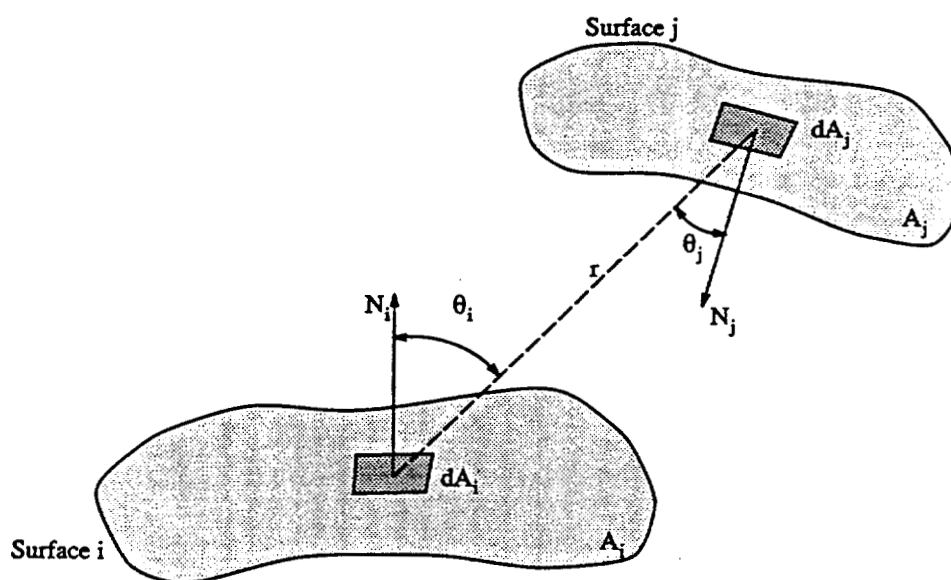


Fig 2-27 Calculation View Factors Between Two Arbitrary Surfaces (Adapted From Ref. 73)

CHAPTER 3

CASE STUDIES

3.1 Component Level Simulation

3.1.1. Modeling of Multi-chip Modules (MCM) with Thermal Vias

In the MCM a 133 Mhz P5 microprocessor, three MX, four DRAM and two SRAM are mounted on a fused multi-layer Alumina ceramic board with epoxy adhesive under the each electronic component (Fig.3-1). The design criteria for the thermal design are as follows:

- The maximum IC temperature for all the components is below 100°C.
- The maximum in-plane dimension of the modules is less than 1.5".
- The packaging board is more than 40 μm and less than 100 μm thick.
- Heat transfer enhancement is allowed.

This thermal design is a typical component level simulation with the combination of multiple factors involved such as the material properties, geometries of the substrate, epoxy adhesive layer, locations of the components, and the factors introduced by any heat transfer enhancement. Since there are ten different components on this package, there are numerous combinations of the configurations to be optimized with the geometries and material properties, an efficient simulation plan is the first step of all the thermal management procedures.

For this engineering implementation, the numerical simulation of the thermal management design for this package is divided into two stages; component level simulation for the individual component, and package level simulation for the combination of the whole package. The first step is to determine the critical components for the individual component level analysis. The critical component is the one with the highest temperature for the thermal issue, and the largest deformation or stress for the structural issue (which has not involved yet for this particular problem). The highest IC

temperature is always associated with the highest power density and less efficient heat transfer paths which provide lower out-heat-flux of the packaging or in-heat-flux adjacent to heat sources. From an electrical layout of this MCM packaging the Pentium processor had the largest power dissipation rate than other components, and it is surrounded by the other ICs, the hottest spot is expected to be associated with it. Therefore, the Pentium microprocessor was the object of the component level simulation at the first stage.

Conduction heat transfer through the substrate is the only way to dump the heat out of the packaging, and the thermal resistance is $R = t / AK$, where t is the substrate thickness, A is the heat conduction area between the Pentium and the substrate which is unchangeable, and k is the thermal conductivity of the substrate. The thermal resistance could be reduced by decreasing the substrate thickness. As a preliminary simulation by the operating requirements, two schematics are setup to find the temperature difference corresponding to two substrate thickness. The simulation cases are:

- a) Chip mounted on a 96 μm thick ceramic substrate,
- b) Chip mounted on a 48 μm thick ceramic substrate.

The outer surface of the substrate is assumed to be at a temperature as high as 90°C. The temperatures are obtained with a FEM model as Table 3-1. The temperature decreased about 14% after decreasing the substrate thickness by 50%, and the temperature was still 116°C which is unacceptable. Because there is no other choice to replace ceramic substrate which has lower thermal conductivity (18W/mK), and the temperature dropped slow with the substrate thickness decrease within the allowable thickness range all of heat transfer enforcement is critical for the success of the 100°C target in the next step.

To enhance the conduction heat transfer through the substrate, there are two directions to dissipate the heat, in-plane and through-plane directions. Generally, in-plane enhancement needs imbedding many metal plates like copper to spread the heat in the planar direction. Through plane enhancement could be done by implanting thermal vias with the high thermal conductivity materials like tungsten through the substrates and boards. The selecting of the direction for heat transfer enhancement depends on the path which is shortest to the cold end. "Shorter" means less thermal resistance, instead of the dimensional "shortest length" from the hot spot to the cold end. It may need heat transfer

enhancement in one direction or both directions. For this type of problem, because the cold surface is at the bottom of the substrate, and there is not enough space to bury more copper plates, from the chip where the hot spot resides to the cold end, thermal vias are better solutions for enhancing the heat transfer.

After the enhancement is selected, the third step is to verify the thermal configuration by simulation. The models are built with tungsten vias in different combinations of the number of the vias, the thickness of the ceramic board. The parametric combinations for the packaging layout examined in this study are:

- c) Chip mounted on a 96 μm thick ceramic substrate with thermal vias
- d) Chip mounted on a 48 μm thick ceramic substrate with thermal vias

Simulation results summarized in Table 3-2 showed that the minimum maximum Pentium temperature was 95°C with the thermal vias and 48 μm thick board. It dropped 18% more compared that without the vias. This component level design has successfully optimized the thermal management configuration focusing on the hottest IC “locally”. Further verification and modification is needed to verify whether the design is good “globally” or at the package level.

The fourth step is to assemble all the other components on a full size board of 1.5" with thermal vias to check the maximum IC temperature. Since for the component level simulation only for the Pentium, there were 200 thermal vias implanted beneath the chip, it took 60,000 elements to get a converged solution. Elements for the whole packaging domain with all the components were failed since the total number of elements exceeded the license limit which is 65,000 element allowance. Under this special circumstance, it is impossible to model the packaging with thermal vias directly. This is very typical to do the electronic packaging modeling due to license limitation,

- insufficient data for material properties,
- software limitation such as modeling generation for special geometries, CFD models,
- other data associated with boundary conditions, load, *et al.*

This requires the analysts who are doing modeling using either approximating approaches with reasonable assumptions for the missing data or using relevant models to

use the logical reasoning to optimize the design. For this case the problem is from the license rather than the lack of data. The second method was utilized to obtain the solution. The models was built with the all the components mounted on a 48 and 96 μm thick ceramic board without thermal vias inside; this allowed considerably finer meshes within the limit of 65,000 elements. The results (Table 3-3) showed that the least maximum temperature on the processor happened when the board was 48 μm thick, and the temperature was 108°C. Let us compare the results from three model configurations:

- I. the component level model with processor-local board only without thermal vias whose temperature is 116°C,
- II. the component level model with processor-local board only with thermal vias whose temperature is 95°C,
- III. the package level model with all components and board without thermal vias whose temperature is 107°C.

Results from I and III indicated that the Pentium temperature decreased after the board was enlarged even though more components were populated around it; the increment of out-heat-flux through the enlarged board is more than the increment of in-heat-flux from other components. That means for the real full model without thermal vias, the processor temperature would be no more than 107°C for model I. And from II we know that corresponding to I, which is 116°C, the temperature is 95°C, if then we change to 107°C, the temperature in case II can be predicted less than 95°C, which is less than the design specification of 100°C. This means that in some cases, the thermal management optimization can be achieved without direct modeling.

The layout of the MCM packaging from thermal solution analysis is described as a 133 Mhz P5 microprocessor, three MX, four DRAM and two SRAM are mounted on a 1.5" squared, 48 μm thick, multi-layer Alumina ceramic board with 200 tungsten thermal vias embedded by epoxy adhesive under the each electronic component.

These cases were also investigated with and without a silver epoxy adhesive. All the studies were conducted by means of finite element analysis using the ANSYS code. The solid models were three dimensional based on the packaging layout design. All the

operations were simulated under the actual operating thermal loads such as different power dissipation on each individual components and temperature boundary conditions. Steady-state conduction and convection heat transfer conditions were simulated among seven solid components with different materials. The mapping of the geometry was very complex. The maximum dimension was the length of the board (1.5"), and the minimum dimension is the radius of the vias (0.004"). The ratio between the maximum and minimum dimension was 375. The unstructured mesh specification is required for this modeling procedure. The shape of the thermal vias was changed from cylindrical to square cross-section pillars, detailed discussion related to this procedure are given in Chapter 4. For region near the power dissipating components, finer mesh was needed. The mesh density along the in-plane direction was less than that along the normal direction of the substrate.

Different size components are located on the same surfaces. This made the mesh difficult to generate because on each surface many materials in different sizes involved and resulted in difficulty to size the element without exceeding the element limit of the software license and exceeding the tolerance of the distortion for the elements. The large number of vias inside the ceramic board is another factor that increased the task of generating the volumes for the vias and size the element in different values as well. For this particular problem, the best strategy involved using the Ansys Parametric Design Language (APDL) to write the relevant program macros.

In the preprocessing stage, the material properties for the seven kinds of solid materials, the dimensions of all the solids were defined by parameters. This strategy made it efficient to change model dimensions by changing the parameters. Solid 3-dimensional elements were chosen for the thermal analysis. These were either the 8-node brick or the 4-node tetrahedron. The maximum number of volumes was 1400 filled by 65000 elements. The volumes were generated by the duplicating a predefined unit of one component one by one and then assembling all volumes together.

For the present schematic with vias, chips, ceramic board, epoxy layer, the cylinder needed more elements to avoid distortion of the element especially for the large ratio of depth to the radius of the cylinder. By using cylindrical solids for the vias to

match the actual geometry and to satisfy the requirement for the distortion tolerance, the total number of elements exceeded the license limit of the software.

To solve this problem the approach using rectangular section vias to replace the cylindrical vias approach was deemed a reasonable solution. If the length of the rectangular via is the same as the cylindrical vias, its edge is then equal 1.77 times as much as the radius of the cylindrical via.

In the solution process, converting the power dissipation to heat generation rate and applying as body heat source by

$$\dot{Q} = \frac{P}{V} \quad (3-18)$$

where P is the power dissipation for each component in Watts, and V is the volume of each component in cubic meters.

At the bottom of the whole packaging, the temperature was fixed at the value of 90°C. The side surfaces of the board were adiabatic, and the surfaces over the components were set to a natural convection boundary condition by applying the value of convective heat transfer coefficient and room temperature. This is represented the first phase of the study.

The second phase of the study involved temperature prediction of the P5 microprocessor only. The solid model was simplified into a three-dimensional quarter symmetry model (Fig.3-2, 3-3) of the P5 chip, ceramics board, with and without 196 tungsten thermal vias. The bottom surface of the package was constrained at 90°C, while all other surfaces were adiabatic. Appropriate symmetry boundary conditions were imposed on the two planes of symmetry. The heating rate in the P5 was 8.3 Watts. All other material property and geometry data was specified based on actual operating conditions. Detailed finite element analysis results on the model according to the conditions stated earlier in the chapter was conducted.

Temperature profiles for the P5 mounted on the 96 μm thick ceramic board with Tungsten vias are shown in Table 3-2 and Fig.3-4. Temperature profiles for the P5 mounted on the 96 μm thick ceramic board without tungsten vias are shown in Table 3-1 and Fig.3-5. Temperature profiles for the P5 mounted on the 48 μm thick ceramic board

with Tungsten vias are shown in Table 3-2 and Fig.3-6. Temperature profiles for the P5 mounted on the 48 μm thick ceramic board without Tungsten vias are shown in Table 3-1 and Fig.3-7. Chip and board temperature profiles for the existing layout are shown in Table 3-3 and Fig.3-8.

Two more simulations were conducted; one is for the worst-case scenario layout are shown Fig.3-9, the other is for a reduced size ceramic board where chips are mounted considerably closer to each other are shown in Fig.3-10. The purpose for the worst-case scenario simulation is to predict the highest temperature in case that the layout with maximum in-heat-flux surrounding the P5 even though this may not happen, and the results are showed in Table 3-4. The reason for the second additional simulation was try to find a possibility to minimize the size of the packaging such as to reduce the weight, the cost and the size as well. The simulation was completed and the results are shown in Table 3-5. The two simulations predicted there is no obvious temperature change for the P5. It was verified from the thermal aspect that the size of the packaging might be reduced at least 10% in weight and the maximum temperature for the chip increased less than 1%. The simulation concluded that:

1. thermal vias decreased the chip temperature up to 26%,
2. decreasing the thickness of the substrate by 50% could decrease chip temperature up to 14%,
3. decreasing by 50% the thickness and implanting thermal vias decreased chip temperature up to 30%.

It indicated that the size of the whole MCM package may be reduced up to 10%.

3.2 System Level Simulation

3.2.1. Heat Transfer Prediction for In-line Arrays of Modules in Air Channel

In this case study, heat transfer for in-line arrays of rectangular blocks in an air channel flow was developed using both finite element method and finite control volume method. The blocks are situated on the bottom surface inside a rectangular channel which simulates a typical electronic cooling passage. The numerical results were compared with benchmark experimental data. The electronic packaging model⁽¹⁵⁾ contains uniform array

of 10 rows by 6 columns of solid blocks as the chips mounted on an adiabatic wall of a channel in forced convection flow ⁽³⁾(Fig.3-11). Two channel heights ($H/B = 2.25- 4.6$) and two of inlet velocities (3.0 - 6.67 m/s) were simulated. The κ - ϵ turbulence computational fluid dynamics model was used for FEM simulation, algebraic turbulence model was used for FVM simulation.

The domain of the problems contained 60 blocks dissipating thermal energy. The first step was to define as small a boundary as possible. Because the velocity varied in all three directions around each block, there is no way to lower the dimensionality of the problem. But each row has the same flow condition namely same geometry and uniform upstream and downstream flow along the flow direction. The model could thus be converted into one column of the array of blocks inside a flow channel with two symmetric sides to simulate the whole package. The size of whole problem was thus decreased by 90% (Fig.3-12).

The second step was to determine the heat transfer mechanism. Compared with convective heat transfer inside the channel with forced flow and due to a small temperature difference between the two sides of the top and bottom wall, the heat loss across the top and bottom surfaces was ignored so that the two surfaces can be considered as adiabatic.

The third step was to confine the flow. At the inlet, the velocity and fluid temperature were considered to be uniform for the small temperature and velocity difference, for the outlet the relative back pressure is considered zero for there is no blockage. For the two sides of the domain, a zero velocity normal to the sides symmetric boundaries were specified. The fourth step was applying the internal heat-generation rate in the solid blocks. After the simplification and assumptions were made, the dimensions of the solid model are shown in Fig.3-13.

The analyses were performed using a structured mesh and the standard κ - ϵ turbulence model for the turbulent kinetic energy and length scale. Effects of Reynolds number variation from 2540 to 5672 and the channel-to-block height ratio variation from 2.25 to 4.6 were considered. Local heat transfer distributions as well as block-wise average heat transfer were obtained and calculation results compared with experimental

data of Moffat and Anderson⁽²⁾. It was found that thermal development was rapid and the block-wise average heat transfer coefficient attained a constant value after the second block. Numerical prediction of temperatures of modules of such an array was carried out for a three-dimensional uniform in-line array of 10 rows of solid blocks simulating integrated circuit chips mounted on an adiabatic substrate.

The first numerical analysis used a finite element method from a CFD code with a two equation (κ - ε) turbulence model to solve the full Navier-Stokes and energy equations. The code employs monotonic streamline upwinding for the advection terms. Monotonic streamline upwinding is unconditionally bounded, minimizing dissipation errors without introducing dissipation errors. An equal order pressure-velocity coupling scheme was used, and the governing equations were solved using a segregated solution algorithm. This segregated solution approach requires significantly less memory than traditional FEM, allowing in-core solutions⁽¹⁷⁾. This technique parallels those found in many FDM codes where the governing equations are solved sequentially rather than simultaneously⁽⁵⁸⁾. The algorithm requires repeated solutions to the matrix equations during every global iteration. In the case of the pressure equation, exact solutions are required to ensure conservation of mass. In a thermal problem with constant properties, there is no need to solve the energy equation at all until the flow problem has converged. For this problem the solver is the conjugate gradient method which is pre-conditioned with incomplete Choleski decomposition and is used only for the pressure equation in incompressible flows.

The numerical modeling convergence criterion for the CFD solution is monitored by the convergence monitoring parameters. A convergence monitor is calculated for each degree of freedom (DOF) at each global iteration. It is loosely normalized rate of change of the solution from one global iteration to the next and is calculated for each DOF as follows:

$$ConvMon = \frac{\sum_{i=1}^N |\phi_i^k - \phi_i^{k-1}|}{\sum_{i=1}^N |\phi_i^k|} \quad (3-24)$$

where N is total number of in mesh nodes, ϕ is a DOF, k is current global iteration number. The pressure convergence criterion for the problem is set to 10^{-3} and the temperature residual to 10^{-5} .

The model under study is shown in Figure 3-14. The calculation domain is a cut-off slice along the line of symmetry in the flow direction. The domain was discretized with a structured mesh option using rectangular block cells. The near wall regions and higher gradient regions being more restrictive needed a considerably finer mesh to capture the steep gradients of the flow variables since the near wall regions are associated with higher pressure and temperature. Simulation results using FEM method showed a diverge solution (Fig.3-15a). Reasons attributed to this are discussed as followings:

1. mesh too coarse,
2. inadequate turbulence model,
3. insufficient entry length for the air flow to fully develop,
4. singularity point introduced by rectangular corner for blocks,
5. flow separation and reattachment over each block.

The models have been modified based upon the potential problems as above. The first modification was to reduce the domain since there is only 65,000 elements available for the whole domain, and the only way to achieve the finer mesh is to minimize the domain. The principle to reduce the domain is to keep the representative section. For this application, three blocks were kept; one block located at the entry section, one in the flow separation region, one next to the outlet. Since the domain has been changed from 10 blocks to three (Fig.3-16), the element size has been decreased by a factor of 3.3 with 65,000 elements in the mesh. The simulation results showed that the severity was reduced (Fig.3-15b), but it was still divergent. To decrease the element size further, the only thing left was to decrease the model from three dimension to two dimension. Although this distorted flow in one of the direction, it is valuable to do an element size sensitivity analysis. A 2D model with 10 blocks (Fig.3-17) were simulated with the element size 1/18th that of 3D model with 10 blocks, but the result did not converged either (Fig.3-15c). For the 2D model with 3 blocks inside domain (Fig.3-18), the element size is only 1/30th that of 3D full model, and the it is unlikely to converge (Fig.3-15d). The

conclusion from the four element size sensitivity analysis is that convergence level is sensitive to the element size, but for this problem, the reduction of the element size needs other modification to get a converged solution.

Evidently mesh refinement reduced the level of divergence severity, further mesh refinement becomes a non-viable option since the software license limit will be exceeded. Other possible means to improve convergence need to be explored. The next model was to apply the length both at entry and exit sections (Fig.3-19) as:

$$L_{fd} \approx 0.05D Re_D \quad (\text{for laminar}) \quad (2-138)$$

$$10D \leq L_{fd} \leq 60D \quad (\text{for turbulent}) \quad (2-139)$$

The solution was not convergent due to factor of 50 increase the element size being so dramatic. The potential gain of a fully developed entry length was negated by the increase size of elements.

The singularity point introduced by rectangular corners of blocks became the next target to modify the model. By plotting the velocity vector, the front corner of the block is seemed to show higher divergence (Fig.3-20), apparently this a singularity point. The modification was aimed at removing the rectangular corner at 10% location of the edge. More work for model generation is still needed to adjust the damaged topology which was able to provide a structured mesh, and it doubled the work for the model generation. This model gave a converged solution but the result was 52°C versus 78°C. The error is either from the over simplification from 3D model to 2D model or from something else.

By a reattachment analysis using a benchmark test (Fig.3-21) data, it is found the κ - ϵ model has larger error for the reattachment length to solve the problems with the reattachment involved⁽⁷⁸⁾.

In summary, the FEM model is very sensitive to the element size and the mesh quality. Sharp corners may introduce divergence, when flow reattachment occurs, leading to significant errors. But most electronic packages are of rectangular shape and have flow reattachment when flow come across each block. This implies that FEM with κ - ϵ model might not be a good option to do system level analysis.

A three dimension CFD model for the 10 blocks in a symmetric channel was finally done by a FVM code. It provided a series of satisfactory simulation results. Data

from 12 experiments are listed as Table 3-6. The experiments were conducted by Anderson ⁽³⁾, where N_h is the number of the row which is applied by power dissipation; V_{in} is the average velocity at the inlet; H/B is the ratio between the height of the channel and blocks; T_{in} is the ambient temperature; and P is the total power for each block. The geometry and boundary conditions for the system level model were based upon the data listed as Table 3-6. Fig.3-22 showed the velocity vector when the first row is heated. Fig.3-23 showed the temperature contour when the first row is heated. Fig 3-24 showed the flow separation and Fig.3-24 showed the back flow region.

The simulation results are as Table 3-7 to Table 3-10. Further discussion is in Chapter 4.

Table 3-1 Simulated Temperatures (°C) of P5-133 (Without Tungsten Vias)

	Board Thickness=0.096 in	Board Thickness=0.048 in
Maximum Temperature	135.60	116.43
Minimum Temperature	113.62	99.22

Table 3-2 Simulated Temperatures (°C) of P5-133(With Tungsten Vias)

	Board Thickness=0.096 in	Board Thickness=0.048 in
Maximum Temperature	100.99	95.68
Minimum Temperature	100.29	95.16

**Table 3-3 Maximum Temperatures (°C) of Multi-Chip Module (Without Vias)
(Layout 1- Preliminary)**

	Board Thickness=0.096 in	Board Thickness=0.048 in
P5-133	120.40	107.98
DRAM-1	92.43	91.21
DRAM-2	92.35	91.21
DRAM-3	92.44	91.23
DRAM-4	92.34	91.22
32Kx32SRAM-1	96.07	93.71
32Kx32SRAM-2	96.13	93.71
82437MX	103.46	98.36
82438MX-1	101.65	97.56
82438MX-2	101.58	97.84

Table 3-4 Maximum Temperatures (°C) of Multi-Chip Module (Without Vias)
(Layout 2 - the Worst Case)

	Board Thickness=0.096 in	Board Thickness=0.048 in
P5-133	120.55	107.98
DRAM-1	93.53	91.58
DRAM-2	92.75	91.28
DRAM-3	92.07	91.19
DRAM-4	92.05	91.20
32Kx32SRAM-1	96.49	93.79
32Kx32SRAM-2	96.96	93.81
82437MX	104.64	98.50
82438MX-1	102.11	97.77
82438MX-2	101.43	97.70

Table 3-5 Maximum Temperatures (°C) of Multi-Chip Module (Without Vias)
(Layout 3 - Reduced Size)

	Board Thickness=0.096 in	Board Thickness=0.048 in
P5-133	120.60	107.93
DRAM-1	93.84	91.72
DRAM-2	93.65	91.77
DRAM-3	94.00	91.67
DRAM-4	93.74	91.63
32Kx32SRAM-1	96.96	93.90
32Kx32SRAM-2	96.68	93.90
82437MX	104.70	98.47
82438MX-1	102.01	97.82
82438MX-2	101.91	97.78

Table 3-6 Input data for the 12 system level simulations

Case	H/B	V_{in} (m/s)	N_h	T_{in} (°C)	P(W)
1	4.6	3	1	26.072	1.727
2	4.6	3	3	27.101	2.09
3	4.6	3	6	27.395	2.03
4	4.6	6.7	1	28.406	1.85
5	4.6	6.7	3	27.856	2.49
6	4.6	6.7	6	29.209	2.46
7	2.25	3	1	26.247	2.003
8	2.25	3	3	25.803	3.397
9	2.25	3	6	25.03	1.959
10	2.25	6.66	1	27.017	3.049
11	2.25	6.66	3	28.912	2.058
12	2.25	6.66	6	28.462	3.048

Table 3-7 H/B=4.6, V=3 m/s

	case1	case1	case2	case2	case3	case3
n	T_c (°C)					
1	77.3	78.675				
2	28.9	28.711				
3	27.8	27.772	81.6	76.576		
4	27.2	27.379	29.5	30.523		
5	27.1	27.17	28.6	28.912		
6	27.0	27.047	28.0	28.45	80.6	78.421
7	26.9	26.941	27.9	28.2	30.0	30.189
8	26.8	26.876	27.7	28.07	28.9	28.638
9	26.7	26.795	27.6	27.95	28.2	28.228
10	26.6	26.749	27.5	27.891	28	28.046

Table 3-8 H/B=4.6, V=6.7 m/s

	case4	case4	case5	case5	case6	case6
n	$T_c(^{\circ}\text{C})$	$T_e(^{\circ}\text{C})$	$T_c(^{\circ}\text{C})$	$T_e(^{\circ}\text{C})$	$T_c(^{\circ}\text{C})$	$T_e(^{\circ}\text{C})$
1	57.1	59.597				
2	29.1	29.543				
3	28.7	29.073	64.5	61.553		
4	28.6	28.936	28.6	29.630		
5	28.6	28.879	28.2	28.870		
6	28.6	28.823	28.1	28.621	65.7	66.880
7	28.5	28.815	28.0	28.498	30.0	31.192
8	28.5	28.797	28.0	28.438	29.5	30.298
9	28.5	28.772	28.0	28.348	29.4	30.036
10	28.4	28.763	27.9	28.317	29.3	29.934

Table 3-9 H/B=2.25, V=3 m/s

	case7	case7	case8	case8	case9	case9
n	$T_c(^{\circ}\text{C})$	$T_e(^{\circ}\text{C})$	$T_c(^{\circ}\text{C})$	$T_e(^{\circ}\text{C})$	$T_c(^{\circ}\text{C})$	$T_e(^{\circ}\text{C})$
1	78.8	73.213				
2	29.8	29.036				
3	28.2	28.176	102.3	97.554		
4	27.5	27.873	30.0	30.918		
5	27.2	27.753	27.9	28.454		
6	27.1	27.680	27.0	27.722	70.7	66.324
7	27.0	27.641	26.9	27.384	27.9	27.712
8	26.9	27.608	26.8	27.206	26.2	26.382
9	26.8	27.576	26.5	27.066	25.9	25.999
10	26.8	27.563	26.5	26.983	25.8	25.860

Table 3-10 $H/B=2.25$, $V=6.66$ m/s

	case10	case10	case11	case11	case12	case12
n	$T_c(^{\circ}C)$	$T_c(^{\circ}C)$	$T_c(^{\circ}C)$	$T_c(^{\circ}C)$	$T_c(^{\circ}C)$	$T_c(^{\circ}C)$
1	71.2	73.213				
2	28.2	29.036				
3	27.8	28.176	56.2	53.853		
4	27.3	27.873	29.6	30.206		
5	27.3	27.753	29.3	29.608		
6	27.3	27.680	29.2	29.459	70.0	67.199
7	27.2	27.641	29.1	29.407	29.3	30.523
8	27.1	27.608	29.1	29.357	29.0	29.566
9	27.1	27.576	29.1	29.352	28.8	29.295
10	27.1	27.563	29.0	29.324	28.7	29.188

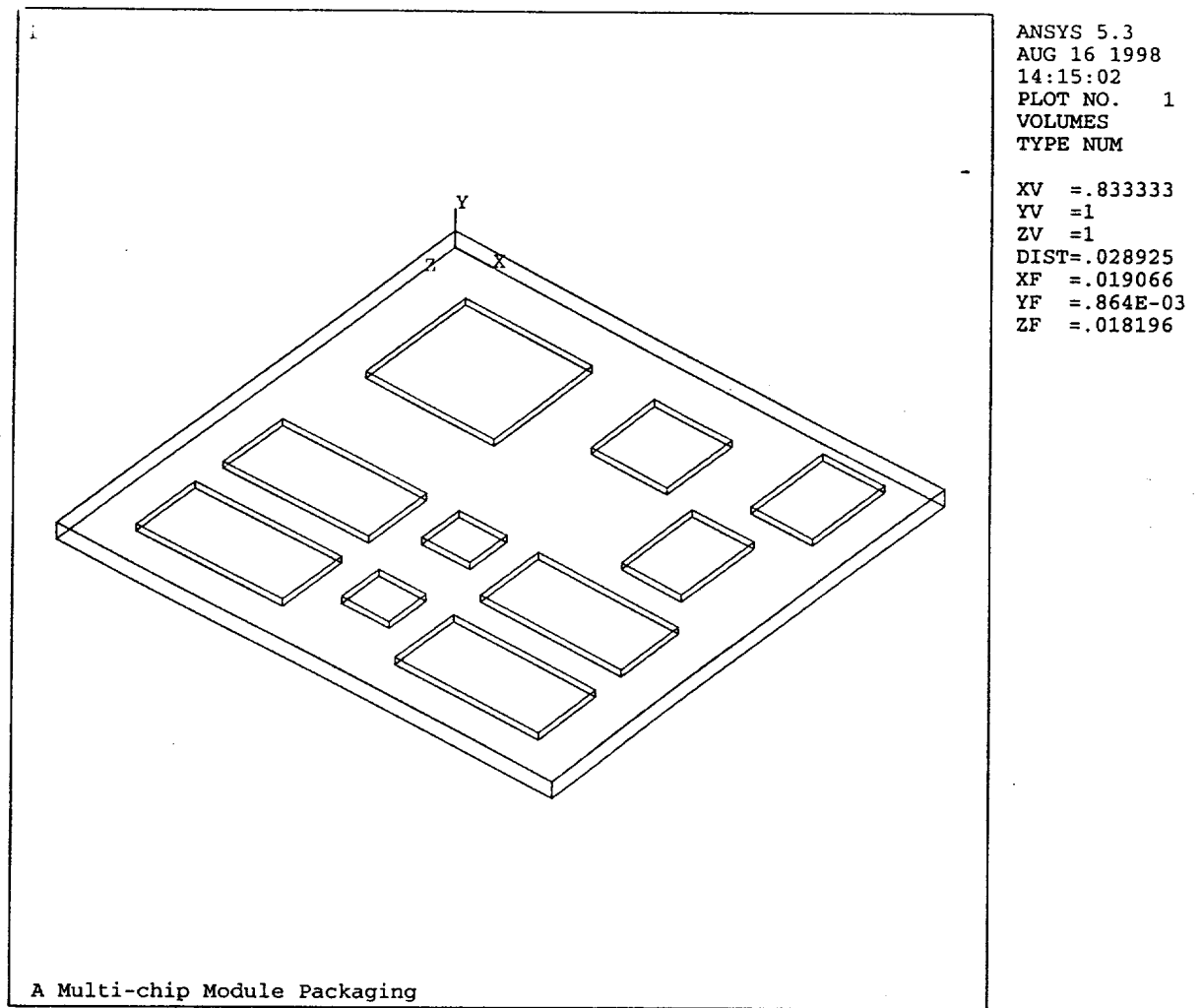


Fig.3-1 The Multi-Chip Module Package

133

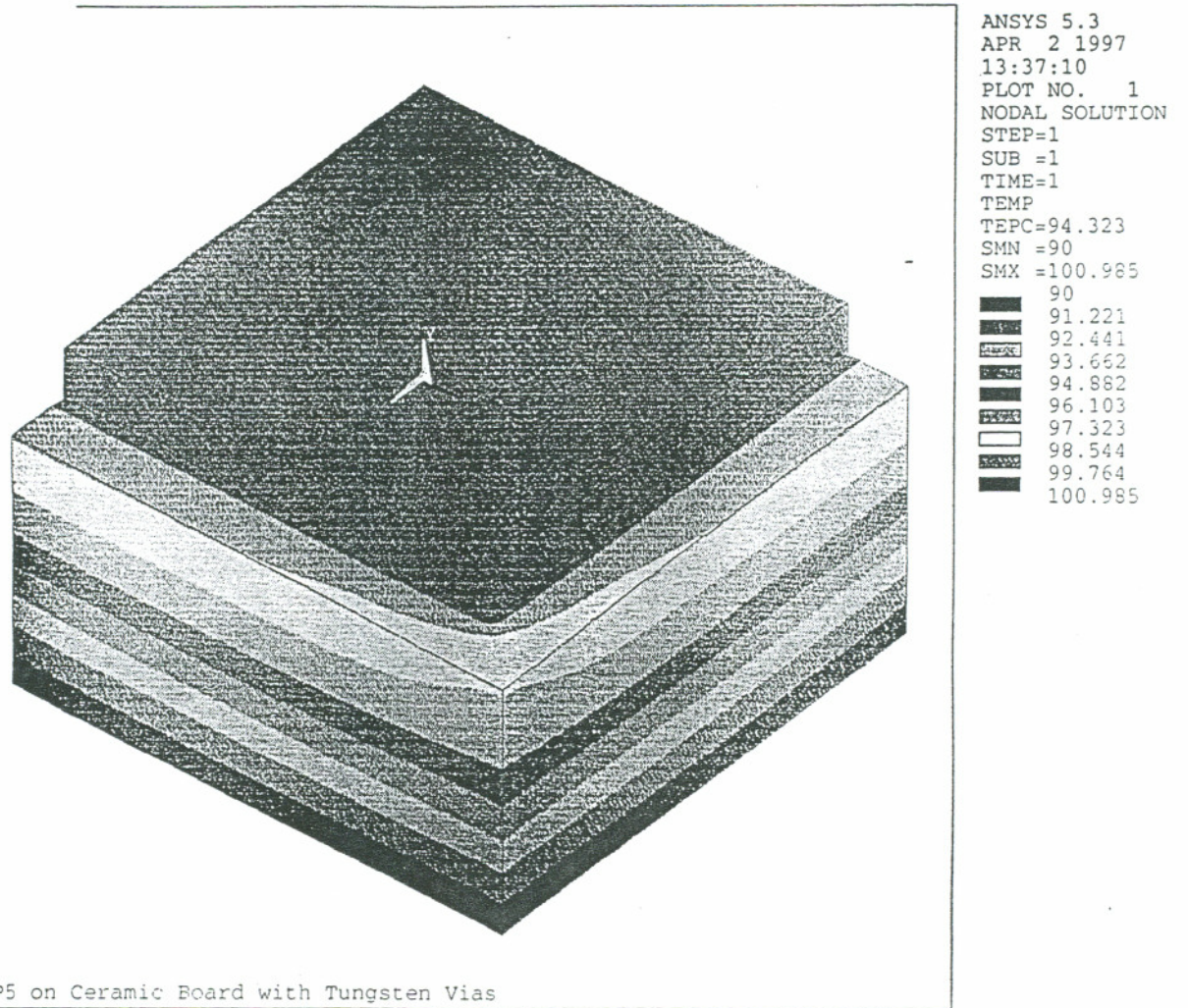


Fig.3-2 Component Level Model For P5 Only

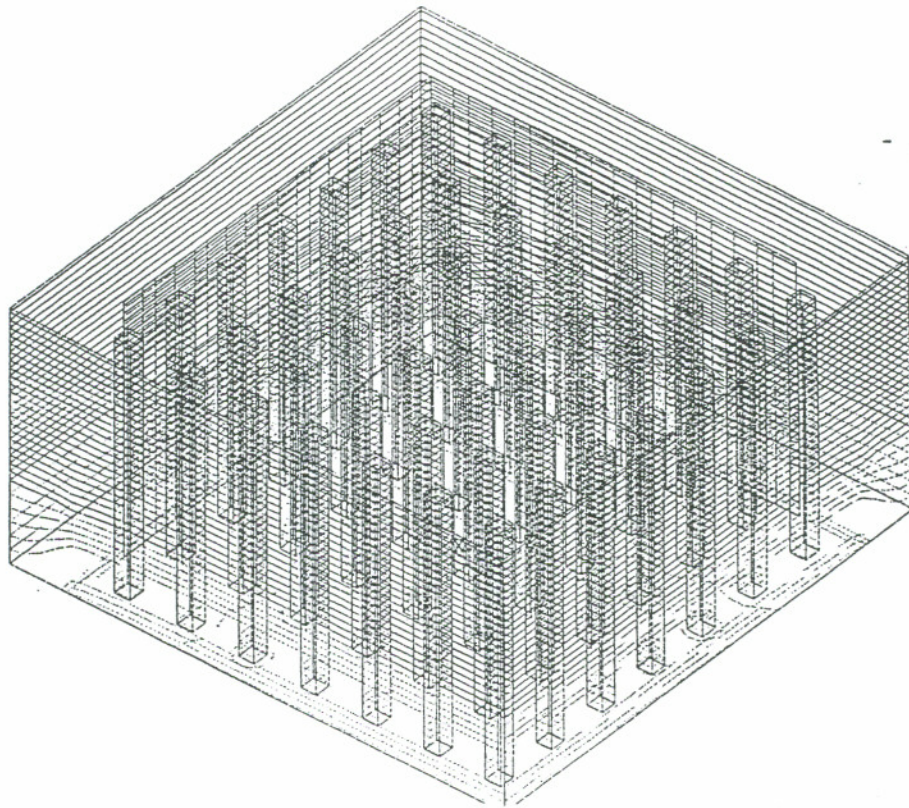


Fig.3-3 Local Board With The Embedded Thermal Vias

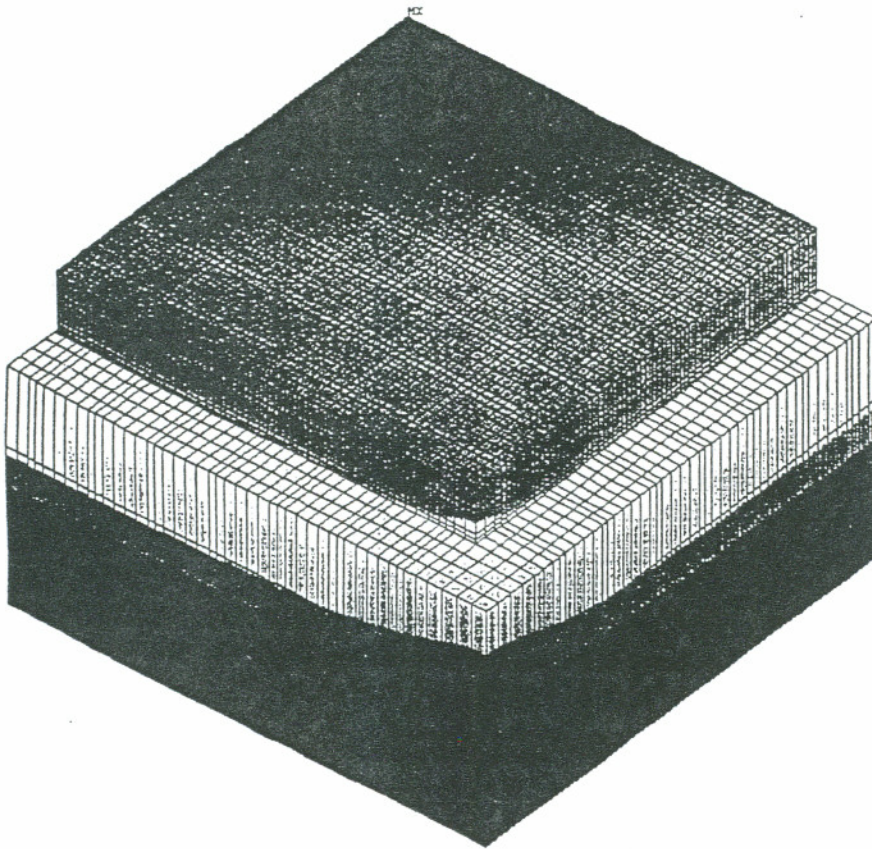


Fig.3-4 Temperature Contours Of Thicker Board With Thermal Vias

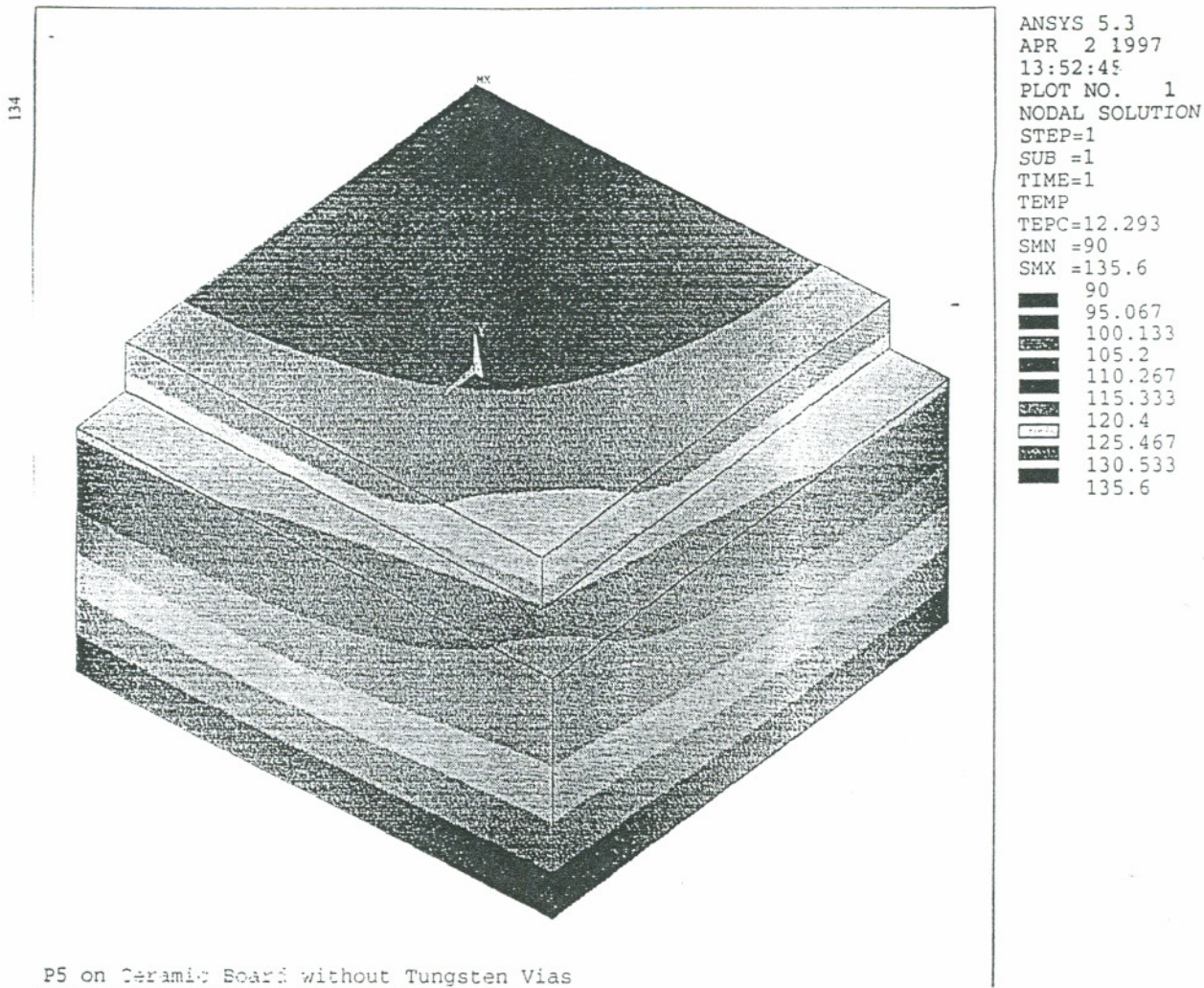


Fig.3-5 Temperature Contours Of Thicker Board Without Thermal Vias

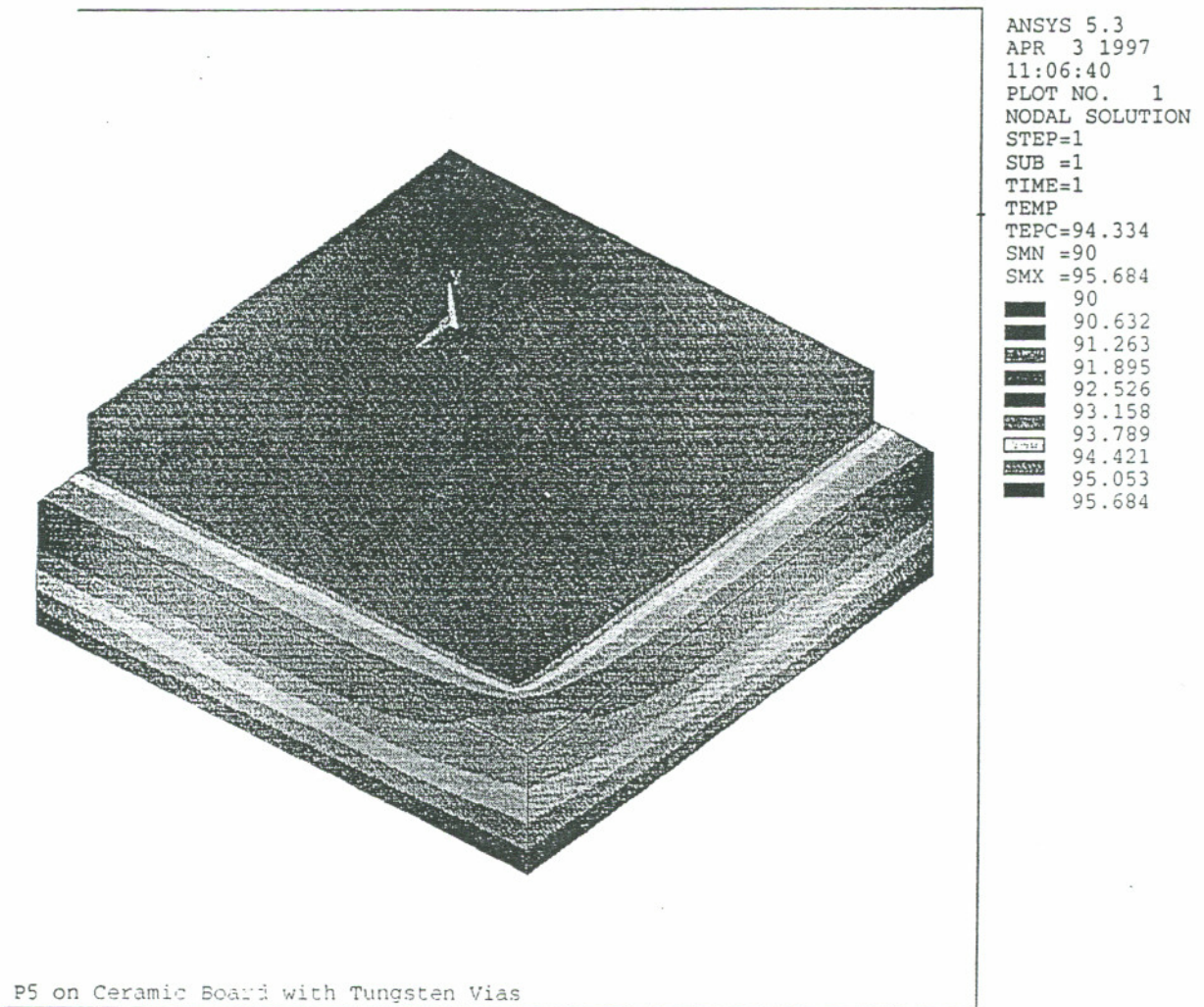


Fig.3-6 Temperature Contours Of Thin Board With Thermal Vias

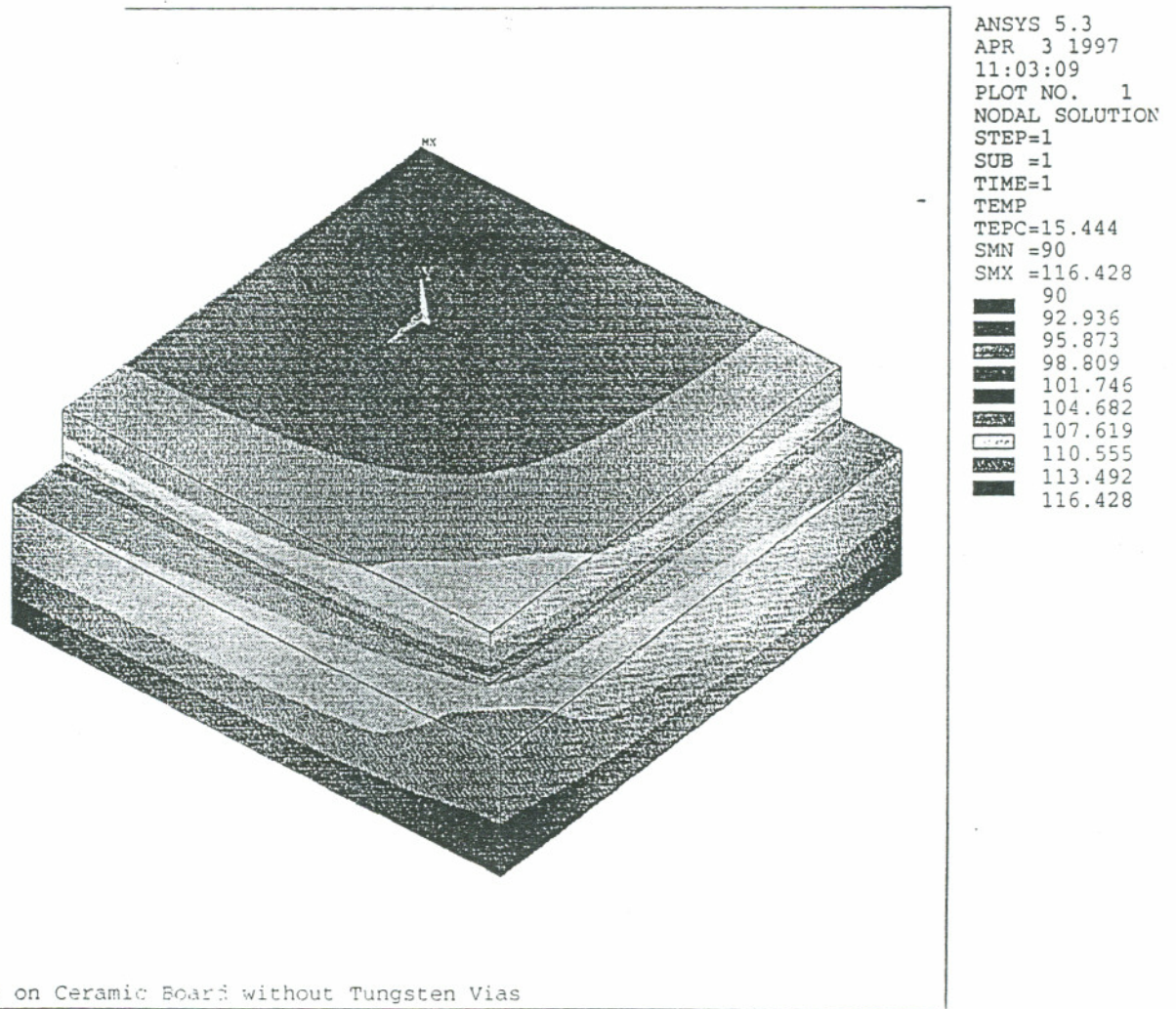


Fig.3-7 Temperature Contours Of Thin Board Without Thermal Vias

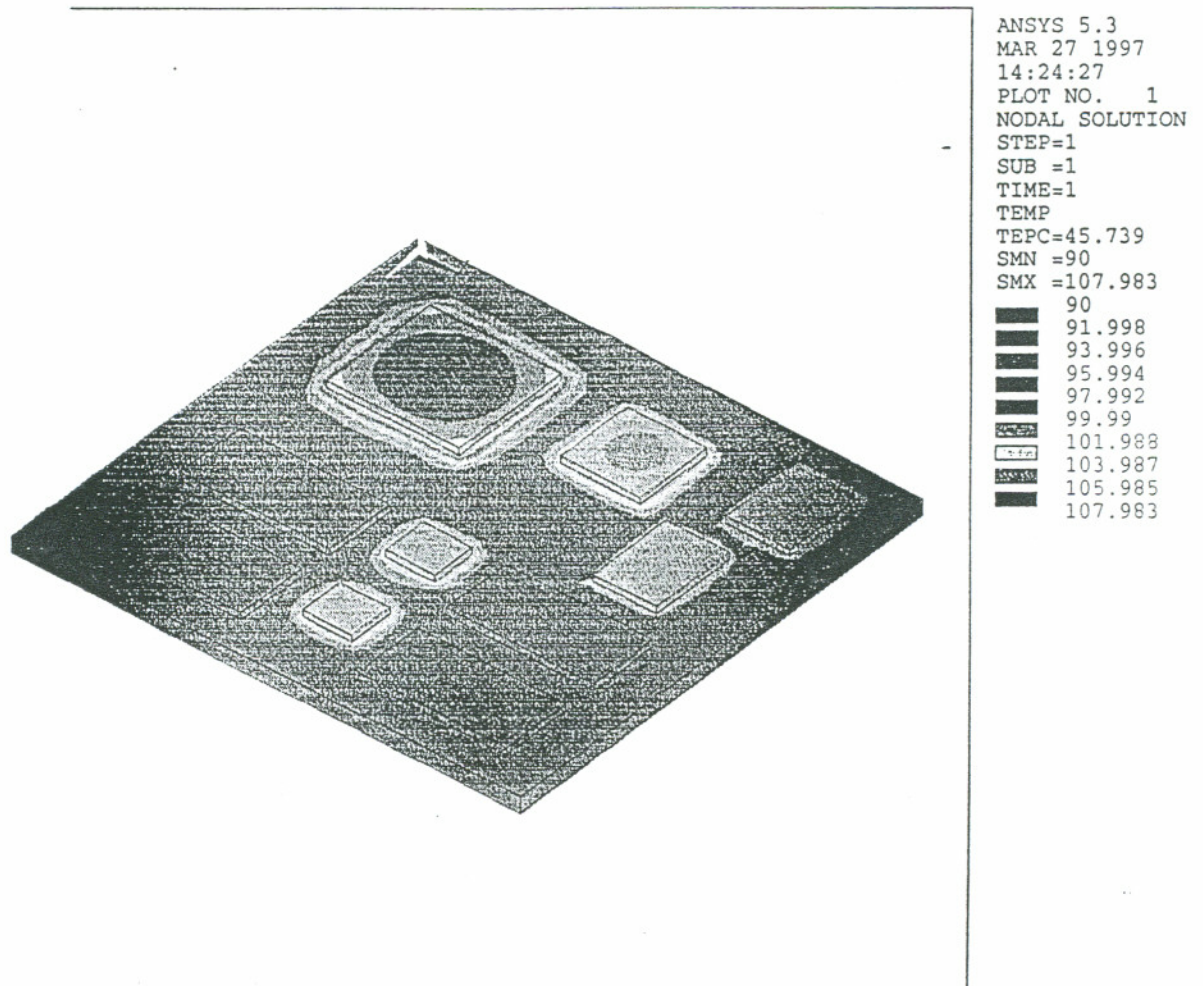


Fig.3-8 Temperature Profiles For The Current Layout

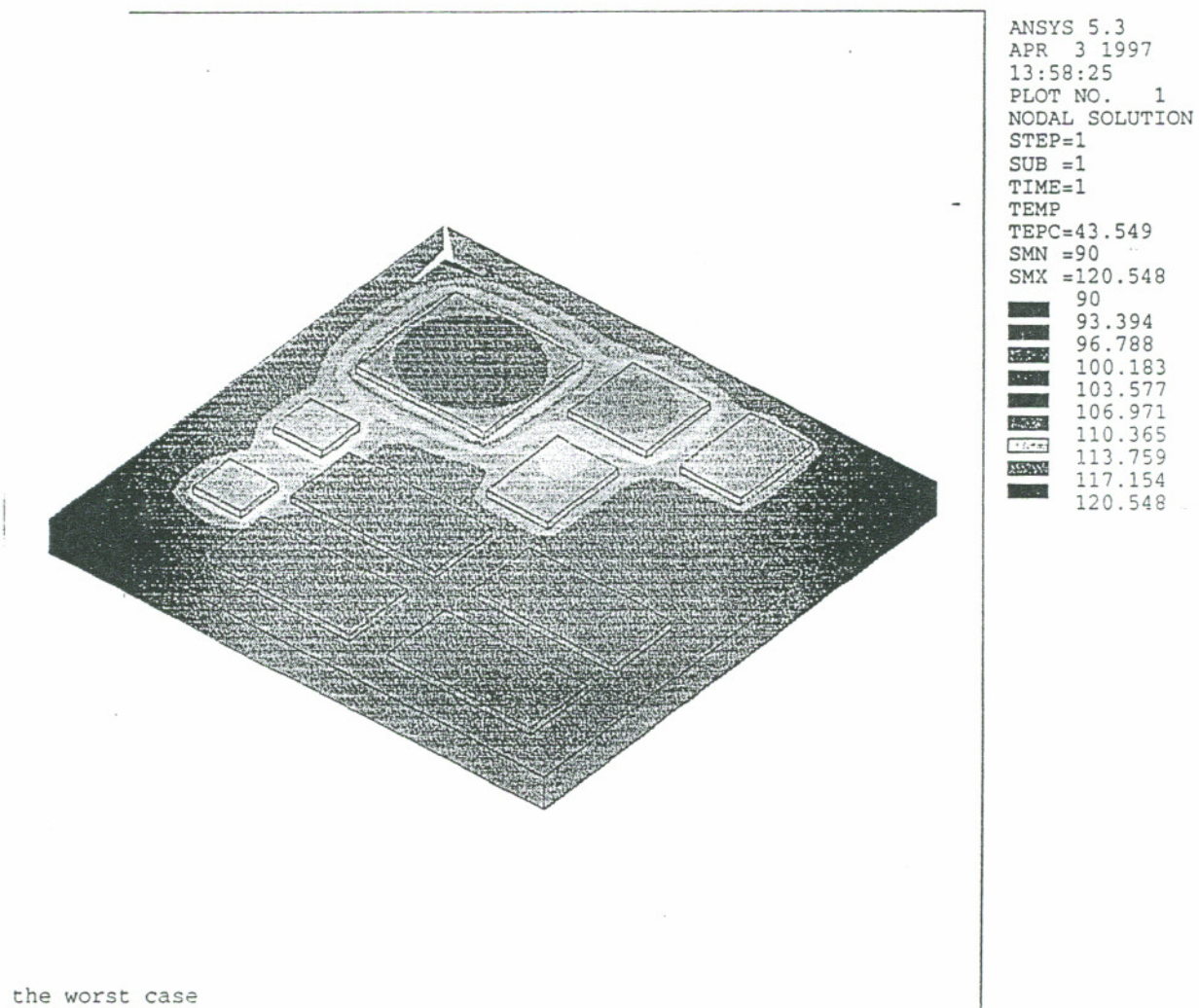


Fig.3-9 **Temperature Profiles For The Worst Case**

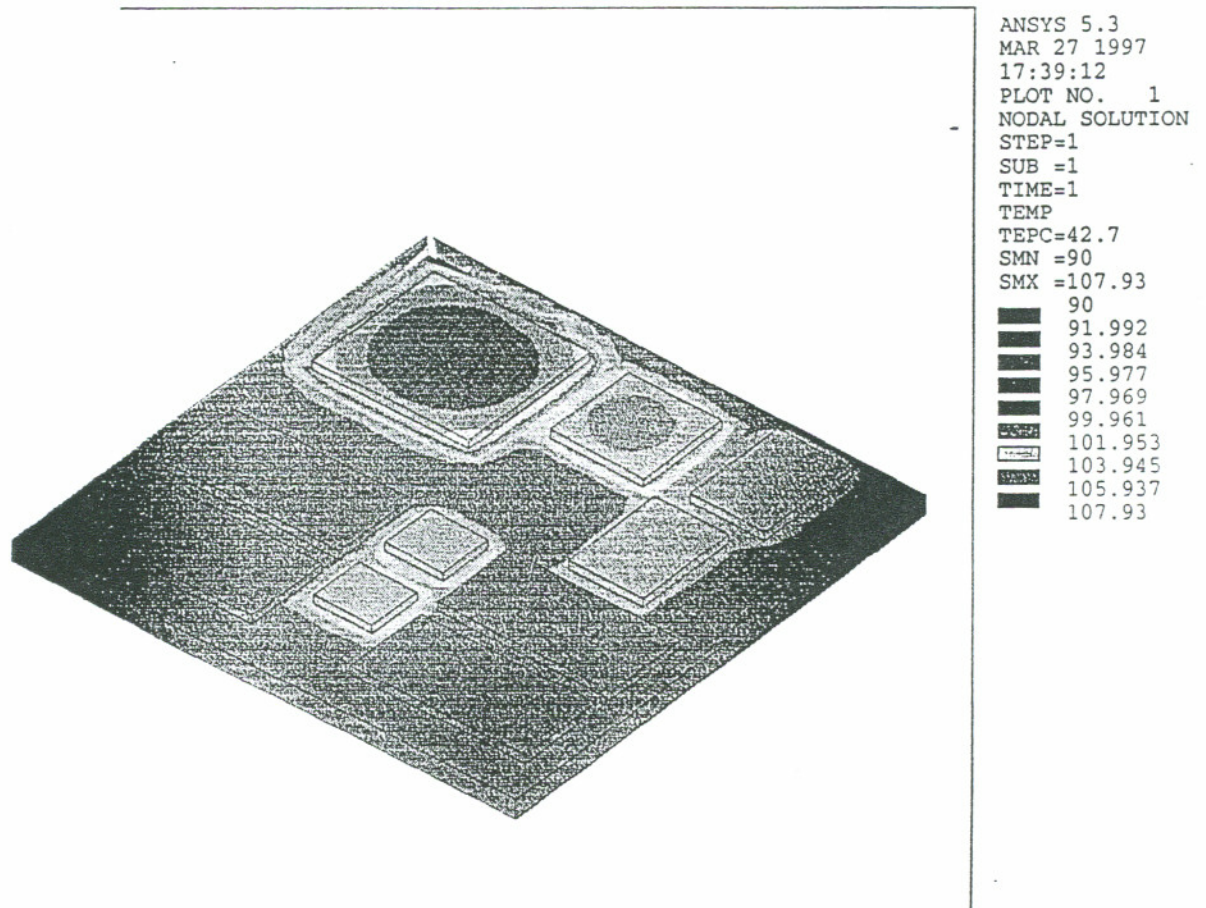
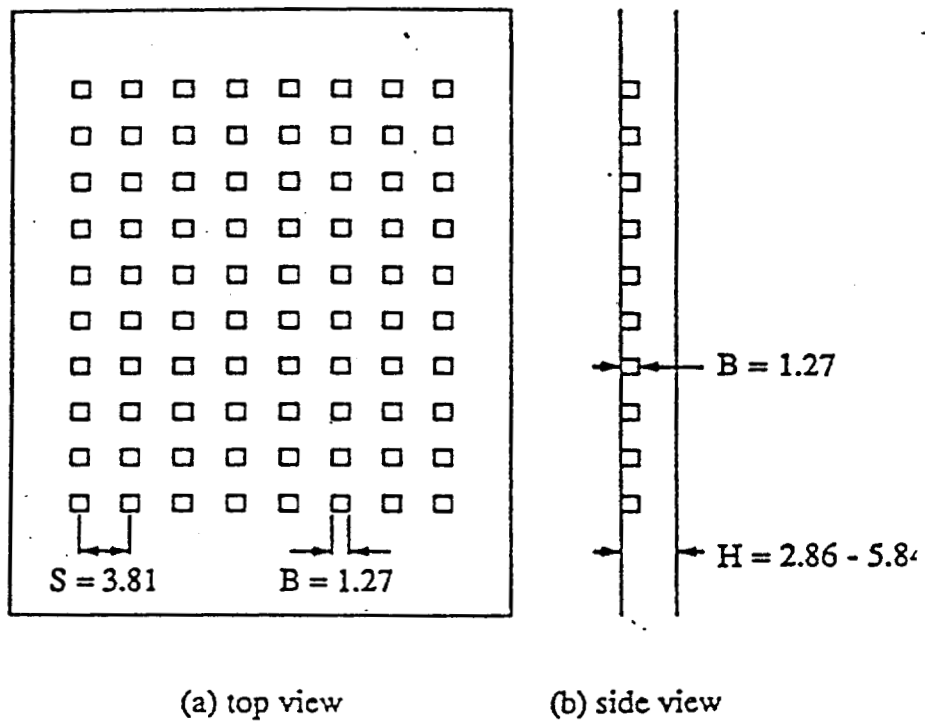


Fig.3-10 Temperature Contours For The Reduced Size Board



Schematic of cube test plate (all dimensions in cm).

Fig.3-11 System Level Benchmark Model

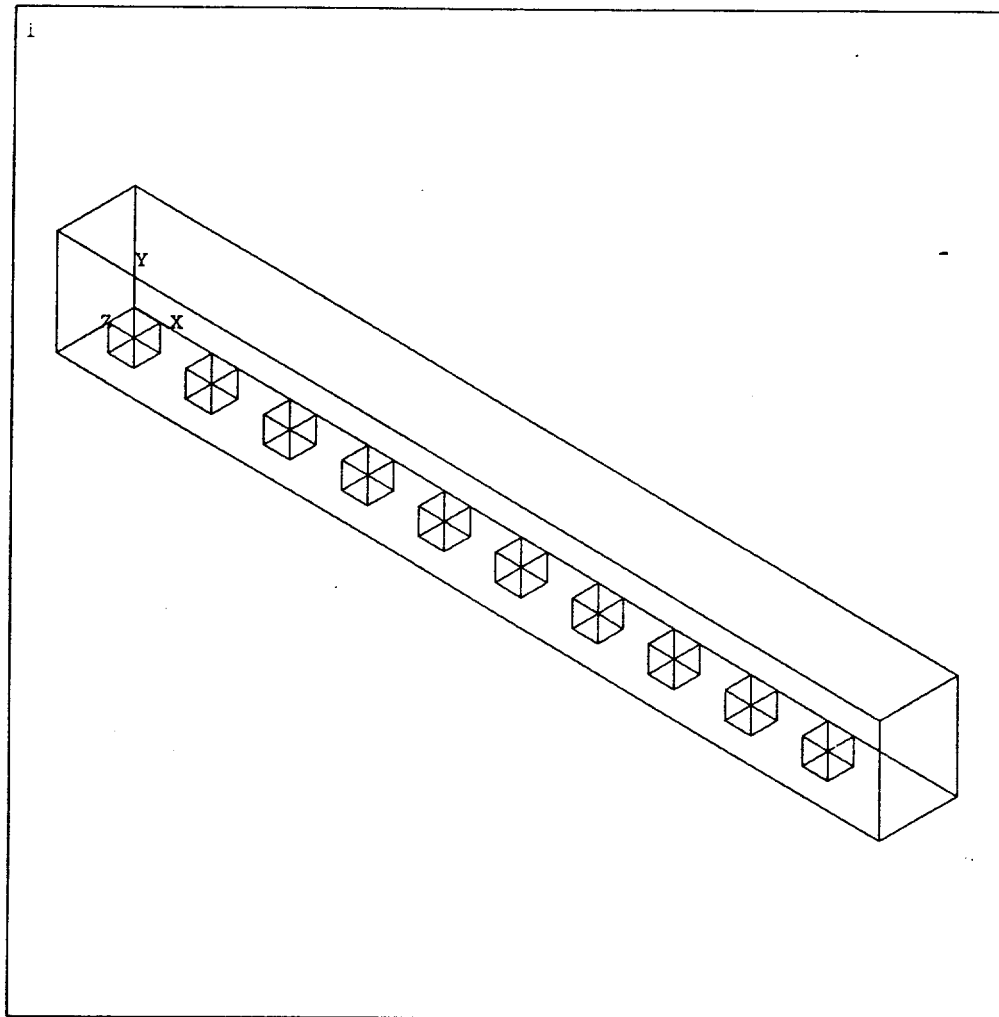


Fig.3-12 **3D Fem Model Simplified With Symmetrical Slice**

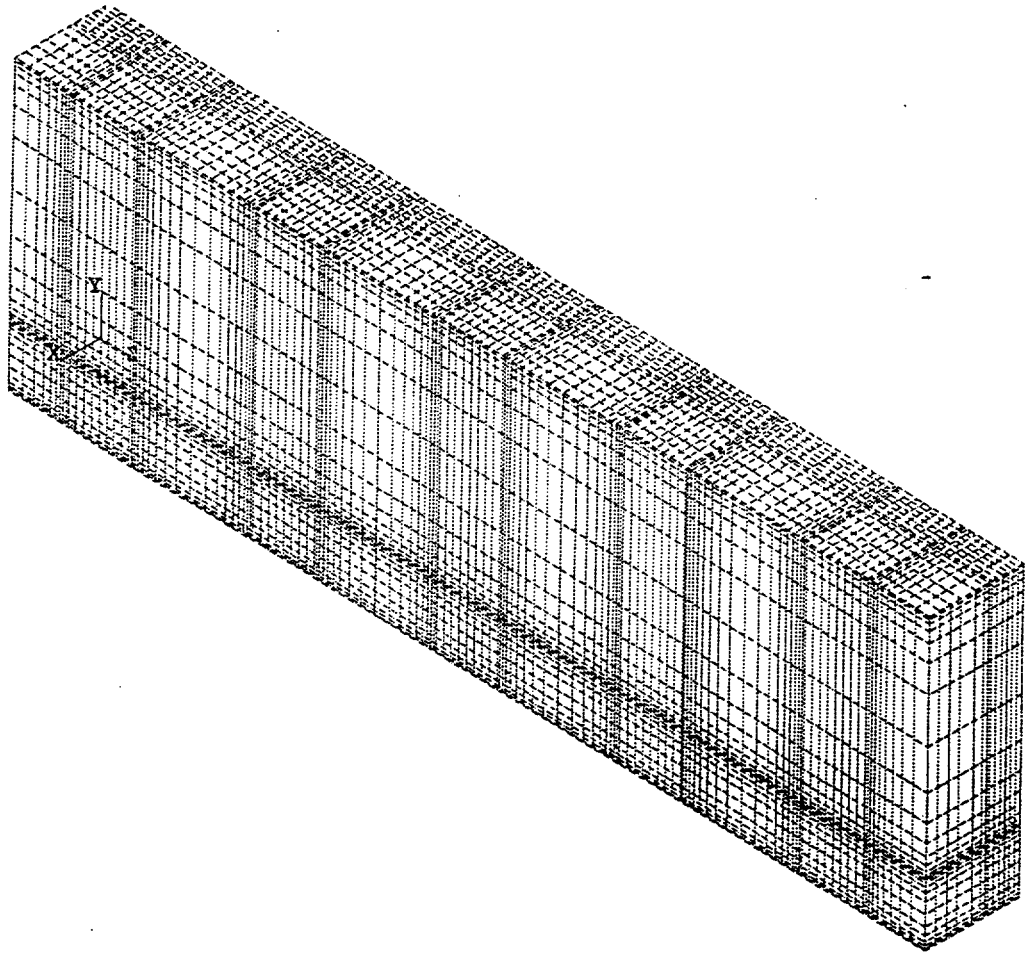


Fig.3-13 **Cut-Off Slice Of The Symmetrical 3D Model And Mesh**

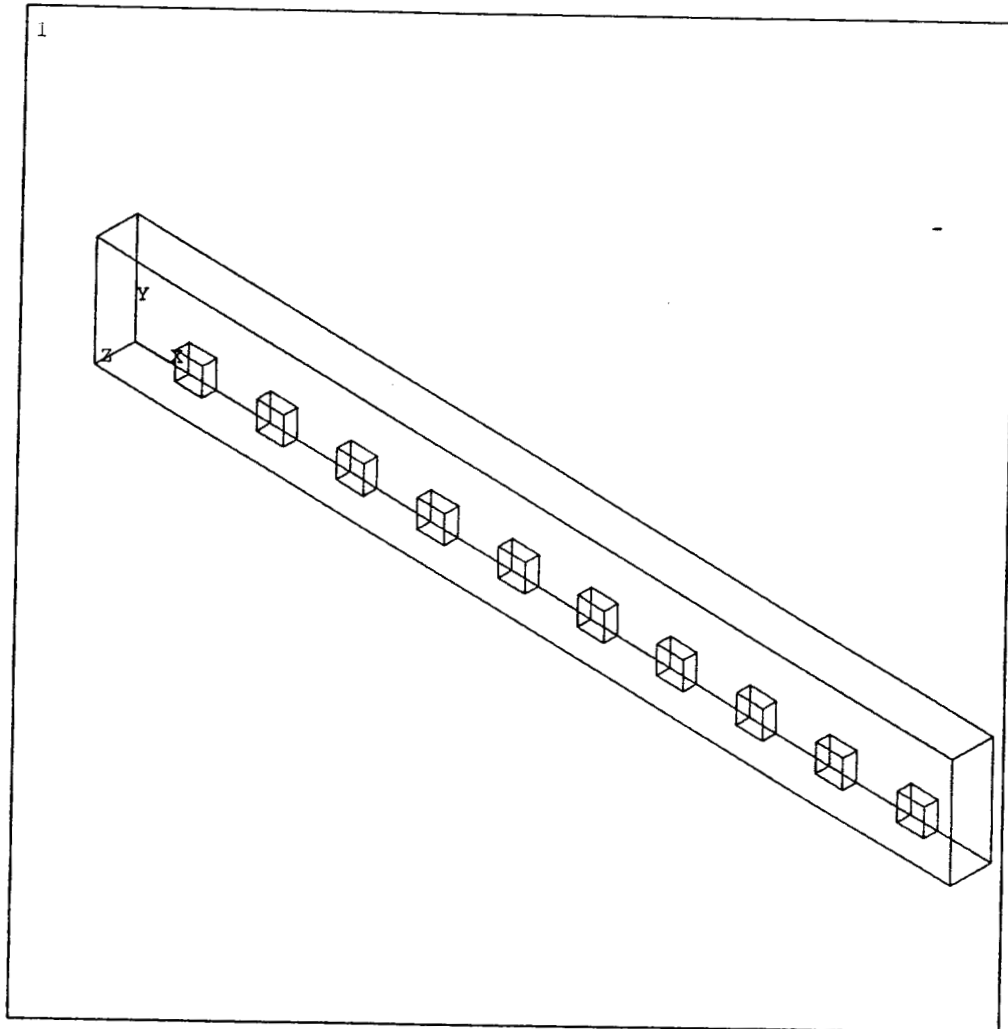


Fig.3-14 Numerical Model With Boundary Conditions

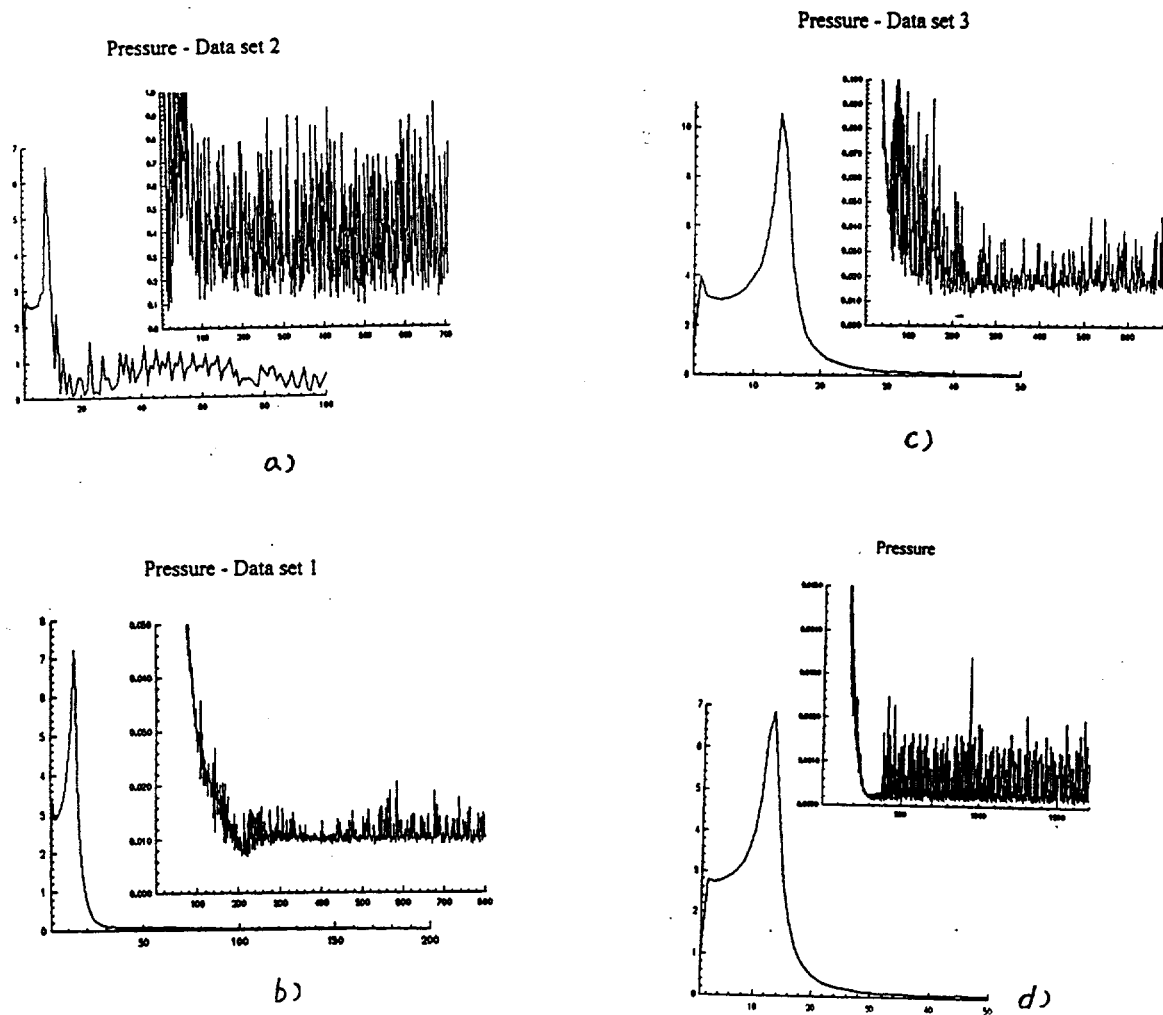


Fig.3-15 Convergence Monitor For Different Size Elements

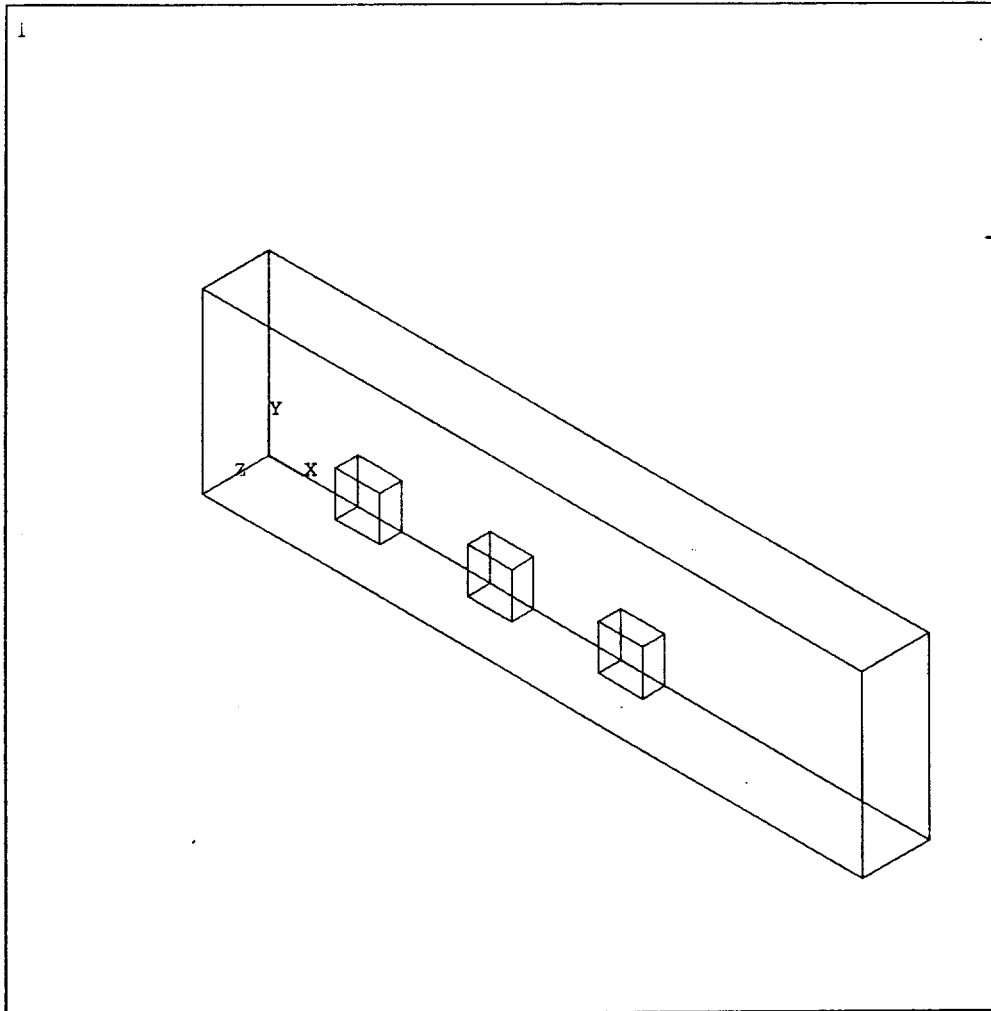


Fig.3-16 **Reduced 3D Domain**

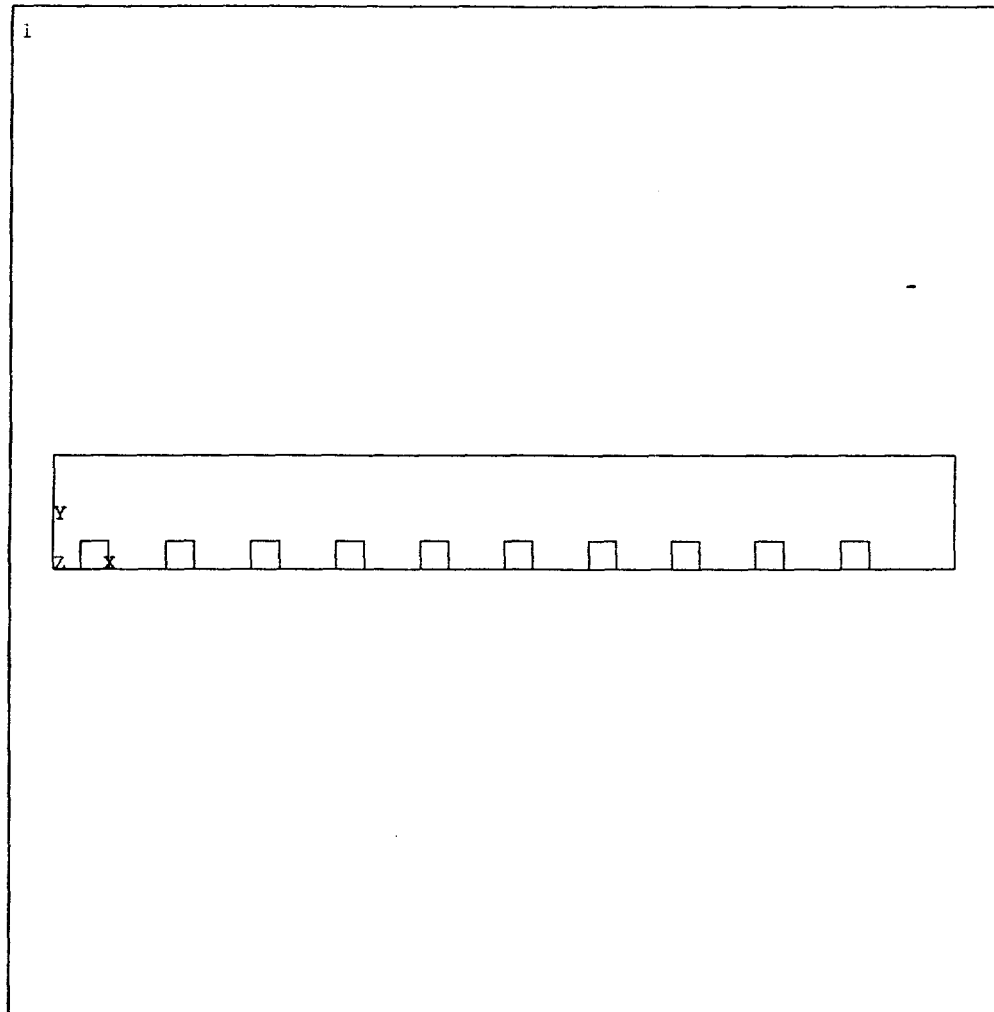


Fig.3-17 **2D Model With 10 Blocks**

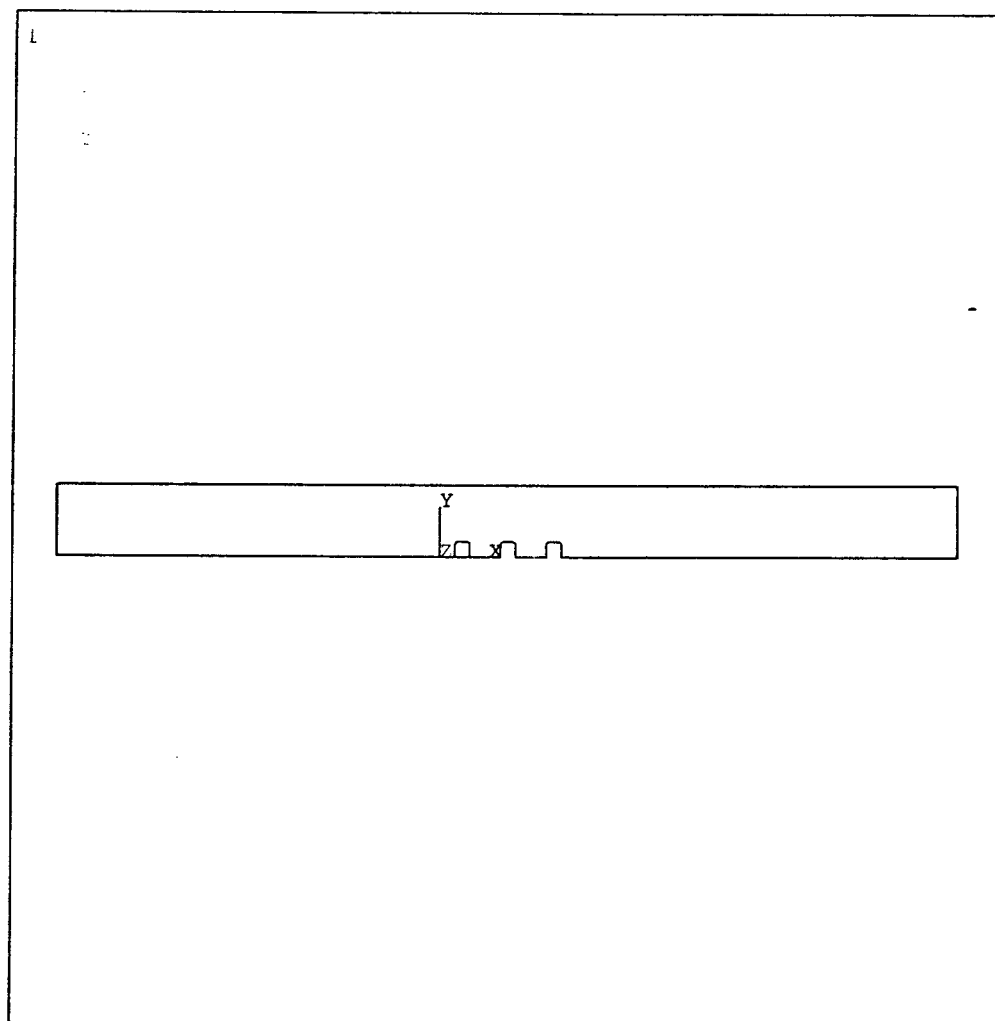


Fig.3-18 **2D Model With 3 Blocks**

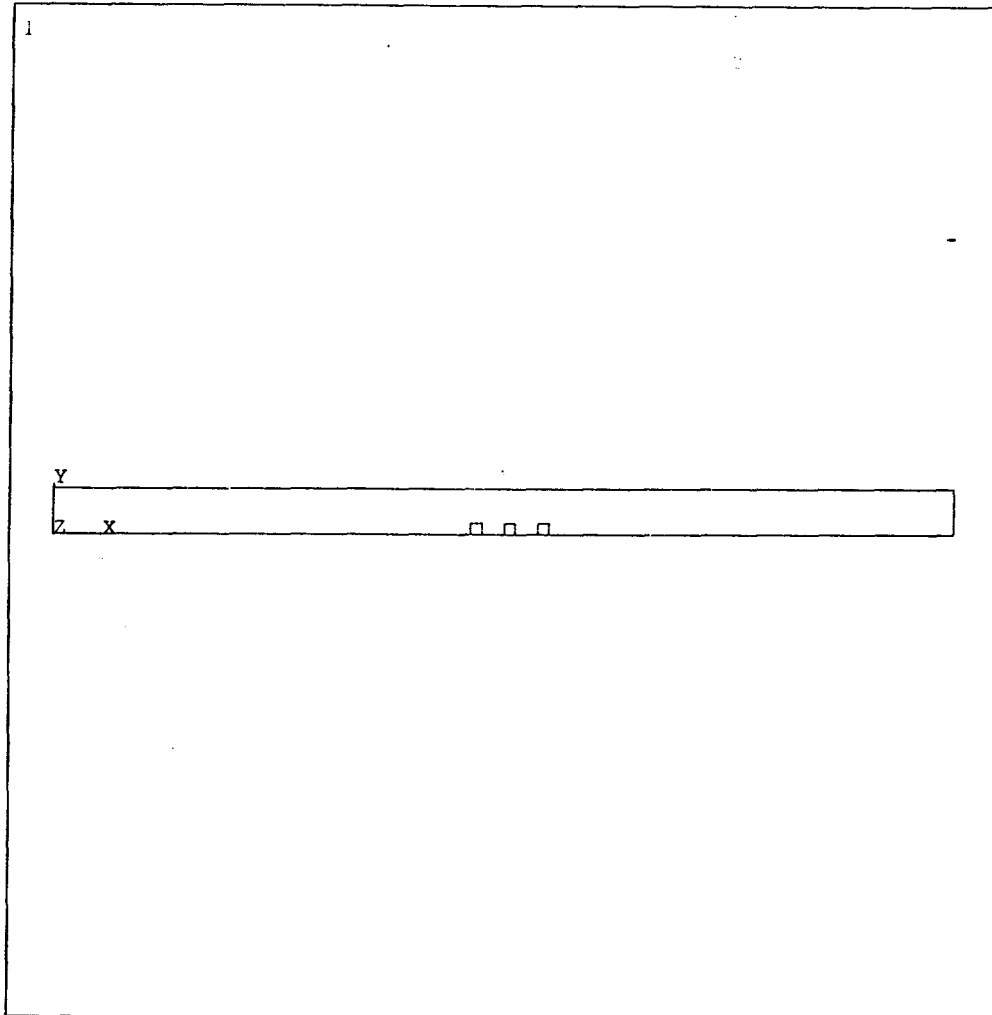


Fig.3-19 2D FEM Model Considering The Entry And Exit Length

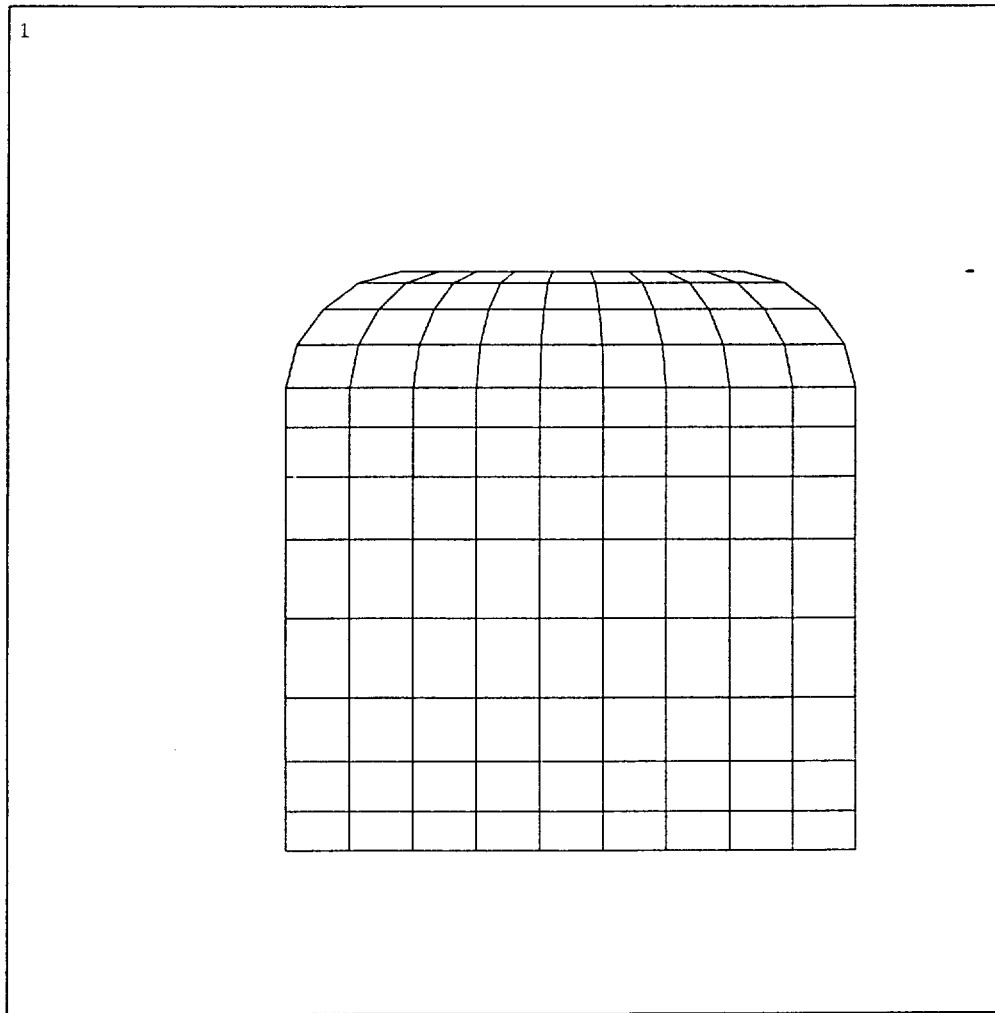


Fig.3-20 Divergence Caused By Singularity Point

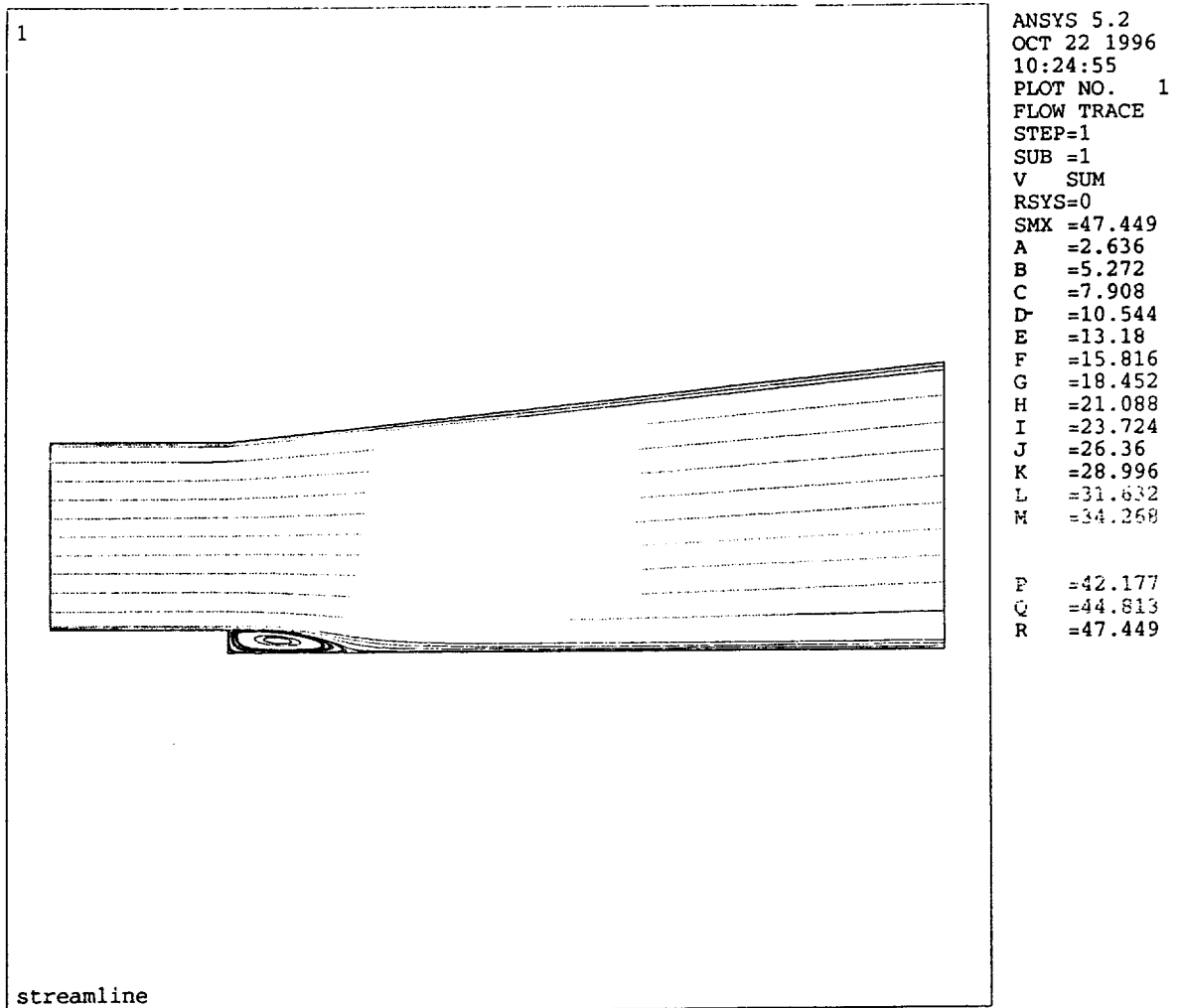


Fig.3-21 Back Flow Reattachment Length

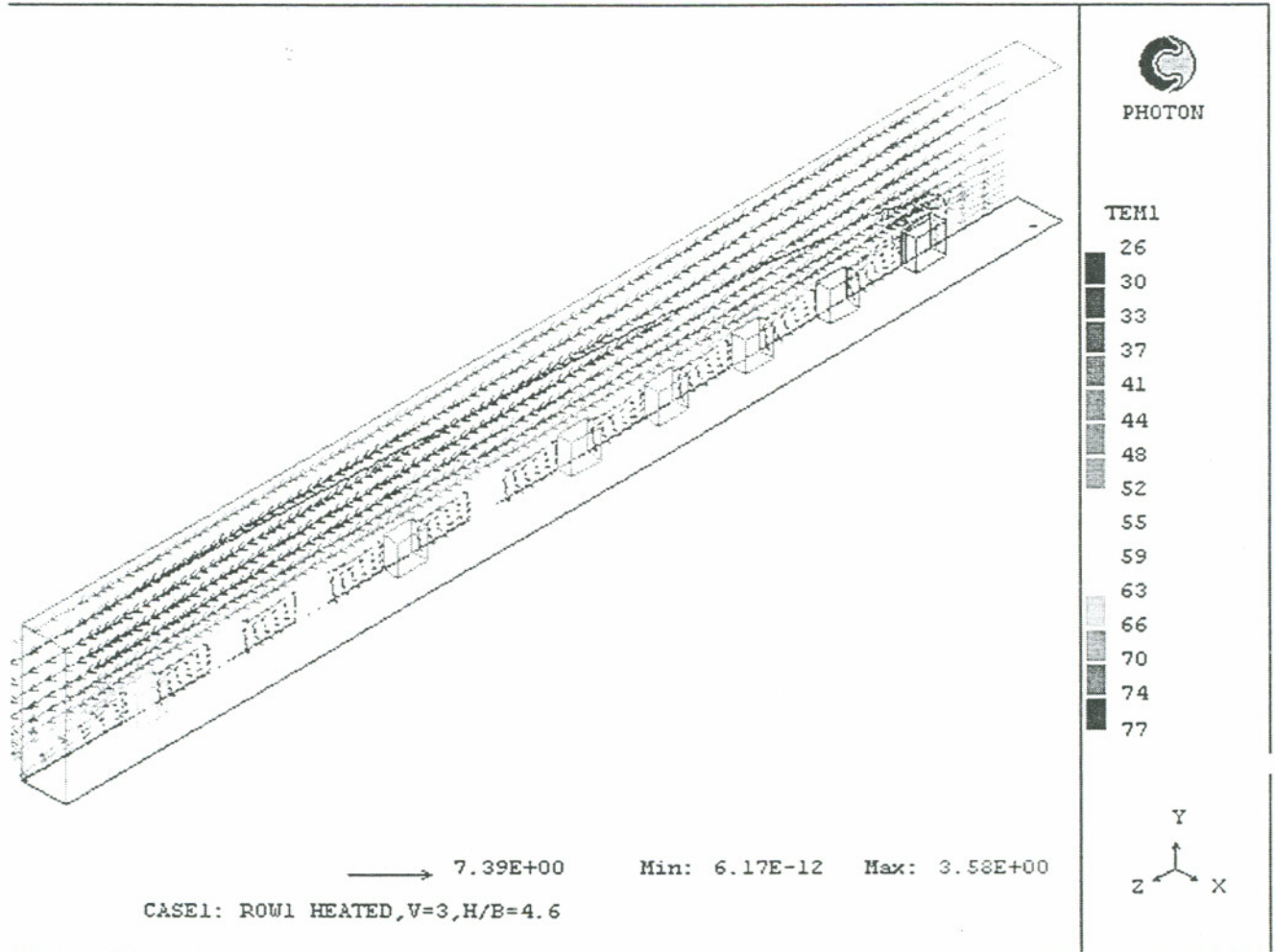


Fig.3-22 Vector Plots With Finite Volume Method

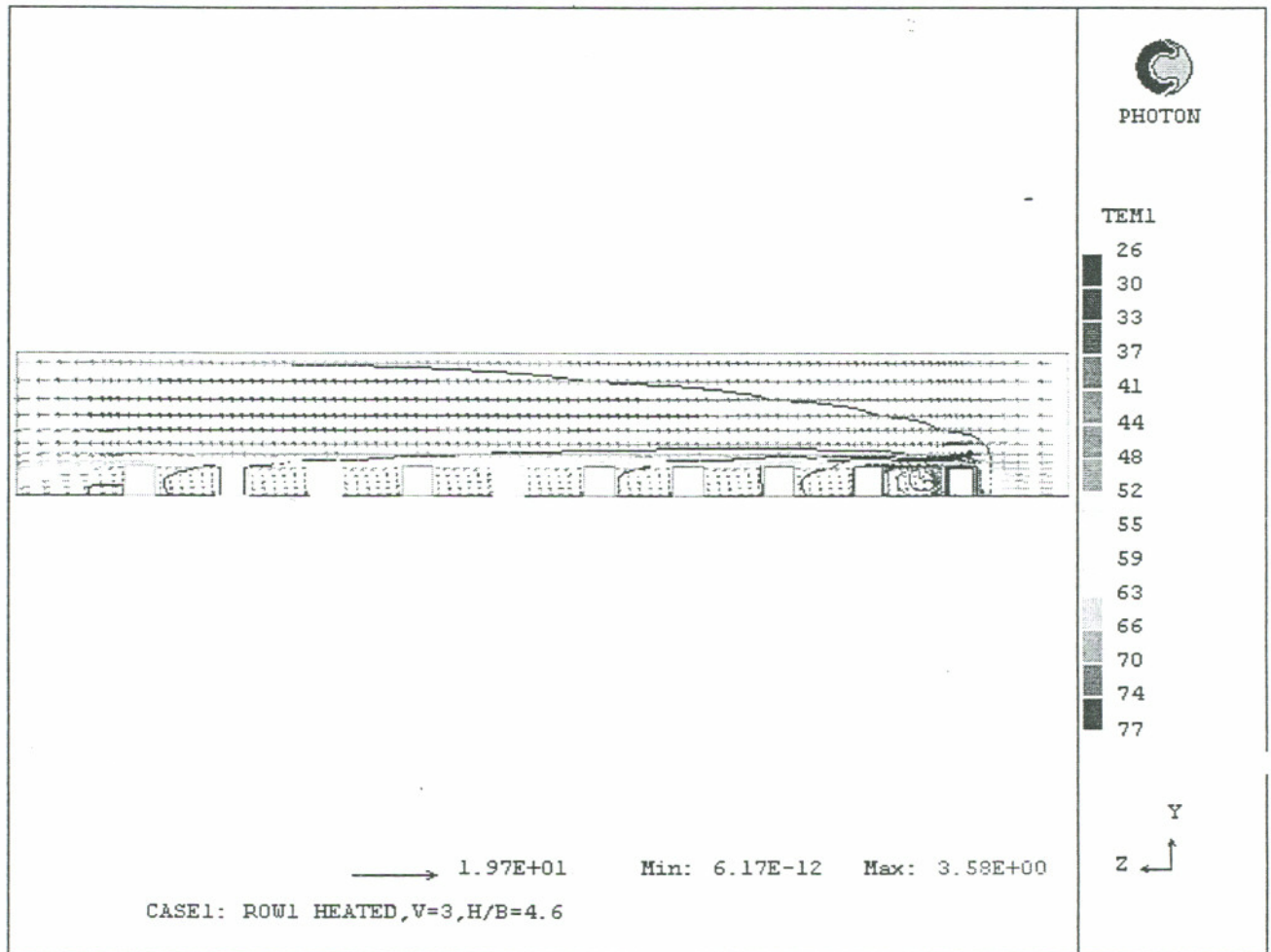


Fig.3-23 **Temperature Fields With 3D Finite Volume Model**

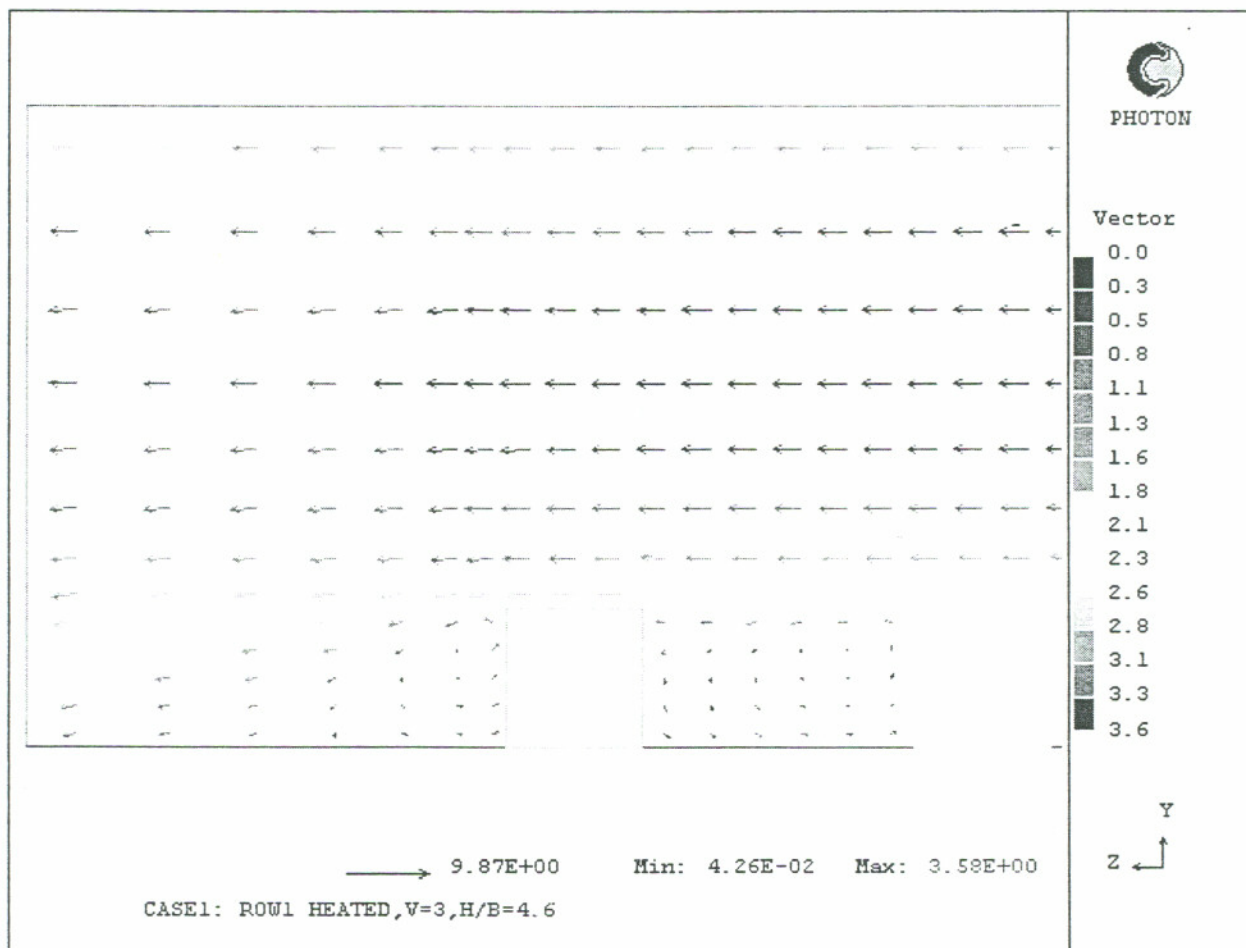


Fig.3-24 Back Flow Region

CHAPTER 4

SPECIAL TOPICS AND DISCUSSIONS

4.1 Component Level Simulation

Maximum temperature due to thermal dissipation of electronic packaging modules need to be kept below a critical value. The component level⁽⁴²⁾(Fig.4-1) simulation involved modeling the heat transfer within chips, boards, and heat sinks. To achieve this end, the effect of material properties, geometry and operating conditions on heat transfer can be investigated. Heat transfer analysis considerations were undertaken in the three main regimes namely conduction, convection and radiation. The link between the flow and heat transfer is by the convective coefficient applied as a boundary condition on the solid surfaces. The convective heat transfer coefficient may be obtained from empirical relationships, experiment, or computed at the system level analysis. There are special features in electronic packaging that make heat transfer modeling considerations complicated. These include:

1. Multiple heat flow paths through small solid objects; heat flows from chip to hundreds of tiny solder bumps, thermal vias or interfacial layer at micron level into the ceramic and case, then it flows into the board at the centimeter level by hundreds of pins and leads or interfacial layers⁽⁷⁷⁾ (Fig.4-2, 4-3).
2. The variable material properties introduced by large temperature gradient due to the variable thermal resistance.
3. Anisotropic material and composite materials such as multi-layer substrates and boards, which bring about the unknown material properties.
4. Complex structures such as implantation of the thermal layers inside the substrates, inlaying of wiring and leads, dies on substrate on the thermal pastes, pin fin heat sinks, *et al.*
5. Imperfect contact between components and layers.
6. Variable thermal load or power dissipation during the operation.

7. Multi-phase heat transfer with the air over the packaging surface and the liquid inside the package.

As a consequence of the above characteristics, component level thermal modeling has its own special features. Since a large number of elements is needed by the many different solid objects in a small domain; this will either increase solution times or can exceed the software limit for the maximum number of elements and the hardware ability in swap space in memory. This problem might be improved by maximizing the aspect ratio of elements in the meshes so as to decrease the total number of elements. But, too large an aspect ratio may cause solution inaccuracies and possible divergent solutions. And, for the different topology interacting objects such as cylinders and blocks in contact, meshing difficulties may result. Nevertheless, unstructured mesh approach is still an effective way to generate the solid model particularly in three dimensions.

The application of variable material properties like thermal conductivity is important for domains with large temperature gradients. This may apply under three circumstances:

- a) an isotropic solid with low thermal conductivity and large temperature gradients across boundaries,
- b) solid objects separated by a interfacial material which has a smaller thermal conductivity or a larger thermal conductivity and higher temperature gradient,
- c) transient heat transfer conditions.

Heat flow for the electronic packaging takes place from the chip through solder bumps, leads, pins, vias, and the ceramic into the boards by conduction. It is impossible, in some situations, or not practical to model the whole solid objects to represent all the flow paths by solders, pins, leads, vias, the model with all the details would lead to tremendously number of cells or elements and excessively long iteration times. From work done in this dissertation it was shown that it becomes less important to match the exact geometry of thermal vias ⁽⁴⁷⁾ (Fig.4-4). It is not practical to build numerical solid models with identical number and geometry detail of real part sizes at the micro level because this will make the number of cells or elements extremely large, and may lead to

impractical CPU time. The following special topic addressed the modeling of via, solder bump or pin, and thin interlayer.

4.1.1 Sensitivity Analysis of Thermal Via Configuration

In this study an attempt to substitute rectangular vias for circular vias was considered. In normal production, vias are circular in cross section. However, for modeling considerations, rectangular vias offer much more promise in the ease of generating elements with a good aspect ratio. Of issue in this consideration is that the shape substitution should not affect the accuracy of heat dissipation. Heat is dumped from chips to the vias and substrate, but since the substrate like ceramic is not a good electrical and thermal conductor, majority of the heat is transferred through the substrate along the axial direction of the cylindrical vias to the board. So, side surface is not a critical factor. On the contrary, the length and cross sectional area of the vias are critical factors. And since the rectangular cylinder via or pillar has similar heat transfer characteristics to that of the cylinder whose heat dissipation is uniform along the radial direction and mainly along the axial direction, cylindrical thermal vias may be replaced by rectangular cylinder with the same height and cross sectional area. The reasons are:

1. the thermal conductivity for the thermal vias like tungsten is largest among all the solids,
2. the side contact surface between the vias and ceramic board is relatively small compared axial direction of the thermal vias.

If we keep the cross section of the rectangular cylinder the same as that cylinder, and its edge a may be determined by:

$$a^2 h = \pi r^2 h \quad (4-1)$$

therefore,

$$a = \sqrt{\pi} r = 1.77r \quad (4-2)$$

where r is the radius of the cylinder; h is the height for both of the rectangular cylinder and the circular cylinder. A number of sensitivity analyses were conducted to explore the impact of geometric details of thermal vias to heat conduction with different substrate thermal conductivity.

Conclusion

Results were summarized in the Table 4-1, Table 4-2 and Table 4-3. The investigation was conducted under room temperature(25°C). T_j , chip junction temperature, and T_{via} , the maximum via temperature are recorded with three different thermal conductivity values. The reason for choosing thermal conductivity value at 20, 80 and 200 (W/m°C) is because, that of 200 represents conditions of a good thermal conductor, 80 is the chip characteristic, and 20 is about the same as that of substrate. They are thus representative for analyzing the temperature sensitivity caused by different material vias. The same principle was applied to a pin and interlayer temperature sensitivity analysis discussed in the next special topic.

The results showed that the relative error range introduced by replacing the circular via with a rectangular one is from 0.047% to 4.56%. Maximum temperature error occurred when thermal conductivity of the via is equal to that of the chip. The error for the via is from 0 to 0.018%. The rectangular via configuration takes only about 12% of the elements for the cylindrical via configuration. The hard disk space taken by rectangular via model is about 9% of cylindrical via model. And the computation time for rectangular via model is only 42% of cylindrical via model. The large the number of vias in the model the better the gains we extract by using square section vias compared to circular section pins. This is with regard to all solution performance metrics namely, solution time, memory and file storage space.

Pertinent Future Research

1. Analyze the combined influence of thermal via and multi-layer circuit board with anisotropic material properties.
2. Analyze the percentage of heat transfer of convection through the surface of the modules, the heat sink surface, and the conduction through the board by via.
3. The thermal resistance influence to efficiency of thermal via from the adhesive interlayer.
4. The optimal number and size of vias.

4.1.2 Sensitivity Analysis for Pins

For those parts with features less than 1mm such as solder bumps (Fig.2-8), leads and pins (Fig.4-2), which are either at the bottom or on the side of the chip, the most efficient way to model these parts is to use a solid pillar between the chips and board. The model could be approached by a rectangular solid pillar which is located between the die and substrate or chip and the board with the same thermal resistance as that of the total bumps or the pins. The total thermal resistance for pins in parallel is described as:

$$R = \sum_{i=1}^n R_i = \sum_{i=1}^n \frac{L}{A_i k_{\text{pin}}} = \frac{L}{n A_i k_{\text{pin}}} \quad (4-3a)$$

where L is the length of the solder or pin, substrate and board, n is its total number of the pins, k_{pin} is its thermal conductivity. A_i is its cross section area which is also contact area of pin to the chip; A_i is equal to r^2 for the rectangular pin or πr^2 for cylindrical bumps or pins, where r is the edge or radius of the cross section.

The thermal resistance of the pillar is described as:

$$R = \frac{H}{B^2 k_{\text{pillar}}} \quad (4-3b)$$

where B is the edge size of the bulk, H is its thickness, k_{pillar} is its thermal conductivity. To keep the same thermal performance, let the two thermal resistance equal, from equation (4-3a) and (4-3b), a relationship between the pillar and pins can be established as:

$$\frac{L}{n A_i k_{\text{pin}}} = \frac{H}{B^2 k_{\text{pillar}}} \quad (4-4)$$

If using the pin length as the pillar thickness, i. e. $L = H$, and same thermal conductivity, which is $k_{\text{pillar}} = k_{\text{pin}}$, the thickness of the pillar is then as:

$$B = \sqrt{n A_i} \quad (4-5)$$

when the pin is rectangular shape:

$$B = \sqrt{n r} \quad (4-5a)$$

when the pin is cylindrical:

$$B = \sqrt{n \pi r} \quad (4-5b)$$

A component level model is shown as Fig.4-5, 4-6, 4-7. The model consists of a component mounted on a circuit board by solder bumps or pins. The ambient temperature is 20°C with natural convection. A heat sink is on top of the device. The 3D thermal/flow model provided a convergence solution with the maximum IC temperature 93°C (Fig.4-8) with a single pillar⁽²⁴⁾. With the development of high performance integrated module, the tendency of the number of pins per module is expected to increase from about 2000 to 5000 in the year of 2000 (Fig.4-3). The percentage of heat transfer by conduction through the pins has been increasing correspondingly. The approach of the pins becomes a very important part to provide the accurate temperature results on ICs. The temperature will be very sensitive to the pin configuration.

A new model was developed using five pillars centrally distributed to the edge of the chip. Compared to the single pillar approached, this one allowed more heat to dissipate into the PCB than that with one pillar located at the center and got greater heat loss from the board and a cooler maximum temperature. The edge for each pillar is defined by

$$B = \frac{1}{m} \sqrt{nA_i} \quad (4-6)$$

where m is the number of the pillars, in this case $m = 5$. The value of m is determined through engineering judgment to create a good representation of the problem at hand in order to get representative and reliable results. There is often a trade-off between accuracy of results and speed of solution. For this problem, the solution from this five-pillar-model gave 86°C (Fig.4-9) which is 7°C lower than one-pillar-model, and it brought an additional 8.1% relative error (Table 4-4).

The two cases both involved heat sinks attached. Studies were conducted using both methods without heat sink were conducted (Fig.4-10), (Fig.4-11). The results show that the maximum IC temperatures were 123°C with one pillar only versus 108°C with five pillars; The 15°C difference brought at least 13.9% relative error from the simulation (Table 4-5). The results also showed that for the conduction dominated case, which is the model without heatsink, the percentage of the heat flux by conduction changed from

37.5% to 50% (Fig.4-12). Under this situation, if we still use one pillar model, it will cause at least 13.9% simulation error on chip temperature.

Conclusion

Pins play a very important role of dissipating heat by conduction into the board under following cases:

- Conduction is the dominant heat transfer mode,
- Conduction and low efficient convection such as natural convection, rarefied gas convection, low Reynolds number flow, no heat sink.
- Conduction and radiation at low temperature level and temperature difference,
- Enhanced conduction heat transfer case like large number of pins, leads, high thermal conductivity solder bumps with more layer boards.

The simulation results comparison between the one pillar model and five pillar model showed that the model with more pillars provided more representative heat transfer, but there is an optimal number of pillars to balance the accuracy and problem solving time. The reason for the inaccuracy of one pillar model is that the model is built based upon the equal thermal resistance assumption. For a single real pin, it is one dimensional flow along the pin length, but when treated as a sold pillar, the effective thermal resistance is no longer one dimensional; using one dimensional conduction approach improperly will cause error. The choice for the number of pin pillars is really problem dependent. It should be judged on a case by case basis. The best way is to model a simple model to check how sensitive the number of pins result in. Using single pin pillar predicted higher temperature and this might result in an over-design.

Pertinent Future Research

Future work could focus on two possible directions:

- Research on establishing the temperature correlations between single-pillar and multi-pillar models.
- For thermal management at component design, arrange the pin pattern not only considering electrical considerations, but also in a heat transfer enhancement formats

for the increasing number of pins has been taking a higher and higher percentage of conduction heat transfer.

4.1.3 Sensitivity Analysis of Interlayer Thickness

The contact region is a heat transfer barrier between two contact ingobjects. This barrier could be a substance inserted between the contact surfaces like thermal paste, soldering bumps, or the physically or chemically interacting regions between the two objects under pressure or thermal load. Usually this interface is very thin (1~3 mil for the adhesive layer for heat sinks). Even though it is tiny; it still possesses a thickness and has its thermal characteristics with rather high thermal resistance which results in large temperature difference at the interface. To model this layer directly with an effective thickness and thermal conductivity is even less practical than modeling hundreds of pins.

For those layers with a third substance in addition to the two contacting objects, there are two ways available to apply them to the numerical model. The first way is to define this layer by a thermal resistance R or a heat-transfer-coefficient h in terms of a linear equation between the heat dissipation rate q and the temperature difference between the two surfaces of the layer as:

$$q = h(T_1 - T_2) \quad (4-7)$$

or

$$q = \frac{(T_1 - T_2)}{R} \quad (4-8)$$

where T_1 and T_2 are the two surface temperatures of the layer. The values of the R or h can be obtained from procedures described in Chapters 1 and 2 of this dissertation. The interior of this layer is not meshed.

The second way is to “magnify” the effective thickness of the layer to match the sizes of their adjacent components so as not only to reduce the number of elements or cells but also to decrease the distortion of the aspect ratio. The following equations are based upon an example of heat transfer among the chip, substrate and adhesive layer:

$$Q = Q_n = -kA \frac{T_1 - T_2}{\frac{t_1}{k_1} + \frac{t_e}{k_e} + \frac{t_2}{k_2}} \quad (4-9)$$

$$Q' = Q \approx Q'_n = -k'_e A \frac{T'_1 - T'_2}{\frac{t_1}{k_1} + \frac{t'_e}{k'_e} + \frac{t_2}{k_2}} \quad (4-10)$$

and

$$T_1 = -\frac{Q}{A} \left(\frac{t_1}{k_1} + \frac{t_e}{k_e} + \frac{t_2}{k_2} \right) + T_2 \quad (4-11)$$

$$T'_1 = -\frac{Q'}{A} \left(\frac{t_1}{k_1} + \frac{t'_e}{k'_e} + \frac{t_2}{k_2} \right) + T'_2 \quad (4-12)$$

where Q is the total heat transferred across all the boundaries. Q_n is heat dissipated across the real contact interface; and Q'_n is the heat dissipated across the pseudo contact interface; A is the contact area; T_1 and T_2 are the temperatures at the two out surfaces for the chip and substrate; k_e is the thermal conductivity of the layer; and k'_e is the thermal conductivity of the pseudo layer; t_e is the effective thickness of the layer; and t'_e is the effective thickness of the pseudo layer.

Assuming the substrate bottom surface is fixed at a constant temperature, and the effective thickness t_e is smaller than its plane edge l , i.e. $\frac{t_e}{l} \rightarrow 0$, in other words, the heat transfer in the in-plane direction is negligible so that $Q \approx Q_n$, then $T'_1 = T_1$ and $T'_2 = T_2$, thus $T'_1 = T_1$, and

$$T'_1 - T_1 = \frac{Q}{A} \left(\frac{t'_e}{k'_e} - \frac{t_e}{k_e} \right) \quad (4-13)$$

If we magnify t_e to

$$t'_e = \alpha t_e \quad (4-14)$$

and if we want to keep the chip or die temperature for the enlarged layer model the same as the that of the original model, let

$$T'_1 - T_1 = \frac{Q}{A} \left(\frac{t'_e}{k'_e} - \frac{t_e}{k_e} \right) = 0 \quad (4-15)$$

then

$$k'_e = \alpha k_e \quad (4-16)$$

That means if the effective thickness of the interface layer has been increased α times, the thermal conductivity of this layer is needed to be increased α times as well.

Generally, α could be chosen at any value as long as $\frac{t'_e}{l} \rightarrow 0$, but the simulation error introduced by α when $\alpha > 1$ is associated with different configurations. If the only or majority of heat transfer occurs at either the top surface of the chip or bottom surface at the substrate with adiabatic boundaries at the sides, α could be any value even as $\frac{t'_e}{l} \rightarrow 1$. But, this does not mean the larger α the easier to model. If the thickness of the layer is equivalent to the smallest thickness between the chip and substrate, the mesh quality is the best. The optimal value for α may be derived from:

$$t'_e \rightarrow \min\{t_1, t_2\} \quad (4-17)$$

or

$$\alpha = \frac{\min\{t_1, t_2\}}{t_e} \quad (4-18)$$

If there are voids inside this layer, α needs to be modified by multiplying it with the void rate $\lambda (< 1)$.

For cases in which the interfacial layer is formed by voids, the interacting materials such as intermetallic compounds and so on, the above method is applicable only if the effective thickness and the thermal conductivity of the layer is available, and the layer thickness is not too small, the void ratio is about zero. But in reality, these condition do not exist. If the contact region is dominated by normal pressure and there is no void, some formulae to calculate the thermal resistance may be used, for example, the equation proposed by Meekisho⁽⁵⁾:

$$\frac{1}{R_c} = 1.25 \left(\frac{P}{H} \right)^{0.95} \quad (4-19)$$

After R_c is obtained, apply it to the thermal resistance definition equation $R_c = \frac{t}{Ak}$, the thermal conductivity for the pseudo layer is then as:

$$k = \frac{t}{AR_c} = \frac{t_e}{AR_c} \quad (4-20)$$

Some numerical codes incorporate contact resistance to deal with the contact problems. For example, Phoenix⁽⁴⁸⁾ uses porosity P_o which is the function of the distances from the cell center to the faces in two solids, thermal conductivity and thermal resistance.

Conclusion

Table 4-6 presents study results on the temperature sensitivity using this approach with three different times enlarged thickness by different quality of mesh (Fig.4-13, 4-14, 4-15). The method is particularly advantageous when there is a significant size difference in layer thickness between the substrate and the chip. No measurable error was realized using enlarged effective interlayer thickness and thermal conductivity. The advantages using this configuration are:

1. the number of elements decreased by up to 12%,
2. the disk space usage decreased by 10%,
3. CPU time decreased by 46%.
4. The choice for the α should not make the thickness of the layer more than the thickness of chips or substrates and boards, otherwise, the number of elements will increase.

Pertinent Future Research

The following are deemed pertinent future research activities:

1. Examine heat transfer performance of the interlayer with voids or multiphase material, composite material for their large thermal resistance to heat flux from the chips.

2. Observe module temperature as a function of thermal conductivity, and thickness.
3. Determine the effect of material properties and the effective thickness of the interlayer.

4.2 System Level Simulation

Unlike component level simulation, system level simulations focuses on the relationship between the fluid flow and the electronic components and circuit boards. It involves the flow profiles across the solid components and circuit boards. It may couple the fluid flow to the heat transfer process. For this simulation, minute details like adhesive layers, dies, substrate, vias, pins⁽⁴⁴⁾, *et al*, were ignored, instead, they were represented as whole units with the same material properties. The analysis domain was the whole cooling system bounded by the walls, inlet where the fans are located, opening for the vents. For the systems in large scale, all the components were represented by the surface roughness of a plate, which represented the electrical circuit board, and their power converted to power dissipation uniformly distributed on the surfaces at different sides of the circuit board.

The interests of the simulations ultimately centered on the convective heat transfer coefficients on the specific board or the location where a specific component mounted on a board. The simulation concerns on how to obtain the best or optimal convective heat transfer coefficients at the certain location for the system design, and what is going on for different system operations for the system operation modeling. The convection ultimately determines the temperature distribution inside the electronic components.

4.2.1 Fan Design

The major issues for the forced air cooling systems are the selections of the fans or blowers, vents, walls, and the ways to distribute the circuit boards. The major difference between a fan and a centrifugal blower is the flow and pressure characteristics. Flow from a fan is radial and parallel to the fan blade axis. A fan delivers a high flow rate

at low pressure. Flow from a blower is perpendicular to the blower axis with lower flowrate but against higher pressure ⁽⁴²⁾(Fig.4-16).

The most common styles of fans are propeller, tube and vane axial. Tube axial fan, also called muffin fan, is most commonly used in electronic cooling because it generates less vortex flow which makes it similar to propeller fan. The fan configuration includes their location, size, number, flow direction, flowrate based on the fan performances which are determined by the fan curves. The vent design covers the number of vents, the location, the direction, the size, and the back pressure of the outlets. The walls composed of internal and external walls, which also governing the flow pattern besides fans and vents, and their location and geometry. The fan location is somehow more important than its CFM performance because its location determines the flow pattern and pressure gradients which affects the fan performance, the magnitude of the mass flow rate, which ultimately determines the heat transfer rate from the boards, components to the air. If a fan is mounted to a place, which makes it operate with large a pressure drop across the fan (static pressure) or at the flat region, the performance may be poor. The fan curve is a critical factor that helps in choosing the right fan. For a linear fan curve, if the flowrate at zero static pressure and the fan static pressure at zero flowrate are known, a characteristic curve can be obtained as ⁽³⁶⁾:

$$\dot{m} = \dot{m}_0 \frac{(p_o - p_{fs})}{p_o} \quad (4-21)$$

where \dot{m} is flowrate at any pressure drop, \dot{m}_0 is the flowrate at zero static pressure, p_o is the pressure at zero flowrate. In reality, the fan curve is nonlinear and the curve is provided by the fan manufactures ⁽²⁰⁾(Fig.4-17). When the flow is not only exiting the fan in a direction normal to fan plane, but also in a direction oriented at an angle θ to the flow direction, the swirl magnitude S needs to be applied as:

$$u_\theta(r) = u_z \left(\frac{r}{R} \right) S \quad (4-22)$$

where $u_\theta(r)$ is the velocity in the revolution direction, u_z is the velocity in the normal fan direction, r is the radial coordinate, R is the outer radius of the fan.

When designing a fan, the following basic equation is often used to define the total cooling air requirement ⁽²⁰⁾:

$$m = \frac{1760 \times KW}{\Delta T_k} \quad (4-23)$$

where m is required air flow in CFM, KW is heat to be dissipated, ΔT_k is allowable temperature rise in degrees Kelvin.

The second step is to define the system characteristic curve of the enclosure from the inlet to the exhaust outlet. The system characteristic curve formula is:

$$\Delta P = K \dot{m}^n \quad (4-24)$$

where K is system characteristic curve ⁽²⁰⁾ (Fig.4-18) constant; and n is the turbulence factor, which is between 1 and 2, (for laminar flow, $n = 1$, for turbulent flow $n = 2$). The system characteristic curve is determined by total system impedance, which is the combination of:

- inlet/outlet,
- filters like screens and guards,
- interior barriers like cables, wires, frames, structures, and
- electronics like ASICs, chips, cards and boards.

The intersection between the fan curve ⁽²⁰⁾ (Fig.4-19) and the system characteristic curve is the operation point. The operating point should not only match the m calculated from equation (4-20), but also locate at the high slope section of the fan curve, in other words, avoid the flat region, such as to minimize the flow rate change caused by the pressure change.

4.2.2 Heat Sink Design

Generally, there are two types of heat sinks according their fin shapes. They are extruded heat sink and pin fin heat sink. There are also other special types of heat sinks according to their special shapes, functions, and cooling, for example, fan heat sink.

The basic heat transfer mechanism of a heat sink is described as ⁽³¹⁾:

$$W = \frac{T_j - T_A}{R_{\theta JC} + R_{\theta CS} + R_{\theta SA}} \quad (4-25)$$

where W is the power dissipation by a semiconductor device or component; T_j is the IC junction temperature; T_c is case or cap temperature, T_s is the mounting surface temperature of heat sink; T_A is air temperature; $R_{\theta jC}$ is thermal resistance ($^{\circ}\text{C}/\text{W}$) from junction of the ICs to its case; $R_{\theta CS}$ is thermal resistance through the ICs case; and $R_{\theta SA}$ is thermal resistance from the heat sink to the air. $R_{\theta jC}$ is usually determined after the IC device are made by the semiconductor manufactures. $R_{\theta CS}$ is obtained from the thermal resistance/pressure curve which is provided by heat sink manufactures under typical operating conditions. If there is no curve available for the design, both system level simulation is most efficient to design or select heat sink. When choosing the adhesive layer or material, maximum shear stress is to be considered based upon its application.

It is important to choose the right type of heat sink; if the flow is not parallel to the extrusion direction of a heat sink, pin fin heat sink is recommended. When the angle between the flow direction and extrusion direction is 45° , pin fin heat sink has the smallest thermal resistance. When the flow is parallel to the extrusion direction of a heat sink, extruded heat sink is the most efficient.

Due to large velocity and temperature gradients at the boundary layer between the solid surface and fluid flow, a relatively fine and a structured mesh is very critical especially near these regions. This is to ensure convergence and reliability of the solution. Since the system domain covers the components, circuit boards, fans, vents, walls, and the flow problems are usually three-dimensional, extraordinarily large numbers of elements are required for solving the CFD problem. This requires high speed computer with large enough memory and file storage space. Unfortunately such demands on a computing system are hard to satisfy, it is often necessary to make simplifying assumptions on the problem, to meet the capability of available computers. The most common assumptions and practices for electronics packaging problems are as follows:

- Newtonian fluid,
- Single phase,
- Incompressible fluid,
- Simplifying the physical domain by use of symmetry

- Lowering the dimensions.

The following case study represents the steps to solve a three-dimensional turbulent forced air cooling system coupled with thermal model.

4.2.3 Results of Heat Transfer Analysis for In-line Arrays of Modules in Air Channel Flows

This model referred to the problem described in Chapter 3. The results were obtained by a finite volume method with three dimensional model. The number of cells are 126,666 cells. The domain was meshed by $18 \times 31 \times 227$ grids along x , y and z directions. The size of the whole domain was $(x, y, z) = (1.905e-02, 5.842e-02, 5.000e-01)$. The tolerance at three directions were all set to $1.000E-05$. The machine-clock time of run was 46380 seconds, and the results were converged.

The curves in Fig 4-21 to Fig 4-34 presented the comparison between the maximum temperatures measured from test and calculated from the simulation. The maximum temperatures happened on the chips heated. The 12 curves were from the simulation for 12 experiment cases with different power dissipation, flow velocities, height of channels. Fig 4-21 to Fig 4-26 showed the module temperatures with the ratio of 4.6 between the channel height and the module height at different air flow rate and power dissipation on different modules. Fig 4-27 to Fig 4-32 showed the module temperatures with the ratio of 2.25 between the channel height and the module height at different air flow rate and power dissipation on different modules.

From the results, the relative errors from simulation are plotted against the Reynolds numbers corresponding to the characteristic dimension of the solid module and the channel as Fig 4-33 and 4-34. Conclusion were made by the above curves:

- 1) The relative errors decreased along the flow direction inside the channel with one exception.
- 2) With the increasing of Reynolds number, the relative error dropped.
- 3) The variation of the Reynolds number of the channel also affected the simulation results the temperature on the modules.

- 4) Finite element analysis was found to be very sensitive to element number/size and turbulence model (hence inadequate for turbulence problems analyzed in this thesis).
- 5) FVM was better to reproduce experimental test benchmark data with a largest error less than 8%.
- 6) FVM was found to be an effective tool to design and predict thermal/flow conjugate problems encountered in system level packages.

Pertinent Future Research

- 1) Explore the sensitivity of temperature to the mesh density in the thermal-flow conjugate problems.
- 2) Examine the percentage of the natural convection to the total forced convective heat transfer. This research should best focus on conditions of temperature difference between air flow and chip temperature under 70°C.
- 3) Explore the correlation between the temperature difference and the component temperature since temperature difference of the flow is the driving force for natural convection.
- 4) Apply fan curve characteristics to the inlet flow since studies completed in this dissertation used uniform velocity profile. It would thus be beneficial to explore temperature sensitivity with the use of both linear and nonlinear fan curve characteristics. A relevant component of this study would be the inclusion of cooling effect with normal flow and reverse flow of the fan.
- 5) Correlate three-dimensional CFD problems involving irregular shapes of components and/or boundaries by using regular geometrical models.
- 6) Analyze the influence of radiation to the forced convection cooling system, and its sensitivity to the module temperature. The investigations could be conducted with normal air and rarefied airflow or high temperature with lower air density.
- 7) Study multiphase flow simulation for the air-water cooling system, which combines the air cooling for the components and water cooling for the cold plates, connected to the substrates or circuit boards.

- 8) Simulate impingement behavior of individual high-power dissipation components with different combination of the impinging distance, velocity and nozzle diameters. Compare the simulation results with benchmark test results to obtain the correlation for the heat transfer coefficient. This study could be combined with a fan heat sink design.
- 9) Use nonlinear models to simulate heat transfer with the incorporation of contact thermal resistance directly to the model. This study can feasibly be conducted with the aid of the ANSYS finite element code.
- 10) Study the thermal performance of the interfacial layer with different materials such as adhesive, thermal paste, intermetallic compounds for different level packaging requirements.
- 11) Modeling of coupled thermal-structural problems with emphasis on the different Coefficient of Thermal Expansion (CTE) of the materials and different temperature ranges or power levels.

Table 4-1 Comparison Of Simulated Results For The Two Vias

Via section	$T_j(^{\circ}\text{C})$	$T_{\text{via}}(^{\circ}\text{C})$	Elements	Disk (Mb)	CPU(times)
Circle	33.553	33.458	207,300	1,128	2.4
Square	33.355	33.458	25,200	100	1

$$k_{\text{via}}=200(\text{W}/\text{m}^{\circ}\text{C})$$

Table 4-2 Comparison Of Simulated Results For The Two Vias

Via section	$T_j(^{\circ}\text{C})$	$T_{\text{via}}(^{\circ}\text{C})$	Elements	Disk (Mb)	CPU(sec)
Circle	38.881	38.144	207,300	1,128	2.4
Square	37.110	36.918	25,200	100	1

$$k_{\text{via}}=80(\text{W}/\text{m}^{\circ}\text{C})$$

Table 4-3 Comparison Of Simulated Results For The Two Vias

Via section	$T_j(^{\circ}\text{C})$	$T_{\text{via}}(^{\circ}\text{C})$	Elements	Disk (Mb)	CPU(sec)
Circle	101.100	99.182	207,300	1,128	2.4
Square	101.052	99.151	25,200	100	1

$$k_{\text{via}}=20(\text{W}/\text{m}^{\circ}\text{C})$$

Table 4-4 Model With Heatsink

Pin	T_j (°C)	Heat Flux by Conduction	Heat Flux by Convection
1 Pillar	92.7	27.5%	72.5%
5 Pillar	86.7	37.5%	62.5%

Table 4-5 Model Without Heatsink

Pin	T_j (°C)	Heat Flux by Conduction	Heat Flux by Convection
1 Pillar	123.3	35%	65%
5 Pillar	108.3	50%	50%

Table 4-6 Simulation Comparison Using Different Pseudo Layer Thickness

α	T_j (°C)	Elements	Disk (Mb)	CPU(times)
1	59.803	3150	15.05	2.2
5	59.803	384	1.60	1
20	59.803	576	8.40	1.6

$k=2$ (W/m°C)

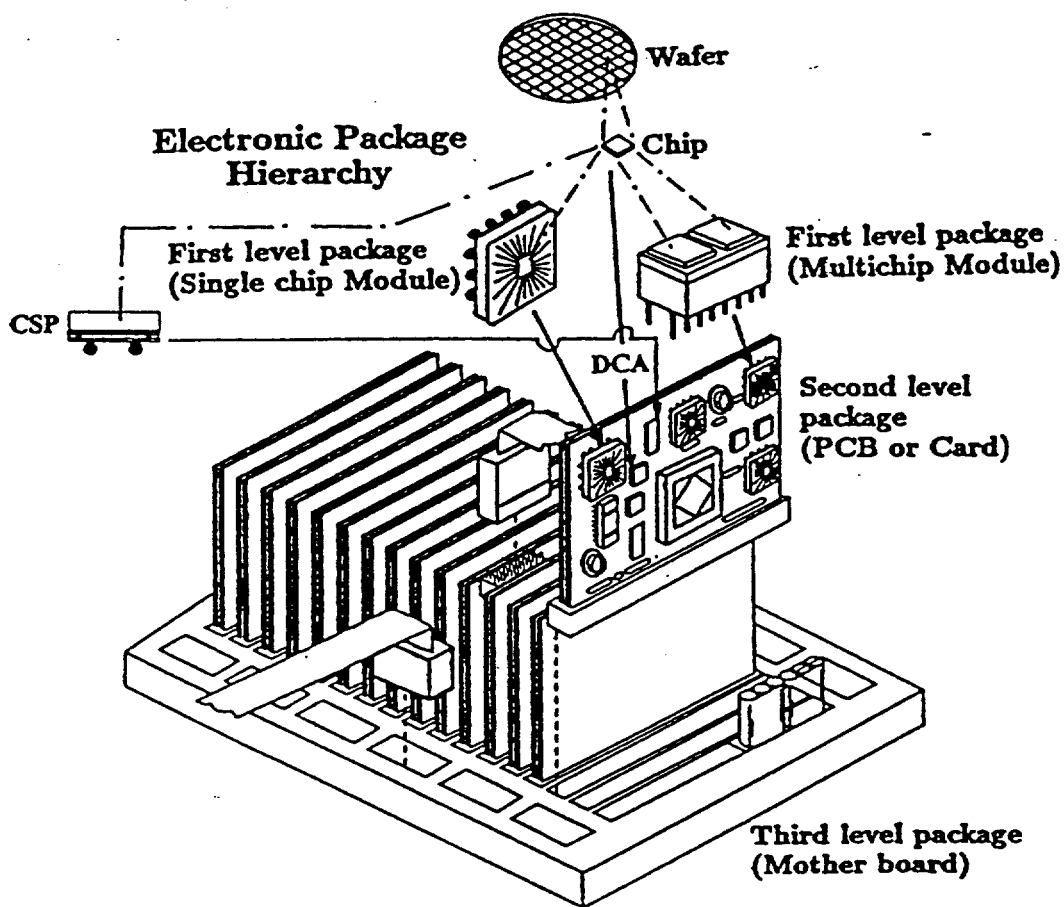


Fig.4-1 Packaging Hierarchy (Adapted From Ref. 42)

Through Hole Package		Surface Mounted Package			
a	A rectangular package with two parallel rows of pins extending from the bottom.	DIP (Dual In-line Package)	g	A rectangular package with pins extending from two opposite sides.	SO or SOP (Small Out-line Package)
b	A rectangular package with pins extending from two opposite sides, similar to DIP but smaller.	SH-DIP (Shrink DIP)	h	A square package with pins extending from all four sides.	QFP (Quad Flat Package)
c	A very narrow rectangular package with pins extending from two opposite sides.	SK-DIP, SL-DIP (Skinny DIP, Slim DIP)	i	A square package with a flat top surface and no visible pins.	LCC (Leadless Chip Carrier)
d	A rectangular package with a single row of pins extending from the bottom.	SIP (Single In-line Package)	j	A square package with pins extending from all four sides, some are longer than others.	PLCC, SOJ (Plastic Leaded Chip Carrier with Butt Leads)
e	A rectangular package with pins extending from the bottom in a zig-zag pattern.	ZIP (Zig-zag In-line Package)	k	A square package with a grid of small circular solder balls on the bottom surface.	BGA (Ball Grid Array)
f	A square package with pins extending from all four sides in a grid pattern.	PGA (Pin Grid Array) or Column Package	l	A square package with a central square area and radiating lines representing wire bonds.	TAB (Tape Automated Bonding)
			m	A very small rectangular package with pins extending from two opposite sides.	CSP (Chip Scale Package)

Fig.4-2 Types Of The Chip Level Packaging (Adapted From Ref. 77)

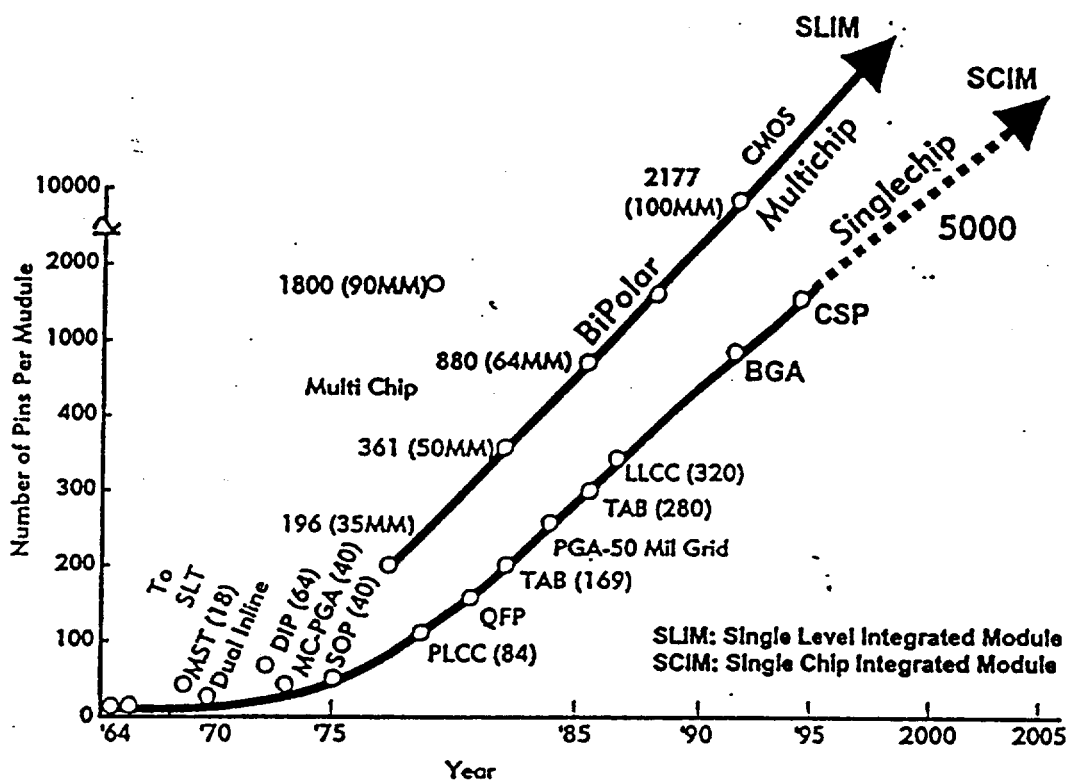


Fig.4-3 Chronological Development of Single-Chip And Multichip Modules (Adapted From Ref. 77)

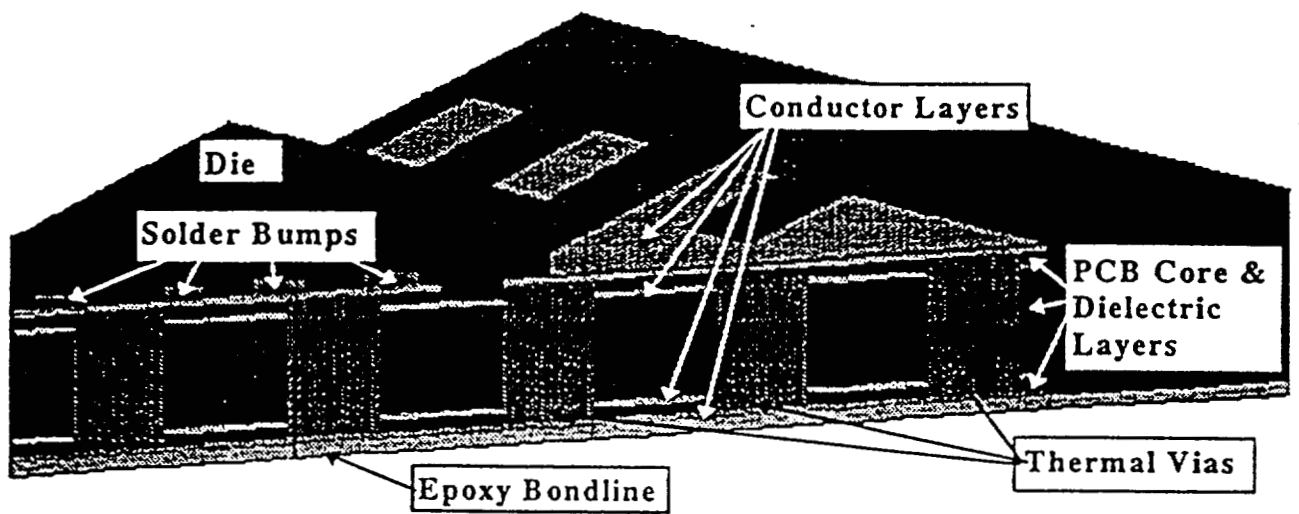


Fig.4-4 Thermal Vias (Adapted From Ref. 47)

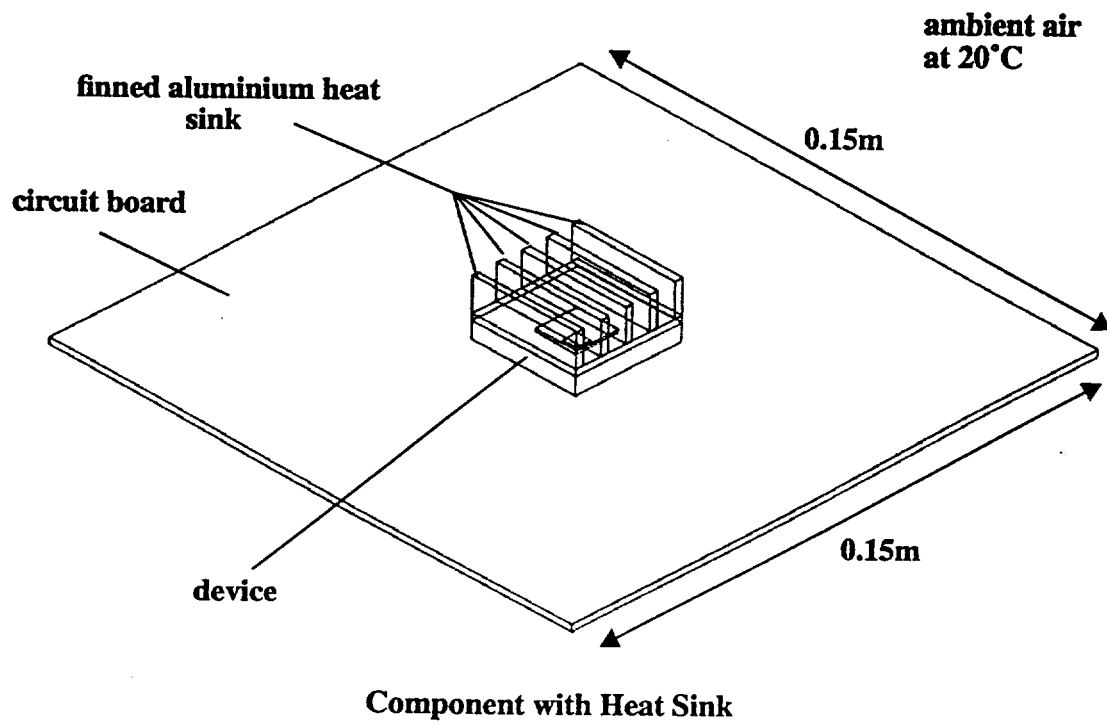


Fig.4-5 **Component With Heat Sink (Adapted From Ref. 24)**

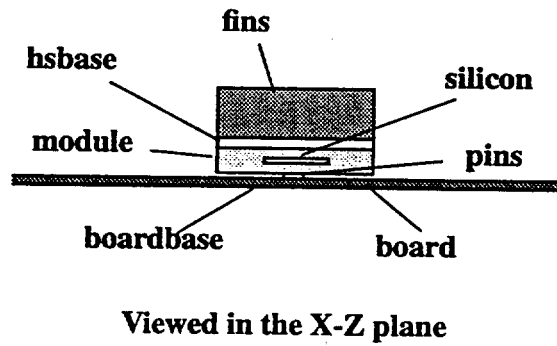


Fig.4-6 **Structure Of The Component (Adapted From Ref. 24)**

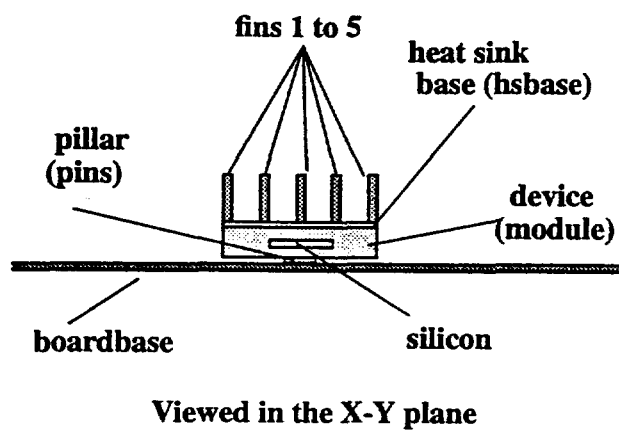


Fig.4-7 **Structure Of The Component (Adapted From Ref. 24)**

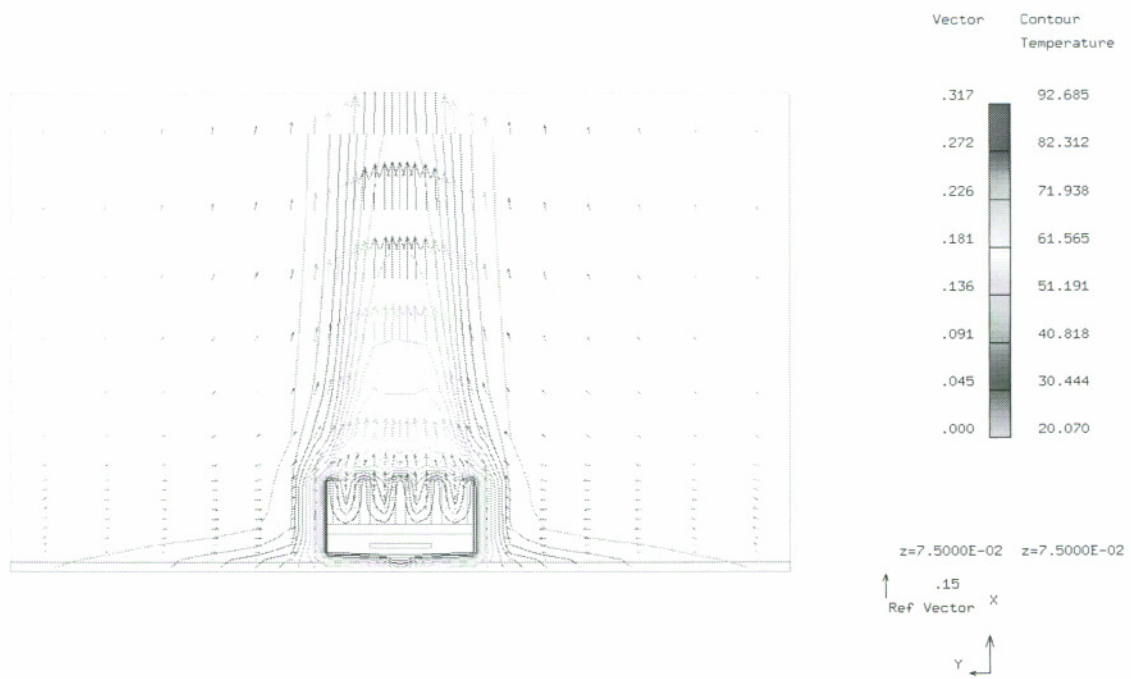


Fig.4-8 Simulation Results Using One Pin Pillar With Heat Sink

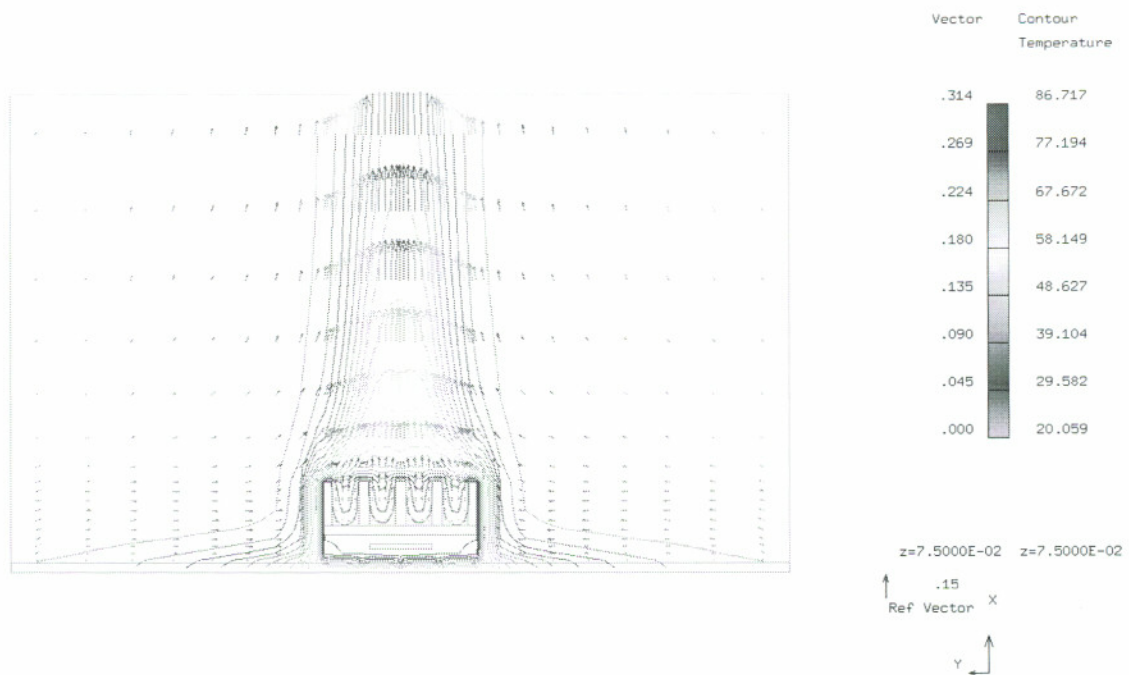


Fig.4-9 Simulation Results Using Five Pin Pillar With Heat Sink

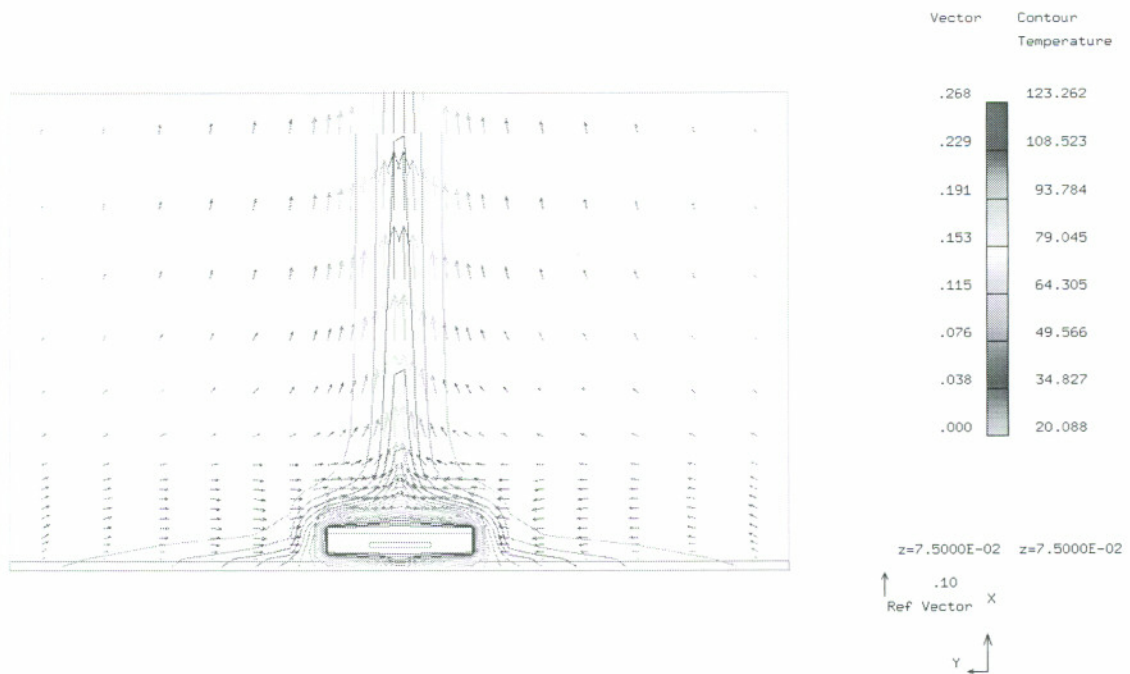


Fig.4-10 Simulation Results Using One Pin Pillar Without Heat Sink

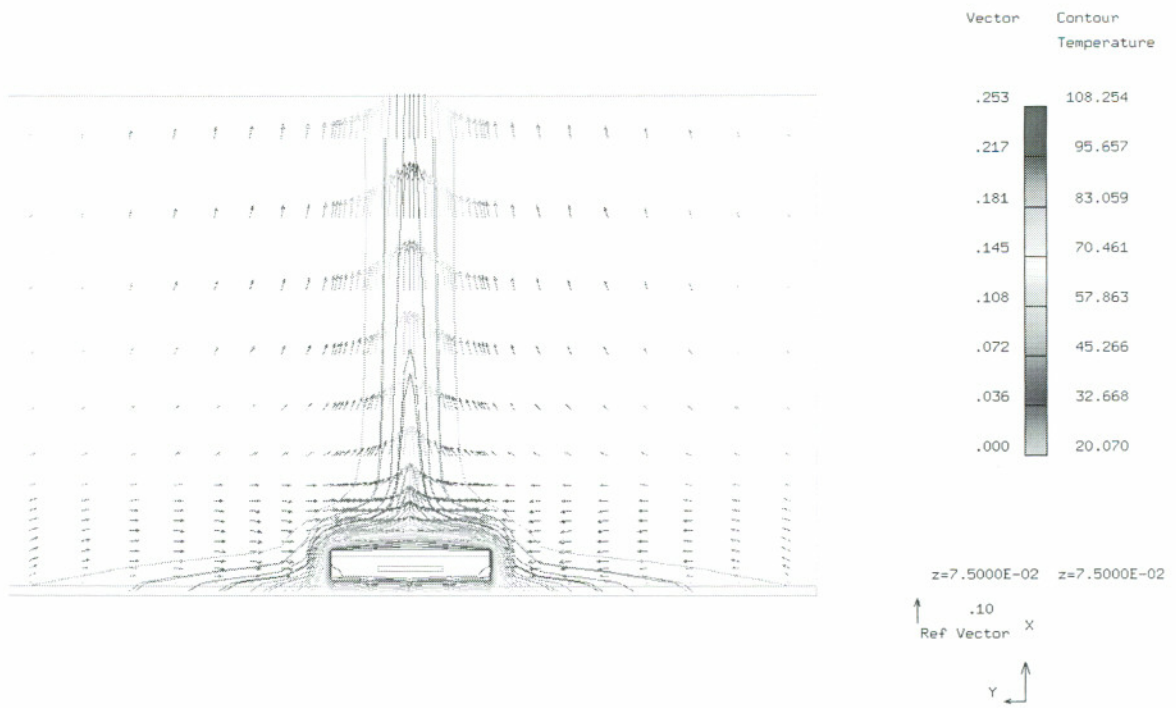


Fig.4-11 Simulation Results Using Five Pin Pillars Without Heat Sink

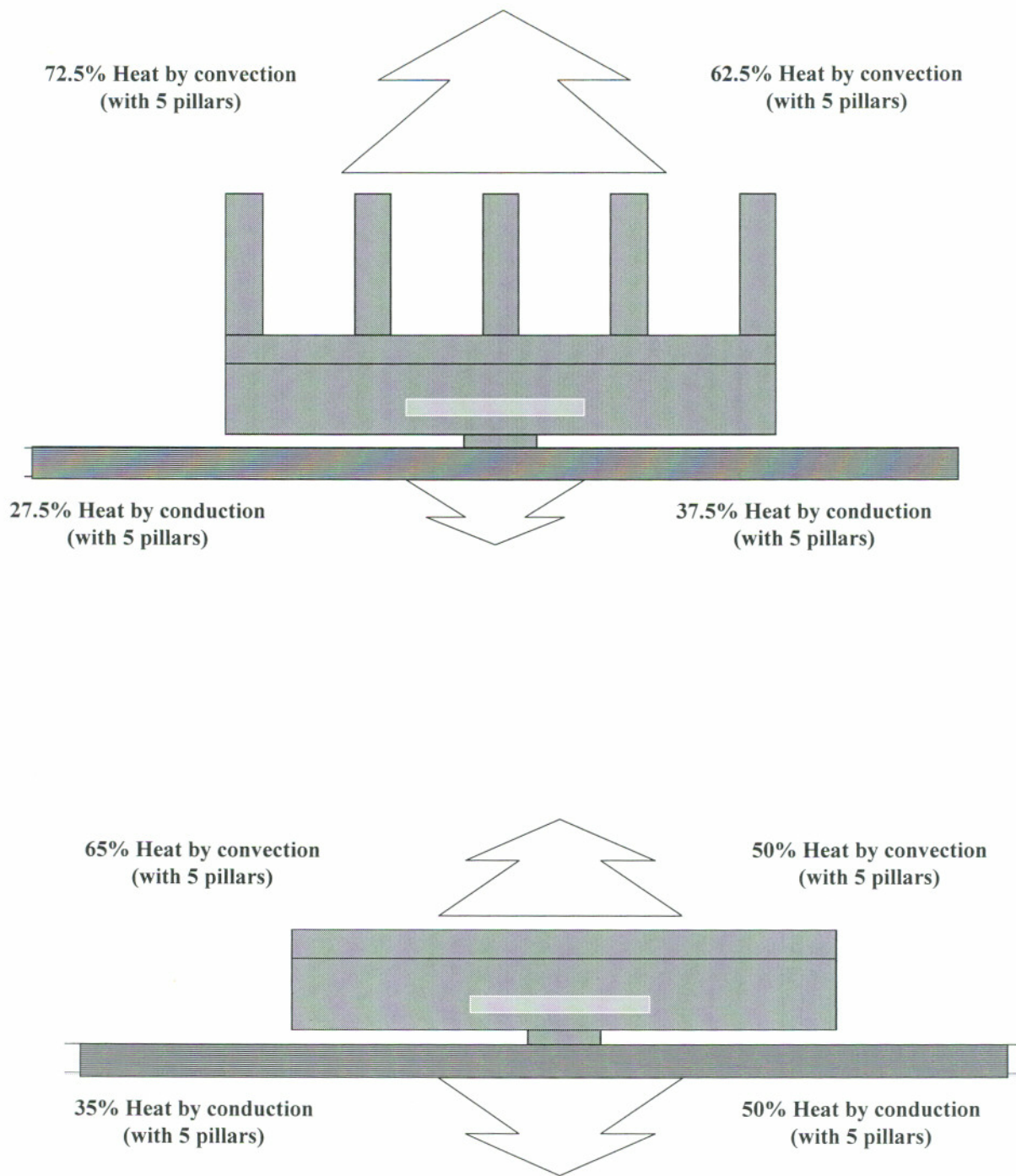


Fig.4-12 Simulation Result Comparison

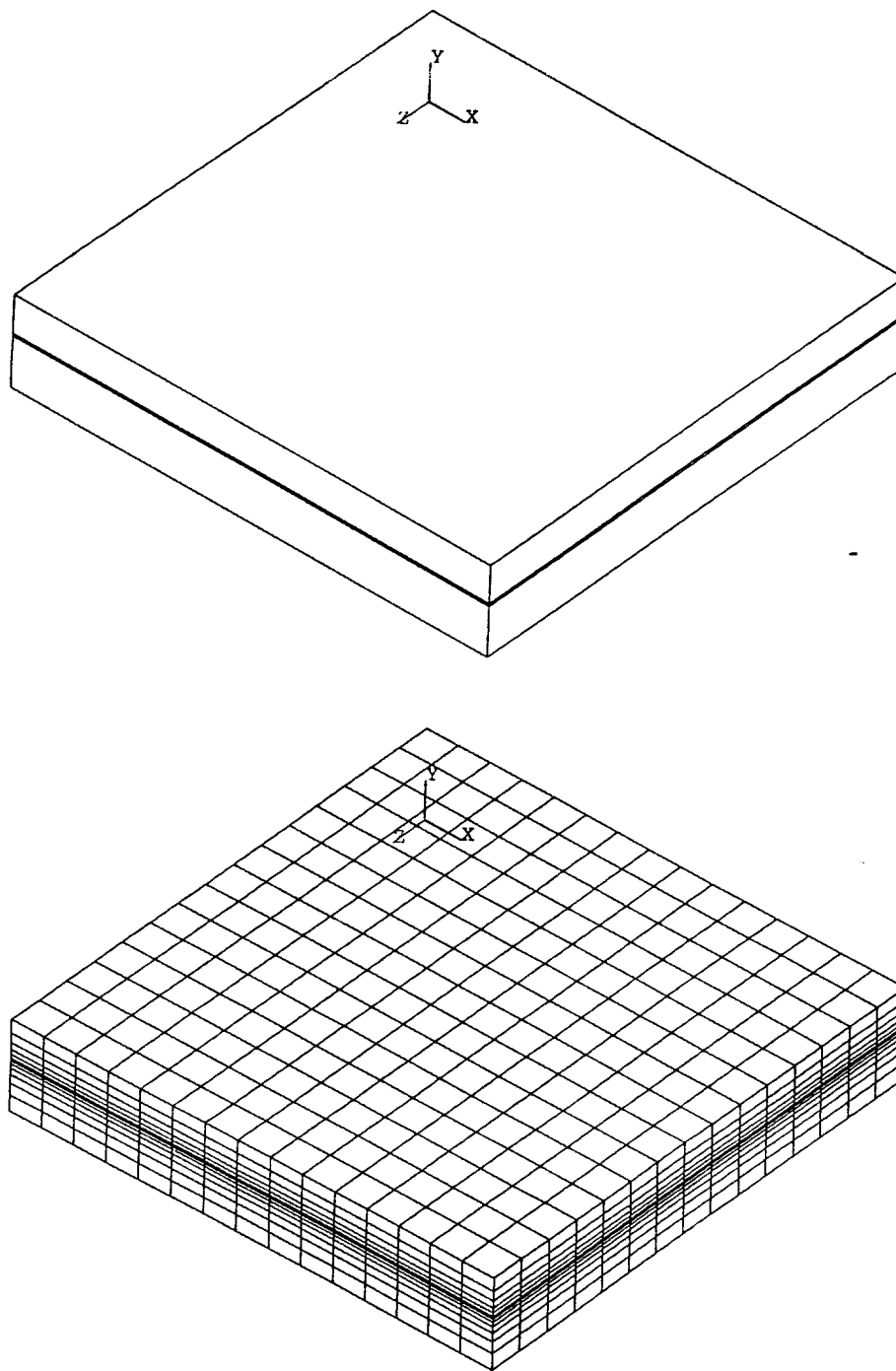


Fig.4-13 Interlayer Simulation With Alpha=1

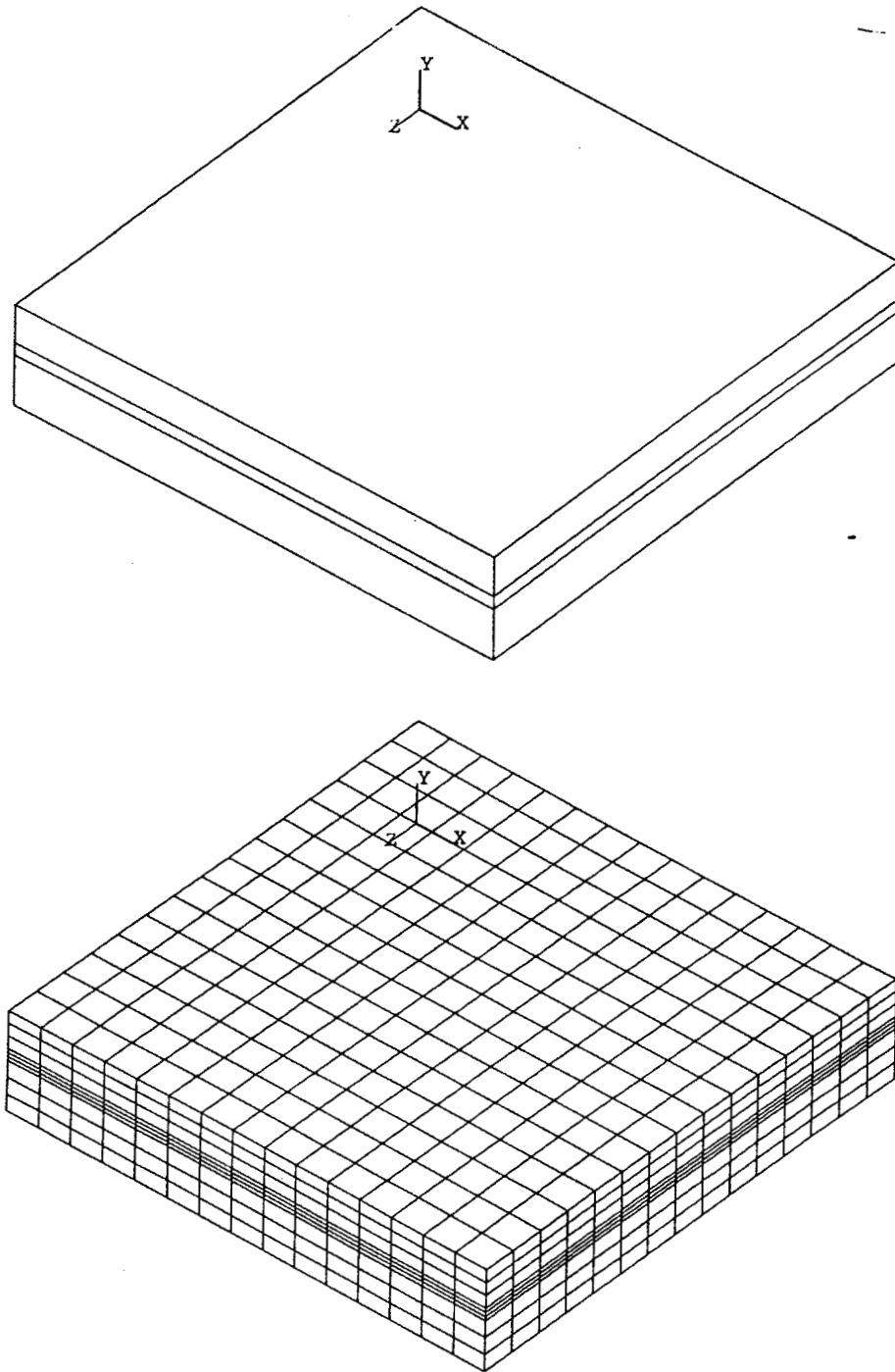


Fig.4-14 Interlayer Simulation With Alpha=5

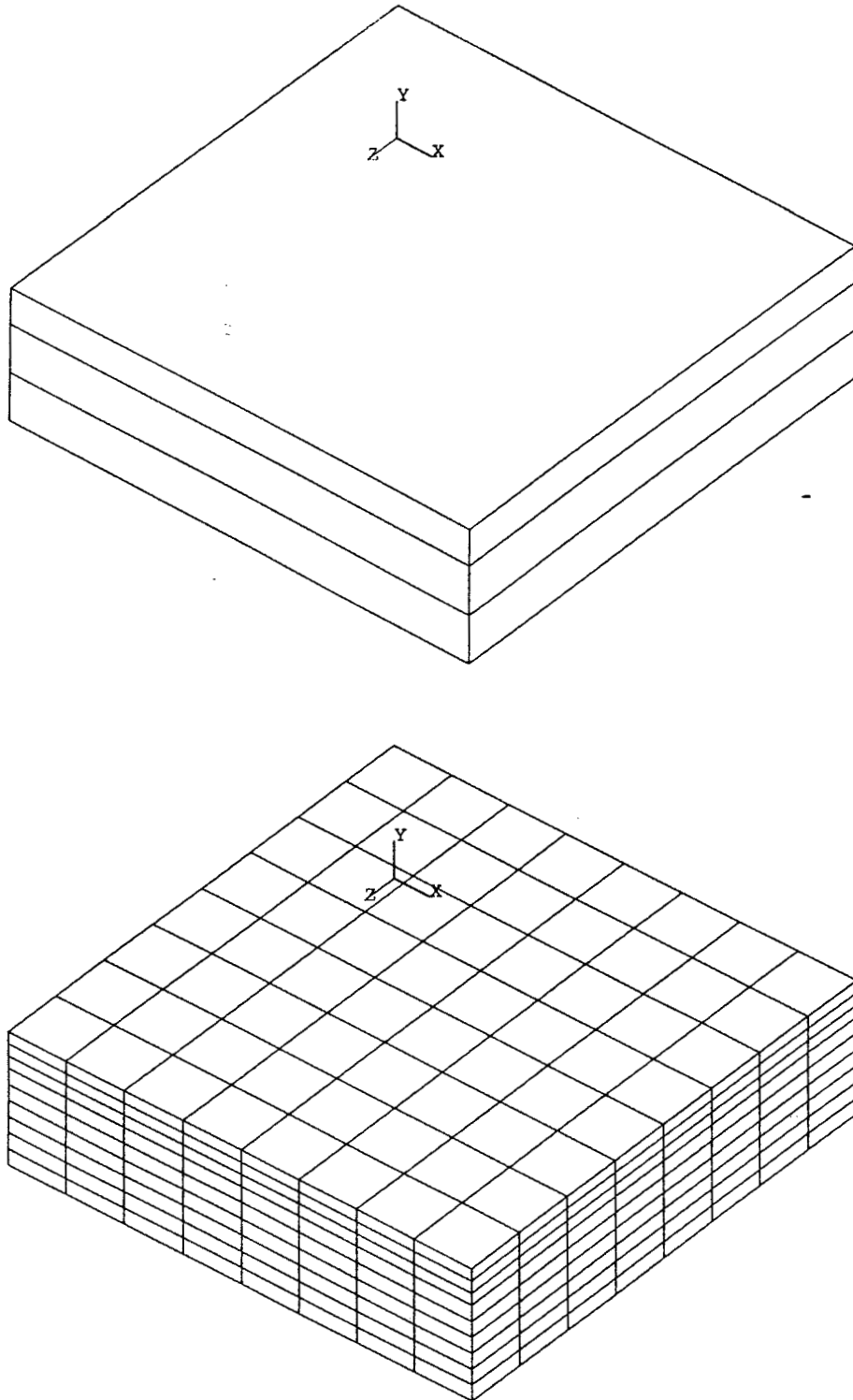
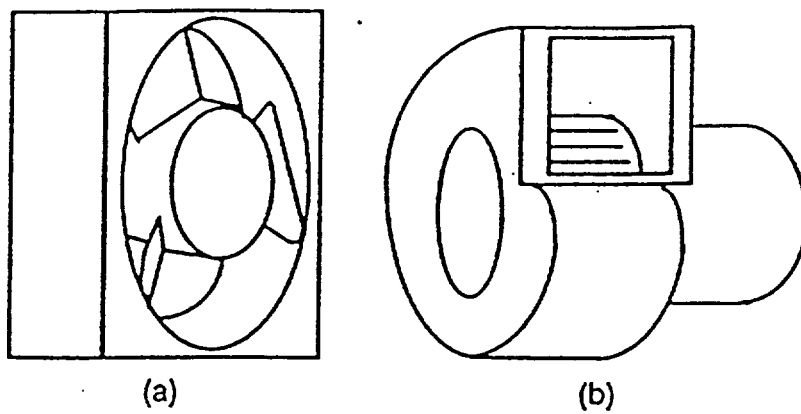


Fig.4-15 Interlayer Simulation With Alpha=20



Air-moving devices; (a) tube-axial fan; (b) squirrel cage blower.

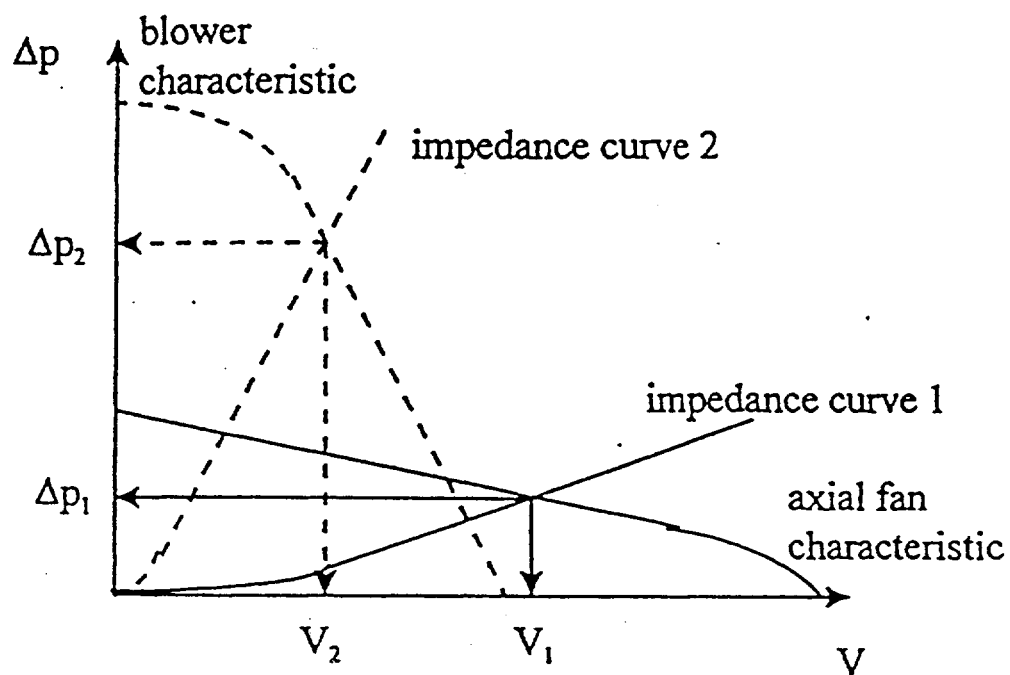


Fig.4-16 Characteristic Curves And Impedance Curves For The Air-Moving Devices (Adapted From Ref. 42)

Fan/Blower Air Performance Comparison

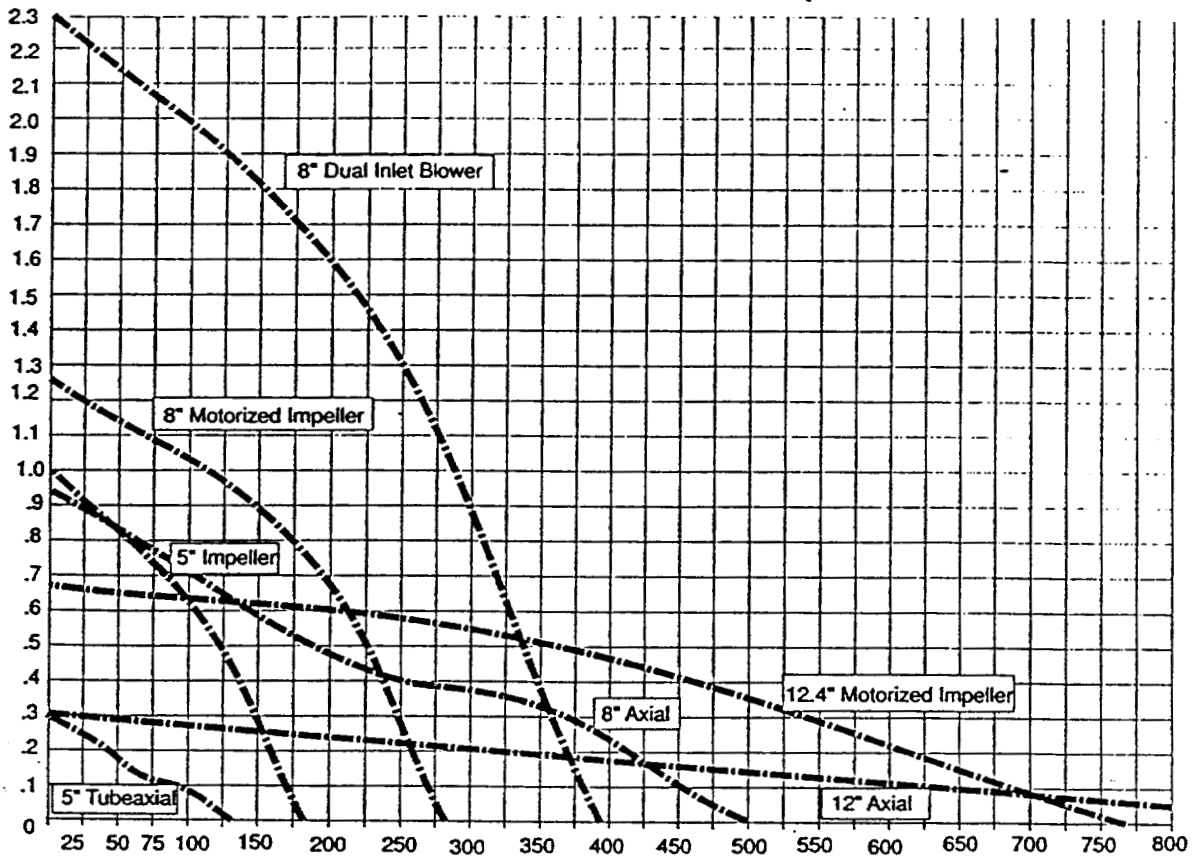


Fig.4-17 Fan/Blower Air Performance Comparison (Adapted From Ref. 20)

Determining STATIC PRESSURE (Resistance of components to air flow)

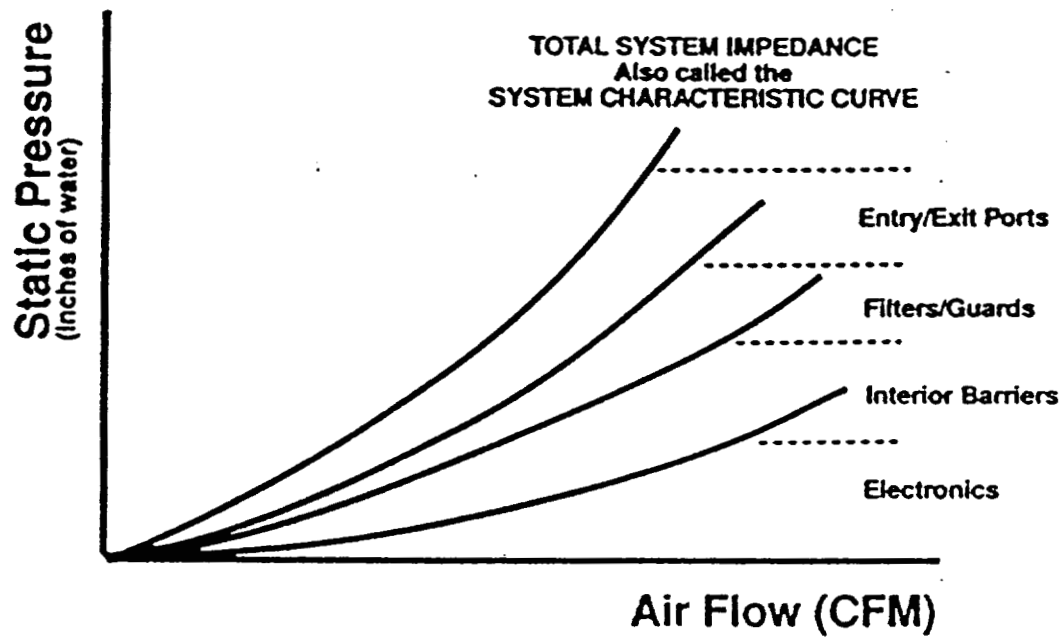


Fig.4-18 Determining Static Pressure (Adapted From Ref.20)

THE OPERATING POINT

(Matching the Air Performance to System Resistance)

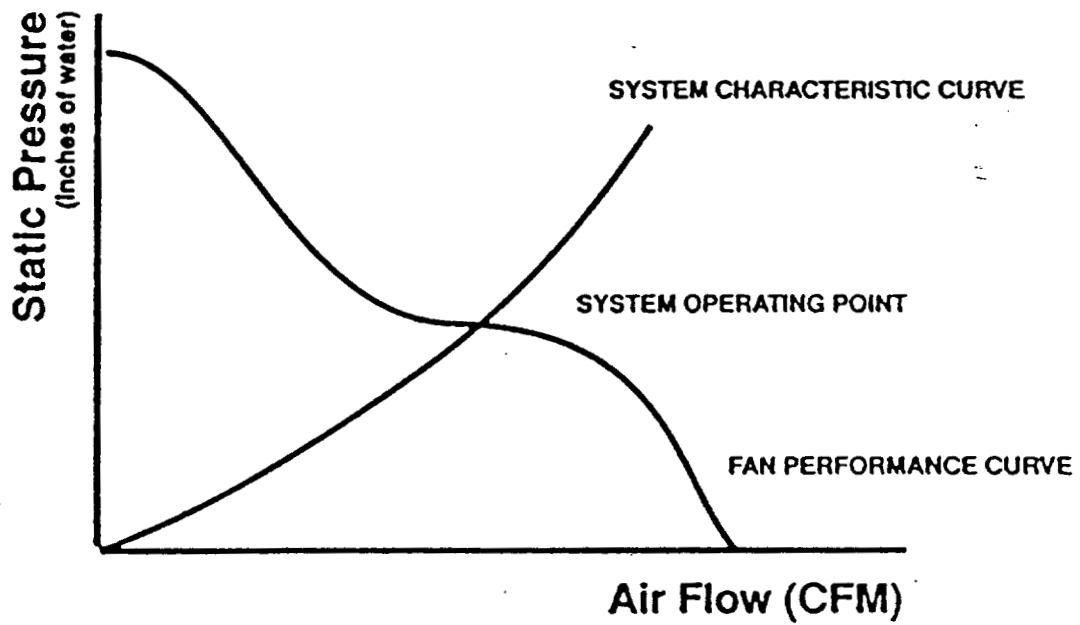
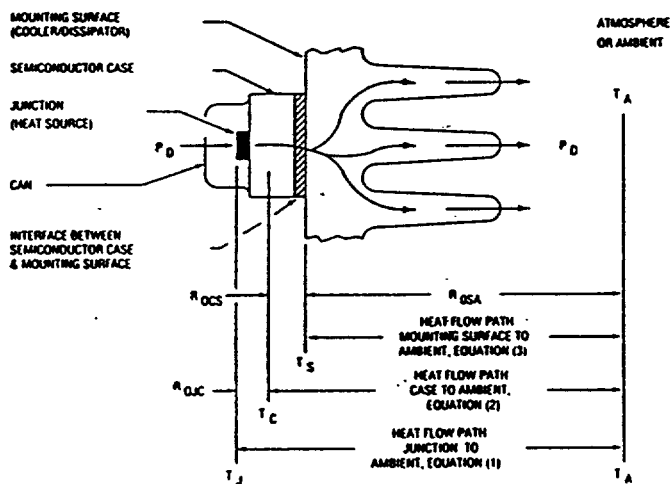


Fig.4-19 The Operating Point (Adapted From Ref.20)



The common practice is to represent the above system with a network of series resistances as shown

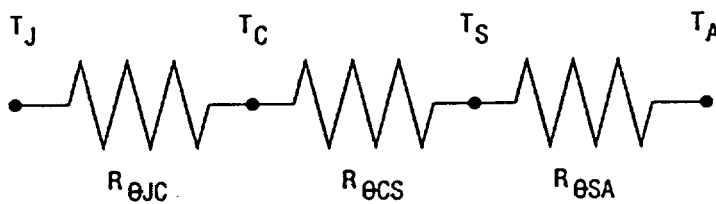


Fig.4-20 Thermal Resistance Configuration For A Typical Heat Sink / Component Packaging (Adapted from Ref. 31)

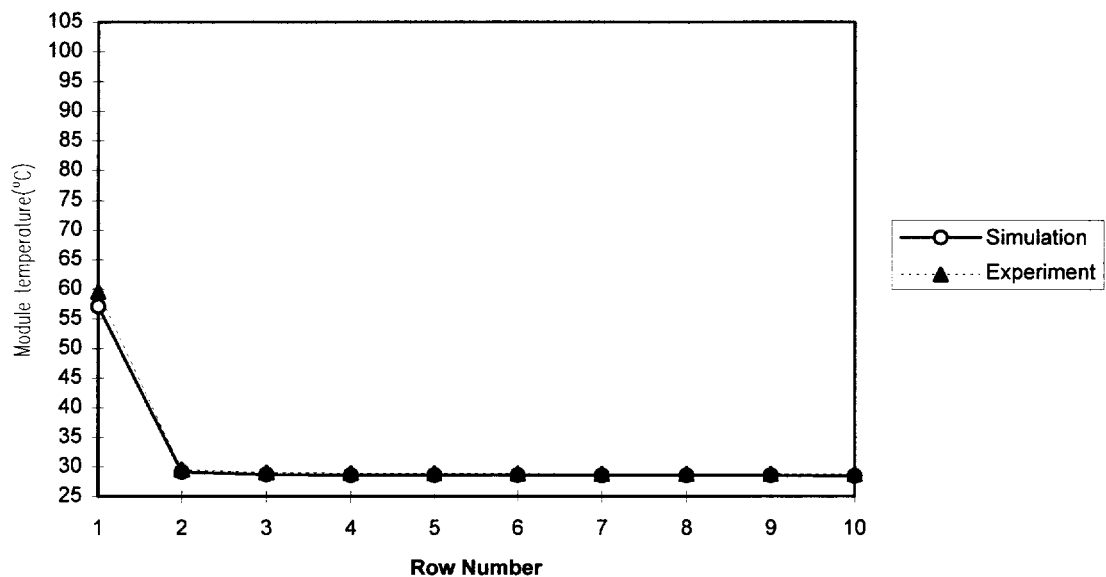


Fig 4-21 Simulated Results By Heated Module (Row 1 Heated, Case1)

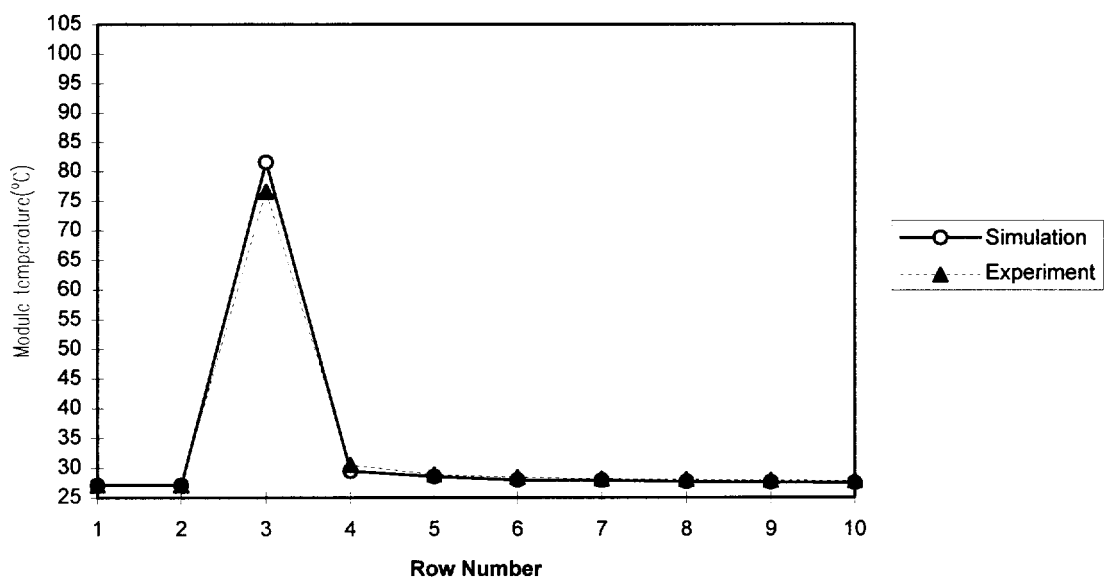


Fig 4-22 Simulated Results By Heated Module (Row 3 Heated, Case2)

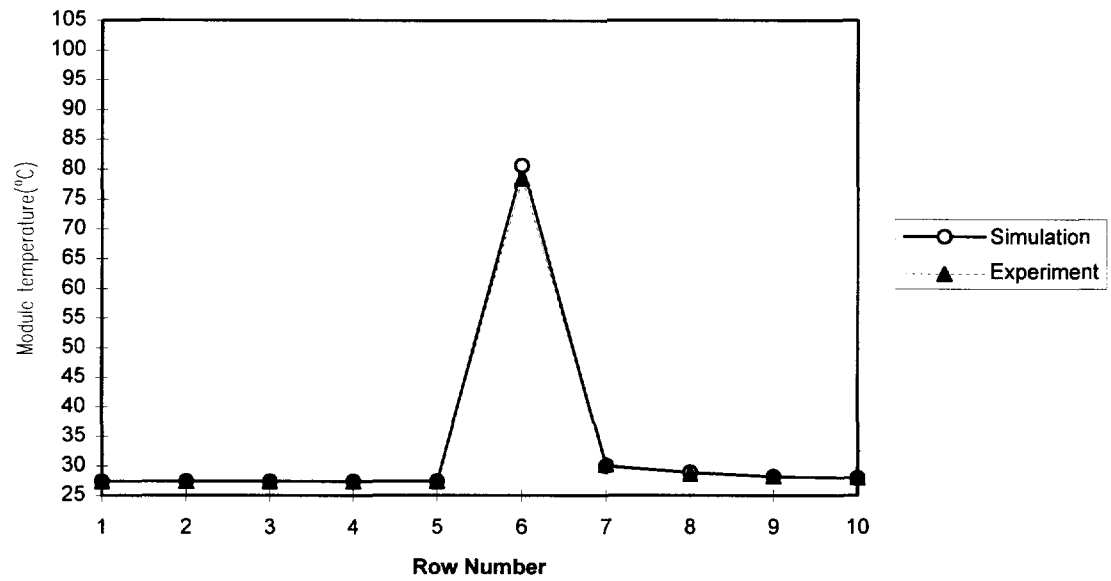


Fig 4-23 Simulated Results By Heated Module (Row 6 Heated, Case3)

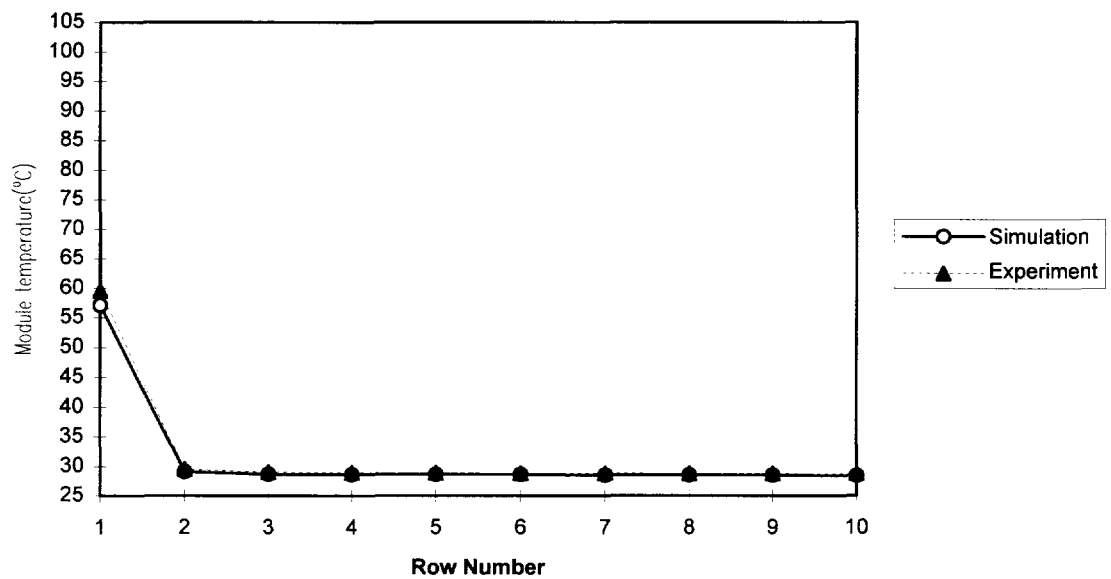


Fig 4-24 Simulated Results By Heated Module (Row 1 Heated, Case4)

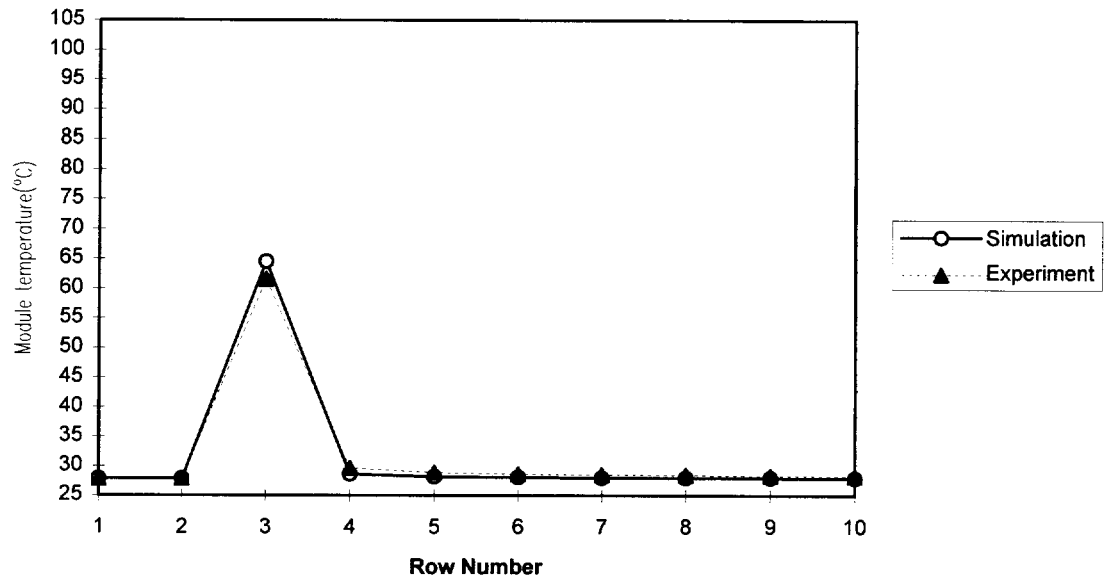


Fig 4-25 Simulated Results By Heated Module (Row 3 Heated, Case5)

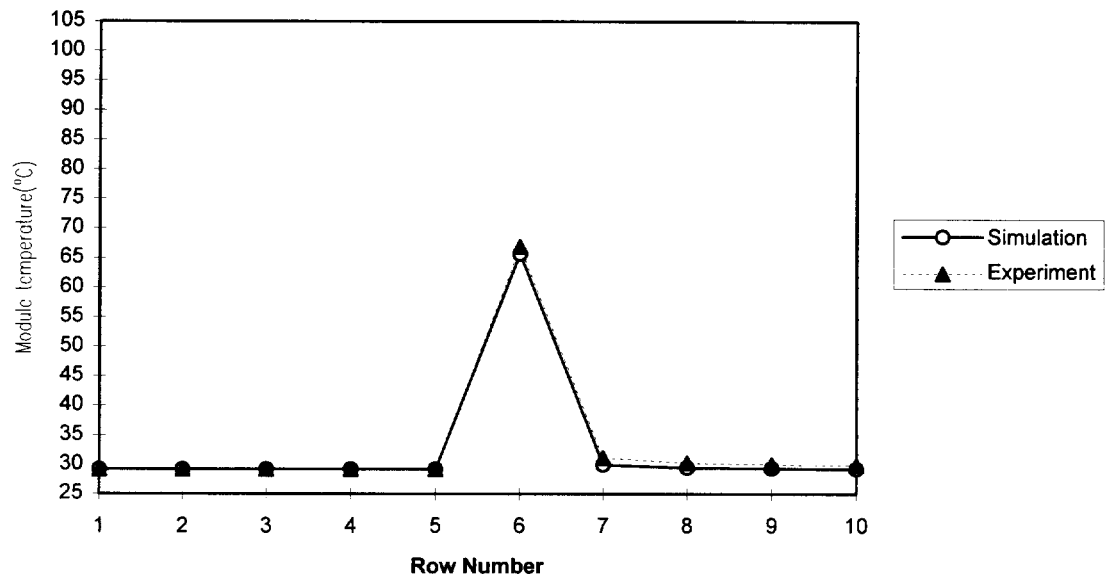


Fig 4-26 Simulated Results By Heated Module (Row 6 Heated, Case6)

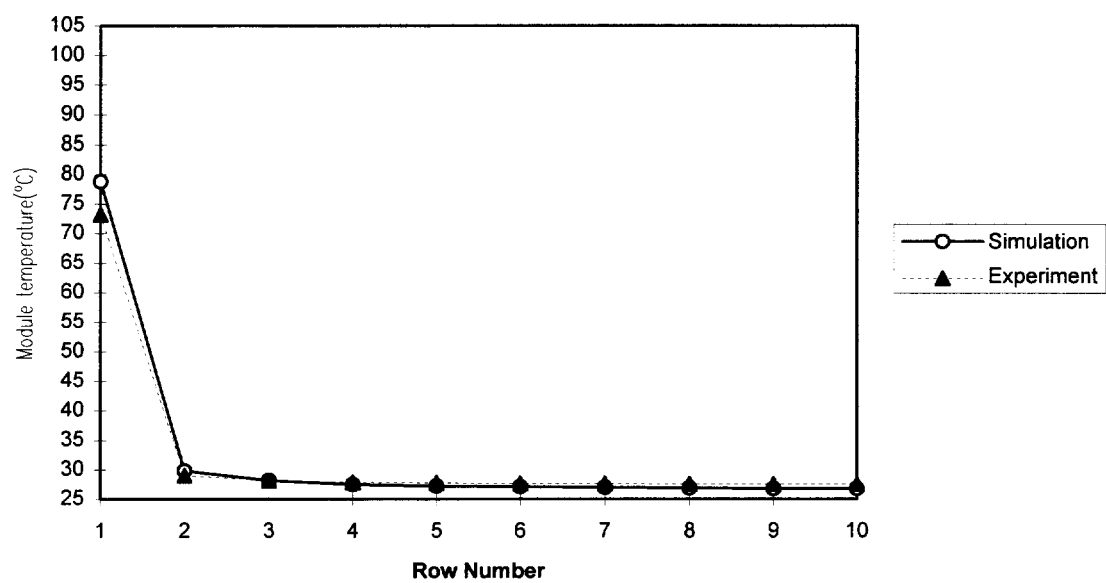


Fig 4-27 Simulated Results By Heated Module (Row 1 Heated, Case7)

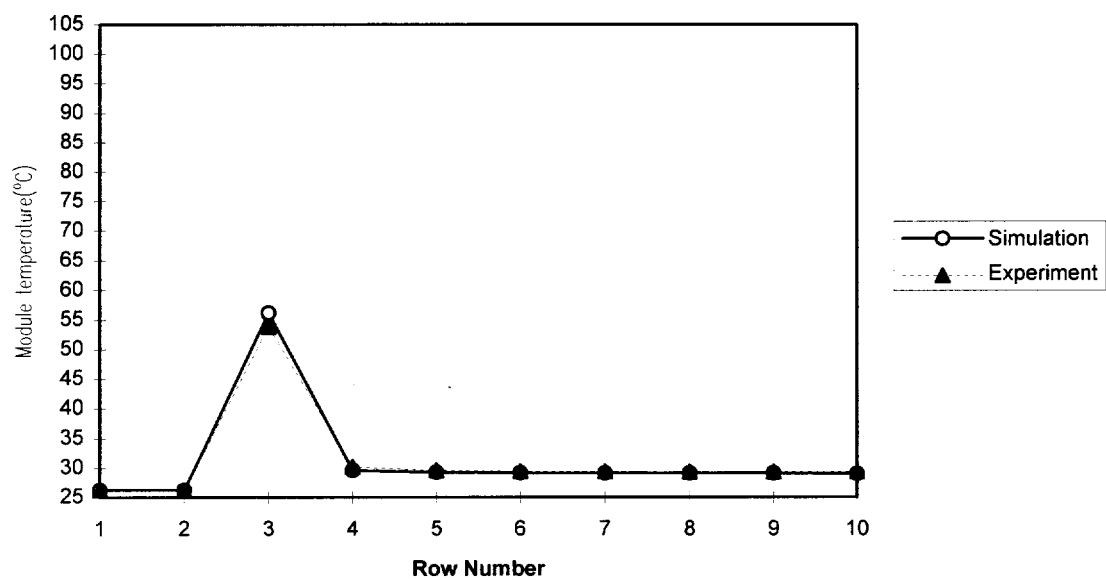


Fig 4-28 Simulated Results By Heated Module (Row 3 Heated, Case8)

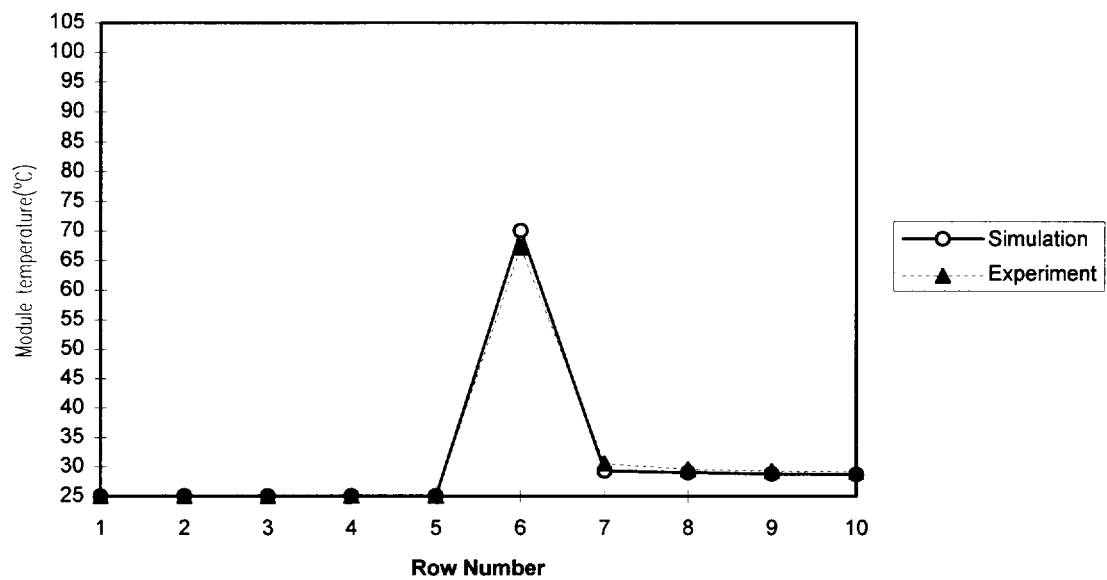


Fig 4-29 Simulated Results By Heated Module (Row 6 Heated, Case9)

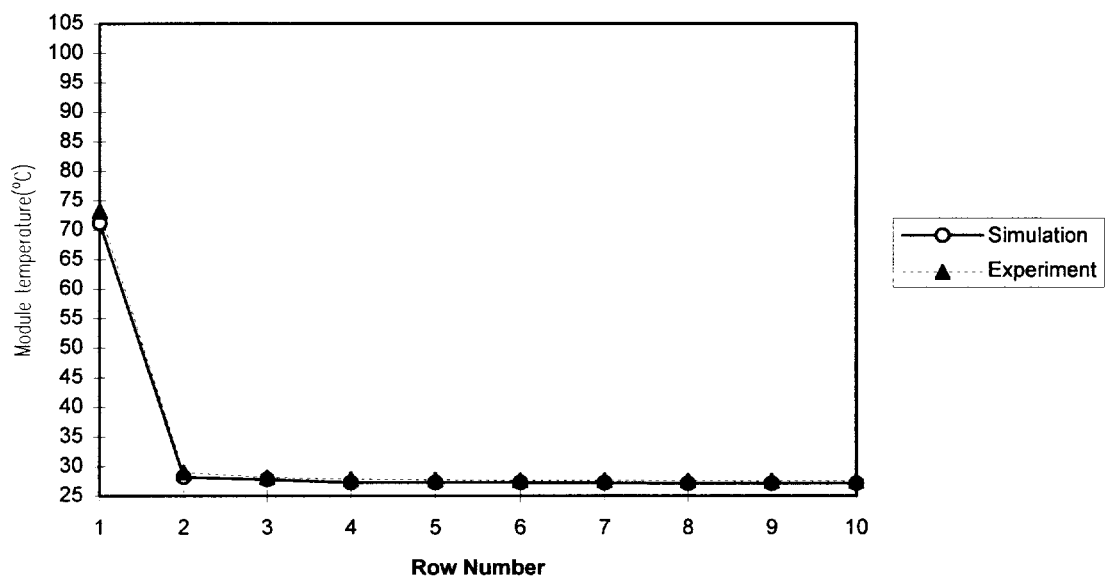


Fig 4-30 Simulated Results By Heated Module (Row 1 Heated, Case10)

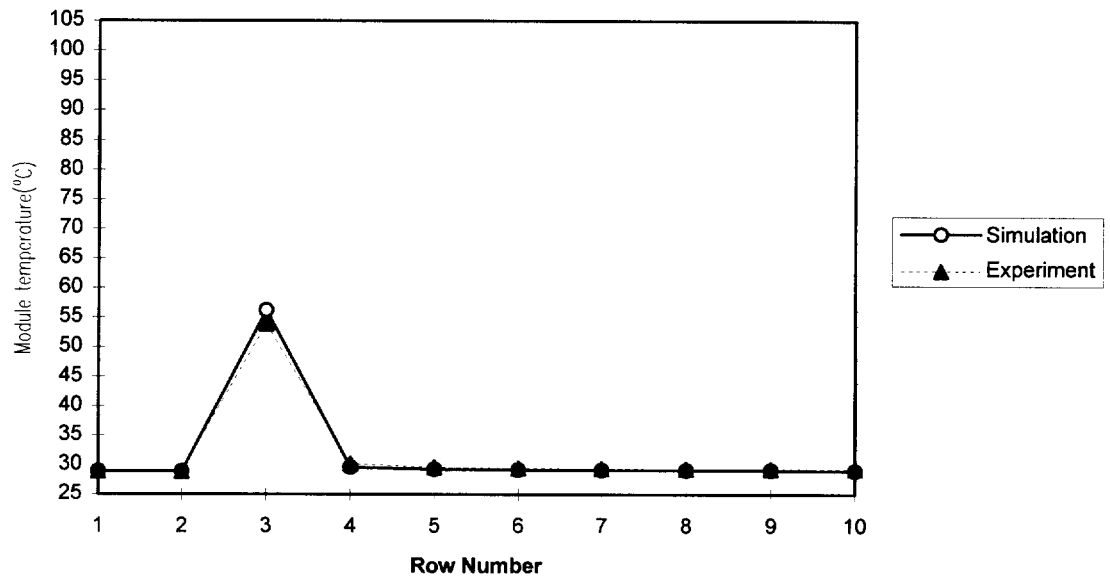


Fig 4-31 Simulated Results By Heated Module (Row 3 Heated, Case11)

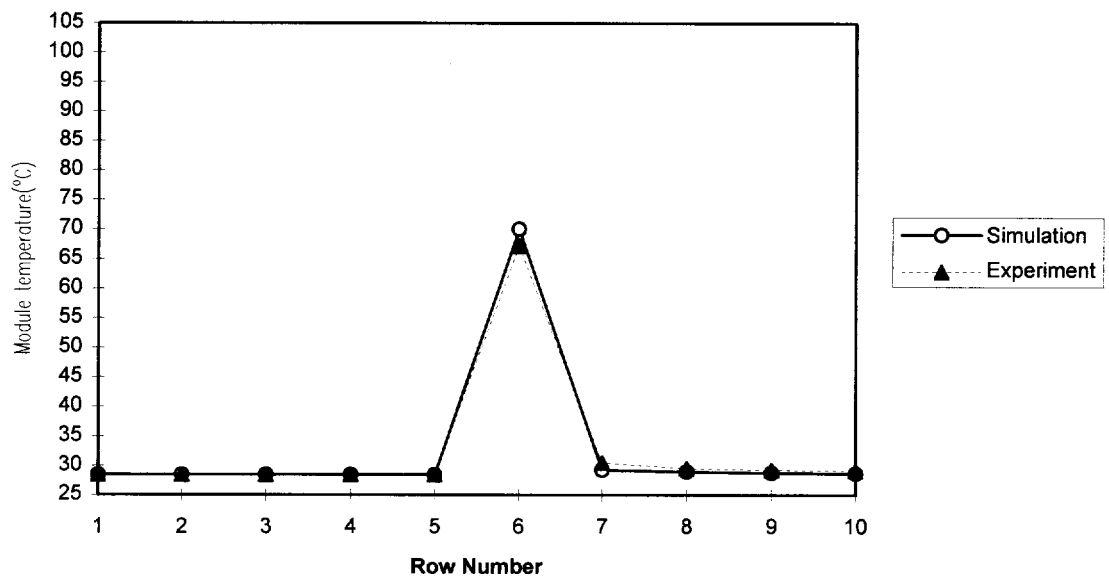


Fig 4-32 Simulated Results By Heated Module (Row 6 Heated, Case12)

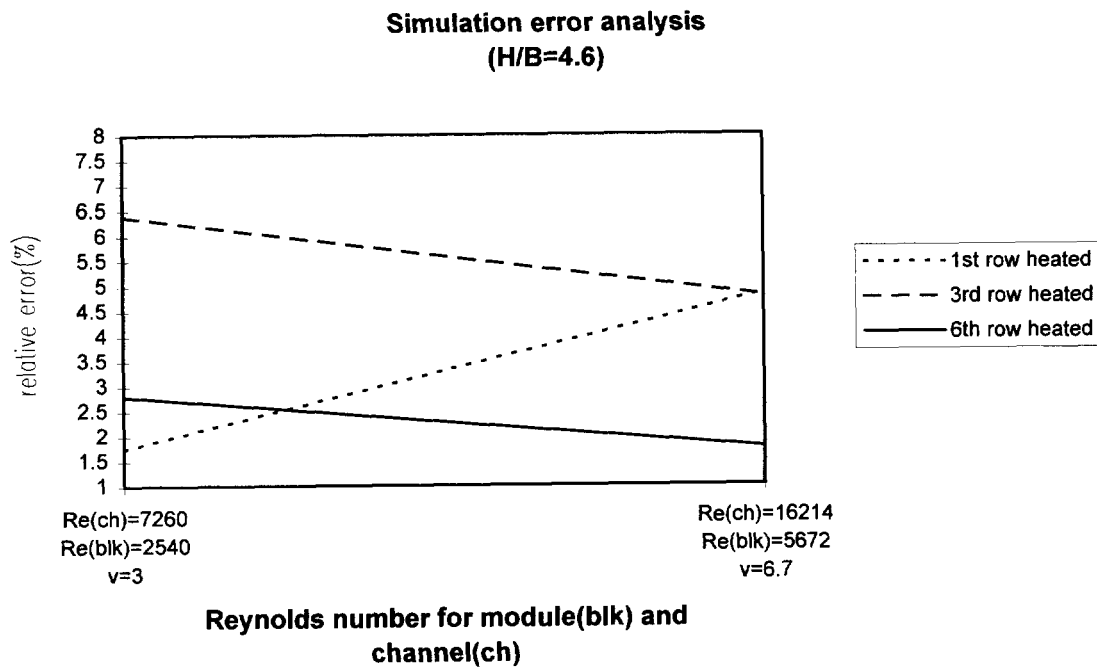


Fig 4-33 Error Analysis At H/B=4.6

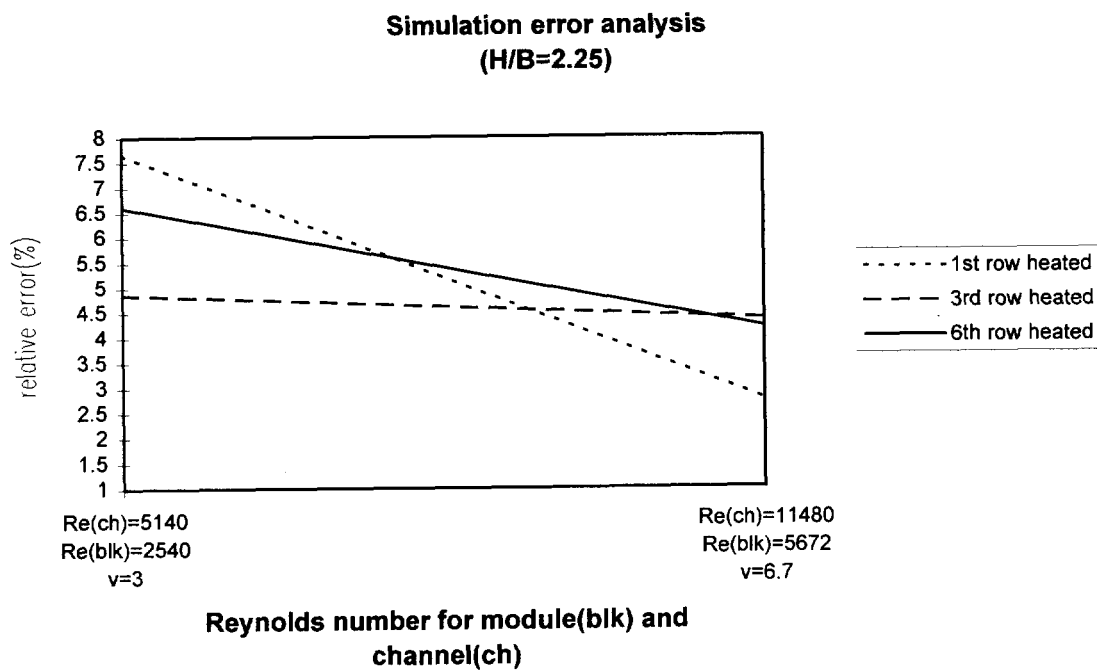


Fig 4-34 Error Analysis At H/B=2.25

REFERENCES

1. Addison, S., Ali, A., "Modeling PCB's with Condition", Flotherm User News, Western Region Edition. No. 5, pp. 9-11, Marlborough, Massachusetts, May 1996.
2. Anderson, A. M., Moffat, R., J., "Applying Heat Transfer Coefficient Data to Electronics Cooling", Journal of Heat Transfer, ASME, Vol. 112, pp. 882, November 1990.
3. Anderson, A., Convective Heat Transfer from Arrays of Modules with Nonuniform Heating: Experiments and Modules, Ph.D. Dissertation, Stanford University, 1990.
4. Arvizu, D. E., Experimental Heat Transfer from an Array of Heated Cubical Elements on an Adiabatic Channel Wall, Ph.D. Thesis, Stanford University, December 1981.
5. Asako, Y., Faghri, M., "Arrays of Heated Square Blocks", Journal of Heat and Mass Transfer, Vol. 32, No. 2, pp. 395-405, 1989.
6. Bar-Cohen, A., "State-of-the-Art and Trends in the Thermal Packaging of Electronic Equipment", Journal of Electronic Packaging, Vol. 114, No. 3, pp. 257-270, 1992.
7. Bar-Cohen, A., "Thermal design and Control", Physical Architecture of VLSI Systems, pp. 564, John Wiley and Sons, New York, 1994.
8. Barkan, P. and Tuohy, E. J., "A Contact Resistance Theory for Rough Hemispherical Silver Contacts in Air and in Vacuum", IEEE Trans. on Power Apparatus and Systems, Vol. Pas-84, No. 12, December 1965.
9. Bathe, K. J., Finite Element Problems in Engineering, Prentice Hall, 1982.
10. Belajev, N. M., Memoirs on the Theory of Structures, Petrograd, 1924.
11. Benson, D. J., Hallquist, J. O., "A Simple Rigid Body Algorithm for Structural Dynamics Programs", International Journal for Numerical Methods in Engineering, Vol. 22, pp. 723-749, March 1986.
12. Biber, C. A., "Surface-Mount Heat Sink Thermal Analysis", FLOTHERM Publishing No. T170-2, pp. 1-6, 5th International FLOTHERM User Conference, Paris, France, September 1996.
13. Biber, C. A., Sammakia, B. G., "Transport From Discrete Heat Components in A Turbulent Channel Flow", ASME Paper No. 86, WA/HT-68, 1986.
14. Boresi, A. B., Sidebottom, O. M., Seely, F. B., Smith, J. O., Advanced Mechanics of Materials, 4th Ed., John Wiley and Sons, 1985.

15. Buragohain, D. N., Shah, V. L., "Curved Interface Elements for Interaction Problems", Proceedings, International Symposium on Soil Structure Interaction, Vol. 1, pp. 197-202, University of Roorkee, India, 1977.
16. Castleberry, G. A., "Analyzing Contact Stresses More Accurately", Machine Design, Vol. 56, No. 7, pp. 92-97, 1984.
17. Chopin, T.,R., "Buoyancy-Driven Flow with large Viscosity Variations in A Square Enclosure", ASME HTD Proceedings, Vol. 317-1, pp. 49-59, Pennsylvanian, 1995..
18. Clausing, A. M. and Chao, B. T., "Thermal Contact Resistance in A Vacuum Environment", Trans. ASME, Vol. 94C, No. 3, pp. 243-251, 1965.
19. Davalath, J., Bayazitoglu, Y, "Forced Convection Cooling Across Rectangular Blocks", Journal of Heat Transfer, Vol. 109/321, pp. 321-328, May 1987.
20. EBM Industries Inc., "How to Select the Best Fan or Blower for Your Application", Fans and Blowers, Catalog F6-954, EBM Industries, Inc., 1995.
21. Faghri, M., Lessmann, R. C., Sridhar, S., Schmidt, R., Asako, Y., "A Preliminary Experimental Study of Forced Air-cooling of Rectangular Blocks Encountered in Electronic Equipment", ASME HTD Proceedings, Vol. 123, pp. 1-6, California, 1989.
22. Flotherm, "The Electronics Cooling Problem: Junction Life Statistics", Flomerics, Surrey, UK, 1996.
(http://www.flotherm.com/Prod_Info/About_FLOTHERM/about_FLOTHERM.htm#problem) Viewed July 16, 1998.
23. Flotherm, "The Electronics Cooling Problem: Major Cause of Electronic Failures", Flomerics Inc., Surrey, UK, 1996.
(http://www.flotherm.com/Prod_Info/About_FLOTHERM/about_FLOTHERM.htm#problem) Viewed July 16, 1998.
24. Flotherm, Instruction Manual: How to Use Flotherm, Version 1.4, FLOTHERM/LC/0993/1/3, Flomerics, Inc., Surrey, UK, 1995.
25. Francavilla, A., Zienkiewicz, O. C., "A Note on the Computation of Elastic Contact Problems", International Journal for Numerical Methods in Engineering, Vol.9, pp. 913-924, 1975.
26. Ghaboussi, J., Wilson, E. L., Isenberg, J., "Finite Elements for Rock Joints and Interfaces", Journal of the Soil Mechanics and Foundations Division, ASCE Publications, No. SM10, pp. 832-848, 1973.

27. Goodman, R. E., Taylor, R. L., Brekke, T., "A Model for Mechanics of Jointed Rock", *Journal of the Soil Mechanics and Foundations Division, ASCE*, No. SM3, Proceedings Paper No. 5937, 1968.
28. Greenwood, J. A. and Williamson, J. B. P., "Contact of Nominally Flat Surfaces", *Proc. Roy. Soc., Series A*, No. 1442, Vol. 295, pp. 300-319, 1966.
29. Greenwood, J. A., "On the Area of Contact Between Rough Surface and Flats", *ASME*. Paper No. 65-Lub-10, 1965.
30. Harper, C. A., *Electronic Packaging and Interconnection Handbook*, 2nd Ed., McGraw-Hill, 1997.
31. Heat Sink Technical Data in Thermalloy, Inc., *Thermal Management Solution*, pp. A10, Dallas, Texas, 1998.
32. Hegazy, A. A., *Thermal Joint Conductance of Conforming Rough Surfaces: Effect of Surface Micro - Hardness Variation*, Ph.D. Dissertation, University of Waterloo, Canada, 1985.
33. Holman, J. P., *Heat Transfer*, 6th Ed., McGraw-Hill, 1986.
34. Huebner, K. H., Thornton, E. A., Byrom, T. G., *The Finite Element Method for Engineers*, 3rd Ed., John Wiley & Sons, 1995.
35. Hughes, T. J., Taylor, R. L., Sackman, J. L., "A Finite Element Method for a Class of Contact - Impact Problems", *Computer Methods in Applied Mechanics and Engineering*, Vol. 8, No. 3, pp. 249-276, 1976.
36. *Icepak Reference Manual 2.0*, Fluent Inc., Lebanon, New Hampshire, 1996.
37. Incropera, F. P., "Convection Heat Transfer in Electronic Equipment Cooling", *Journal of Heat Transfer*, Vol. 110, pp. 1097-1111, 1988.
38. Incropera, F. P., DeWitt, D. P., *Fundamentals of Heat and Mass Transfer*, 3rd Ed., John Wiley & Sons, 1990.
39. Kalker, J. J., "The Computation of Three - Dimensional Rolling Contact with Dry Friction", *International Journal for Numerical Methods in Engineering*, Vol. 14, No. 9, pp. 1293-1307, 1979.
40. Kays, W. M., and Crawford, M. E., *Convective Heat and Mass Transfer*, McGraw-Hill, New York, 1966.

41. Kohnke, P., ANSYS User's Manual for Revision 5.3, Swanson Analysis Systems, Inc, 1994.
42. Lau, J., Wong, C. P., Prince, J. L., Nakayama, W., Electronic Packaging: Design, Materials, Process, and Reliability, McGraw-Hill, 1998.
43. Launder, B. E., "On the Computation of Convective Heat Transfer in Complex Turbulent Flows", Journal of Heat Transfer, Vol. 110, No. 4B, pp. 1112-1128, 1988.
44. Lee, S., "How to Select a Heat Sink", Electronics Cooling, Vol. 1, No. 1, pp.10-14, June 1995.
45. Lee, T. Y., Chambers, B., Mahalingam, M., "Application of CFD Technology to Electronic Thermal Management", Proceedings of 4th IEEE Electronics Comp. and Tech. Conf., pp. 411-420, 1994.
46. Lee, T. Y., Mahalingam, M., "Application of a CFD Tool for System-Level Thermal Simulation", IEEE Trans. Comp., Hybrids, Manufact. Technol., Vol. 17, pp. 564-572, 1994.
47. Linton, R. L., "CFD Modeling of Electric Enclosures", ASME Heat Transfer in Electronic Equipment, ASME HTD Proceedings, Vol. 171, pp. 95-100, 1991.
48. Linton, R., "Thermal Contact Resistance Using Porosity", Lectures on Phoenixics, Phoenixics 2.2, London, England, September 1997.
49. Martin, H., "Heat and Mass Transfer between Impinging Gas Jets and Solid Surfaces," Advances in Heat Transfer, Vol. 13, pp. 1-61, Academic Press, New York, 1977.
50. Meekisho, L. L., Thermal Stress Analysis of Contact Problems by the Finite Element Method, Ph.D. Dissertation, Carleton University, Canada, 1988.
51. Meyer IV, G. A., Toth, J. E., "Alternate Thermal Management Technologies", Thermacore Inc., EUROTHERM Conference, Delft, Netherlands, June, 14-16, 1993. (http://www.flotherm.com/Prod_Info/About_FLOTHERM/about_FLOTHERM.htm#problem) Viewed July 16, 1998.
52. Mithal, P., "Design of Experiment Based Evaluation of the Thermal Performance of A Flipchip Electronic Assembly", ASME EEP Proceeding, Vol. 18, pp. 109-115, ASME, 1996.
53. Mix, D. E., Bar-Cohen, A., "Transient and Steady State Thermo-Structural Modeling of A PDIP Package", ASME paper, 92-WA/EEP-10, pp. 1-12, Anaheim, California, November 1992.

54. Noor, A. K., Kamel, H. A., Fulton, R. E., "Substructuring Techniques, Status and Projections", *Computers and Structures*, Vol. 8, No. 5, pp. 621-632, 1978.
55. Oden, J. T., Carey, G. F., *Special Problems in Solid Mechanics*, Texas Finite Element Series, Vol. 5, Prentice-Hall Inc., New Jersey, 1984.
56. Oosthuizen, P. H., "Effect of a Deflector Wedge on Forced Convection from Heated Rectangular Blocks on a Channel Wall", *Proceedings of the 5th International Conference on Numerical Methods in Laminar and Turbulent Flow*, Vol. 5, Part 2, pp. 1280-1289, Montreal, July 6-10, 1987. Pineridge Press, Swansea, U.K, 1987.
57. Ortega, A., Moffat, R. J., "Cooling Electronic Components: Forced Convection Experiments with An Air-Cooled Array", *Heat Transfer in Electronic Equipment*, ASME HTD Proceedings, Vol. 48, pp. 15-27, 1985.
58. Patankar, S. V., *Numerical Heat Transfer and Fluid Flow*, Hemisphere Publishing Corp., New York, 1980.
59. Paul, B., "Surface and Subsurface Stresses Associated with Non - Hertzian Wheel - Rail Contact", *Symposium on Contact Mechanics and Wear of Rail/Wheel Systems*, pp. 197-207, Vancouver B.C., Canada, 1982.
60. Pilkey, W. D, *Formulas for Stress, Strain, and Structural Matrices*, John Wiley & Sons, 1994.
61. Przekwas, A. J., Athavale, M. M., Ho, Y. H., "High Resolution Thermal Design Tools for Air-cooled Electronics Components and Systems", *ASME EEP Proceedings*, Vol. 18, pp. 27-32, ASME, 1996.
62. Reddy, J. N., Gartling, D. K., *The Finite Element Method in Heat Transfer and Fluid Dynamics*, CRC Press, 1994.
63. Sambasivam, M., Ghoshal R., "Novel Epoxy Composition for Microelectronic Packaging Applications", *ASME EEP Proceedings*, Vol. 18, pp. 55-59, 1996.
64. Schlichting, H., *Boundary Layer Theory*, 7th Ed., McGraw-Hill, New York, 1979.
65. Schmidt, R. C., Patankar, S. V., "A Numerical Study of Laminar Forced Convection Across Heated Rectangular Blocks in A Two Dimensional Duct", *ASME Paper*, 86-WA/HT-88, 1986.
66. Seigal, Robert, and Howell, John R., *Thermal Radiation Heat Transfer*, 2nd Ed., Hemisphere, 1981.

67. Seraphim, D. P., Lasky, R. C., Li, Chen-Yu, Principles of Electronic Packaging, McGraw-Hill, 1989.
68. Shigley, J. E., Mechanical Engineering Design, 3rd. Ed. McGraw - Hill, 1977.
69. Shlykov, Y. P. and Ganin, Y. A., "Thermal Resistance of Metallic Contacts", International Journal of Heat and Mass Transfer, Vol. 12, No. 10, pp. 79-83, 1965.
70. Spalding, D. B., Launder, B. E., "The Numerical Computation of Turbulent Flows", Computer Methods in Applied Mechanics and Engineering, Vol. 3, No. 2, pp. 269-289, 1974.
71. Sparrow, E. M., Niethammer, J. E., Chaboki, A., "Heat Transfer and Pressure-Drop Characteristics of Arrays of Rectangular Modules Encountered in Electronic Equipment", International Journal of Heat and Mass Transfer, Vol. 25, No. 7, pp. 961-973, July 1982.
72. Sze, S. M., VLSI Technology, 2nd Ed., McGraw-Hill, 1988.
73. Thermal Analysis, ANSYS User's Manual for Revision 5.3 Tutorial, Swanson Analysis Systems, Inc., 1994.
74. Thomas, H. R., Hoersch, V. A., "Stress Due to the Pressure of One Elastic Solid upon Another", University of Illinois Engineering Experimental Station Bulletin, No. 212, 1930.
75. Tien, C. L., "A Correlation for Thermal Contact Conductance of Nominally Flat Surfaces in A Vacuum", Proceedings of 7th Conference on Thermal Conductivity, NBS/SP 302, pp. 755-759, 1968.
76. Tummala, R. R., Rymaszewski, E. J., Klopfenstein, A. G. Microelectronics Packaging Handbook, 2nd Ed., Chapman & Hall, 1997.
77. Tummala, R. R., Rymaszewski, E. J., Klopfenstein, A. G., Microelectronics Packaging Handbook, 1st Ed., Chapman & Hall, 1989.
78. Wilcox, D. C., Turbulence Modeling for CFD, 2nd Ed., DCW Industries, Inc. La Canada, California, 1998.
79. Wilcox, L. E., "An Exact Analytical Method for Calculating Stresses in Bevel and Hypoid Gear Teeth", No. 3, Vol. 2, pp. 387-396, Gleason Machine Division, New York, 1970.

80. Wilson, E. A., Parsons, B., "Finite Element Analysis of Elastic Problems Using Differential Displacements", *International Journal for Numerical Methods in Engineering*, Vol. 2, pp. 387-395, 1970.
81. Yang, Shiming, *Heat Transfer*, People's Education Press, Beijing, China, 1981.
82. Yovanovich, M. M., "Recent Developments in Thermal Contact, Gap and Joint Conductance Theories and Experiment", *Keynote Paper, International Heat Transfer Conference*, pp. 35, San Francisco, California, 1986.
83. Yovanovich, M. M., "Theory and Application of Constriction and Spreading Resistance Concepts for Microelectronics Thermal Management", *Cooling Techniques for Computers*, Department of Mechanical Engineering, University of Waterloo, Ontario, Canada, 1991.
84. Yovanovich, M. M., "Thermal Contact Resistance in Microelectronics", *Proceedings of the Technical Program*, pp. 177-188, *National Electronic Packaging and Production Conference*, Anaheim, California, March 1978.
85. Zahn, Bret A., "Evaluating Thermal Characterization Accuracy Using CFD Codes: A Package Level Benchmark Study of IcePak and Flotherm", *Proceeding of the Sixth Intersociety Conference on Thermal and Thermomechanical Phenomena in Electronic Systems*, pp. 322-329, Seattle, May 1998.
86. Zienkiewicz, O. C., "Adaptivity and Mesh Generation", *International Journal for Numerical Methods in Engineering*, Vol. 32, No. 4, pp. 783-810, 1991.
87. Zienkiewicz, O. C., *The Finite Element Method*, McGraw - Hill, 1977.
88. Zimmerman, E. B., "Prevention of Overheating and Frequent Thermal Cycling of Outdoor Electronic Cabinets Cooled by Forced Air Convection in Cold Climate", *EEP-Vol. 18*, pp. 83-87, ASME 1996.

VITA

Wen Wei was born on May 28, 1963 in Beijing, China.

He joined the Department of Power Machinery Engineering at Xi'an Jiaotong University in 1980 and graduated with a BS degree in Engineering in 1984. His major area of study was Internal Combustion.

He was employed as an Assistant Engineer at the Science and Technology Research Institute of Transportation in Hebei, China between 1984-1985.

Between 1985-1987 he was in the Department of Power Machinery Engineering of the Shanghai Institute of Mechanical Engineering, Shanghai, China, where he graduated with the MS degree.

Between 1987-1991 he was employed as a Mechanical Engineer in the Ministry of Machinery and Electronics Industry of China, Beijing, China.

He was a, Ph.D. Candidate and Research Assistant at the Institute of Engineering Thermophysics at the Chinese Academy of Sciences, Beijing, China between 1991-1993.

He joined the Department of Materials Science and Engineering of the Oregon Graduate Institute of Science and Technology, Oregon in 1993 and graduated with the Ph.D. degree in 1998.

He has been a Senior Mechanical Design Engineer specializing in Thermal Management in Microelectronics at Credence Systems Corporation, Beaverton, Oregon from 1997 to the present.